Nye typer bygningsintegrerede ventilationsløsninger med flere funktioner

Hviid, Christian Anker; Olesen, Bjarne W.; Nielsen, Toke Rammer; Svendsen, Svend

Publication date:
2010

Document Version
Publisher's PDF, also known as Version of record

Building integrated passive ventilation systems

Christian Anker Hviid

Industrial Ph.D. Thesis
in collaboration with ALECTIA A/S

Department of Civil Engineering
Technical University of Denmark

2010

Building integrated passive ventilation systems

Printed by DTU-Tryk
Department of Civil Engineering
Technical University of Denmark
1601-2917

Preface

You never change something by fighting the existing reality. To change something, build a new model that makes the existing model obsolete.
R. Buckminster Fuller

Man knows so much and does so little.
R. Buckminster Fuller

This thesis is submitted in partial fulfilment of the requirements for the Danish Ph.d. degree.

Copenhagen 7$^{\text{th}}$ of April 2010

Christian Anker Hviid

Acknowledgements

I wish to express sincere appreciation to Professor Svend Svendsen, Professor Bjarne W. Olesen, Associate Professor Toke Rammer Nielsen, all of them DTU Byg, and Head of Research Lars D. Christoffersen and senior civil engineer Ejvind Løgberg, both ALECTIA A/S, for their assistance in the preparation of this thesis.

The gratitude is also extended to the Birch & Krogboe Foundation, ALECTIA and the Danish Ministry of Science, Technology and Innovation for their financial support.

Thanks also to the colleagues of the Building Physics and Services Section at DTU Byg for their valuable input. A special thanks goes to Steffen Petersen for valuable ping-pong, for taking the time again and again to discuss issues and to bear with my constant interruptions.

Last but not least, I would like to extend my most sincere thanks and gratitude to my beloved ones Irina and my son Anton, for bearing the unsociable aspects of a Ph.D., for their invaluable patience and for their acceptance of my lack of time and attention. It is for them I dedicate this thesis.

List of Papers

Published

Paper I
Hviid, C.A., Nielsen, T.R., Svendsen, S., 2008. Simple tool to evaluate the impact of daylight on building energy consumption. Solar Energy 82 (9) 787-798

Submitted

Paper II
Hviid, C.A., Svendsen, S., 2010. Analytical and experimental analyses of a low-pressure loss heat exchanger suitable for passive ventilation. Submitted to Energy and Buildings

Paper III
Hviid, C.A., Svendsen, S., 2010. Experimental and numerical analysis of perforated suspended ceilings as diffuse ventilation air inlets. Submitted to Energy and Buildings

Paper IV
Hviid, C.A., Svendsen, S., 2010. Detailed whole-year simulation of a building integrated ventilation concept with heat recovery and night cooling for low-energy offices. Submitted to Energy and Buildings

Paper V
Hviid, C.A., Svendsen, S., 2010. A morphological method for investigation of the problem complex of choosing the ventilation system for a new building. Submitted to Building and Environment

Published conference papers

Paper VI
Hviid, C.A., Svendsen, S., 2008. Passive ventilation systems with heat recovery and night cooling. In: Proceedings of the 29th AIVC Conference, Kyoto, 99-104

Paper VII
Hviid, C.A., Svendsen, S., 2007. A method for evaluating the problem complex of choos-

ing the ventilation system for a new building. In: Proceedings of Clima Conference, Helsinki

Paper VIII
Hviid, C.A., Nielsen, T.R., Svendsen, S., 2008. Simple tool to evaluate the impact of daylight on building energy consumption. Proceedings of Building Physics Symposium in the Nordic Countries, Copenhagen, 119-126.

Abstract

Ventilation of a building is the process of supplying outdoor air to the occupants of a building and extracting the same amount of used or contaminated air. Despite the constant improvements of conventional ventilation technologies, it is not possible to meet tomorrow's demand of better indoor climate while cutting energy consumption as demanded by the risk of global warming. This leads to a widening gap between the required fossil fuel reductions and the demand for improved indoor climate. One solution is to shift the ventilation use from active (mechanical) to passive ventilation systems. Passive in this context means ventilation solutions that exploit natural driving forces and the building envelope physics to establish and maintain a satisfying indoor climate without the consumption of electrical energy. The concept has particular potential in temperate climates where high wind speeds and large daily temperature differences prevail.

In order for a passive ventilation system to be competitive, efficient heat recovery, filtration and low risk of draught are essentials. This thesis proposes a one-mode hybrid ventilation system with very small pressure loss yet with superior or equal indoor climate compared to conventional mechanical ventilation systems.

The objective of the proposal is to achieve whole-year comfort ventilation at extremely low fan power consumption, low primary energy consumption and to provide sufficient free cooling by night ventilation using the supply ducts. A parallel objective is to use components with measured performances whether they are commercially available or prototypes. The system proposed here employs a newly developed heat recovery concept, filtration by electrostatic precipitators and diffuse ceiling ventilation for air distribution. The proposal is backed by detailed simulation of the heat and mass transfer in a test case building. Furthermore, it discusses air flow control, thermal comfort, filtration, operation/maintenance, and cost as a whole.

To obtain the best performance hybrid ventilation is often characterized by solutions that integrate the building, the building operation and the ventilation system in a holistic manner. This means that during the earliest design phase, the ventilation system design and the building design are part of an integrated process with three goals: better indoor climate, lower energy consumption and architecture. This has led to a growing awareness that to achieve low-energy buildings with satisfactory indoor climate the designer has to be aware of the consequences of critical design decisions as early as possible in the design process to obtain a good final whole-building cost-benefit ratio.

The design of ventilation systems for low-energy offices requires insight of the engineer/architect into multiple fields of building design and ventilation. Analysing problem complexes like choosing the ventilation system for a new building presents us with a number of methodological difficulties. The issue involves both quantifiable and non-quantifiable

variables that are correlated to some extent and perhaps incomplete, with missing or undetermined information due to the early stage in the design phase or simply the subjective nature of judgements. A software tool has been developed together with a methodology which promises a quick holistic approach sufficiently accurate to estimate the performance variability of different scenarios. The tool employs a thermal model, a ventilation model that accounts for stack and wind and a daylight model that accounts for the effect of solar shading on the variable artificial lighting load.

The issue of economy is investigated through three very different sources all of which state that low-pressure ventilation, whether it is a mechanical or a hybrid solution, has an installation economy comparable to conventional mechanical ventilation.

The thesis comprises a summary based on five articles submitted to international, scientific journals. The abstract of each paper is reported below.

Paper I This paper presents a simple building simulation tool for integrated daylight and thermal analysis. The tool is capable of importing the thermal and visual properties for different glazings and shading positions from the Window Information System (WIS) program. A coupled ray-tracing and radiosity methodology is used to derive the daylight levels for different sky conditions. Both detailed daylight distribution for a particular day and time and hourly discrete values on a yearly basis may be obtained. For an integrated simulation the hourly daylight levels are fed into an existing simple thermal simulation program capable of calculating energy demand and the indoor environment. Straightforward control systems for general and task lighting systems have been implemented together with a shading control strategy that adjusts the shading according to the indoor operative temperature, the risk of glare and the profile angle of the sun. The implemented daylight calculation method allows for shades from the window recess and overhang, and for distant shades blocking the sky vault. Comparisons with the ray-tracing program Radiance show that the accuracy of this approach is adequate for predicting the energy implications of photoresponsive lighting control. The amount of input is small, which makes the tool useful for integrated daylight optimisation in the early design process.

Paper II A core element in sustainable ventilation systems is the heat recovery system. Conventional heat recovery systems have a high pressure drop that acts as blockage to naturally driven airflow. The heat recovery system we propose here consists of two separated air-to-liquid heat exchangers interconnected by a liquid loop powered by a pump ideal as a component in a heat recovery system for passive ventilation systems. This paper describes the analytical framework and the experimental development of one exchanger in the liquid-loop. The exchanger was constructed from the 8 mm plastic tubing that is commonly used in water-based floor-heating systems. The pressure loss and temperature exchange efficiency was measured. For a design airflow rate of 560 L/s, the pressure loss was 0.37 Pa and the efficiency was 75.6%. The experimental results agree well with the literature or numerical fluid calculations. Within the analytical framework, the total heat recovery of two liquid-coupled exchangers was calculated to be in the range 64.4–74.9%, depending on the parasitic heat loss in the experimental setup. The total pressure drop of the heat recovery

system is 0.74 Pa. Moreover, preliminary improvement calculations promise a future total efficiency of 80% with a pressure drop of 1.2 Pa.

Paper III Experimental and simulation analyses are reported in this paper for a diffuse ceiling ventilation concept. The analyses were carried out with two different porous surfaces mounted in a suspended ceiling: perforated tiles of aluminium and of gypsum. The experiments were carried out in a climate chamber, and the simulations were performed with CFD. The experiments documented an air change efficiency equal to fully mixed conditions with a pressure drop of 0.5 Pa and with no evidence of thermal discomfort. Furthermore, the measurements documented that the ceiling acts as a radiant cooling surface which increases the potential and applicability of the concept. The numerical analyses used an approximate method to model the pre-heating in the porous ceiling and generally supported the experimental conclusion, but it also showed risks of downdrafts especially in areas where thermal plumes do not counteract the cool supply air.

Paper IV Hybrid ventilation systems seek to exploit the advantages of both natural ventilation and mechanical ventilation. Hybrid systems are typically two-mode with two fully autonomous systems or mixed-mode systems where a fan helps the natural ventilation system. Here we present a one-mode system of balanced mechanical ventilation with substantial assistance from stack and wind. The state-of-the-art building simulation program ESP-r is used to model heat and air flows in a fictive building and indoor climate and energy consumption is quantified. The system employs heat recovery with a newly developed heat exchanger, filtration with an electrostatic precipitator and distributes air using diffuse ceiling ventilation. Conventional blade dampers control the airflow and free cooling is provided as night ventilation through the existing supply ducts. The pressure loss is 5 Pa, and the specific fan power (SFP), which is commonly used to compare the energy performance of different ventilation systems, is calculated to 155 J/m^3 including the power consumption of the electrostatic precipitator. The SFP value is approx. 6% of the currently upper limit for VAV systems in the Danish Building Code. The total primary energy consumption of the building is 18.9 kWh/m^2 which makes the ventilation concept suitable for near-zero emission buildings.

Paper V The application of a ventilation system in a new building is a multidimensional complex problem that involves both quantifiable and non-quantifiable data e.g. energy consumption, indoor environment, building integration and architectural expression. This paper presents a structured method for evaluating the performance of a ventilation system in the design process by treating quantifiable and non-quantifiable datasets together. The method is based on general morphological analysis and applies cross-consistency assessment to reduce the problem complex, thus treating the multi-dimensionality, the uncertainty and the subjectivity that arise in the design process on a sound methodological and scientific basis. Using a distance analysis of the shared values, the solution scenarios may be plotted relative to each other, which provides the designer with an illustrated 'space of solutions'. Herein the designer may view multiple ventilation solutions and navigate between

them, evaluate the differences and choose the best ventilation system scenario in terms of energy consumption, indoor environment and architectural quality.

Resumé

Bygningsventilation er en proces, hvor brugt eller forurenet luft fjernes og frisk luft tilføres til bygningen og dens beboere. Trods fortsatte forbedringer af konventionelle ventilationsteknologier, er det imidlertid ikke muligt at opfylde fremtidens krav om bedre indeklima og reduktioner i energiforbruget i en grad som risikoen for global opvarmning påkræver. Dette fører til en stadig større kløft mellem kravet om energibesparelser og kravet om et forbedret indeklima. En løsning er at benytte mere passiv ventilation som erstatning for aktiv (mekanisk) ventilation. Passiv betyder i denne forbindelse ventilationsløsninger, der udnytter naturlige drivkræfter og bygningens fysik til at opretholde et tilfredsstillende indeklima uden brug af elektricitet. Begrebet har et særligt stort potentiale i tempererede klimazoner med høje vindhastigheder og store daglige temperaturforskelle.

For at et passivt ventilationssystem skal være konkurrencedygtigt, er effektiv varmegenvinding, filtrering og lav trækrisiko væsentlige elementer. I denne afhandling udvikles en hybrid ventilationsløsning, der, med små tryktab til trods, har et lige så godt eller bedre indeklima end konventionelle mekaniske ventilationsanlæg. Den hybride løsning er karakteriseret ved at være et mekanisk system som i høj grad udnytter vind og opdriftskræfter.

Formålet med løsningen er at opnå komfortventilation med ekstremt lavt elforbrug til ventilatorer, lavt primært energiforbrug samt tilstrækkeligt med natteventilation via de eksisterende ventilationskanaler. En parallel målsætning er at bruge komponenter med målte egenskaber, hvad enten de er kommercielt tilgængelige eller prototyper. Løsningen anvender et nyudviklet varmegenvindingskoncept, filtrering med aktive elektrostatiske filtre og diffus loftsventilation til rumluftfordeling. Løsningsforslaget bakkes op af detaljerede simuleringer af varme og massetransport i en fiktiv testbygning. Endvidere drøftes styring af luftstrømmen, termisk komfort, filtrering, drift/vedligeholdelse og omkostninger som helhed.

For at opnå den bedste ydeevne er hybride ventilationsanlæg ofte kendetegnet ved en holistisk tilgang, der integrerer bygning, bygningsdrift og ventilationsanlæg. Det betyder, at i den første idéfase er ventilationssystemet, bygningskroppen og bygningens drift alle en del af en integreret designproces med tre mål: bedre indeklima, lavere energiforbrug og arkitektur. Dette har ført til en voksende bevidsthed om, at for at opnå lavenergibygninger med tilfredsstillende indeklima er bygningsdesigneren nødsaget til at være klar over konsekvenserne af kritiske designbeslutninger så tidligt som muligt i processen for at få et godt cost-benefit resultat.

Ventilationsanlæg til lavenergibygninger kræver indsigt af ingeniøren/arkitekten i flere områder indenfor bygningsdesign og ventilation. En analyse af et komplekst problem som det at vælge det bedste ventilationssystem til en ny bygning har en række metodiske problemer. Analysen bør omfatte både kvantificerbare og ikke-kvantificerbare variable, nogen

korrelerede, andre måske ufuldstændig, eller med manglende eller ubestemte oplysninger grundet det tidlige stadium i konstruktionsfasen eller blot pga. variabelvurderingens indbyggede subjektivitet. Et softwareværktøj er udviklet til formålet sammen med et forslag til en metode, der på en hurtig og holistisk måde kan vurdere de forskellige systemers præstationer tilstrækkeligt nøjagtige på et tidligt stadie. Værktøjet består af en termisk model, en ventilationsmodel, som indbefatter vind og opdrift og en dagslysmodel, som sammen med solafskærmningssstyring medtager den variable termiske last fra kunstlyset.

Økonomi og konstruktionsomkostninger er undersøgt gennem fire meget forskellige kilder, som tilsammen konkluderer, at lavtryksventilation, hvad enten det er en mekanisk eller en hybrid løsning, har installationsomkostninger, der kan sammenlignes med traditionelle mekaniske ventilation.

Afhandlingen består af et udvidet resumé baseret på fem artikler indsendt til internationale, videnskabelige tidsskrifter. Resuméet fra hver artikel er refereret herunder.

Artikel I Artiklen præsenterer et enkelt bygningsimuleringsværktøj til integreret dagslys og termisk analyse. Værktøjet er i stand til at importere de termiske og visuelle egenskaber for forskellige rudetyper og solafskærmninger fra programmet Window Information System (WIS). En koblet ray-tracing og radiosity metode bruges til at beregne dagslysniveauet for forskellige himmeltyper. Både detaljeret dagslysberegning for en bestemt dag og tidspunkt samt timebaserede værdier på årsbasis kan beregnes. I en integreret simulering bliver de timebaserede dagslysværdier anvendt i en eksisterende simplificeret termisk model, som kan beregne energibehov og indeklima. Kontrolsystemer til almen og arbejdsbelysning er programmeret som sammen med en solafskærmningsstrategi justerer afskærmningen i henhold til operativ temperatur, risiko for blænding og solens profilvinkel. Modellen medtager også effekten af murindbygning, udhæng og fjerne objekter, som blokerer himmelhvælvingen. Sammenligninger med ray-tracing programmet Radiance viser, at nøjagtigheden af den beskrevne tilgang er tilstrækkelig til at forudsige energikonsekvenserne for daglysstyret belysning. Mængden af input er lille, hvilket gør værktøjet nyttigt til integreret dagslysoptimering i den tidlige design proces.

Artikel II Et centralt element i bæredygtige ventilationsanlæg er varmegenvindingssystemet. Konventionelle varmegenvindingssystemer har et højt trykfald, der fungerer som en effektiv blokering for naturligt drevne luftstrømme. Det varmegenvindingssystem som foreslås her består af to adskilte luft-til-væske varmevekslere indbyrdes forbundet med et væskekredsløb drevet af en pumpe. Konceptet er ideelt som genvindingssystem til passive ventilationssystemer. Artiklen beskriver den analytiske ramme samt eksperimentelle udvikling af en varmeveksler i væskekredsløbet. Vekslerindmaden består af 8 mm plastslanger, der er almindeligt anvendt i vandbaserede gulvvarme-systemer. Tryktabet og genvindingseffektiviteten blev målt. For en ønsket volumenstrøm på 560 L/s blev tryktabet målt til 0,37 Pa og effektiviteten var 75,6%. De eksperimentelle resultater stemmer godt med litteraturkilder eller numeriske fluidberegninger. Analytisk set var den samlede varmegenvinding af to væske-koblede varmevekslere beregnet til at være i størrelsesordenen 64,4 til 74,9% afhængig af varmetabet i forsøgsopstillingen. Det samlede trykfald i varmegenvindingssystem er

0,74 Pa. Desuden viser foreløbige bergninger at en fremtidig samlet virkningsgrad på 80% med et trykfald på blot 1,2 Pa er mulig.

Artikel III Artiklen rapporterer eksperimentelle og numeriske analyser af et diffust loftsventilationskoncept. Analyserne blev udført med to forskellige porøse loftsflader monteret i et nedhængningssystem: perforerede plader af aluminium og gips. Forsøgene blev udført i et klimakammer, og simuleringerne blev udført med CFD. Forsøgene dokumenterede et effektivt luftskifte svarende til fuld opblanding med et trykfald på 0,5 Pa uden tegn på termisk diskomfort. Desuden dokumenterede målingerne, at loftet virker som en køleflade, som øger mulighederne og anvendeligheden af konceptet. De numeriske analyser benyttede en tilnærmet metode til at modellere forvarmningen i loftet og generelt støttede de målingerne, men de viste også risiko for kuldenedfald især i områder, hvor termisk opdrift ikke modvirker den kølige indblæsningsluft.

Artikel IV Hybride ventilationssystemer er udviklet til at udnytte fordelene ved både naturlig ventilation og mekanisk ventilation. Hybridsystemer er typisk two-mode med to fuldt autonome ventilationssystemer eller mixed-mode, hvor en ventilator assisterer det naturlige drivtryk. Her præsenteres et one-mode system karakteriseret ved balanceret mekanisk ventilation med væsentlig bistand fra opdrift og vind. State-of-the-art bygningsimuleringsprogrammmet ESP-r blev anvendt til at simulere varme og luftstrømme i en fiktiv bygning, og indeklima og energiforbrug blev kvantificeret. Ventilationssystemet anvender varmegenvinding med en nyudviklet varmeveksler (Paper II), filtrering med et aktivt elektrostatisk filter og distribuerer luften ved hjælp af diffus loftsventilation (Paper III). Konventionelle spjæld kontrollerer luftstrømmen, og frikøling med natteluft sker gennem de eksisterende kanaler. Tryktabet er 5 Pa, og det specifikke elforbrug (SEL), der almindeligvis bruges til at sammenligne den energimæssige ydeevne af forskellige ventilationssystemer, er beregnet til 155 J/m^3, herunder indgår strømforbrug til det elektrostatiske filter. SEL-værdien er ca. 6% af den nuværende øvre grænse for VAV-systemer i det danske bygningsreglement. Det samlede primære energiforbrug i bygningen er $18,9\,kWh/m^2$, hvilket gør ventilationskonceptet egnet til en fremtidig near-zero energiklasse.

Artikel V Udvælgelsen af et ventilationssystem i en ny bygning er et flerdimensionalt komplekst problem, der involverer både kvantificerbare og ikke-kvantificerbare data, f.eks energiforbrug, indeklima, integrering i byggeri og arkitektonisk udtryk. Denne artikel præsenterer en struktureret metode til vurdering af et ventilationssystem i designprocessen ved at behandle kvantificerbare og ikke-kvantificerbare datasæt sammen. Metoden er baseret på generel morfologisk analyse og anvender cross-consistency assessment til reduktion af problemkomplekset. Således behandles meget komplicerede og flerdimensionale usikkerheder samt den subjektivitet, der opstår i designprocessen på et forsvarligt metodologiske grundlag. Ved hjælp af en afstandsanalyse af de simulerede scenarier kan de visualiseres i forhold til hinanden, hvilket giver designeren et illustreret 'løsningsrum'. Heri kan designeren se flere ventilationsløsninger og navigere mellem dem, evaluere forskelle og udvælge det bedste ventilationssystem i form af energiforbrug, indeklima og arkitektonisk kvalitet.

Table of Contents

Chapter 1

Aim and objective

The main aim of this thesis is to produce low-energy buildings at a low cost. Focus is on ventilation because fan energy consumption constitutes a major part of the total energy consumption in modern buildings.

The objective is to develop the concept and components for future ventilation of buildings. A parallel objective is to develop the holistic tools that, prior to the design phase, enable the ventilation engineer to select the ventilation system that performs best, thereby obtaining a good final whole-building cost-benefit ratio.

Chapter 2

Introduction

Building developers and designers are constantly straining to produce end-user buildings with low energy consumption and high indoor environmental performance. Reducing energy consumption while improving the indoor environment is, however, today two opposing aspects. This has led to an increased focus on solutions to reduce the building energy consumption.

In low-energy buildings the energy consumption is dominated by power consumption. Power is used for ventilation, artificial lighting, pumps and sometimes heating and domestic hot water. Power is expensive to produce in terms of investment, fossil-fuelled power plants or wind turbines alike, and in terms of CO_2. Therefore, savings of power with comfort preservation is sensible.

Conventional ventilation technologies are constantly improving energy-wise and efficiency-wise, yet it is not possible to meet tomorrow's demand of better indoor climate while cutting energy consumption as demanded by the risk of global warming. While the solution to save artificial lighting is to improve daylighting through proper facade design, the solution for ventilation is to shift the ventilation use from active (mechanical) to passive ventilation (Aggerholm et al., 2008). Passive in this context means ventilation solutions that exploit natural driving forces, fully or in part, and the building physics to establish and maintain a satisfying indoor climate without the consumption of electrical energy. Passive ventilation has particular potential in temperate climates where high wind speeds and large daily temperature differences prevail. However, passive systems suffer from a lack of components and concepts that can render them competitive with conventional mechanical solutions in terms of thermal comfort and heat loss.

This thesis constitutes the work of three and a half year study developing components and a concept for ventilation with ultra-low energy consumption. An important point of reference for the study was to develop solutions that are implementable in practise for the concept to be accepted and used by practitioners. This is achieved by comprehensive investigation and documentation in three articles submitted to international, scientific journals. A fourth, submitted article is dedicated to obtain the best performance of passive ventilation systems which is often characterized by solutions that integrate the building, the building operation and the ventilation system in a holistic manner. A fifth, published article expands the meaning of truly holistic by including the effect of daylight, shading and thermal load from artificial lighting into the simulation model. Thus the framework

for power-savings is put into place.

The thesis comprises five articles, an extended summary with literature review, a chapter on the installation costs of passive ventilation and a general conclusion. The frame for this thesis constitutes work within the following specific research topics:

- one-mode hybrid ventilation
- diffuse ceiling ventilation
- heat transfer with liquid-coupled tube banks
- yearly daylight simulations
- design via morphological analysis

2.1 Background

The European building sector is responsible for about 40% of the total primary energy consumption. To promote cost-effective improvement of the overall energy performance of buildings, the European Union launched in 2002 the Energy Performance of Buildings Directive (EPBD 2002/91/EC) (EPBD, 2010). One of the key issues of the directive is set a holistic approach on energy performance of buildings that covers the energy needs for space and hot water heating, cooling and lighting. Another key issue is the revision of requirements every five years. In the Danish context, the revisions are set to reduce the 2006 level in two steps with 25% in 2010 and 50% in 2015 denoted low-energy class 2 and low-energy class 1. In addition to this, the Danish Council of Ministers has in December 2009 initiated considerations on a near-zero energy class by 2020. The magnitude of reduction is unknown — earlier principle decisions mention 25% of present consumption (equal to 24 kWh/m^2) — but the technical progress of the building sector has major influence on the reduction level. Therefore, it is important to show feasible technical solutions that can comply with the requirements of 2020.

In the socioeconomic sense reductions in energy consumption are considered as being reasonable. Furthermore, productivity is increased by improving the indoor environment. Several investigations document the effect of indoor climate on the performance of office workers (Seppänen et al., 2006). The same conclusion can be drawn from studies on school children exposed to higher ventilation rates and better thermal comfort (Wargocki et al., 2007b,a). Other investigations show that the productivity increase of an improved ventilation system with higher air change and better temperature control is significantly larger than the total costs of the ventilation system (Wargocki and Djukanovic, 2005). A good indoor climate in large buildings is ensured in practice today by installation of mechanical ventilation with cooling. Based on the current knowledge and ventilation practice it is difficult to improve indoor air quality without increasing energy consumption for installations excessively. Further improvements in the ventilation system performance therefore call on a paradigm shift in ventilation technique.

Power consumption in new buildings due to ventilation and lighting constitutes a major part of the total energy consumption. Conventional mechanical ventilation solutions

Table 2.1: Typical properties of different ventilation schemes.

	Natural	Mechanical	Passive
Heat recovery	☹	☺	☺
Fan power	☺	☹	☺
Free cooling	☺	☹	☺
Airflow control	☹	☺	☺
Thermal comfort	☹	☺	☺

are usually based on costly plant installations, space-consuming duct penetrations and energy consuming fans. Generally, installations are not integrated in the building at an early stage in the design process, because it historically has been customary to divide the design of buildings in segregated activities each related to the construction side or the installation side. By considering the ventilation as an installation separated from the rest of the building the interaction with the building is ignored.

Natural ventilation solutions require a different approach to building design. The ventilation scheme makes active use of the building rooms to supply and extract air and in general the ventilation design and building design are not segregated activities. Rather the design of natural ventilation requires the gap between architecture and function to be bridged. However, supplying fresh air through openings in the facade close to the occupied zone causes draught and complaints especially during the winter season (Larsen et al., 2006).

Table 2.1 illustrates some current, typical properties of natural and mechanical ventilation schemes. Natural ventilation suffers from heat loss and comfort risks while mechanical ventilation excel in theses areas but at the price of high power consumption. The hybrid ventilation approach is to combine the advantages of both systems to achieve mechanical control, thermal comfort and heat recovery with low power consumption.

Most hybrid systems are two-mode or mixed-mode. Two-mode schemes require two fully autonomous installations of a natural and a mechanical system, and mixed-mode systems operate by natural stack ventilation and a helping fan. The former requires an inordinate investment and the operation is challenging during transitional seasons, and the latter suffers from draught and/or lack of heat recovery.

In the future, when near-zero energy consumption and improved indoor environment are essential demands, two-mode and mixed-modes systems perform inadequately. Consequently, the one-mode system should be developed further with components developed specifically for this type of system to provide the airflow control, the thermal comfort and the heat recovery of mechanical systems and the power consumption and the free cooling of natural systems. Furthermore, through greater integration with the building, the physics can be exploited for passive air-conditioning without consumption of power, but still with a heating, alternatively cooling function. A ventilation system that air-conditions passively, that provides comfort ventilation with very little fan power and night ventilation by natural means, that has limited heat loss, and that does not suffer from inadequate indoor environment, that is a 'building integrated passive ventilation system'.

2.2 Ventilation running costs

Earlier it was stated that the energy for ventilation contributes substantially to the total energy demand. To illustrate this Figure 2.1 shows the hourly relations of external temperature and the cost due to heating demand and air transport for three types of ventilation. The mechanical systems have an SFP-value of 2100 and 100 J/m^3, respectively. The data has been generated with the simplified, yet dynamic building simulation program iDbuild which has been developed at the Technical University of Denmark (Petersen and Svendsen, 2010; Nielsen, 2005) and (Paper I). The input was an open plan office space in indoor climate class 2 (EN15251, 2007) with a heat load of 10 W/m^2 and double-layer glazing covering 40% of the facade. Furthermore we use weather forecast-based setpoint prediction to maximize the efficiency of the night cooling without compromising the level of comfort. We assume that the natural system is able to provide sufficient comfort and night ventilation at all times.

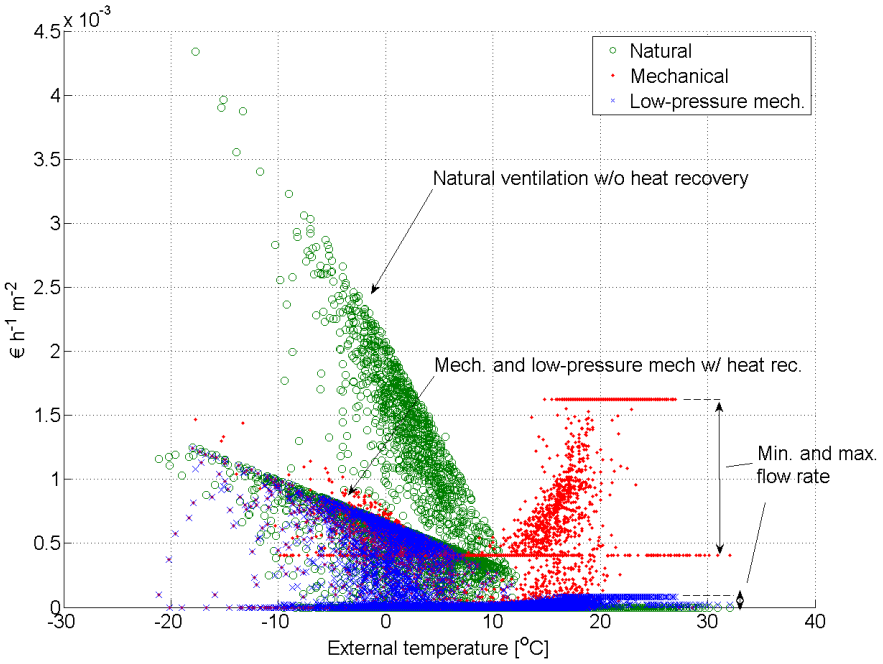

Figure 2.1: Running costs of natural, mechanical ventilation and low pressure mechanical ventilation.

The figure shows that for low temperatures conventional mechanical and low-pressure mechanical systems are more cost-effective than natural systems. For external temperatures above approx. 14 °C removal of excessive heat gains by conventional mechanical ventilation is less cost-effective due to the high price of air transport. Figure 2.1 also reflects the CO_2-emissions of the different systems because the ratio between natural gas and electricity production is the same for heating price and electricity price.

Chapter 3

State-of-the-art

3.1 Hybrid ventilation

The research in ventilation of buildings is vast. A recent textbook on ventilation systems design is by (Awbi, 2008). Another recent textbook on the aspects of indoor climate and ventilation energy efficiency is by (Nilsson, 2003). In the framework of the International Energy Agency, several research project annexes were on ventilation design. In recent years the Annex 35 (Delsante and Vik, 2002) has been committed to develop and explore various mixed approaches of naturally and mechanically driven ventilation. Historically natural and mechanical ventilation developed separately towards minimal energy use and comfortable indoor environment. The annex was started in recognition by experts that the ventilation must provide indoor air quality *and* passive cooling and that this dual task reaches beyond the limit of fully natural or fully mechanical systems (de Gids, 2001; Heiselberg, 2002; Aggerholm et al., 2008). Lately the ongoing Annex 44 was started in 2004 to investigate the influence of building responsive elements and as a consequence of this, building integrated ventilation.

The motivation for hybrid ventilation is access to both ventilation modes and therefore the advantages of both systems while eliminating some disadvantages of both systems. Basically three categories covers the hybrid approach (Heiselberg, 2002):

- Two-mode system of natural and mechanical ventilation
- Mixed mode system of fan-assisted natural ventilation
- One mode system of stack- and wind-assisted mechanical ventilation

The first category provides fresh air by two fully autonomous ventilation systems where the active system typically is mechanical when heat recovery is needed and natural when night cooling is used. Apart from that any of the two systems may be active depending on time, building and season. The second category is a mixed mode system where the ventilation primarily is driven by natural ventilation but in periods of insufficient natural driving pressure or the need for heat recovery an assisting fan is switched on. The third category does not fully comply with the hybrid definition of a two-mode system and is in reality a low-pressure balanced mechanical ventilation system. Due to the low pressure drop, pressure rise from stack and wind aids in driving the air flow. This difference from

conventional ventilation that fully relies on mechanical pressurization to work, however, justifies the hybrid label. The distinction between the second and third category is vague and indeed different sources are observed enlisting the same project in both categories (Heiselberg, 2002; Wouters et al., 1999; Tjelflaat, 2000).

Annex 35 was committed to develop and explore various hybrid approaches, but only a few detailed simulations on energy performance are reported (Seifert et al., 2001; Heikkinen et al., 2002; Jeong and Haghighat, 2002). By detailed we mean simulations on a macroscopic level with a combined thermal and airflow model that includes heating and electricity consumption, indoor air quality and thermal comfort. Indeed combined thermal and airflow simulation is a powerful tool for whole-year analysis of hybrid ventilation buildings (Heiselberg, 2002) and is also reported to show good accuracy with measurements (Meinhold and Rösler, 2002; Wachenfeldt, 2003). In one Finnish study simulated in IDA ICE (Equa, 2010) a fan-assisted natural ventilation system of a five-storey building is found to consume 15% less energy compared to a mechanical VAV system and 73% less fan energy (Heikkinen et al., 2002). The annual primary energy consumption is 92 $\mathrm{kWh/m^2}$ when electricity is multiplied with 2.5.

While the estimated pressure drop in the Finnish study is < 100 Pa in bypassed mode and < 500 Pa otherwise, a Norwegian state-of-the-art implementation reaches a measured total of approx. 100 Pa (Tjelflaat, 2000). The Mediå School in Grong, Norway is considered a successful practical implementation of a balanced mechanical ventilation system with substantial assistance from stack and wind (Schild, 2001). The ventilation system has central intake through an underground culvert that dampens the seasonal fluctuations of the outdoor temperature and central exhaust through a stack-enhancing wind tower. Heat is recovered by liquid-coupled heat exchangers and filtering is partly done through settlement of particles in the culvert, partly in a EU7 filter. The primary energy consumption is measured to 107 $\mathrm{kWh/m^2}$. A combined thermal and airflow simulation of the school was performed using ESP-r (Jeong and Haghighat, 2002; ESRU, 2008), but the model was cursory and the simulation period limited.

3.2 Heat recovery

One of the conclusions of Annex 35 was that there is a general lack of components for hybrid ventilation systems. Most often this leads to the installation of two-mode hybrid systems with components specific for natural ventilation and components specific for mechanical ventilation.

In a passive system with no or very little fan power consumption, the energy reduction can be eliminated by the lack of heat recovery. An early attempt in the field of heat recovery for passive or natural ventilation solutions was based on a vertical counter-flow air-to-air heat exchanger and achieved a heat recovery efficiency of 40% (Schultz, 1994). Another concept used a system of stack chimneys. Passive heat pipes were interjected into the chimneys and experiments showed a heat recovery efficiency close to 43% with a total pressure loss of 1 Pa (Shao et al., 1998). However, both attempts suffered from the inherited flow obstruction that arises when the induced flow direction is counteracted by the local buoyancy forces in the heat exchanger or heat pipes. They also lacked control of the airflow and had little flexibility in the building design.

A different concept with two air-to-liquid heat exchangers in the supply air and in the exhaust air, and connected with a pump-powered liquid loop was found to have an efficiency of 43% at a total pressure loss of 1 Pa (Overgaard et al., 2002). This approach had many advantages in that the building integration was more flexible, the supply and exhaust airflows did not have to meet, and the buoyancy forces in the exchangers were fully exploited. But the total heat recovery efficiency of the system was somewhat less than the Danish Building Code requirement of 65% heat recovery for mechanical ventilation (EBST, 2010). Paper II presents a heat recovery concept that has been developed specifically for innovative passive ventilation systems with heat recovery and night cooling suitable for temperate climates. The concept that is presented is a newly developed heat exchanger with properties designed for passive ventilation. These include very low pressure loss (< 1 Pa) and high efficiency ($\approx 70\%$). If the concept is integrated as a core element at the earliest stages of building design, it takes no more office space than conventional mechanical ventilation systems.

3.3 Diffuse ceiling ventilation

The conventional mixing principle supplies air from one or multiple diffusers. The diffusers are placed outside the occupant zone, and mixing is induced by a high impulse air stream that acts through entrainment of the room air. Numerous mixing diffusers has been tested and reported in the literature (Lee et al., 2007). The displacement principle exploits the thermal load in the room and the associated buoyancy effects to create stratification that replaces the contaminated air with fresh air.

Mixing ventilation is generally often the better choice in single offices where the heat load is limited, while displacement has proven superior in rooms with high occupant density and high thermal load, e.g. conference rooms and classrooms (Skistad et al., 2002). To avoid draught both principles require optimization and accurate operating control of two basic design parameters: inlet temperature and supply air velocity. The former parameter is achieved through the installation of heating and cooling coils which induce high pressure drops in the ventilation system. The latter parameter is achieved through fan-powered pressurization and dampers.

An alternative ventilation concept of supplying fresh air is through perforations in the ceiling. The concept is known as diffuse ceiling ventilation and is characterized by air being supplied over a very large surface area occupying a substantial part of the ceiling. The inlet velocity is very small and with no fixed jet direction, hence the term diffuse. In comparison with mixing air terminals, diffuse ceiling ventilation only requires very low pressurization. Paper III documents good ventilation performance for pressure drops down to 0.5 Pa which makes it a suitable concept for passive ventilation. Furthermore, the contact with the upper concrete deck allows for more exposed thermal mass and therefore more pre-conditioning of the supply air. This effect, however, is not investigated in detail.

One, and quite common, application is in livestock buildings where diffuse ceiling ventilation is a cheap method of providing fresh air to the animals (Jacobsen, 2008). Because of the non-impulse supply from the ceiling area the mixing is dependent on the buoyant forces present from the thermal loads. The advantage is that the system does not produce draught by itself.

Application of the diffuse ceiling concept to indoor spaces occupied by humans is known in practise, but the research is limited and early results are very few (Klimatechnik, 1986). A recent work included laboratory experiments and numerical analysis (Jakubowska, 2007) of a two-persons office. The experiments included measurements of local air velocities and temperatures for draught ratings and investigated the ventilation effectiveness with tracer-gas. The diffuse ceiling was made from 30 mm acoustic mineral fibre with a painted surface and the suspension system was an upside-down T. The painted low-permeable surface caused most of the inlet air to penetrate through cracks between tiles and suspension. The overall conclusion was very beneficial for the diffuse ceiling. Compared to other means of air supply the diffuse inlet exhibited superior performance in terms of possible concurrent flow rate and low inlet temperature without causing draught in the comfort zone (Nielsen and Jakubowska, 2009). Similar findings was reported by Jacobs et.al. (Jacobs et al., 2008) in a study of a classroom with two different types of perforations.

3.4 Integrated design tool

The design of ventilation systems for low-energy offices requires insight of the engineer/architect into multiple fields of building design and ventilation. Integrated design process is a holistic method that facilitates the design of buildings in the initial design phase. By use of a simplified calculation model the number of input is minimized and computational time is reduced (drastically), so that an appropriate solution space can be established at an early stage in the design process, thereby maximizing the synergies of building integration. Synergies will make it possible to reduce or eliminate the need for fans, ducts and conditioning units while meeting increased requirements for both indoor climate and energy consumption in an economically feasible way.

3.4.1 Coupled thermal, daylight, and ventilation model

For a truly holistic model designed to minimize heating *and* power consumption, integrated simulation of daylighting and artificial lighting plays a significant role on energy consumption, indoor environment and environmental impact as the fenestration system influences heat loss, solar gains and daylight penetration (Lee et al., 1998; Jenkins and Newborough, 2007; Tzempelikos and Athienitis, 2007).

Sparked by innovations in dynamic fenestration and shading systems and increasingly sophisticated characterizations of glazings and shading devices (van Dijk and Oversloot, 2003; Andersen and de Boer, 2006; Huizenga et al., 2007) some detailed simulation programs like ESP-r (ESRU, 2008), and EnergyPlus (Crawley et al., 2002) now link daylight and thermal simulation in an integrated manner (Clarke and Janak, 1998; Crawley et al., 2002). However to run these programs they require expert knowledge and large amounts of input data for even the simplest simulation, rendering them impractical in the early design stage when information is scarce. This calls for tools that are capable of rapid and dynamic calculation of the impact of fenestration and shading provisions on lighting demand, cooling demand and occupant glare.

Such rapid whole-year algorithms are starting to emerge (Lehar and Glicksman, 2007; Walkenhorst et al., 2002), but they still lack interactivity with the thermal domain.

Franzetti et al. (2004) implemented a daylighting software module with a thermal model, but the validity of the model was restricted to internal working plane illuminances below 1000 lux. Athienitis and Tzempelikos (2002) developed an integrated model based on clear and overcast sky formulations for external illuminances and radiosity for internal illuminances. This approach, however, assumes that direct light is diffused in the shading devices and that incident diffuse light on the outside of the window is transmitted uniformly. An existing simplified thermal simulation tool BuildingCalc (Nielsen, 2005) and a daylight simulation tool LightCalc (Nielsen et al., 2005) formed the starting point for the work, the BC/LC tool. To further enhance the applicability of the design tool in ventilation solutions design and to enable the advisory engineers to make an intelligent choice regarding the materials and design, the ideal ventilation model in the tool was supplemented with stack and wind effects.

3.4.2 Morphological analysis

Other pre-design tools that employ a holistic approach are developed by Massachusetts Institute of Technology (MIT, 2010) and by Lawrence Berkeley National Lab (LBNL, 2010). Both tools are based on arbitrary scenario generation and thus neglects the method to produce energy-efficient scenarios. Rather, the methodology is trial and error, i.e. no methodology. In the IEA Annex 35 a simple method was developed that enables the building designer to determine the feasibility of natural or hybrid ventilation systems in a given building based on the site and permeability of the building envelope (Fracastoro et al., 2002). An even simpler design guide chart was meant to quantify the probability of success for natural, hybrid and mechanical systems (Heiselberg, 2002).

None of these methods provide the advisory engineer with the appropriate 'space of solutions'. Instead of freeing the design engineer to explore all feasible solutions, the existing tools are based on conventional solutions that set constraints and boundaries on the feasible solutions. This may be perfectly alright in a practical design situation where the shear number of arbitrary solutions must be limited.

This contribution proposes to use morphological analysis to decompose and structure the problem complex into both objective (technical) and subjective (psychological) variables while treating incomplete information in a structured manner. One of the advantages of morphological analysis is that such combinations are valid. General morphological analysis was developed by Fritz Zwicky (Zwicky, 1969) and has been used for many purposes in relation with buildings e.g. for integral design methods or to improve the comfort of various ventilation concepts (Quanjel et al., 2006; Zeiler et al., 2006). Coupling morphological analysis with cross-consistency assessment (CCA) (Ritchey, 2006) and multidimensional scaling (MDS) (Cox and Cox, 2001) enables the engineer to establish the feasible 'space of solutions' for various ventilation schemes within various building envelopes. This process is time-consuming, but it can be automated if it is implemented in a dynamic building simulation program. For this purpose a transparent building simulation application developed at the Technical University of Denmark is useful (Nielsen, 2005; Petersen and Svendsen, 2010) and (Paper I). The application works on room level to facilitate the design of the building to maximize the indoor climate and minimize the energy consumption at the pre-design stage where changes are cost-free. Here we explain

a method by which the software application can be expanded specifically in terms of it's ventilation design capabilities but the morphological approach with multidimensional scaling can also with relative little effort be implemented generally in the program.

Chapter 4

Components

The development of a passive ventilation concept requires the development of different sub-concepts that again require the development of components. This chapter summarizes three sub-concepts that are suitable for low-pressure ventilation systems. In the following two are described in more detail and a third is discussed. They are:

Heat recovery with ultra-low pressure loss and efficient recovery (Paper II)

Diffuse ceiling ventilation as air distribution device with low pressure loss and efficient mixing (Paper III)

Filtration with embedded culvert and electrostatic precipitator

4.1 Heat recovery

The heat recovery concept is based on a well-known principle of two inter-connected air-to-liquid heat exchangers: one exchanger is placed in the inlet air and one in the outlet air, and they are inter-linked with a liquid loop powered by a pump. A schematic of the principle is depicted in Figure 4.1. Cold fresh air enters the heat exchanger in the inlet, heat is transferred from the hot liquid to the colder air resulting in a temperature rise in the supply air. The now cooled liquid is pumped to the heat exchanger in the outlet where it is heated by the hot exhaust air leaving the building. The warm liquid returns to the inlet heat exchanger and the cycle is repeated continuously.

The main advantage of the liquid-coupled heat exchanger principle is the flexible placing of inlet and outlet in the ventilation system because the airstreams are not required to meet. This flexibility is particularly advantageous for ventilation systems partly or purely driven by stack effect and wind pressures instead of mechanical means such as fans. The approach allows for optimum placement of the heat exchangers in the building to exploit the natural driving pressure differences fully.

The heat exchanger is of an approximate counter-flow type which have the highest efficiency potential. The counter-flow type is based on a heat exchange process where a hot and a cold fluid enter the heat exchanger from opposite ends; the cold fluid is warmed and the hot fluid is cooled. Because the hot input is at its maximum temperature, it can

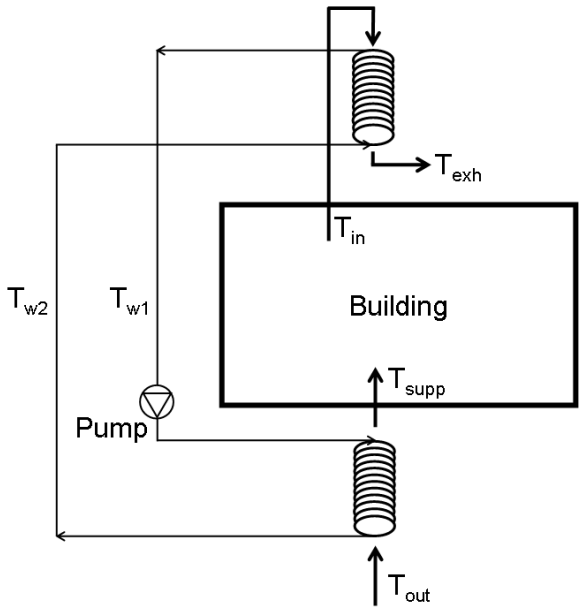

Figure 4.1: Schematic of the heat recovery concept.

warm the exiting hot fluid to near its own temperature. In parallel the cold input can cool the exiting cold fluid to near its own (low) temperature; in other words, the fluids 'swap' temperatures. To maintain an effective heat transfer the wall material between the fluids must have negligible heat transfer resistance compared to the surface resistances and the capacity flow of the fluids must be equal. To keep the exchanger simple and with low material costs, round PE plastic tubing is used which are commonly used for water-based floor-heating systems. Oval or even wing shaped tubes have better heat transfer and lower drag coefficient (Horvat et al., 2006), but round tubes require less meticulous production procedures. The tubing used here is mass-produced, cheap, flexible and requires no fittings as it is produced in a continuous cycle and shipped on large cable drums.

In Figure 4.2 two parallel tubes criss-cross the airflow. The choice of two parallel tubes was governed by the possible bend radius of a single tube, where two neighbouring single bends would overlap at both ends. With two parallel tubes there is space for both tube bends at both ends. This is a compromise between the concept of counterflow and practical implementation. When the tubes are locked into the brackets that forms a radiator, multiple radiators can be combined with an inter-longitudinal offset between adjacent radiators. Thus putting multiple radiators together makes the exchanger fully scalable.

4.1.1 Results

Figure 4.3 shows the measured pressure drop characteristic on the air side of the exchanger. Figure 4.4 compares the measured pressure drop with two literature sources and the numerical fluid calculation performed in Comsol (Comsol, 2010). It is clear that the literature sources overestimate the pressure drop across the tube banks when compared to the measured data. Particularly the model by Khan et al. (2006) which was used in

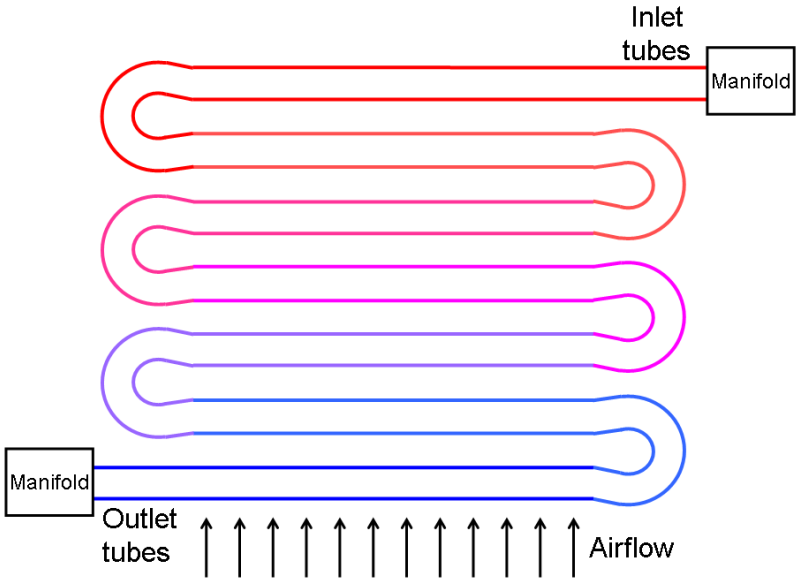

Figure 4.2: Layout of two parallel tubes in a radiator in crossflow.

the design phase of the exchanger overestimates the pressure drop by more than a factor of 4. The model is based on experimental data fitting but does not quantify the fitting error. The model by Zhukauskas (1972) is valid for $Re > 10$ and shows marginally better agreement but it also overestimates the pressure drop. The numerical fluid calculation predicts the pressure drop well in most of the calculation range. The bar plot illustrates the relative error which is in the range of 3–30% with the larger error in the smaller pressure drops.

The total system temperature exchange efficiency when two exchangers are employed is illustrated in Figure 4.5, where the design airflow yields an efficiency between 64.4–74.9% depending on the source. However, if we use the Nusselt numbers from Beale (1997) and Colburn (1964) the interval is 67.5–71.0%, also well within the measured and the corrected values and very close to the initial design value of 70%. The corrected values are a result of an estimate of the parasitic heat loss from the test exchanger.

Further details on the test methods and an in-depth discussion of the test results are found in Paper III. The paper also quantifies the pressure loss on the water side and suggests some preliminary improvements. The heat exchanger has been subjected to indoor experiments under controlled ambient conditions and has not yet been subjected to realistic operation conditions in a building where fluctuating ventilation flow and unexpected parasitic heat losses may exist. However, in a parallel project a prototype of the heat exchanger has been developed and constructed (Paper IV shows a photo), and work has been initiated to test the exchangers in a real building under real conditions.

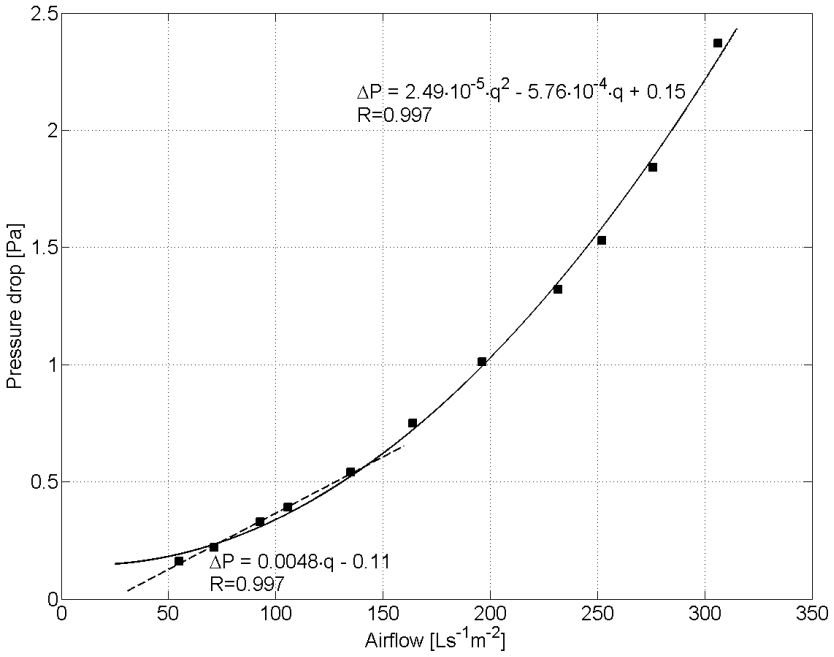

Figure 4.3: Pressure drop characteristic of tube bank. Below an airflow rate of 150 $\mathrm{Ls^{-1}m^{-2}}$ the characteristic corresponds closely to a linear relationship.

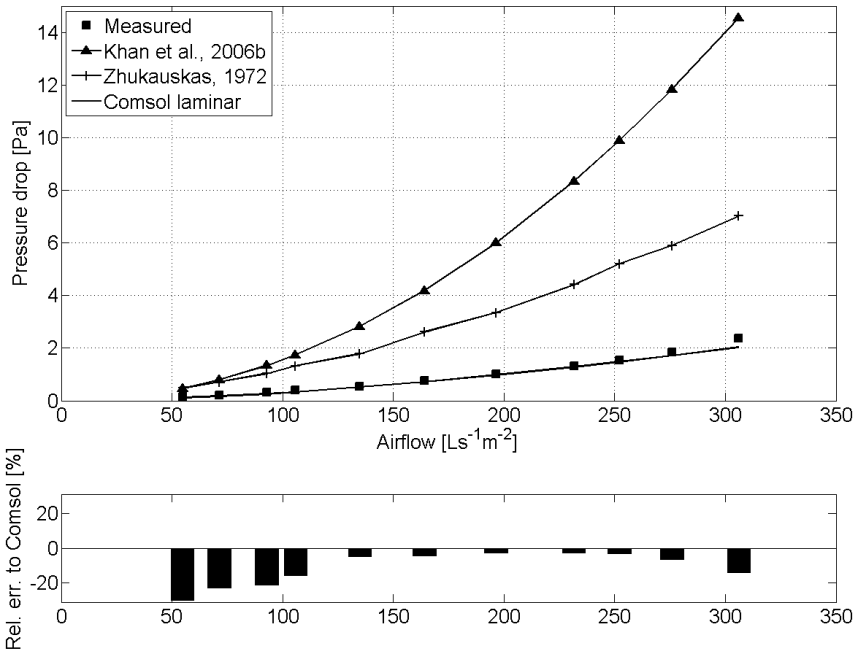

Figure 4.4: Comparison of measured pressure drop with the literature and Comsol. The bar plot denotes the relative error between measurements and the Comsol-derived pressure drops.

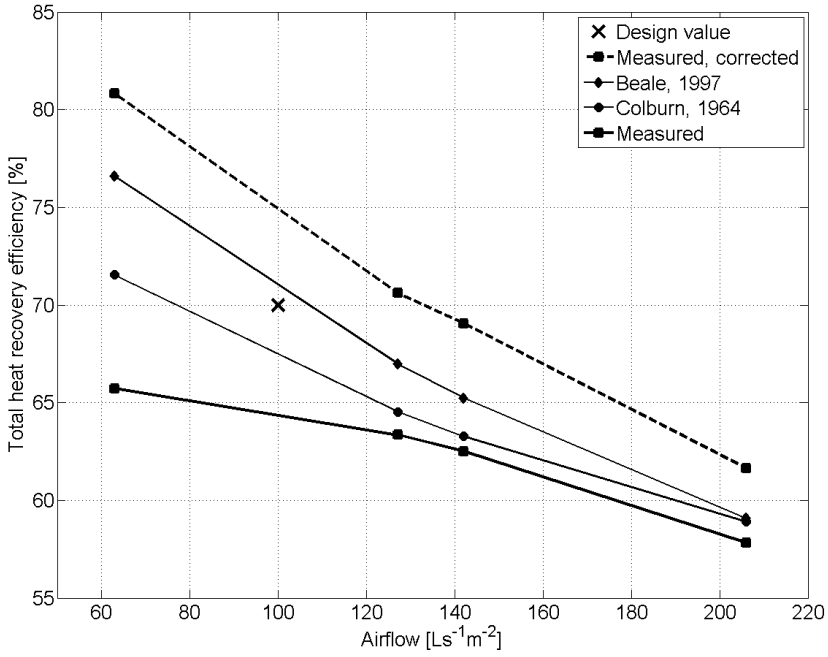

Figure 4.5: Total heat recovery efficiency. Comparison of measured and corrected values with the literature.

4.2 Diffuse ceiling ventilation

In a conventional mechanical ventilation system fresh air is supplied to the room through mixing or displacement diffusers. The diffusers act through a pressure drop that is too large for non-conventional systems. In recent years a new concept where fresh air is supplied through perforations in the acoustic suspended ceiling has been investigated (Jakubowska, 2007; Jacobs et al., 2008; Nielsen and Jakubowska, 2009; Nielsen et al., 2010). The concept is known as diffuse ceiling ventilation or vertical ventilation and is characterized by air being supplied over a very large surface area occupying a substantial part of the ceiling. The inlet velocity is very small and with no fixed jet direction, hence the term diffuse. The plenum space above the acoustic ceiling is used as a pressure chamber reducing ductwork and diffusers.

Diffuse ceiling ventilation does not mix or displace the room air by itself. Rather it depends on the buoyant forces in the room to mix the air. Jacobsen et al. (2004) showed how the location of the heat sources governs the prevailing air flow pattern in livestock buildings with diffuse ceiling ventilation. The thermal plume is the strongest current in the enclosure, and it acts by deflecting the downward cool air current from the ceiling. Thus the ventilation pattern takes the form of room size vortices that act through a mixture of displacement and mixing.

In the study reported in Paper III the properties of the suspended acoustic ceiling is exploited to provide ventilation through perforations in the ceiling tiles. Two types of suspended ceilings with two types of tiles are assessed in terms of thermal comfort, air change efficiency and pressure drop. One tile is a perforated aluminium sheet, and another

is a perforated gypsum board. Both tiles are commercial products and are sold as acoustic ceiling tiles. Figure 4.6 illustrates the perforation characteristics.

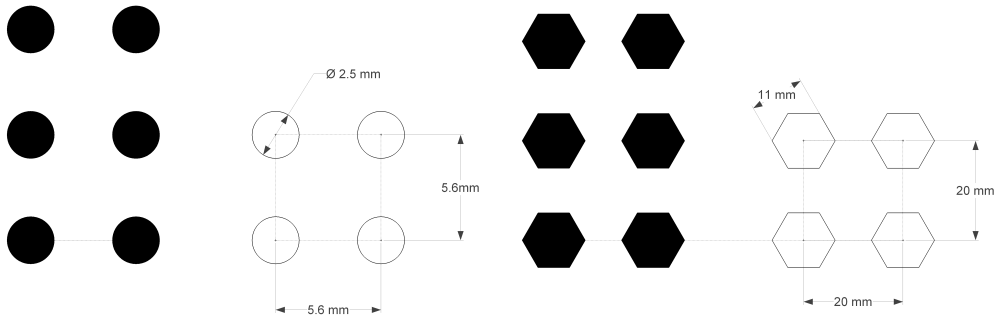

(a) Alu-16 (b) Gyp-17

Figure 4.6: Schematic of ceiling tile perforations.

4.2.1 Measured results

Figure 4.7 illustrates the pressure drop for tiles when they are mounted in the suspension system. For comparison the pressure drop of single tiles is included.

The air change efficiencies are illustrated in Figure 4.8. It shows almost perfect mixing (50%) for all test cases and ceiling types with a slight transition into displacement ventilation for high air change rates, something that could indicate increased risk of downdrafts.

Evidence of cold downdrafts are further investigated in Figure 4.9 which shows local discomfort due to draught in the occupied zone in different locations. The figure does not allow for a conclusive statement on draught risk in terms of overall air change or ceiling type, but a slight tendency towards higher ratings at ankle height may be observed. Furthermore, the two corner points 7 and 9 shows elevated readings. This could indicate downdrafts that, when they hit the floor, spill out and cause elevated readings at ankle height of the closest occupants in points 3b and 6b. It is worth noting, however, that within the occupied zone, the velocities have dropped to values that places the diffuse ventilation into category B of ISO7730 (ISO7730, 1994).

The inlet air is heated in plenum by the concrete deck and when it passes the porous ceiling. The pre-heating in the ceiling is marked in Table 4.1 with **bold**. The pre-heating potential is discussed in more detail in Paper III.

4.2.2 CFD simulations

In Figure 4.10 the temperature distribution of the numerical test cases are illustrated. Streamlines that emanate from the lower surface of the porous ceiling is plotted to illustrate the downdrafts that occur in all cases. The numerical figures illustrates well the phenomena that the thermal plumes counteract the colder supply air and push it to the nearest corner where it drops down and flows unto the floor. This downdraft is also observable, however

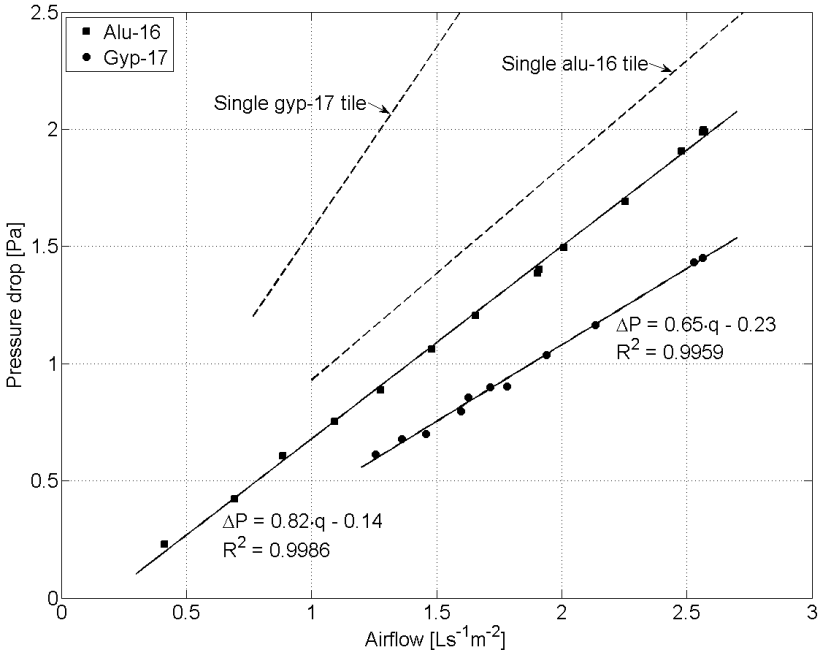

Figure 4.7: Correlation between pressure drop and airflow for two mounted suspended ceilings. Comparison with single tiles.

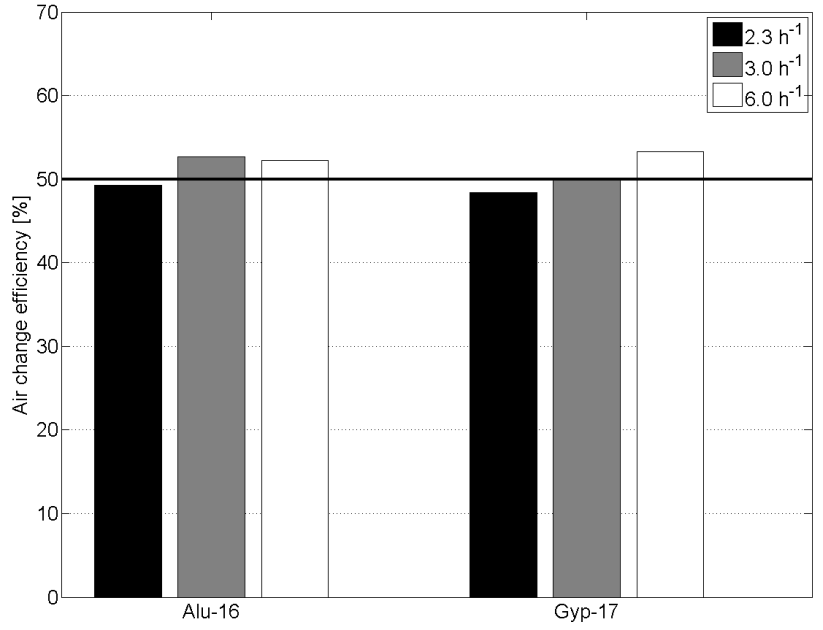

Figure 4.8: Air change efficiency.

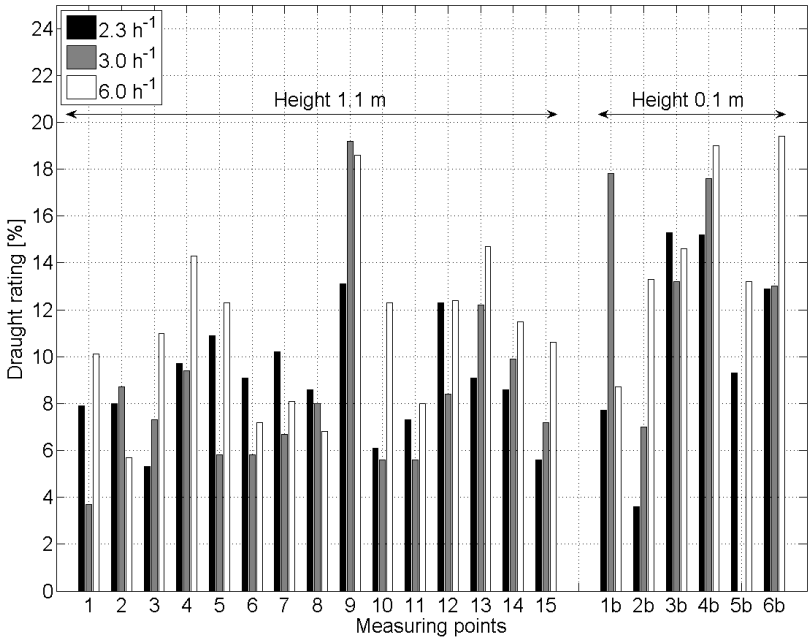

(a) Alu-16

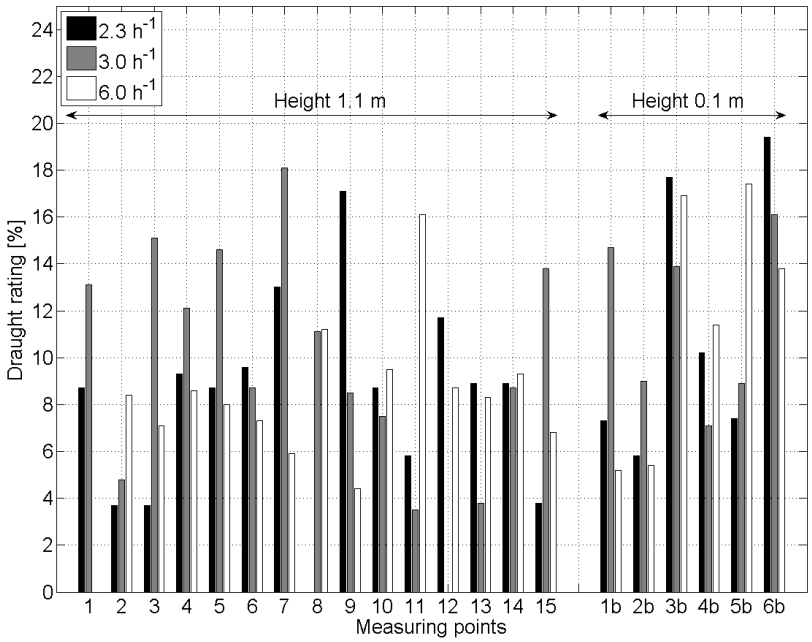

(b) Gyp-17

Figure 4.9: Draught ratings at the height of 1.1 m and 0.1 m.

Table 4.1: Measured temperatures during the experiments. The temperature of the suspended ceiling is measured on the lower side.

		Gyp-17				Alu-16			
Case	ACR h^{-1}	Inlet °C	Susp. ceil. °C	$\Delta T_{in \to ceil}$ °C	ΔT_{ceil} °C	Inlet °C	Susp. ceil. °C	$\Delta T_{in \to ceil}$ °C	ΔT_{ceil} °C
1	2.3	-3.2	15.0	18.2	**4.4**	-2.2	14.3	16.4	**5.7**
2	3.0	3.2	17.7	14.5	**3.7**	3.2	16.0	12.7	**4.7**
3	6.0	11.2	17.6	6.4	**5.2**	11.6	16.9	5.3	**4.7**

weak, in Figure 4.9(b) where draught ratings in the two corners of the inlet wall (point 7 and 9) are slightly elevated. The effect is repeated in the readings at ankle height which are also elevated.

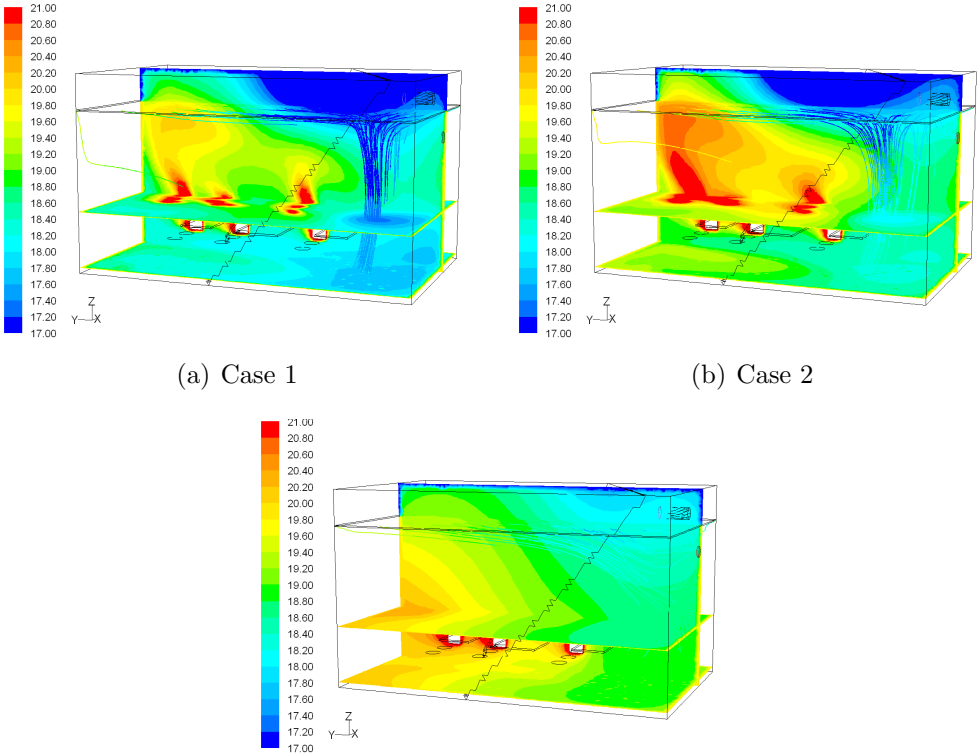

(a) Case 1

(b) Case 2

(c) Case 3

Figure 4.10: Temperature distribution for three test cases.

4.3 Filtration

Filtration has two objectives: to filter outdoor pollutants, primarily pollen and traffic soot, and to protect the inlet heat exchanger and the duct system from soiling. Filtering is conventionally done in mechanical ventilation systems by bag filters which are soiled

during ventilation operation with subsequent negative impact on the indoor air quality (Bekö et al., 2008, 2009). In this concept we employ two types of filtration, passive settlement of particulate matter in an embedded culvert and active filtration by an electrostatic precipitator. The former type is documented in one study of a 15 m long culvert where the decrease of $>0.3\,\mu$m particles is 85% and 95% for larger particles (Schild, 2001). This emphasizes the need for the duct to be passable for manual cleaning.

The latter type is an electrostatic precipitator which is an active efficient filtration devices that minimally impede the airflow through the device and easily removes fine particulate matter such as dust and smoke from the airstream. An electrostatic precipitator charges passing particles and aerosols and remove them with an electrical field and like bag filters they must be cleaned regularly to avoid depletion of the efficiency. The pressure drop of an electrostatic precipitator is a fraction of a conventional bag filter and therefore is used in some hybrid ventilation projects (Schild, 2001). The filter employed here induces 2 Pa pressure drop at the design flow speed (Terkildsen, 2009). On the down-side electrostatic precipitators are costly to buy and run, because they are power consuming. The power consumption depends on the amount of ionized particles and the ionization level of each particle. Therefore, it is difficult to accurately quantify the power consumption of an electrostatic precipitator, especially in a relatively particle free environment after a long culvert. Only vague sources are available stating a power consumption of 75 W for a flow rate of 1700 m^3/h (Terkildsen, 2009). An in-depth investigation of the aspects of filtration efficiency, pressure drop, fan power and filter power is beyond the scope of this thesis. In general the power consumption of the filter is added to the total energy consumption as well as to the reported specific fan power of the ventilation system.

4.4 Conclusion

The dual-sided issue of indoor environment and energy consumption have become increasingly important in building design. One possible solution is to ventilate by passive means, such as stack effect and wind pressure, but this requires the development of new concepts and components. The components investigated in this chapter are all developed with the primary objective of providing low-pressure loss alternatives to conventional solutions. To be competitive, the secondary objectives have been high efficiency and low total cost. The outline of a heat recovery concept is presented. The concept is suitable for passive ventilation systems where the available driving pressure is well below 10 Pa. Cost optimization is achieved through the selection of plastic tubing as the main material. The diffuse ceiling ventilation concept is cost-optimized by exploiting the existing suspended acoustic ceiling to provide ventilation equal in performance to mixing ventilation. Filtration is achieved passively as well as actively through a culvert and an electrostatic precipitator. This allows for very efficient filtration and thus better indoor climate. The next chapter utilizes all three concepts for a proposal of a building integrated passive ventilation system.

Chapter 5

Concept proposal

5.1 Proposal

The hybrid ventilation system that is presented here is a one-mode system of balanced mechanical system with extremely low pressure losses. We believe that the hybrid approach where only one mode exists has several advantages in temperate climatic conditions:

- One-mode systems do not require the implementation and inordinate investment of two separate ventilation systems in the same building
- One-mode systems require only one control system which makes it simpler to control
- Ducted systems distribute fresh supply air as intended because conventional dampening systems may be applied
- Ducted systems may easily employ heat recovery and filtration
- Ducted systems with heat recovery do not suffer from draught risks in the occupied zone
- Frequency-controlled fans ensures steady and continuous performance by levelling out natural fluctuations while allowing stack and wind to assist
- One-mode systems do not suffer from shifts in the neutral plane due to thermal stratification (Li et al., 1999)
- One-mode systems may exploit the stack from temperature drop in summer nights to provide night ventilation
- Conventional low-pressure mechanical systems suffer from uncontrollable stack. In the approach here the system is designed to actively exploit the stack effect

Figure 5.1 illustrates the building integrated ventilation concept. The concept is designed for maximum stack effect and for maximum responsive building integration. A 30 m long embedded concrete duct leads the fresh air through an electrostatic precipitator, through the heat recovery coil and distributes it to the floors via the main shaft placed in the atrium. On each floor supply ducts feeds the diffuse ceiling ventilation system, see

Paper III. The extract air flows from all floors via the atrium to another heat recovery coil above the roof. Heat is recovered by linking the recovery coils with a pump-powered liquid loop. The properties of the employed coils are described in detail in Paper II.

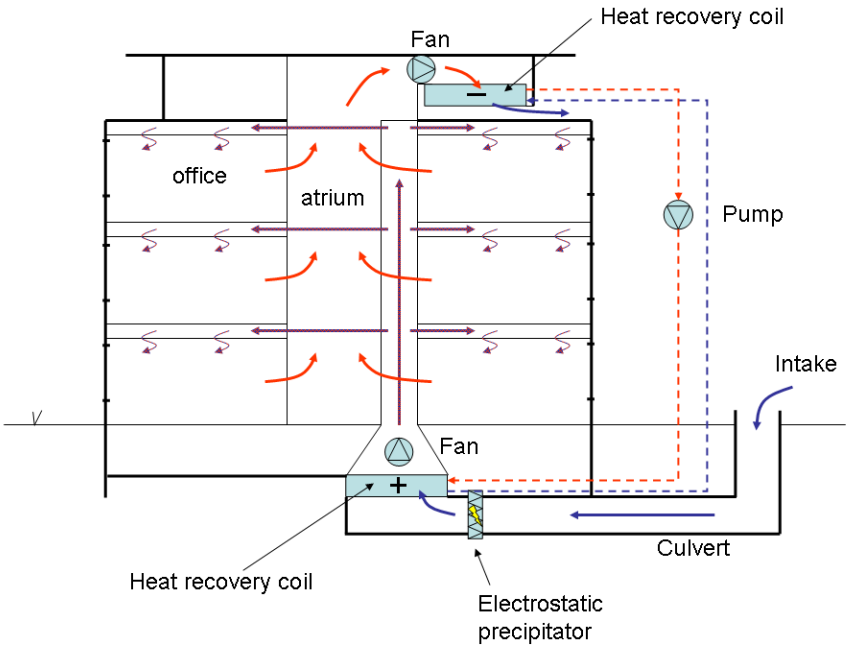

Figure 5.1: Building integrated ventilation concept.

The objective of the design is to achieve whole-year comfort ventilation at extremely low fan power consumption as well as total energy consumption and to provide sufficient night cooling through the same system purely by stack. A parallel objective is to use components with measured performances whether they are commercially available or developed prototypes.

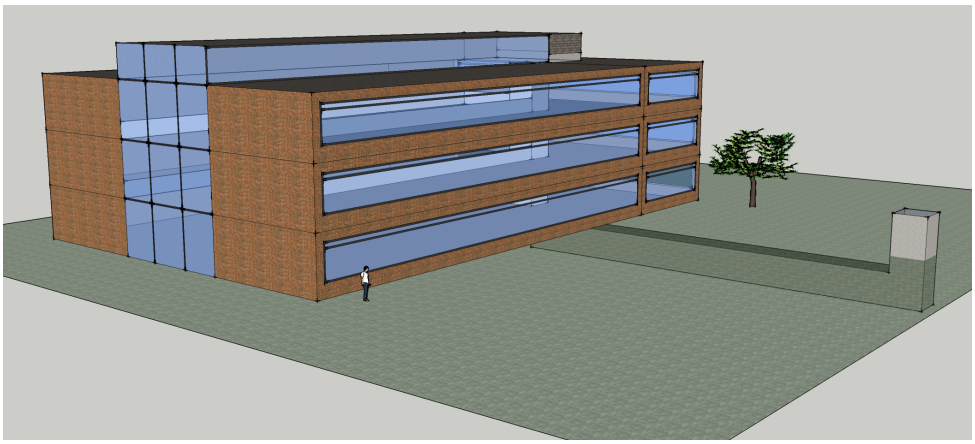

Figure 5.2: 3D schematic of the test case building.

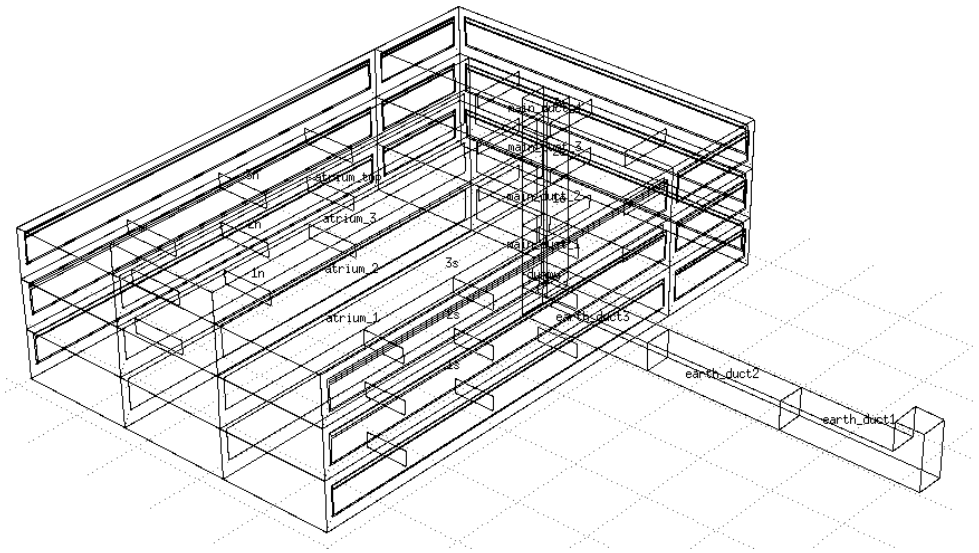

Figure 5.3: Model in ESP-r.

The above-mentioned principles are used in a fictive test case office building with three stories, see Figure 5.2 and Figure 5.4. The design of the building is intended to match many newly erected office buildings while showing the applicability and energy savings of building integrated ventilation. It comprises three blocks forming a U-shape around an atrium with the open face of the atrium pointing westward. This means that a substantial part of the offices are facing either North of South which is worst-case scenario. The footprint of the building is $38 \times 24\,\mathrm{m}$ with a total floor area of $2256\,\mathrm{m}^2$. The office floor area is $2016\,\mathrm{m}^2$ and the floor height is $3.4\,\mathrm{m}$.

The system with it's components is designed to provide sufficient ventilation during winter and most of the transitional periods without fans. However, during the day in the summer season the stack effect is eliminated and a helping fan is required to create driving pressure. Therefore, the reported results include yearly simulations of the test case building with fans. At night, when the outdoor temperature drops, the stack is exploited to create night ventilation without the help of fans. The exchangers and fans are bypassed but to avoid soiling of the inlet ducts, the electrostatic precipitator is active. The consumed energy for this purpose is included in the reported total energy consumption.

The ventilation system is simulated using the state-of-the-art building simulation program ESP-r from University of Strathclyde, Glasgow, Scotland (ESRU, 2008). ESP-r is capable of combined thermal and airflow modelling and has been used to model natural ventilation with good accuracy (Wachenfeldt, 2003; Høseggen et al., 2009) and has a comprehensive validation history (Strachan et al., 2008). Also it has several build-in HVAC plant components that we use for the dynamic heat recovery loop. On the down-side ESP-r is, although improving, less than user-friendly, and requires a strong opinion on the physics of buildings and environmental systems. It is run on a Microsoft Windows machine using the Linux-emulator Cygwin. The used version was 11.6. Figure 5.3 illustrates the model of the test case building in ESP-r. For more details on the airflow and thermal model and the control strategies, the reader is referred to Paper IV.

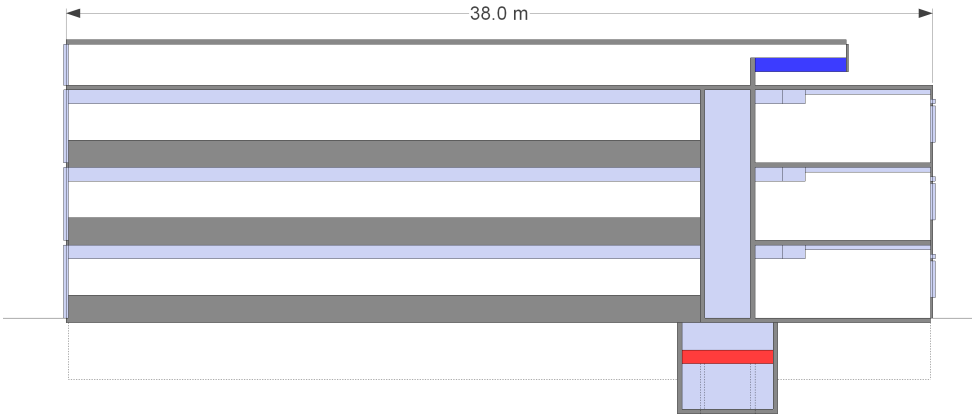

(a) North view

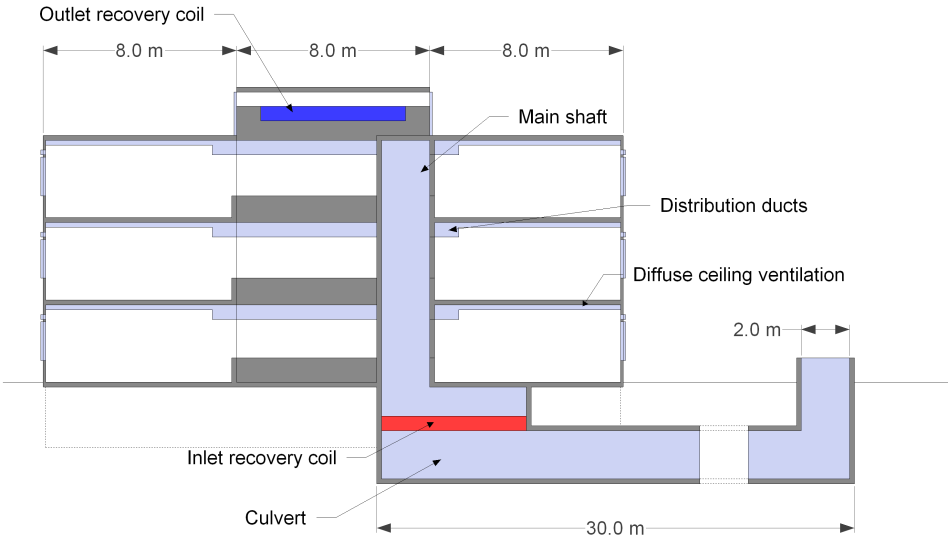

(b) East view.

Figure 5.4: Schematic of cross sections of atrium building with passive ventilation system components. The dimensions of the ventilation system are correct relative to the building dimensions.

5.2 Results

The building was simulated with and without fans. Only the results with fans are reported here. For results without fans, the reader is referred to Paper IV. The ventilation and thermal performance results for the yearly simulation are reported as footprints for the occupied time in all offices and duration curves for selected offices (Figure 5.5) and Figure 5.6). The figures document that the system complies with the minimum indoor climate requirements in indoor class II (EN15251, 2007). The thermal comfort was achieved by night ventilation, effective solar shading, effective lighting and the embedded culvert. Figure 5.7 shows the yearly necessary fan pressure rise.

The primary energy consumption is reported in Table 5.1. Yearly lighting and hot water was separately calculated with an external program (SBi, 2008) which is normally used to document the primary energy consumption in Denmark. The only major difference between the two cases is the heating consumption which is due to differences in ventilation heat loss. The power required for fans is extremely small. This is supported by Figure 5.7 which illustrates that the required fan pressure rise is very low (<5 Pa) and only necessary during the warm season. This is comparable with the pressure loss in natural ventilation which is typically less than 10 Pa (Aggerholm et al., 2008). Some of the low fan power is replaced by the power consumption in the electrostatic precipitator. This results in a mean specific fan power of 155 J/m^3 including fans, pumps and filter. In Table 5.2 the contributors to the mean SFP is listed. The SFP values were calculated by the mean value of the sum of all power consumption divided with the total amount of comfort ventilation. For comparison the maximum SFP value in the Danish Building Code (EBST, 2010) is 2500 J/m^3. The total energy consumption is 18.9 kWh/m^2 with a heat recovery efficiency of approx. 66% and a pressure drop of approx. 5 Pa. This is significantly lower than the values obtained by (Tjelflaat, 2000), and by (Heikkinen et al., 2002). Also it is worth noting that no gains are achieved by raising the efficiency of the heat recovery except for minimum supply temperatture. However, Paper IV documents that the supply temperature is never colder than 8 °C below room temperature.

Table 5.1: Comparison of yearly primary energy consumption. Conversion factor to primary energy: 2.5.

Primary energy kWh/m^2	w/o fans	w/ fans
Heating	4.93	3.63
Cooling	0.00	0.00
Fans	0.00	0.03
Filter	2.20	2.20
Pumps	0.03	0.03
Hot water	6.05	6.05
Lighting	6.95	6.95
Total	20.16	18.90
Mean SFP [J/m^3]	155.6	155.0

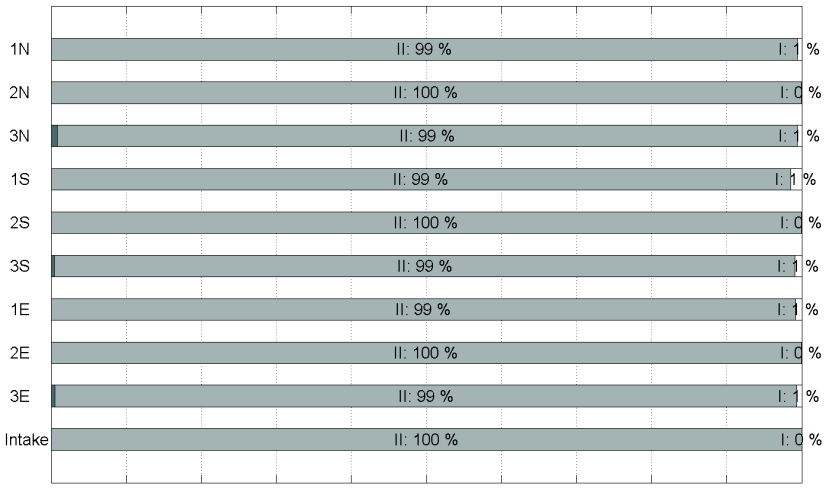

(a) Ventilation footprint

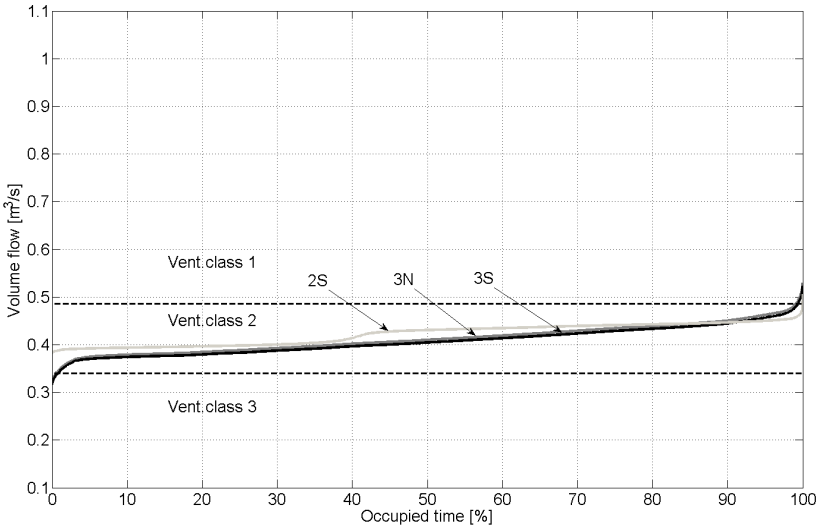

(b) Selected ventilation duration curves

Figure 5.5: Compliance with the ventilation requirements according to EN15251 (2007) in the different offices.

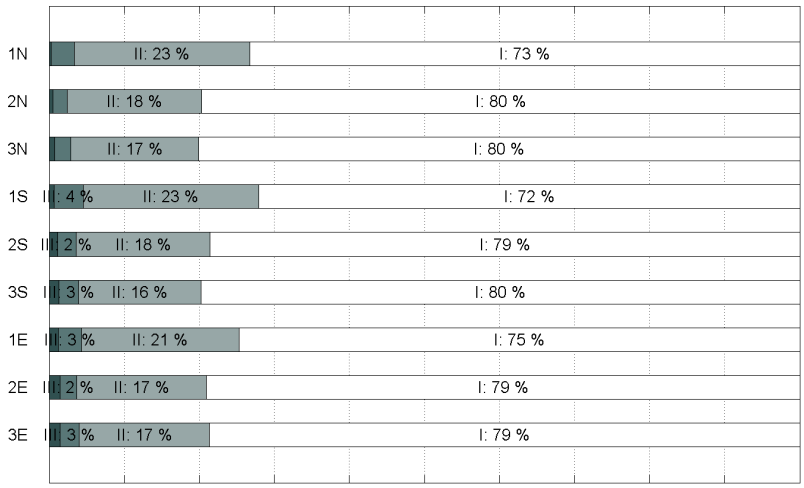

(a) Operative temperature footprint

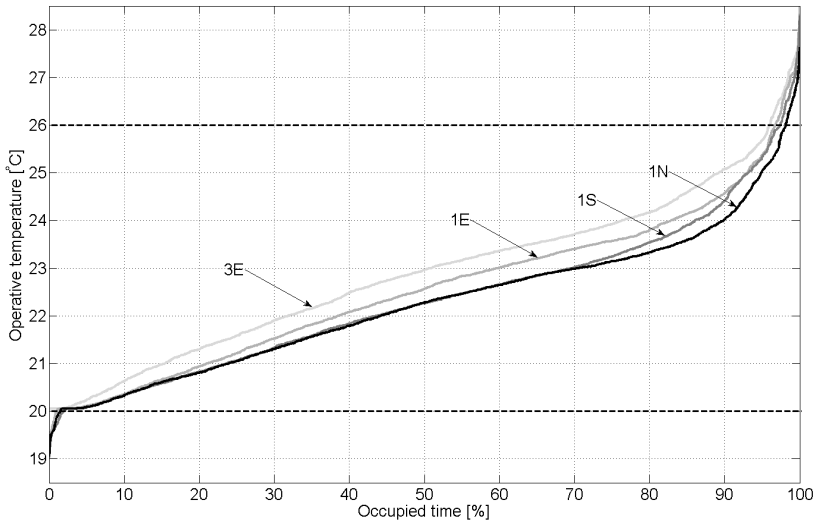

(b) Selected temperature duration curves

Figure 5.6: Compliance with the thermal requirements according to EN15251 (2007) in the different offices.

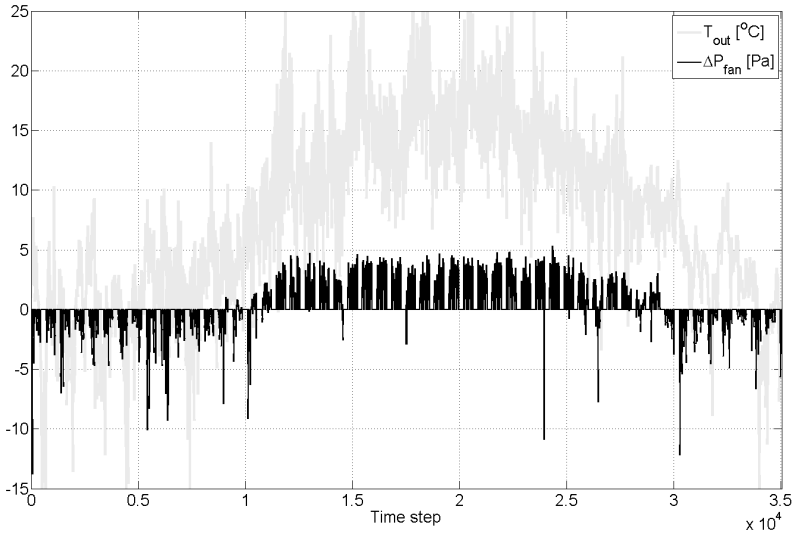

Figure 5.7: Fan pressure rise.

Table 5.2: Breakdown of mean SFP.

Specific fan power J/m^3	w/o fans	w/ fans
Fans	0	1.1
Pumps	19.7	16.4
Filter	135.9	137.5
Sum	155.6	155.0

5.3 Conclusion

With the results in Paper IV it is made probable that a realistic building can be ventilated by a one-mode hybrid ventilation system. The building is almost naturally ventilated, employs heat recovery, filtration and flow control and uses a fraction of the energy required in a new building by the Danish Building Code. The total energy consumption lies below a possible near-zero energy class from 2020. The indoor air quality is improved because filtration is performed with an electrostatic precipitator where the fresh air is not polluted by dirty bag filters, and the thermal comfort is maintained through an embedded culvert and free cooling by night ventilation without fans using the existing supply ducts. The major cost difference to a conventional mechanical system is due to the culvert, the main concrete shaft, and the heat exchanger coils. On the up-side no air-conditioning coils are necessary, no office space is consumed for ventilation purposes, and increased ventilation rates, e.g. due to higher future indoor climate demands, are 'free'. In total, it is made probable that buildings with near-zero emissions are within reach without employing costly renewables.

Chapter 6

Selection of optimal ventilation solution

Energy performance and indoor environment have become increasingly important in building design. Building developers and designers are straining to produce end-user buildings with a low energy consumption and high indoor environmental performance. This has lead to a growing awareness that to achieve low-energy buildings with satisfactory indoor climate the designer has to be aware of the consequences of critical design decisions as early as possible in the design process to obtain a good final whole-building cost-benefit ratio (Petersen and Svendsen, 2010). The design of ventilation systems for low-energy offices requires insight of the engineer/architect into multiple fields of building design and ventilation. Integrated design process is a holistic method that facilitate the design of buildings in the initial design phase. The process is to combine architectural and functional quality of a building at an early stage.

Analysing problem complexes like choosing the ventilation system for a new building presents us with a number of methodological difficulties. The issue involves both quantifiable and non-quantifiable variables that are inter-correlated to some extent and perhaps incomplete, with missing or undetermined information due to the early stage in the design phase or simply the subjective nature of judgements.

The rationale behind the developed tool and method is a quick holistic yet formalized approach sufficiently accurate to estimate the performance of different scenarios. In Section 6.1 the developed software tool is described and in Section 6.2 a methodology that uses the tool to find the optimal ventilation solution is suggested.

6.1 Coupled thermal, daylighting and ventilation model

The software tool used for evaluating the performance of different ventilation schemes is the sum of three major algorithms. They comprise a thermal model (BuildingCalc), a daylighting model (LightCalc), and a stack ventilation model. These models can be used in conjunction through a user interface and provide evaluation of thermal indoor environment and heating and cooling loads in a building with very few input parameters while providing the option of sophisticated system controls. The amount of input is small which renders the tool practical in the early stages of design or as simulation foundation

for an integrated design process where it is essential to quantify and create awareness of the consequences of design decisions. Indeed a second user interface was developed specifically as part of an integrated design process (Petersen and Svendsen, 2010) allowing the user to specify low, medium, and high values for all variables. Thus the name of the tool has changed to Integrated Design of Buildings, iDbuild.

6.1.1 Thermal model

The foundation of the simulation software is a simplified thermal model (Nielsen, 2005) by the name of BuildingCalc. The thermal model is based on a two-nodal equation system with one node representing the air temperature and one the internal temperature of the constructions. The mean surface temperature represents the internal surfaces where heat is exchanged with the indoor air and the effective heat capacity of the constructions. The equation system has an analytical solution and by the end of each time step the temperatures are calculated based on the initial temperatures of the time step. The systems control strategy is ideal yet satisfactory for quick design suggestions. During each time step the systems are activated to control the indoor air temperature which changes the analytical solution and causes the equation system to be solved several times within a time step to achieve a given setpoint.

6.1.2 Daylighting model

The daylighting algorithm employs the radiosity method for internal daylight reflections, while the incident initial light is calculated by tracing the rays emanating from the sky to the room surfaces (Paper I). This gives a reasonable balance between accuracy and calculation time.

A critical element in the daylight calculation routine is the light transmittance of the combined glazing/shading system. For this purpose the European software tool called WIS (van Dijk and Oversloot, 2003) is used. This tool is capable of calculating the light transmittance of a transparent system for both direct and diffuse light. It calculates the thermal and solar performance of multilayered window systems, allowing the user unlimited combinations of glazing and solar shading devices. This makes WIS a very powerful tool for evaluating various integrated daylight designs. The daylighting algorithm comprises a comprehensive database of pre-defined window/shading systems yet it also has an interface that reads WIS generated data files.

The daylighting tool may be used in two ways: (1) for detailed daylight distribution in a room for a particular day, time and sky luminance distribution and (2) coupled with the thermal domain to quantify the impact of daylight on the building energy consumption.

In a combined simulation the shading control is based on a two-conditional strategy and the cut-off angle. When any of the two conditions: indoor operative temperature or risk of glare are exceeded the cut-off strategy is activated. In the case of adjustable blinds they are lowered and adjusted to the slat angle where the direct sun is just blocked. This strategy maximizes the incoming amount of daylight while blocking the main contributor to glare and indoor overheating. In the case of screens the control is limited to screen up or screen down.

To assess the risk of glare a glare probability index is used (Wienold and Christoffersen, 2006). The DGP index is defined in the interval [0.2; 0.8] and is directly correlated with the percentage of disturbed persons. According to Wienold and Christoffersen (2006) the correlation between the linear function of vertical eye illuminance and DGP is stronger than all other tested functions. If E_v denotes the vertical eye illuminance (lux), the daylight glare probability is calculated from Equation 6.1:

$$\mathrm{DGP} = 5.87 \times 10^{-5} E_v + 0.16 \tag{6.1}$$

This means that DGP values of 0.2 (20% disturbed) approximately corresponds to a vertical eye illuminance of 700 lux.

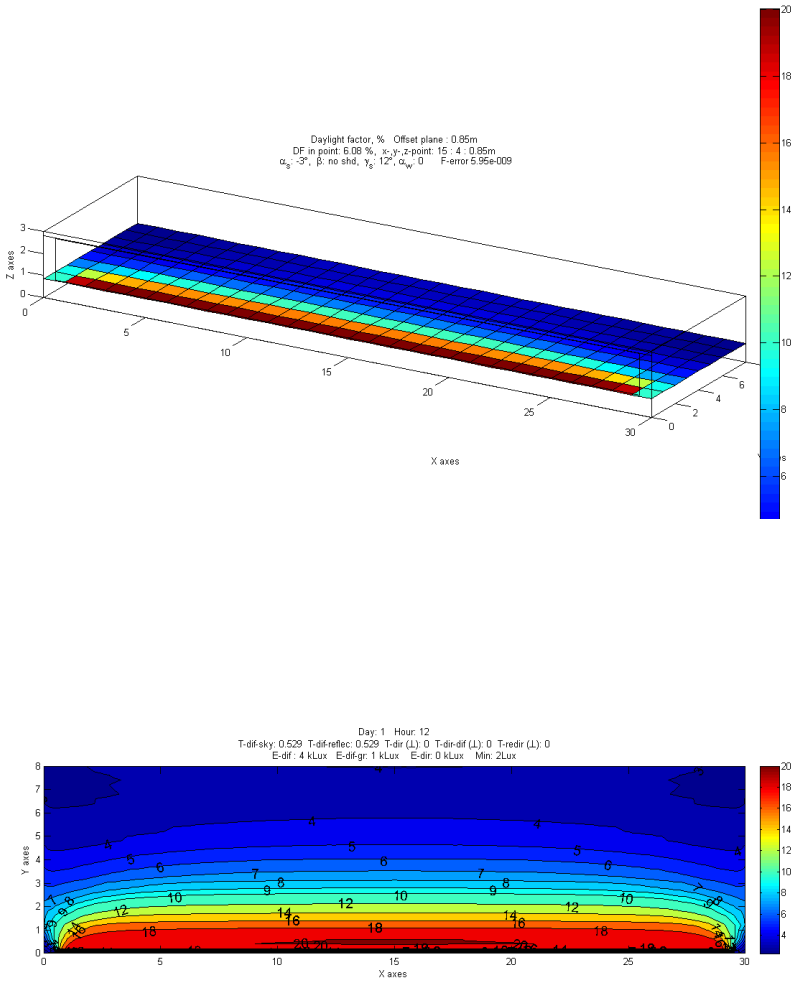

(b) Contour plot

Figure 6.1: Daylight factor in open plane office.

One example of output from a detailed daylight simulation is depicted in Figure 6.1 showing the daylight factor contour lines from a CIE standard overcast sky with internal

subsurfaces the size of 1×1 m. The room size and glazing properties are the same as those used in the test case building in Paper IV. Indeed the daylight factor was used to calculate the lighting energy consumption. For validation of the results with RADIANCE (Ward and Shakespeare, 1998), the reader is referred to Paper I. Another example of output in Figure 6.2 is from a coupled simulation that encompasses hourly values for the daylight level in two arbitrary points and the artificial lighting load

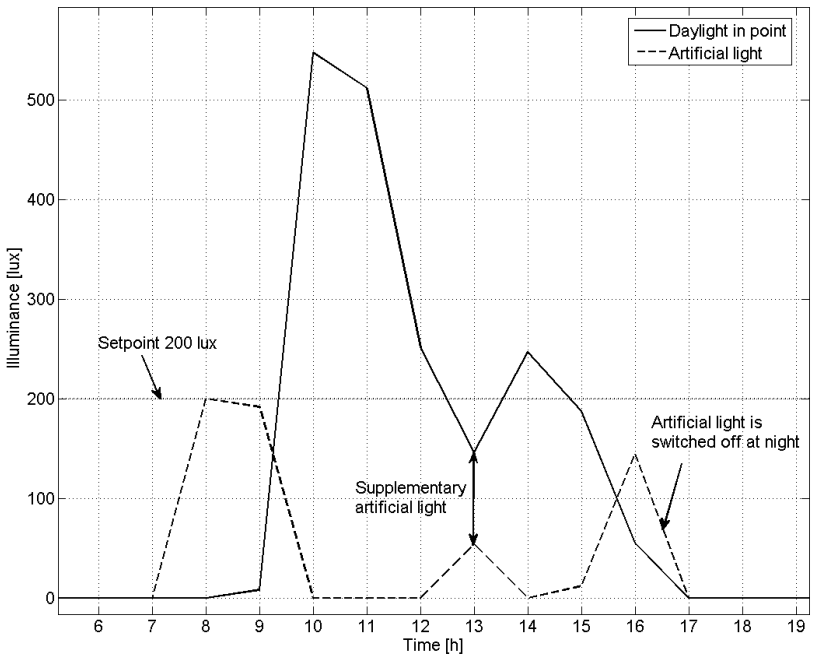

Figure 6.2: The artificial lighting system continuously complements the daylight to reach a user-specified setpoint.

6.1.3 Ventilation model

The stack ventilation model expands the ideal ventilation model in the iDbuild tool by introducing stack and wind effects in the ventilation system (Paper V). In order to properly evaluate different ventilation concepts as part of an integrated design process, e.g. natural ventilation versus mechanical ventilation, the natural driving forces become important especially for low-pressure systems. Figure 6.3 depicts a schematic of the model with two possible inlets, either central inlet or facade inlet. All heights relate to the ground level and can be selected arbitrarily, i.e. inlet and outlet heights can be equal, e.g. with air-to-air heat recovery. 6.4(b) illustrates the user interface for the simplified ventilation model.

6.1.4 Coupling

The integration of daylight, stack and thermal domain requires a sophisticated coupling to calculate the incoming daylight, the effect of shading on thermal load and indoor air

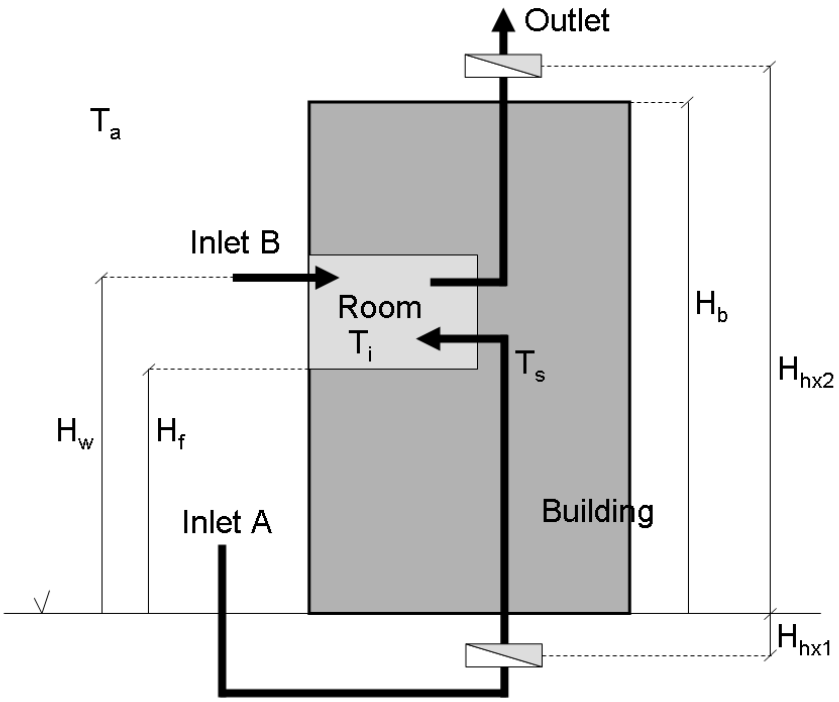

Figure 6.3: Stack model.

temperature and the subsequently the effect on the stack. Figure 6.5 gives a schematic overview of the coupling. The procedure pre-calculates the hourly daylight levels in the room without shading and the wind pressure difference between inlet and outlet. The thermal load is then calculated as well as the available ventilation rate due to wind and stack and possibly a helping fan in the ventilation system. The stack algorithm employs a forward advancing routine that uses the indoor air temperature from the previous time step. No iterations between stack model and thermal model is performed. This saves calculation time in a tool meant for quick estimation and the error is deemed small due to the time constant of the temperature.

After the pre-calculations of daylight, the thermal model is initiated. It evaluates the hourly indoor operative temperature with respect to the cooling setpoint, possibly lowers the shading and adjusts the slat angle (for blinds) to cut off direct sunlight, and calculate the daylight levels and thermal load again. If the operative temperature still exceeds the cooling setpoint, other measures like venting, increased ventilation, and mechanical cooling are employed in that order. Thus the tool encompasses a fully integrated thermal, ventilation and daylighting simulation with detailed hourly output of daylight level, the electrical energy consumption for lighting and fans, heating load, cooling load and indoor operative temperature.

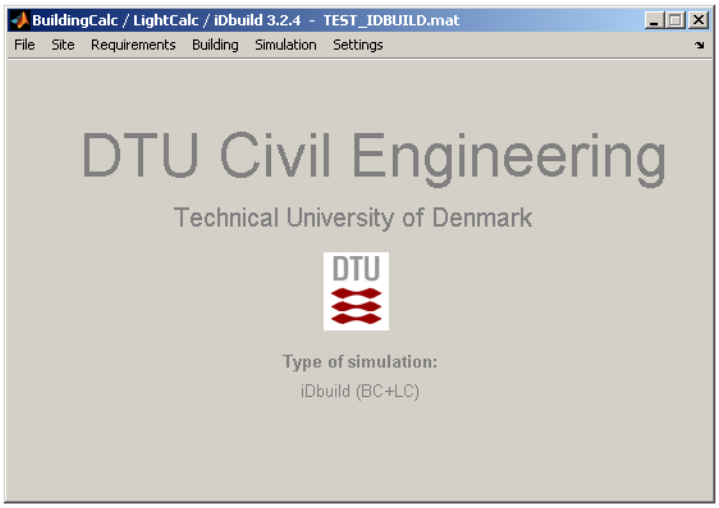

(a) Startup screen

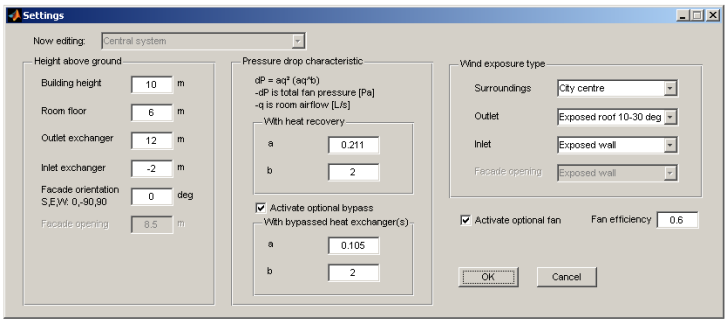

(b) Ventilation user interface

Figure 6.4: iDbuild and the ventilation model user interfaces.

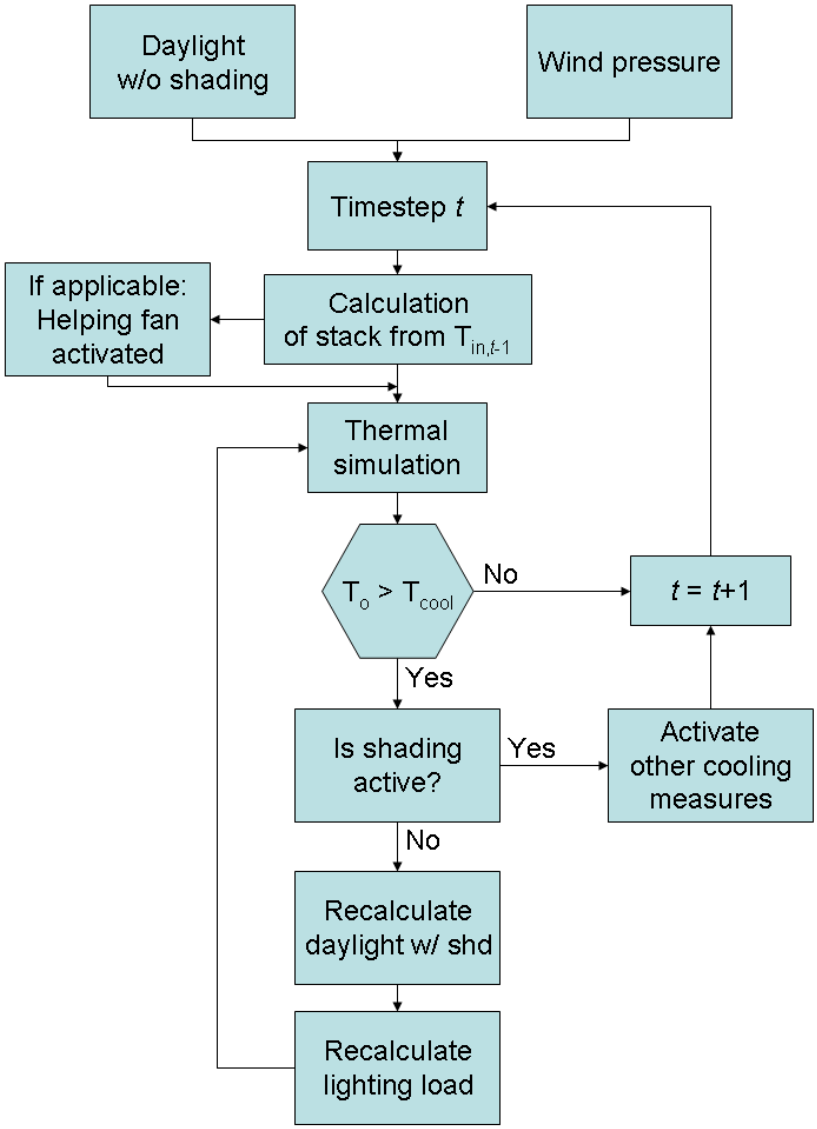

Figure 6.5: Calculation procedure for the integrated thermal, daylight and stack ventilation.

6.2 Morphological analysis

Morphological analysis may be used to decompose and structure problem complexes into both objective (technical) and subjective (psychological) variables while treating incomplete information in a structured manner. One of the advantages of morphological analysis is that such combinations are valid. General morphological analysis was developed by Fritz Zwicky (Zwicky, 1969) and has been used for many purposes in relation with buildings e.g. for integral design methods or to improve the comfort of various ventilation concepts (Quanjel et al., 2006; Zeiler et al., 2006). Here we propose a coupling of morphological analysis with cross-consistency assessment (CCA) (Ritchey, 2006) and multidimensional scaling (MDS) (Cox and Cox, 2001) to establish the feasible 'space of solutions' for various ventilation schemes within various building envelopes. This process is time-consuming, but it can be automated if it is implemented in a dynamic building simulation program, e.g. in iDbuild.

The decomposed problem is put into a 'box', which is depicted as a chart in Table 6.1 with example values. The dimensions and variables are listed in the left-hand columns and the values are listed in rows. The imaginative values (high, medium, low) are exchanged with real numbers that the user regards as representing high, medium and low values whenever possible. The values may be arbitrarily selected or based on e.g. three classes from a standard. The depicted chart does not encompass all the possible ventilation variables and indeed has been reduced for the purpose of illustration. The number of non-quantifiable variables is unlimited and the number of quantifiable parameters is only limited by the software tool.

The suggested method is tested on a simple case to illustrate the possible outcome. Figure 6.6 illustrates the procedure that starts with selecting the simulation variables and inputting the non-quantifiable variables as well. Four quantifiable variables and one non-quantifiable were simulated. For the method of cross consistency assessment and economical optimization, the reader is referred to Paper V.

The simulation generated $3^n = 3^4 = 81$ scenarios which took approx. 120 minutes on a laptop with a Pentium M processor running at 1.86 GHz and with 1 GB of RAM. Yearly daylight simulation was included.

Figure 6.7 depicts most of the simulated scenarios. With the software tool it should then be possible to pick the most interesting scenarios, typically with respect to low energy consumption and low draught risk (DR-hours). The calculation of DR-hours is performed with empirical formulae which are explained in greater detail in Paper V. By holding the mouse over the scenario, the properties should 'pop up'. The refence shows an example of a 'pop up' box with scenario information. In Figure 6.7 some interesting scenarios 1–13 are pre-selected which will be used in the next section.

6.2.1 Multidimensional scaling

One of the most important goals in visualizing data is to provide the viewer with a sense of the distance between the plotted points. While it is straightforward to plot scenarios based on two criteria, e.g. energy consumption and DR-hours, the designer is not provided with the overall picture. With more dimensions than 3, it is very difficult to visualize distances, unless the number of dimensions may be reduced to two or three. Consequently

Table 6.1: Morphological box for the ventilation system in a building. Input are example values.

		Values		
	Dimensions and variables	Low $i = 1$	Medium $i = 2$	High $i = 3$
$k = 1$	Comfort-dimension			
$j = 1$	Ventilation rate[a]	Class III	Class II	Class I
$j = 2$	Ventilation effectiveness[b]	0.7	1.0	1.3
$j = 3$	Thermal comfort[a]	Class III	Class II	Class I
$j = \ldots$	Supply method[c]	Wall jet	Circular diffuser	Displacement
	Draught rating[d]	Class C	Class B	Class A
$k = 2$	Building-dimension			
	Site	City	Urban	Open field
	Inlet exch. coil height, m	2.7	3.2	3.4
	Outlet exch. coil height, m	10.0	12.0	15.0
	Room floor height, m	2.7	3.2	3.4
	Room height, m	2.7	3.2	3.4
	Internal gain, W/m^2	5	10	20
	Thermal capacity[e]	Light	Middle light	Middle heavy
	Window size, % of facade	20	40	60
	Solar shading	None	Blinds	Screen
$k = \ldots$	Cost-dimension			
	Material costs, €/m^2	50	100	300
	Energy price, €/kWh	0.15	0.25	2.0
	Fan efficiency, -	0.4	0.6	0.8
	Running time, hours	2000	2500	4000
	Air handling unit[f], Pa	50	100	200
	Length[g], m	20	30	50
	Heat recovery, -	0.65	0.75	0.9
	Night ventilation, -	None	Venting	Mech. vent.
	Heating system eff., -	0.6	0.8	1.0
	Cooling system eff., COP[h]	2.0	3.0	5.0
$k = n$	Psychological-dimension			
	Aesthetics (integration)	Visible	Invisible	Somewhat visible
$j = m$	Occupant satisfaction	No control	Low control	Individual control

[a] (EN15251, 2007)

[b] Example values for natural ventilation, mechanical mixing and mechanical displacement.

[c] A fourth option, linear slot diffuser, is also available.

[d] (ISO7730, 1994)

[e] Influences the thermal load that has to be removed by ventilation/cooling system.

[f] Additional losses due to air handling unit.

[g] Local losses in the ductwork should be included as equivalent lengths.

[h] Coefficient of performance

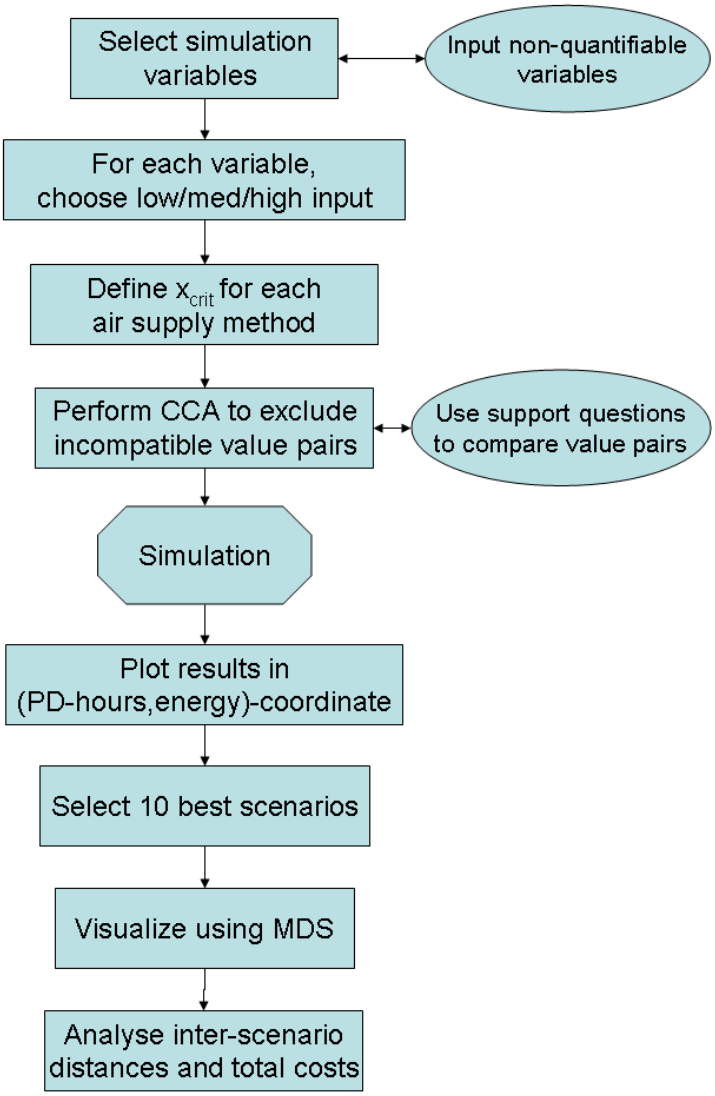

Figure 6.6: Method procedure.

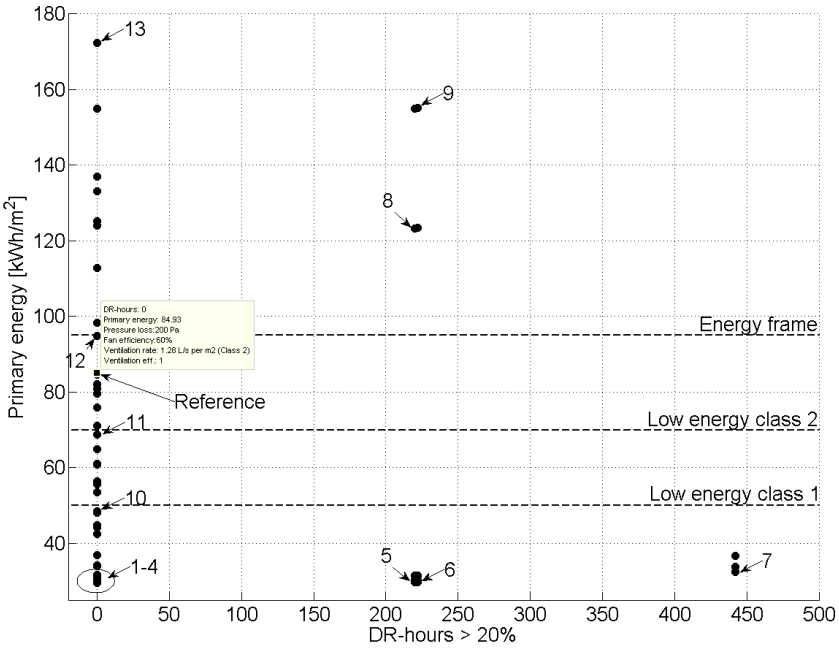

Figure 6.7: The simulated scenarios are depicted with respect to draught and energy.

a reduction in the number of dimensions is necessary. Non-metric multidimensional scaling (MDS) is a set of statistical methods for addressing this type of problem. The methods are available in a toolbox in Matlab and we use them to plot the selected scenarios relative to each other to obtain an instant sense of the distances between them. The inter-scenario distances are not Euclidean but the configurational or technical distances, or more precisely the pairwise dissimilarities between the scenarios. So a technical distance of 1 between two scenarios indicates that they have been produced from the same set of values except for one value that has been replaced by its horizontal neighbour in the morphological box. A technical distance of 2 means that two values have been replaced by its horizontal neighbour. It is evident that a certain amount of distortion has to be tolerated when a multidimensional dataset is reduced to two or three dimensions. In typical MDS applications, an investigation into the significance of the error can be conducted using Kruskal's normalized stress criterion (stress1) (Kruskal, 1964), in which values below 0.05 are good and values above 0.20 are poor. If the criterion is exceeded, the user must reduce the number of selected scenarios or raise the number of depicted dimensions from two to three.

In Figure 6.8 we establish a linear correlation between bubble size and energy and use the MDS method to plot the selected scenarios relative to each other. The bubble size could also have been dependent on the total cost.

The distances between the bubble centroids are expressed in terms of 'technical distance'. Where two bubbles are closely spaced, this represents two ventilation scenarios that are very similar to one another. The MDS method visualizes the morphological chart for the engineer, and he is then able to navigate between them and explore their dissimilarities

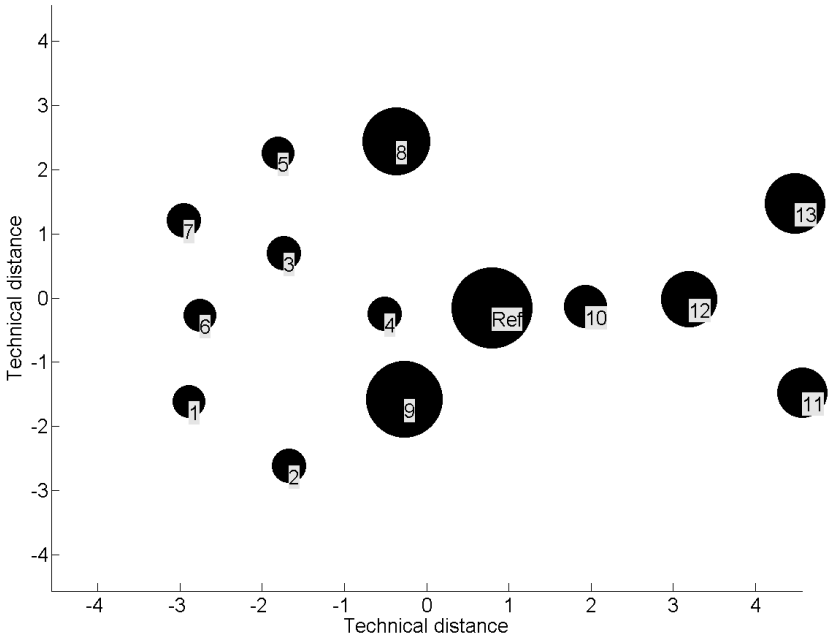

Figure 6.8: Distance analysis chart.

simply by clicking on the bubbles with the mouse. The low-energy scenarios 1–7 are all close together which means that the poor draught performance when going from scenario 1–4 to 5–7 is due to small solution changes. If scenario 1 is not entirely acceptable to the engineer or the architect, they can go to scenario 2, 3, and 4 which are close by. The reference is made of medium values for all variables and thus is close to the middle. Quite interestingly it is close to both scenario 4, which is very good, and scenario 9 which is very poor. This emphasizes the importance of making the correct design decisions on the final performance of the building.

6.3 Conclusion

This chapter describes a tool capable of estimating the performance of a ventilation solution from very few input. The tool is based on a conflated routine of simplified thermal, ventilation and daylight algorithms which makes the tool quick and suitable for design decisions at the very earliest stage. Furthermore the chapter sketches the idea for an optimization methodology using the tool for ventilation solutions. The methodology is based on a morphological approach with subsequent scaling of the n-dimensional problem complex into two dimensions. The different solutions are related to on another by multidimensional scaling showing the 'closeness' or distance of alternatives. One great advantage of the method is that it does not exclude non-quantifiable variables but visualizes them with the quantifiable variables side-by-side. With this methodology the architect and the ventilation engineer together have a tool that enables them to find a common optimal solution.

Chapter 7

Economy

7.1 International hybrid ventilation projects

Various literature sources discusses the economy of ventilation solutions which in some way differs from conventional mechanical ventilation. One of the most comprehensive sources is a technical report within the framework of the IEA Annex 35 on Hybrid Ventilation (van der Aa, 2002). The report is based on several international buildings with a majority located in the Nordic countries. Figure 7.1 documents the mechanical and electrical costs of the hybrid ventilation system compared to a high and a low mechanical reference. What constitutes mechanical and electrical costs is described in detail in the report.

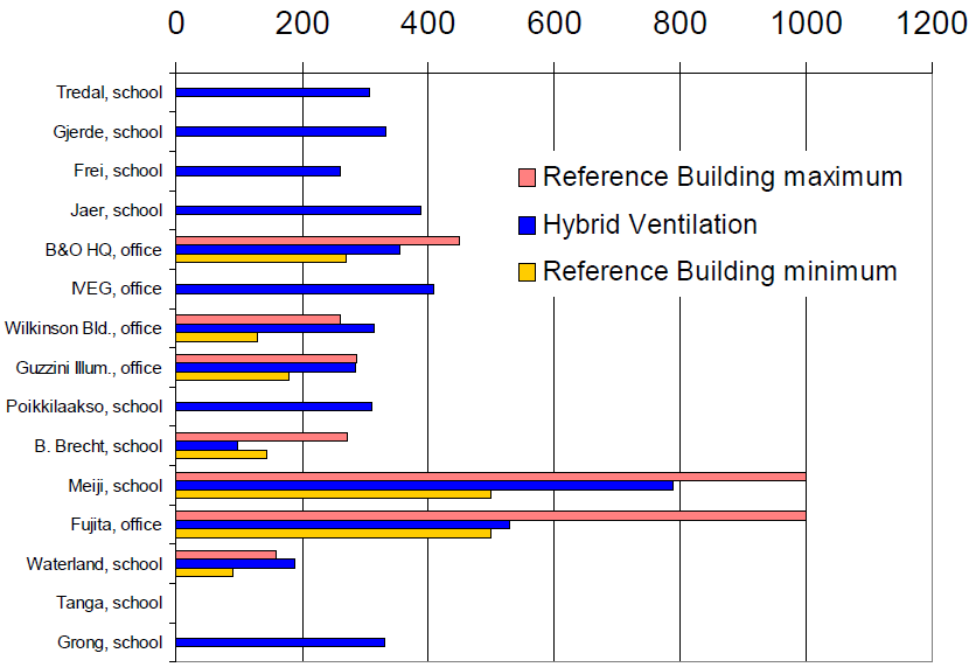

Figure 7.1: Costs of hybrid system versus mechanical reference in €.

Rather than looking at the ventilation system as a separate part of the building, hybrid systems are often dependent on the building design. Therefore, the total building costs

should be looked upon. Figure 7.2 illustrates the total building costs

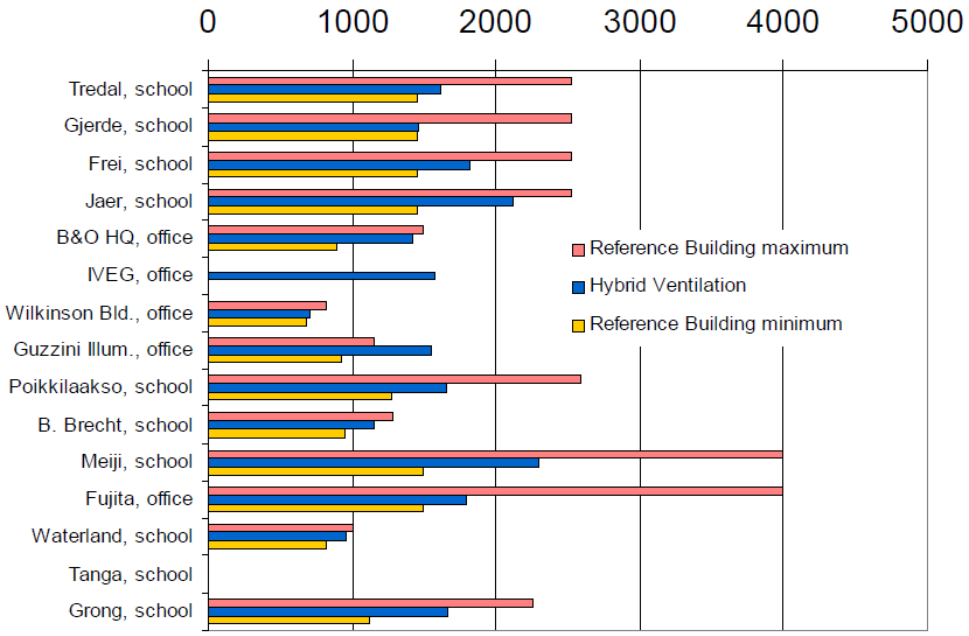

Figure 7.2: Total building costs in €.

There is one conclusion that may be drawn from Figure 7.1 and Figure 7.2 which is that buildings that are designed to operated with hybrid systems are neither as costly as the maximum reference nor as cheap as the minimum reference. Unfortunately, the 'reference' is not elaborated in the report, nor is the data split into type of hybrid system.

7.2 Danish hybrid ventilation projects

To further elaborate and document the construction costs of low-pressure ventilation systems, three recent and very different sources are presented. None of the sources are backed by realization. Rather they are the result of development projects between industry partners who wished to extend their product portfolio. Hence the construction cost is only an accurate estimation, however, performed by very knowledgeable people.

7.2.1 New ALECTIA location in Odense

An old high rise warehouse in Odense, Denmark, is retrofitted into a modern office building. The building was initially not ventilated and ALECTIA wished to investigate the economic feasibility of different ventilation schemes. The total floor area was 2700 m^2, and the necessary ventilation rate was 8000 m^3/h for indoor climate class II (EN15251, 2007). A drawing of the building is shown in Figure 7.3. Table 7.1 lists the installation costs of three ventilation schemes in the building.

Natural ventilation Cross ventilation on each floor provided by openings in the facade above the comfort zone.

Figure 7.3: Drawing of warehouse to be retrofitted in Odense.

Mixed-mode hybrid ventilation Same as above but stale air is exhausted through central staircase. Stack effect is exploited and exhaust fan at the top of the stairwell provides pressure rise if necessary.

One-mode hybrid ventilation Intake fan provides fresh air ventilation to offices through ducts and exhaust fan extracts stale air through central staircase. Stack effect is exploited, energy for air transport is low compared to conventional mechanical ventilation and it is possible to implement heat recovery and cooling.

Table 7.1: Construction costs of different ventilation schemes.

Ventilation scheme	Max ACR h^{-1}	Construction costs €	Costs per m^2 €/m^2
Cross ventilation	4–5	450000	98
Mixed-mode hybrid w/ext. fan	4–5	500000	109
One-mode hybrid w/heat rec.	1.5	370000	80
As one-mode + cooling	1.5	440000	95

7.2.2 INTEND project

A project with industry partners including Ph.D. supervisor Svend Svendsen from DTU Byg was initiated by contractor MT Højgaard to develop a relatively simple yet modern office building, see Figure 7.4. The objective was to estimate the construction costs required to bring the building to meet different energy frame demands of the Danish

Building code 2006-2020. The price was calculated by the contractor and sub-contractors and therefore carries great credibility. Consequently the costs of the different ventilation schemes in Table 7.2 include the entire building costs.

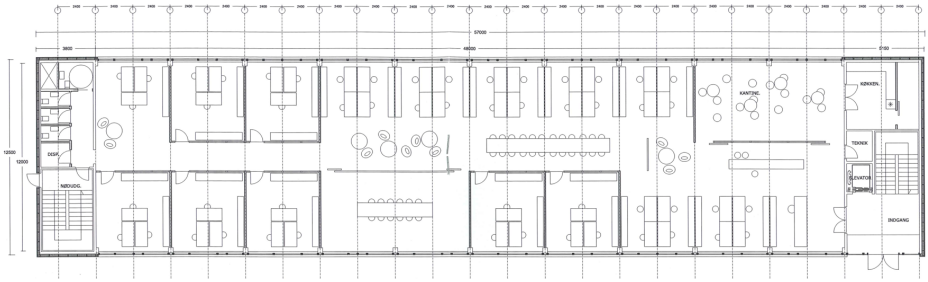

(a) Floor plan

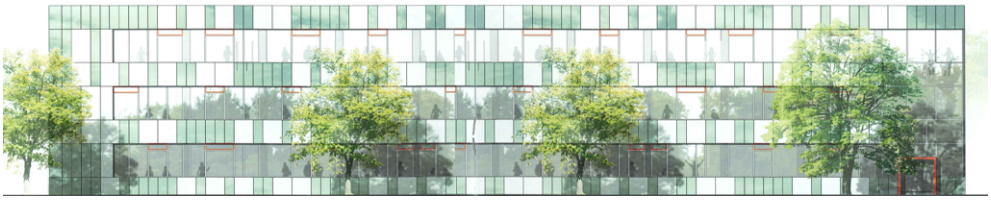

(b) Facade

Figure 7.4: Suggested building design in INTEND-project.

Table 7.2: Building construction costs including different ventilation schemes. BC2015–2020 denotes the year of promotion from option to building code.

Ventilation scheme	Energy frame	SFP kJ/m^3	Costs €/m^2	Increase %
Mechanical VAV	Building code 2009	2.47	84	-
Mech. VAV lower pres.	Low energy class 2 (BC2015)	1.52	107	27
Mech. VAV low pres.	Low energy class 1 (BC2020)	1.26	112	33

7.2.3 HVAC magazine article

A popular article published in May 2009 (in Danish) (Førland-Larsen et al., 2009) states the life-cycle costs of different ventilation schemes with respect for thermal indoor climate, energy consumption, the price of energy and an interest rate of 4%. For calculation of the primary energy demand heating and power is weighted according to the Danish Building Code 2006. For more detailed input descriptions than those below the reader is referred to the many input tables of the published article.

- Natural cross ventilation by openings in the facade above the comfort zone. Free cooling is provided by cold night air down to 20 °C.

- Same as previous in summer and decentralized mechanical ventilation with 80% heat recovery in winter. By decentralized the authors of the article mean:

  > ... decentralized air handling units below the ceiling. Alternatively the hybrid solution can be established by a number of decentralized air handling units distributed throughout technical rooms in the building.

  The decentralized units provide ventilation at a mean specific fan power of 2.1 kJ/m^3.

- Constant air volume with 80% heat recovery and mean specific fan power 2.1 kJ/m^3.

- Variable air volume with 80% heat recovery and mean specific fan power 2.1 kJ/m^3.

- Same as previous with cooling COP = 3.

Table 7.3: Yearly normalized key figures.

	Natural vent.	Hybrid vent.	CAV	VAV	VAV + cooling
Heating	1.9	1.0	1.3	1.1	1.1
Power	1.0	4.0	18	15	16
Primary energy	1.4	1.0	2.4	2.0	2.1
Indoor climate: h>26 °C	1.0	1.0	1.4	1.5	0.0
Total costs (20 years)	1.0	1.7	1.7	1.9	2.0

The results of the calculations are presented in condensed form in Table 7.3. The results are normalized to natural ventilation for direct and quick comparison between the schemes and shows very beneficial values for the natural ventilation scheme. However, the mean fan energy consumption is set to a very high value of 2.1 which just in the previous section (Section 7.2.2) was shown to be reduced to 1.26. However, the case is relevant because in Table 7.4 the construction costs of the schemes are listed, and it shows that while the difference bewteen natural and mechanical ventilation is significant, hybrid ventilation is neither cheaper, nor more expensive. Thus the article supports the conclusion of this chapter.

Table 7.4: Construction costs for the five ventilation schemes per unit air.

		Natural vent.	Hybrid vent.	CAV	VAV	VAV + cooling
Construction costs	€ $m^{-3}h^{-1}$	7.30	16.30	14.70	17.30	18.70
Max airchange per hour	h^{-1}	5	5	4	4	4

7.3 Conclusion

While the running cost savings of passive ventilation systems are well-documented, e.g. in Paper IV, the issue of installation costs is much more disputed. The issue is unfortunately riddled with personal agendas and undocumented summations besides the challenge of comparing performance across multiple systems. This chapter is not intended to clear up these issue but only to add to the general conclusion that hybrid/passive systems are neither less nor more expensive than conventional ventilation installations.

Chapter 8

Conclusion

This thesis has two objectives: to develop the concept and components for future ventilation of buildings and to develop a holistic tool, that prior to the design phase, enables the ventilation engineer to select the ventilation system that performs best, thereby obtaining a good final whole-building cost-benefit ratio.

With the results in this thesis it is made probable that a realistic building can be ventilated by a one-mode hybrid ventilation system. The building is almost naturally ventilated, employs heat recovery, filtration, diffuse ceiling ventilation and flow control while using a fraction of the energy for air transport required in a new building by the Danish Building Code. Heat recovery units with very low pressure loss and adequate efficiency have been developed together with a diffuse ceiling ventilation concept. In both components the issue of low cost has been essential. In the exchanger unit it has materialized by using cheap material for the kilometer long tubing, and in the diffuse ceiling ventilation by exploiting the existing acoustic suspended ceiling. The latter also reduces ductwork and increases the room height. In addition the proposed concept does not occupy any costly office space for ventilation.

The indoor air quality is improved because filtration is performed with an electrostatic precipitator where the fresh air is not polluted by dirty bag filters, and the thermal comfort is maintained by using (1) an embedded culvert and (2) free cooling by night ventilation using the existing supply ducts. Heating coils and cooling coils are obsolete.

The proposed ventilation concept is not optimized with regard to investment and running costs but it is made probable that buildings with near-zero emissions are within reach. Furthermore, a tool that can be used to quickly assess multiple ventilation solutions in a given situation was developed. This tool together with the suggested morphological methodology may subsequently be used to perform economical optimization and maybe to discover new ventilation concepts.

Thereby, the main aim of this thesis of producing low-energy buildings at a low cost is fulfilled.

8.1 Concluding remarks

- The heat recovery unit is soon being tested in a real operating situation. The experiences from that will be used in an updated version — at least the producer

has shown interest — that forms the tubing from two foils. This process will make the unit easier to build, more robust and even cheaper. The full scale test will also include an electrostatic precipitator and the performance of this will be investigated. Unfortunately the test setup will not allow for investigations into the passive settlement of particles in an embedded culvert.

- The diffuse ceiling ventilation concept is scheduled to a thorough practical test in a class room in building 118, DTU. In this project the effect of the thermal mass on the thermal comfort will be quantified and a proper numerical radiation model for a porous zone will be developed.

- The hybrid ventilation proposal has already been used in a competition entry by ALECTIA. The low fan energy consumption saved photovoltaics for about 15 MDKR. The competition proposal was runner-up.

Chapter 9

Research contribution to Academia and Industry

The results of this thesis are expected to have a major impact on shaping the future of the ventilation of buildings and on increasing the priority of installations in the design process so that the buildings will have a rational design with respect to the functioning of the installations. The impact stems from the research performed on the following topics:

- one-mode hybrid ventilation
- heat transfer with liquid-coupled tube banks
- diffuse ceiling ventilation
- yearly daylight simulations
- design via morphological analysis

While the research on hybrid systems is plenty, one-mode hybrid systems are only cursorily touched in the literature. Perhaps due to the believe that natural forces in mechanical systems only create problems. By performing very detailed simulations of a one-mode system with measured component properties it is shown that ventilation can and should be designed to exploit stack and wind. Thus this thesis helps in a paradigm shift that will replace active ventilation with (partly) passive ventilation. Furthermore, in relation to the future Building Code requirements, the results show that a near-zero energy class is a feasible option. This is important to the authorities as well as the industry. From the consulting engineers perspective increased knowledge about combined ventilation solutions, coupled with increased demands on energy consumption and indoor climate, will increase the value of consultant services and contribute to a significantly stronger profile within ventilation, work space design and indoor climate.

Historically passive systems have suffered from a lack of components that could render them competitive with conventional mechanical solutions in terms of thermal comfort and heat loss. Research and development is reported in this thesis to eliminate that deficiency. It is shown that heat recovery for naturally driven airflow is possible in an economically feasible way and that diffuse ceiling ventilation has equal performance to mixing ventilation

at a pressure drop of only 0.5 Pa. This knowledge can be used by the industry to open a new market by developing heat recovery for passive ventilation systems or to use their products in an alternative way, thereby creating products with higher value.

Conflated daylighting, solar shading control and thermal model has historically not been an option in thermal simulation. The implementation and validation of conflated daylight and thermal algorithms have substantially expanded the holistic approach of the integrated design process. An alternative approach to the process has been suggested which helps in guiding the building designer towards low-energy buildings. This complex process has been extended with visualization of scenarios by multidimensional scaling, thereby presenting all feasible solutions in an interactive way. To the consulting engineer this is valuable, especially in a competition phase where out-of-the-box thinking is important.

Bibliography

Aggerholm, S., Heiselberg, P., Bergsøe, N.C., 2008. Hybrid ventilation i kontorer og institutioner. Tech. rep., Statens Byggeforskningsinstitut.

Andersen, M., de Boer, J., 2006. Goniophotometry and assessment of bidirectional photometric properties of complex fenestration systems. Energy and Buildings 38 (7), 836–848.

Athienitis, A.K., Tzempelikos, A., 2002. A methodology for simulation of daylight room illuminance distribution and light dimming for a room with a controlled shading device. Solar Energy 72 (4), 271–281.

Awbi, H., 2008. Ventilation systems - Design and performance.

Beale, S.B., 1997. Tube banks, Single-phase heat transfer. International Encyclopedia of Heat and Mass Transfer. CRC Press Inc.

Bekö, G., Clausen, G., Weschler, C.J., 2008. Is the use of particle air filtration justified? Costs and benefits of filtration with regard to health effects, building cleaning and occupant productivity. Building and Environment 43 (10), 1647–1657.

Bekö, G., Fadeyi, M.O., Clausen, G., Weschler, C.J., 2009. Sensory pollution from bag-type fiberglass ventilation filters: Conventional filter compared with filters containing various amounts of activated carbon. Building and Environment 44 (10), 2114–2120.

Clarke, J., Janak, M., 1998. Simulating the thermal effects of daylight-controlled lighting. In: anonymous (Ed.), Building Performance (BEPAC UK).

Colburn, A.P., 1964. A method of correlating forced convection heat-transfer data and a comparison with fluid friction. International Journal of Heat and Mass Transfer 7 (12), 1359–1384.

Comsol, 2010. Comsol Multiphysics 2010.

Cox, T., Cox, M., 2001. Multidimensional scaling, 2nd Edition. Chapman Hall/CRC.

Crawley, D.B., Lawrie, L.K., Pedersen, C.O., Strand, R.K., Liesen, R.J., Winkelmann, F.C., Buhl, W.F., Huang, Y.J., Witte, M.J., Henninger, R.J., Glazer, J., Fisher, D.E., Shirey, D., 2002. Energyplus: New, capable and linked. In: anonymous (Ed.), esim. pp. 244–251.

de Gids, W., 2001. Hybrid ventilation concepts, classification and challenges. In: anonymous (Ed.), HybVent Forum 01. IEA Annex 35.

Delsante, A., Vik, T.A., 2002. Hybrid ventilation - State-of-the-art review. IEA Annex 35.

EBST, 2010. Danish Building Code 2010 (05-04-2010).

EN15251, 2007. Indoor environmental input parameters for design and assessment of energy performance of buildings addressing indoor air quality, thermal environment, lighting and acoustics. European StandardNot read.

EPBD, 2010. Energy Performance Building Directive 2010 (29-03-2010).

Equa, 2010. IDA ICE.

ESRU, 2008. ESP-r.

Fracastoro, G.V., Perino, M., Mutani, G., 2002. A simple tool to assess the feasibility of hybrid ventilation systems. Tech. rep., IEA Annex 35.

Franzetti, C., Fraisse, G., Achard, G., 2004. Influence of the coupling between daylight and artificial lighting on thermal loads in office buildings. Energy and Buildings 36 (2), 117–126.

Førland-Larsen, A., Tranholm, G.T., Hagelskjær, S., 2009. Hybridventilation er fremtiden i kontorbygninger. HVAC magasinet 45, 52–55.

Heikkinen, J., Heinonen, J.S., Laine, T., Liljeström, K., Vuolle, M., 2002. Performance simulation of hybrid ventilation concepts. Tech. rep., IEA Annex 35.

Heiselberg, P., 2002. Principles of Hybrid Ventilation. Hybrid Ventilation Centre.

Horvat, A., Leskovar, M., Mavko, B., 2006. Comparison of heat transfer conditions in tube bundle cross-flow for different tube shapes. International Journal of Heat and Mass Transfer 49 (5-6), 1027–1038.

Høseggen, R., Mathisen, H.M., Hanssen, S.O., 2009. The effect of suspended ceilings on energy performance and thermal comfort. Energy and Buildings 41 (2), 234–245.

Huizenga, C., Arasteh, D., Curcija, D., Klems, J., Kohler, C., Mitchell, R., Yu, T., 2007. Window 6.1 Research Version.

Hviid, C.A., Nielsen, T.R., Svendsen, S., 2008. Simple tool to evaluate the impact of daylight on building energy consumption. Solar Energy 82 (9), 787–798.

Hviid, C., Svendsen, S., 2010a. Analytical and experimental analyses of a low-pressure loss heat exchanger suitable for passive ventilation. Submitted to Energy and Buildings.

Hviid, C., Svendsen, S., 2010b. Detailed whole-year simulation of a building integrated ventilation concept with heat recovery and night cooling for low-energy offices. Submitted to Energy and Buildings.

Hviid, C., Svendsen, S., 2010c. Experimental and numerical analysis of perforated suspended ceilings as diffuse ventilation air inlets. Submitted to Energy and Buildings.

Hviid, C., Svendsen, S., 2010d. A morphological method for investigation of the problem complex of choosing the ventilation system for a new building. Submitted to Building and Environment.

ISO7730, 1994. Moderate thermal environments - Determination of the PMV and PPD indices and specification of the conditions for thermal comfort. International Standard.

Jacobs, P., van Oeffelen, E.C., Knoll, B., 2008. Diffuse ceiling ventilation, a new concept for healthy and productive classrooms. In: anonymous (Ed.), Indoor Air.

Jacobsen, L., 2008. Air motion and thermal environment in pig housing facilities with diffuse inlet. Ph.d., Aalborg University.

Jacobsen, L., Nielsen, P.V., Morsing, S., 2004. Prediction of airflow patterns in livestock buildings ventilated through a diffuse ceiling. In: anonymous (Ed.), Roomvent.

Jakubowska, E., 2007. Air distribution in rooms with diffuse ceiling inlet. M.sc., Aalborg University.

Jenkins, D., Newborough, M., 2007. An approach for estimating the carbon emissions associated with office lighting with a daylight contribution. Applied Energy 84 (6), 608–622.

Jeong, Y., Haghighat, F., 2002. Modeling of a hybrid-ventilated building. Journal of Ventilation 1 (2), 127–139.

Khan, W.A., Culham, J.R., Yovanovich, M.M., 2006. Optimal design of tube banks in crossflow using entropy generation minimization method. In: anonymous (Ed.), 44th AIAA Aerospace Sciences Meeting and Exhibit.

Klimatechnik, A.D., 1986. Handbuch der Klimatechnik band 2: Berechnung und Regelung. Handbuch der Klimatechnik.

Kruskal, J., 1964. Multidimensional scaling by optimizing goodness of fit to a nonmetric hypothesis. Psychometrika 29, 1–27.

Larsen, T.S., Jensen, R.L., Kalyanova, O., Heiselberg, P., 2006. Indeklimaundersøgelser hos Københavns Energi. Tech. rep., Aalborg Universitet.

LBNL, 2010. Building Design Advisor.

Lee, E.S., DiBartolomeo, D.L., Selkowitz, S.E., 1998. Thermal and daylighting performance of an automated venetian blind and lighting system in a full-scale private office. Energy and Buildings 29 (1), 47–63.

Lee, E., Khan, J.A., Feigley, C.E., Ahmed, M.R., Hussey, J.R., 2007. An investigation of air inlet types in mixing ventilation. Building and Environment 42 (3), 1089–1098.

Lehar, M.A., Glicksman, L.R., 2007. Rapid algorithm for modeling daylight distributions in office buildings. Building and Environment 42 (8), 2908–2919.

Li, Y., Delsante, A., Chen, L., 1999. Integrating thermal stratification in natural and hybrid ventilation analysis. In: anonymous (Ed.), HybVent Forum 99. IEA Annex 35.

Meinhold, U., Rösler, M., 2002. Hybrid ventilation in the Bertolt-Brecht Gymnasium - Results of the monitoring phase. In: anonymous (Ed.), HybVent Forum 02. IEA Annex 35.

MIT, 2010. The Design Advisor. Massachusetts Institute of Technology.

Nielsen, P.V., Jakubowska, E., 2009. The performance of diffuse ceiling inlet and other room air distribution systems. In: anonymous (Ed.), Cold Climate HVAC 2009.

Nielsen, P.V., Jensen, R.L., Rong, L., 2010. Diffuse ceiling inlet systems and the room air distribution. In: anonymous (Ed.), Clima 2010, 10th REHVA World Congress. Rehva.

Nielsen, T.R., 2005. Simple tool to evaluate energy demand and indoor environment in the early stages of building design. Solar Energy 78 (1), 73–83.

Nielsen, T., Nielsen, T.R., Svendsen, S., 2005. Calculation of daylight distribution and utilization in rooms with solar shadings and light redirecting devices. In: anonymous (Ed.), 7th Symposium on Building Physics in the Nordic Countries. pp. 1011–1018.

Nilsson, P.E., 2003. Achieving the desired indoor climate - energy efficiency aspects of system design. Studentlitteratur.

Overgaard, L.L., Nørgaard, E., Jensen, S.Ø., Madsen, K.B., 2002. Komponenter til naturlig ventilation - Del 2 - Luft-til-væske varmeveksler. Tech. rep., Teknologisk Institut Energidivisionen.

Petersen, S., Svendsen, S., 2010. Method and simulation program for informed decisions in the early stages of building design. Energy and Buildings In press.

Quanjel, E., Zeiler, W., Borsboom, W., Spoorenberg, H., 2006. Integral design methodology for collaborative design of sustainable roofs. In: anonymous (Ed.), Passive and Low Energy Architecture, PLEA2006. pp. 195–200.

Ritchey, T., 2006. Problem structuring using computer-aided morphological analysis. Journal of the Operational Research Society 57 (7), 792–801.

SBi, 2008. Be06.

Schild, P.G., 2001. An overview of Norwegian buildings with hybrid ventilation. In: anonymous (Ed.), HybVent Forum 01. IEA Annex 35.

Schultz, J., Saxhof B., 1994. Natural ventilation with heat recovery. Air Infiltration Review 15, 9–12.

Seifert, J., Perschk, A., Rösler, M., Richter, W., 2001. Coupled air flow and building simulation for a hybrid ventilated educational building. Tech. rep., IEA Annex 35.

Seppänen, O., Fisk, W., Lei, Q., 2006. Ventilation and performance in office work. Indoor Air 16 (1), 28–36.

Shao, L., Riffat, S.B., Gan, G., 1998. Heat recovery with low pressure loss for natural ventilation. Energy and Buildings 28 (2), 179–184.

Skistad, H., Mundt, E., Nielsen, P.V., Hagström, K., Railio, J., 2002. Displacement ventilation in non-industrial premises. Rehva Guidebook 1.

Strachan, P.A., Kokogiannakis, G., Macdonald, I.A., 2008. History and development of validation with the ESP-r simulation program. Building and Environment 43 (4), 601–609.

Terkildsen, S., 2009. Udvikling af ventilationsanlæg med lavt elforbrug. M.sc., Technical University of Denmark.

Tjelflaat, P.O., 2000. Pilot study report: Mediå school, Grong, Norway. Tech. rep., IEA Annex 35.

Tzempelikos, A., Athienitis, A.K., 2007. The impact of shading design and control on building cooling and lighting demand. Solar Energy 81 (3), 369–382.

van der Aa, A., 2002. Costs of hybrid ventilation systems. Tech. rep., IEA Annex 35.

van Dijk, D., Oversloot, H., 2003. WIS, the European tool to calculate thermal and solar properties of windows and window components. In: anonymous (Ed.), IBPSA, Building Simulation. pp. 259–266.

Wachenfeldt, B.J., 2003. Natural ventilation in buildings - Detailed prediction of energy performance. Ph.d., Norwegian University of Science and Technology.

Walkenhorst, O., Luther, J., Reinhart, C., Timmer, J., 2002. Dynamic annual daylight simulations based on one-hour and one-minute means of irradiance data. Solar Energy 72 (5), 385–395.

Ward, G.L., Shakespeare, R.A., 1998. Rendering with Radiance - The art and science of lighting visualization, 2nd Edition. Morgan Kaufmann.

Wargocki, P., Djukanovic, R., 2005. Simulations of the potential revenue from investment in improved indoor air quality in an office building. ASHRAE Transactions - Technical and Symposium Papers presented at the 2005 Annual Meeting of the American Society of Heating, Refrigerating and Air-Conditioning Engineers and ASHRAE Transactions 111 PART 2, 699–711.

Wargocki, P., Wyon, D.P., Wargocki, P., 2007a. The effects of moderately raised classroom temperatures and classroom ventilation rate on the performance of schoolwork by children (RP-1257). HVAC and R Research 13 (2), 193–220.

Wargocki, P., Wyon, D.P., Wargocki, P., 2007b. The effects of outdoor air supply rate and supply air filter condition in classrooms on the performance of schoolwork by children (RP-1257). HVAC and R Research 13 (2), 165–191.

Wienold, J., Christoffersen, J., 2006. Evaluation methods and development of a new glare prediction model for daylight environments with the use of CCD cameras. Energy and Buildings 38 (7), 743–757.

Wouters, P., Heijmans, N., Delmotte, C., Vandaele, L., 1999. Classification of hybrid ventilation. In: anonymous (Ed.), Hybvent Forum. IEA Annex 35.

Zeiler, W., Savanovic, P., Borsboom, W., 2006. Integral design workshop for sustainable comfort systems to improve ventilation concepts. In: anonymous (Ed.), Healthy Buildings. pp. 131–136.

Zhukauskas, A., 1972. Heat Transfer from Tube in Cross Flow. Vol. 8 of Advances in Heat Transfer. Academic Press.

Zwicky, F., 1969. Discovery, invention, research - through the morphological approach. The Macmillan Company.

Appendix A

Industrial PhD programme

In the industrial PhD programme the student is employed by a company, and timeshares 50/50 between university and the company. Approx. 50% of the company's expenses are reimbursed by the Ministry of Science, Technology and Innovation. The student is enrolled in a Ph.D. graduate school at a University with the same requirements as for an ordinary Ph.D. In addition the industrial Ph.D. must complete a business course and a business report that reflects on the commercial aspects of the project. Teaching obligations are not required by the industrial Ph.D. programme, but the obligations regarding disseminating knowledge are the same as for en ordinary Ph.D. The purpose of the Industrial Ph.D. programme is to educate scientists with an insight in the commercial aspects of R&D, increase R&D and innovative capacity in private companies and to build networks disseminating knowledge between universities and private companies.

Appendix B

Published or submitted papers

Paper I

Published in Solar Energy, 2008

Available online at www.sciencedirect.com
ScienceDirect
Solar Energy 82 (2008) 787–798
SOLAR ENERGY
www.elsevier.com/locate/solener

Simple tool to evaluate the impact of daylight on building energy consumption

Christian Anker Hviid [a,b,*], Toke Rammer Nielsen [b], Svend Svendsen [b]

[a] Alectia AlS, Teknikerbyen 34, DK-2830 Virum, Denmark
[b] Department of Civil Engineering, Brovej Building 118, Technical University of Denmark, DK-2800 Kgs. Lyngby, Denmark

Received 29 January 2007; received in revised form 16 February 2008; accepted 6 March 2008
Available online 3 April 2008

Communicated by: Associate Editor J.-L. Scartezzini

Abstract

This paper presents a simple building simulation tool for integrated daylight and thermal analysis. The tool is capable of importing the thermal and visual properties for different glazings and shading positions from the Window Information System (WIS) program. A coupled ray-tracing and radiosity methodology is used to derive the daylight levels for different sky conditions. Both detailed daylight distribution for a particular day and time and hourly discrete values on a yearly basis may be obtained. For an integrated simulation the hourly daylight levels are fed into an existing simple thermal simulation program capable of calculating energy demand and the indoor environment. Straightforward control systems for general and task lighting systems have been implemented together with a shading control strategy that adjusts the shading according to the indoor operative temperature, the risk of glare and the profile angle of the sun. The implemented daylight calculation method allows for shades from the window recess and overhang, and for distant shades blocking the sky vault. Comparisons with the ray-tracing program Radiance show that the accuracy of this approach is adequate for predicting the energy implications of photoresponsive lighting control. The amount of input is small, which makes the tool useful for integrated daylight optimisation in the early design process.

Keywords: Simulation; Daylight; Validation; Radiosity; Integrated design; Building design

1. Introduction

Energy performance and indoor environment have become increasingly important in building design. Building developers and designers are straining to produce end-user buildings with a low energy consumption and high indoor environmental performance. This has lead to a growing awareness that to achieve low energy buildings with satisfactory indoor climate the designer has to be aware of the consequences of critical design decisions as early as possible in the design process to obtain a good final whole-building cost-benefit ratio (Petersen and Svendsen, submitted for publication). In this context, integrated simulation of daylighting and artificial lighting plays a significant role on energy consumption, indoor environment and environmental impact as the fenestration system influences heat loss, solar gains and daylight penetration (Lee et al., 1998; Jenkins and Newborough, 2007; Tzempelikos and Athienitis, 2007).

Sparked by innovations in dynamic fenestration and shading systems and increasingly sophisticated characterizations of glazings and shading devices (van Dijk and Oversloot, 2003; Andersen and de Boer, 2006; Window 6.1 Research Version, 2007) some detailed simulation programs like ESP-r (University of Strathclyde, 2008), and EnergyPlus (US Department of Energy, 2008) now link daylight and thermal simulation in an integrated manner (Clarke and Janak, 1998; Crawley et al., 2002). However,

* Corresponding author. Tel.: +45 8819 1365; fax: +45 4588 4578.
E-mail address: crh@alectia.com (C.A. Hviid).

0038-092X/$ - see front matter © 2008 Elsevier Ltd. All rights reserved.
doi:10.1016/j.solener.2008.03.001

Nomenclature

A	area, m^2
E	illuminance, lm m^{-2} (lux)
d	slat distance, m
dh	diffuse horizontal illuminance, lm m^{-2} (lux)
L	luminance, lm m^{-2} Sr^{-1}
lv	relative luminance
m	total number of subsurfaces
Mo	exitance, lm m^{-2} (lux)
w	slat width, m
α	azimuth, rad
β	slat angle, rad
γ	elevation, rad
η	luminous efficacy, lm W^{-1}
θ	profile angle, rad
ξ	angle of incidence, rad
ρ	reflectance
σ	visible proportion
τ	visual transmittance
χ	normalization factor
Φ	solid angle, Sr

Indices

Build	opposing building
cut-off	angle that cuts off direct light
dir	direct light
dir → dif	diffused direct light
redir	redirected light
g	glazing
ground	ground vault
n	normal
sky	sky vault
sun	solar disc
v	vertical

to run these programs they require expert knowledge and large amounts of input data for even the simplest simulation, rendering them impractical in the early design stage when information is scarce. This calls for tools that are capable of rapid and dynamic calculation of the impact of fenestration and shading provisions on lighting demand, cooling demand and occupant glare.

Such rapid whole-year algorithms are starting to emerge (Lehar and Glicksman, 2007; Walkenhorst et al., 2002), but they still lack interactivity with the thermal domain. Franzetti et al. (2004) implemented a daylighting software module with a thermal model, but the validity of the model was restricted to internal working plane illuminances below 1000 lux. Athienitis and Tzempelikos (2002) developed an integrated model based on clear and overcast sky formulations for external illuminances and radiosity for internal illuminances. This approach, however, assumes that direct light is diffused in the shading devices and that incident diffuse light on the outside of the window is transmitted uniformly. The tool described in this article employs the radiosity method for internal daylight reflections, while the incident initial light is calculated by tracing the rays emanating from the sky to the room surfaces. This gives a reasonable balance between accuracy and calculation time.

The tool encompasses a fully integrated thermal and daylighting simulation with detailed hourly output of the daylight level, the electrical energy consumption for lighting, heating load, cooling load and indoor operative temperature. The main objective is to help design professionals with interest in – but no expert knowledge of – daylighting to develop climate-responsive daylighting design concepts, to optimize façade layout and orientation with respect to daylight and energy use and to quantify energy savings from manual and photocell controlled dimming. The amount of input is small which renders the tool practical in the early stages of design or as simulation foundation for an integrated design process where it is essential to quantify and create awareness of the consequences of design decisions (Petersen and Svendsen, submitted for publication).

An existing simplified thermal simulation tool BuildingCalc (Nielsen, 2005) and a daylight simulation tool LightCalc (Nielsen et al., 2005) formed the starting point for the work, the BC/LC tool. In the following, the implemented sky model and algorithms for externally and internally reflected light are described together with the shading control strategy and the coupling procedure. The daylight simulation tool is validated by comparison with Radiance (Ward and Shakespeare, 1998) and the impact on energy demand is discussed.

2. Calculation procedures

2.1. External light distribution

External daylight may be divided into direct light from the solar disc, diffuse light due to the scattering properties of the atmosphere, and diffuse light reflected from the ground and surroundings.

The diffuse light is modelled using the approach in Robinson and Stone (2006) and summarized here.

An upper sky dome for atmospheric light and a lower (inverted) sky dome for ground reflections (one above and one below the horizontal plane) are used to model diffuse light. Each sky vault is divided into 145 patches using a discretization scheme proposed by Tregenza (1987). Each patch subtends a similar solid angle Φ (Sr), which enables every patch to be treated as a point source with insignificant error. The sky vault is divided into seven azimuthal

bands of equal angular height ($\sin\gamma_{i,\max}$–$\sin\gamma_{i,\min}$), in which the azimuthal range $\Delta\alpha$ increases towards zenith (12°, 12°, 15°, 15°, 20°, 30°, 60°).

$$\Phi_i = \Delta\alpha_i(\sin\gamma_{i,\max} - \sin\gamma_{i,\min}) \tag{1}$$

Let L be the luminance (lm m^{-2} Sr^{-1}) of the ith patch, ξ the mean angle of incidence (rad), σ ($0 \leqslant \sigma \leqslant 1$) the visible proportion of the patch, then the illuminance E_{sky} on an external plane due to diffuse light from the sky vault is expressed as

$$E_{\text{sky}} = \sum_{i=1}^{145}(L\Phi\sigma\cos\xi)_i \tag{2}$$

Let E_{n} be the direct normal illuminance and ξ the incidence angle, then the illuminance on an external inclined plane due to direct light is

$$E_{\text{sun}} = E_{\text{n}}\cos\xi \tag{3}$$

Having determined the light sources, the reflecting ground can be represented as a luminous up-side down sky with constant brightness. Let L^* be the ground patch luminance, then the illuminance due to reflected light E_{ground} is expressed as

$$E_{\text{ground}} = \sum_{j=i}^{145}(L^*\Phi\sigma\cos\xi)_j \tag{4}$$

where L^* is expressed as a function of the total horizontal diffuse illuminance E_{sky} and the direct illuminance E_{sun} on a horizontal plane and the mean ground reflectance ρ (albedo)

$$L^* = \frac{\rho}{\pi}(E_{\text{sun}} + E_{\text{sky}}) \tag{5}$$

Fig. 1 shows the principle of how the luminosity of the sky may vary while the ground luminosity is uniform.

The European Solar Radiation Atlas (Scharmer and Greif, 2000) recommends the use of the Perez all-weather model (Perez et al., 1993) or the Muneer model (Muneer et al., 1998) for modeling anisotropic sky radiation. The Perez model is chosen because it is amenable to implementation in a computer program while maintaining good overall performance. The luminance of a sky point L_i is given here:

$$L_i = \frac{lv_i\text{dh}}{\sum_{j=1}^{145}(lv\Phi\cos\xi)_j} \tag{6}$$

where the relative luminance, lv, defined as the ratio between the luminance of the considered sky point and the luminance of an arbitrary reference sky point (usually the zenith luminance), is normalized to diffuse horizontal illuminance dh as recommended by Perez et al. (1993). Diffuse horizontal and direct normal illuminances are obtained from measured horizontal and direct normal irradiances, respectively by a luminous efficacy η given in Perez et al. (1990).

The visible proportion σ is calculated by establishing a 10×10 grid of each patch and evaluating the visibility of each grid point for every internal surface. The incidence angle ξ is calculated from the weight-averaged visible proportion of the sky patch. Thus, σ is a function of both distant objects (other buildings, the landscape) and near shades like the window recess and overhang.

Reflected light from opposing building façades is treated in two ways. For building surfaces below the horizontal plane, their reflectances are part of the average albedo. For buildings that cover parts of the upper sky dome, the algorithms for incident light on inclined surfaces in Perez et al. (1990) are used. The incident light on the opposing building surface E_{build} is then multiplied by the specified reflectance of the building ρ_{build} ignoring any specular effects or interfaçade reflections. The sky patch luminance L_i' then substitutes the luminance of the covered patch with respect to the visible proportion σ: $L_i' = L_i\sigma_i + E_{\text{build}}\rho_{\text{build}}(1-\sigma_i)$. Thus, only one 'bounce' of light is taken into consideration and we ignore the interreflections that deep urban canyons produce.

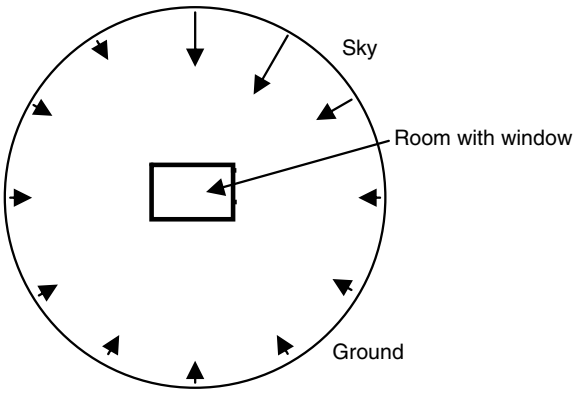

Fig. 1. Room with window surrounded by sky hemisphere and ground hemisphere. Above the horizon the sky model luminosity is applied, below the ground a constant luminosity is applied.

2.2. Internal daylight distribution

The calculation of the internal distribution of light was based on the luminous exitance method. This method is analogous to the radiosity method, in that all the restrictions and assumptions are the same. Internal subsurfaces hit by transmitted direct and diffuse light act as light sources with the initial exitance Mo, if we assume these surfaces have Lambertian optical characteristics and reflect incident light perfectly diffusively and ignore any specular properties. The methodology and implementation of the daylight distribution algorithms are described in Park and Athienitis (2003).

2.3. Coupling of external and internal light distribution

2.3.1. Diffuse light

To establish the initial light exitance Mo (lm m^{-2}) of a subsurface the amount and the direction of the light and

the reflectance of the surface have to be known. Therefore, the external and internal light distributions were coupled in a simple ray-tracing approach that assumes the luminance of the sky hemisphere and ground hemisphere patches can be considered as point sources.

For diffuse sky and ground light penetrating into the room, the exitance for each kth internal subsurface was calculated using (2) and (4) multiplied by the light transmittance τ and the surface reflectance ρ:

$$\mathrm{Mo}_k = \rho_k \left(\sum_{i=1}^{145} (L \Phi \sigma \cos \xi \tau)_i + \sum_{j=1}^{145} (L^* \Phi \sigma \cos \xi \tau)_j \right) \tag{7}$$

The light transmittance is calculated by the WIS program (WinDat, 2006), see Section 2.4, but WIS only calculates uni-directional, profile angle dependent transmittances. The profile angle θ is defined as the line of elevation (usually to the sun) projected unto the vertical normal plane of a surface. We may also name it the perpendicular incidence angle on a vertical surface. For clear glazings and shading systems with isotropic optical properties we use the profile angle dependent transmittances directly with corresponding incidence angles. For anisotropic optical shadings like blinds we multiply the transmittance with the profile angle so τ is replaced with τ_θ in (7) and (8).

2.3.2. Direct light

For direct solar light a different approach is applied. It is evident that all direct light transmitted through the glazing hits a subsurface. Subdividing the internal surfaces however may result in false prediction of the amount of incoming direct light. Let E_{dir} denote the incident sun light on the window plane obtained by (3), A_g the glazing area, A_k the area of the kth internal subsurface and m the total number of internal subsurfaces. If we define a normalization factor $\chi = E_{\mathrm{dir}} A_g \tau / \sum_{k=1}^{m} E_n A_k \tau \cos \xi_k$ then the initial exitance Mo of the kth subsurface is written:

$$\begin{aligned} \mathrm{Mo}_k &= E_n \rho_k \tau \cos \xi_k \chi \\ &= E_{\mathrm{dir}} A_g \rho_k \tau \cos \xi_k \left(\sum_{k=1}^{m} A_k \cos \xi_k \right)^{-1} \end{aligned} \tag{8}$$

When the direct light is transmitted through the glazing, some of the direct light may be transformed into diffuse light in a diffusing device, e.g. blinds placed in conjunction with the glazing. This effect is taken into consideration by calculating the light contribution from sun, sky, and ground on the window plane by using (2)–(4). The exitance of the inner glazing surface Mo_g is determined by multiplying the total light contribution by the light transmittance for direct light that diffuses when it passes the glazing + shading: $\tau_{\mathrm{dir}\to\mathrm{dif}}$. This light transmittance is calculated by WIS, see Section 2.4.

$$\mathrm{Mo}_g = (E_{\mathrm{dir}} + E_{\mathrm{sky}} + E_{\mathrm{ground}}) \tau_{\mathrm{dir}\to\mathrm{dif}} \tag{9}$$

Devices that redirect the incoming light, e.g. a specular light shelve are modelled using a simple implementation. It is achieved by setting a special redirecting light transmittance τ_{redir} to a value between 0 and 1 where 0 means that no light is redirected and 1 that all incoming light is redirected. This means that for an incoming ray of light with a profile angle θ the following applies: $\tau_\theta + \tau_{\mathrm{dir}\to\mathrm{dif},\theta} + \tau_{\mathrm{redir},\theta} = 1$. The inclination angle β of the slat or light shelve determines the reflection angle. Only fully specular devices are considered and any specular interreflections between slats and between the slats and glazing are ignored. In Fig. 2, the principle is illustrated.

2.4. Light transmittances

A critical element in the daylight calculation routine is the light transmittance of the combined glazing/shading system. For this purpose the European software tool called WIS (WinDat, 2006; van Dijk and Oversloot, 2003) is used. This tool implements algorithms from the standard ISO 15099 (ISO, 2003) capable of calculating the light transmittance of a transparent system for both direct and diffuse light.

WIS calculates the thermal and solar performance of multilayered window systems, allowing the user unlimited combinations of glazing and solar shading devices. This makes WIS a very powerful tool for evaluating various integrated daylight designs. Currently, the improvement and verification of WIS, and its database format and database population are the responsibility of the EU Thematic Network WinDat, which consists of major European research institutions and manufacturers of window components (glazings, solar shadings, etc.).

The output from a WIS calculation is in the format of a text file. The file include the light transmittances and solar energy transmittances for different solar profile angles

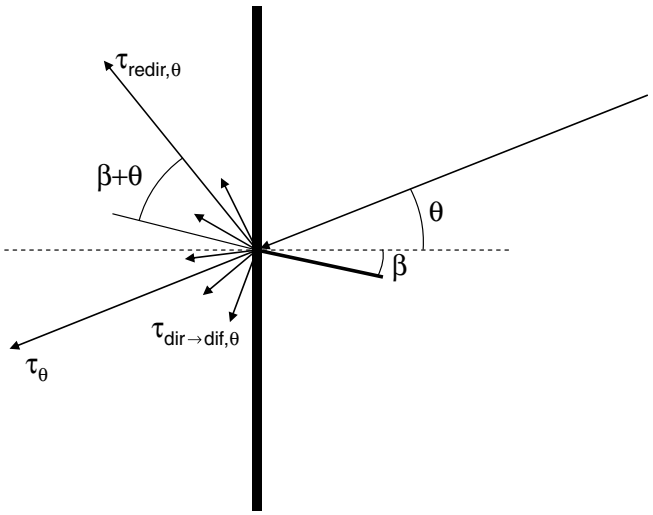

Fig. 2. Illustration of how an incoming ray of light from the sky, sun or ground is transmitted directly, diffused in the combined glazing and shading system, or redirected specularly with equal angle of incidence and reflection.

(−90–90° at 10° increments), and may be loaded seamlessly into the BC/LC tool. If the shading device has multiple shading positions, e.g. Venetian blinds, the user may generate and load files for every position required. The tool will linearly interpolate between the transmittance data loaded, thus making the number of loaded positions a question of desired accuracy.

Because the employed method of calculating incident light on internal subsurfaces is equivalent to a ray-tracing technique, the WIS transmittance for direct light is employed for both diffuse and direct light. WIS cannot yet handle specular shading devices, e.g. light shelves or light redirecting devices. The tool described in this article, however, accepts transmittance data for redirecting devices obtained in other ways, e.g. from Radiance.

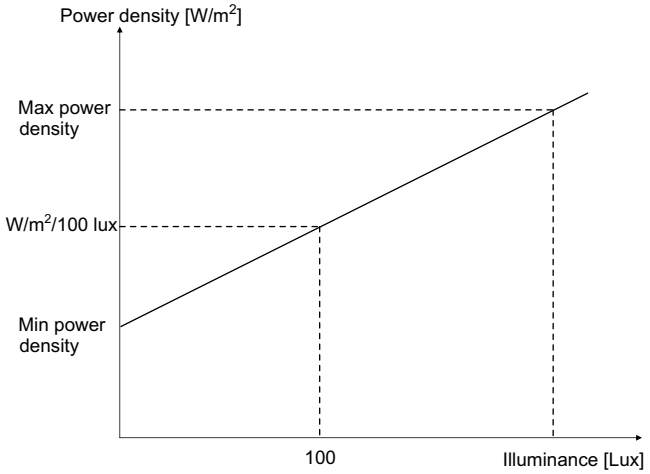

Fig. 3. Definition of illuminance and power density relationship for lighting systems in the BC/LC tool.

3. Control strategies

3.1. Thermal simulation

The simplified thermal model in the BC/LC tool is described in detail in Nielsen (2005). It is capable of evaluating the thermal indoor environment and heating and cooling loads in a building with very few input parameters while providing the option of sophisticated system controls. The model is based on a two-nodal equation system with one node representing the air temperature and one the internal temperature of the constructions. The mean surface temperature represents the internal surfaces where heat is exchanged with the indoor air and the effective heat capacity of the constructions. The equation system has an analytical solution and by the end of each time step the temperatures are calculated based on the initial temperatures of the time step. The systems control strategy is ideal yet satisfactory for quick design suggestions. During each time step systems are activated to control the risk of glare and the indoor air temperature which changes the analytical solution and causes the equation system to be solved several times within a time step to achieve a given setpoint.

3.2. Artificial lighting

The artificial lighting system can be divided into general and task lighting which may be defined and controlled separately. Both systems are defined by the power consumption of the lighting fixtures in W/m^2 when providing an illuminance of 100 lux, and the minimum (standby) power consumption. The relationship between power consumption and illuminance on the workplane is assumed to be linear and is depicted in Fig. 3. The values for power density and corresponding illuminance are often supplied by the producers of lighting fixtures, and the maximum illuminance is calculated using the maximum power density.

For each time profile, the implemented control strategies are 'always on', 'always off', 'on-off', and 'dimming'. The tool evaluates the hourly incoming daylight at two arbitrary points determined by the user and switches the lighting systems on and off or dims them according to the chosen lighting control strategy. The 'on-off' control switches between the maximum and minimum power consumption when the daylight level is below or above the illuminance setpoint. The 'dimming' control interpolates linearly between the maximum and minimum power consumption in order to meet the specified setpoint. Electrical losses in the ballast must be included in the power density.

3.3. Shading

The task of the shading in an office room is multipurpose: it should block direct sunlight to minimize the risk of glare and high contrasts which are discomforting to the occupants while allowing the maximum amount of daylight to enter the room on overcast days. At the same time it should block excessive solar gains to avoid overheating

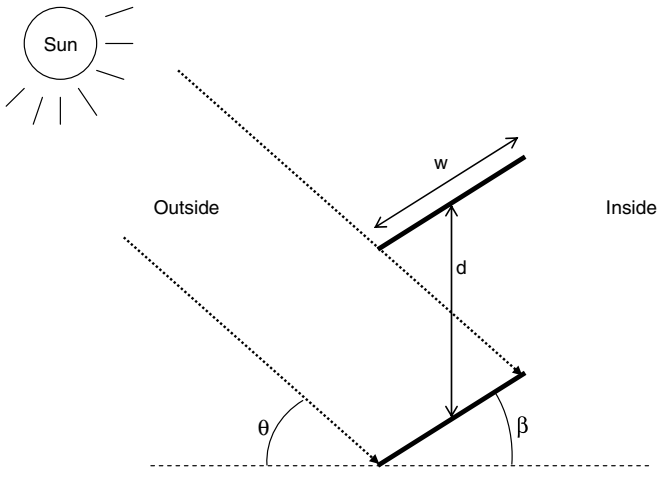

Fig. 4. Illustration of the cut-off shading control strategy for adjustable slats. Sun is projected unto the plane perpendicular to the window plane.

while preserving a good view to the outside. Some shading devices are also capable of controlling and redirecting the incoming direct sunlight and pass it on to the room as diffuse light. To accommodate the various demands the BC/LC tool is provided with a shading control based on a two-conditional strategy and the cut-off angle.

When any of the two conditions: indoor operative temperature or risk of glare are exceeded the cut-off strategy is activated. In the case of adjustable blinds they are lowered and adjusted to the slat angle where the direct sun is just blocked, see Fig. 4. This strategy maximizes the incoming amount of daylight while blocking the main contributor to glare and indoor overheating. In the case of screens the control is limited to screen up or screen down. The cut-off angle β is calculated from:

$$\beta_{\text{cutoff}} = \arcsin\left(\frac{d\cos\theta}{w}\right) - \theta \tag{10}$$

The distance between two slats is defined by d (m), θ is the profile angle of the sun (°), and w is the width of the slats (m).

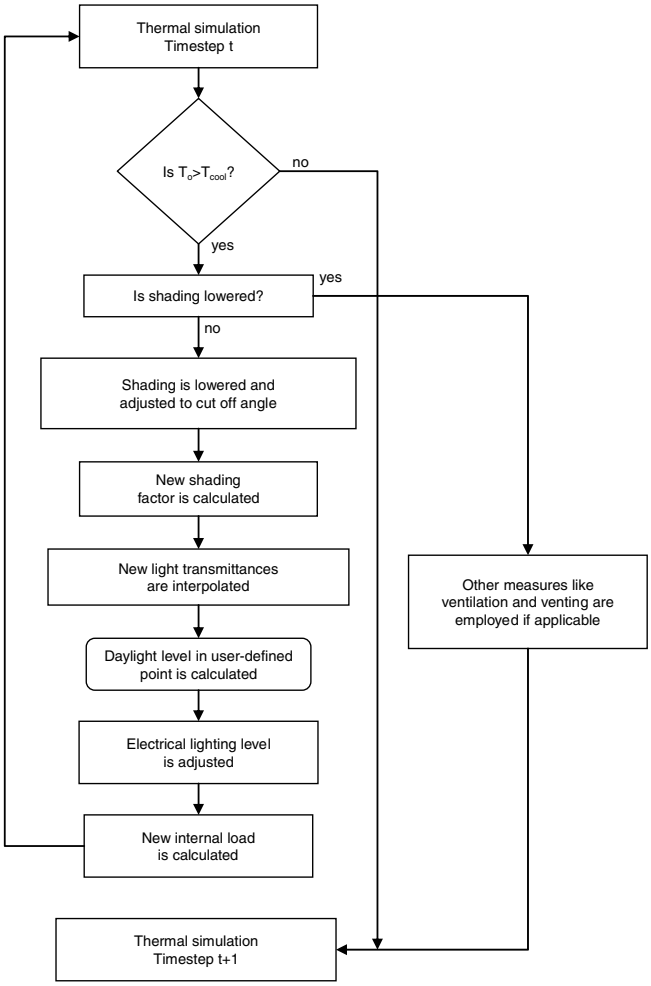

Fig. 5. Calculation procedure for the integrated daylight and thermal simulation.

3.4. Glare

To calculate the risk of glare we use a daylight glare probability index which is proposed by Wienold and Christoffersen (2006). The DGP index is defined in the interval [0.2; 0.8] and is directly correlated with the percentage of disturbed persons. According to Wienold and Christoffersen (2006) the correlation between the linear function of vertical eye illuminance and DGP is stronger than all other tested functions. If E_v denotes the vertical eye illuminance (lux), the daylight glare probability is then written:

$$\text{DGP} = 5.87 \times 10^{-5} E_v + 0.16 \tag{11}$$

This means that DGP values of 0.2 (20% disturbed) approximately corresponds to a vertical eye illuminance of 700 lux.

3.5. Thermal simulation coupling

The integration of the daylight and thermal domain requires a sophisticated coupling to calculate the incoming daylight, the effect of shading on daylight levels, and electrical lighting consumption and indoor air temperature. Fig. 5 gives a schematic overview of the coupling. The algorithm controls the shading device by linking the incoming daylight with the effect of shading on daylight levels, artificial lighting load and indoor air temperature. This is achieved by pre-calculating the hourly daylight levels in the room without shading, initiate the thermal simulation, evaluate the hourly indoor operative temperature with

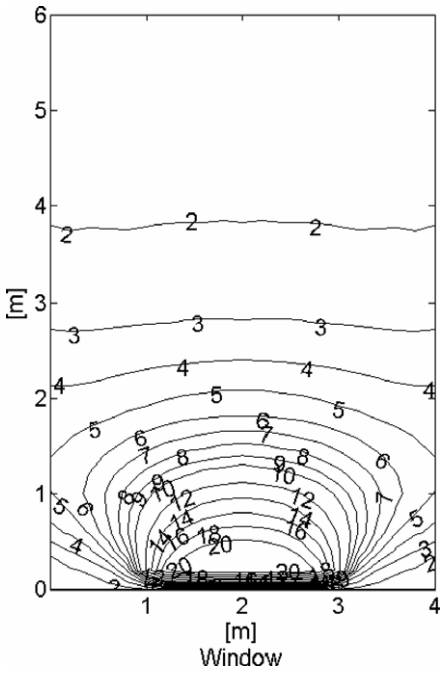

Fig. 6. Detailed daylight factor [%] distribution output from the BC/LC tool on a fictive working plane (0.85 m).

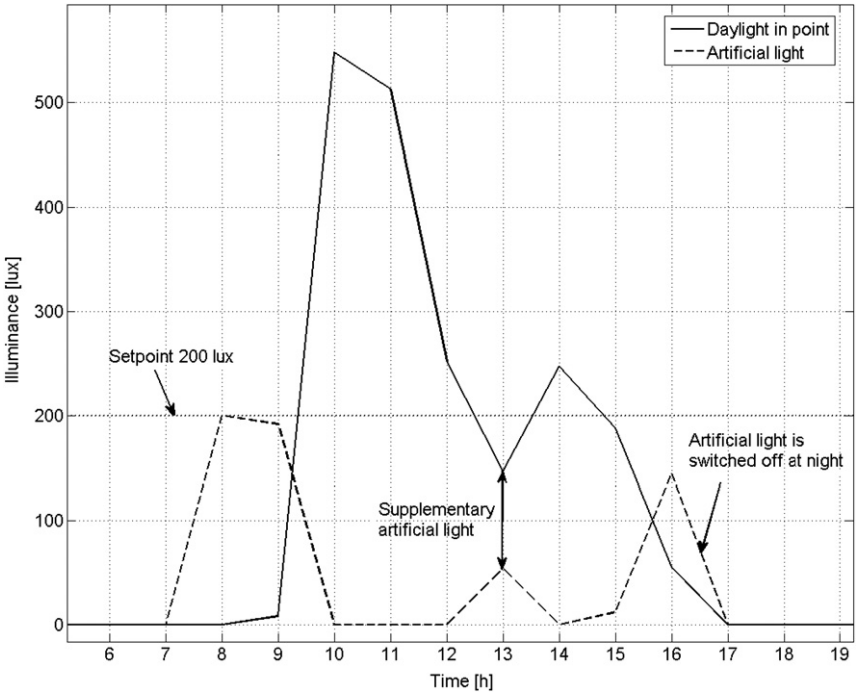

Fig. 7. The artificial general lighting system complements the daylight to reach a user-specified setpoint.

respect to the cooling setpoint, possibly lower the shading and adjust the slat angle (for blinds) to cut-off direct sunlight, and calculate the daylight levels again. If the operative temperature still exceeds the cooling setpoint, other measures like venting, increased ventilation, and mechanical cooling are employed in that order.

4. The tool

The tool may be used in two ways: (1) for detailed daylight distribution in a room for a particular day, time and sky luminance distribution and (2) coupled with the thermal domain to quantify the impact of daylight on the building energy consumption. An example of output from a detailed daylight simulation is depicted on Fig. 6 showing the daylight factor contour lines from a CIE standard overcast sky with internal subsurfaces the size of 0.5×0.5 m.

The output from a coupled simulation encompasses hourly values for the daylight level in two arbitrary points and the artificial lighting load together with results from the thermal domain: heating and cooling demand, ventilation airflow, indoor operative temperature, shading factor, PMV and PPD. The results are presented graphically in figures and by tables. Fig. 7 depicts some of the results from a coupled simulation. A whole-year simulation with retractable blinds takes approx. 6 min on a laptop with a Pentium M processor running at 1.86 GHz and 2 GB of RAM. The subsurface size was set to 2×2 m, because this has a significant impact on simulation speed and only introduces an error in the magnitude of 1% compared to 0.5×0.5 m. Fig. 7 shows how the tool can quantify the implications of exploiting daylighting and reducing the artificial lighting load with photoresponsive controls.

The tool is programmed in Matlab (MathWorks, 2008) and uses a graphical user interface to get input from the user and to provide results from simulations. Its simple input makes it easy and quick to estimate the impact on building energy consumption for different daylight and shading designs. The program exists both in a version to run in Matlab and a version to run as a windows program for people who do not have Matlab. The former includes all the source code while the latter requires the installation of Matlab runtime libraries. Both program versions are available from the web address <http://www.dtu.dk/centre/BFI/Fagomraader/energirigtigtbyggeri/integrateddesign.aspx> or by contacting the corresponding author.

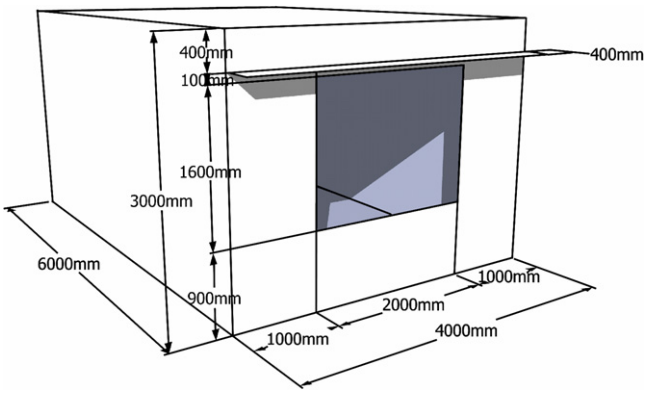

Fig. 8. Dimensions of the validated room.

Table 1
Data assumptions for validation

Room dimensions	Height × width × depth	3 m × 4 m × 6 m
Glazing	Height × width	1.6 m × 2.0 m
	Offset	Symmetrical, 0.9 m from floor
	Type	Double glazing with low-*E* coating (4-15Ar-SN4)
	Light transmittance ⊥	0.782 (transmissivity = 0.852) (void glass glazing 0 0 3 .852 .852 .852)
	Overhang	Length: 0.4 m, 0.1 m above window, reflectance: 0 Not used for CIE overcast sky validation
Shading devices	Blinds WIS code: WinDat #01	Slat width: 0.08 m, slat distance: 0.072 m Slat thickness: 0.5 mm No curvature, no specular properties Diffuse reflectance: 0.096 (void plastic blinds 0 0 5 .096 .096 .096 0 0)
	Screen WIS code: Verosol SilverScreen	Light transmittance: 0.0354 (void trans screen 0 0 7 1 1 1 0 0 0.0354 0.82)
Diffuse reflectances	Walls	0.7 (void plastic walls 0 0 5 .7 .7 .7 0 0)
	Ceiling	0.8 (void plastic ceiling 0 0 5 .8 .8 .8 0 0)
	Floor	0.3 (void plastic floor 0 0 5 .3 .3 .3 0 0)
	Glazing	0.215 (cannot be specified)
	Albedo	0.2 (-g option to gensky)
Calculation settings	Subsurface size	0.5 m × 0.5 m
Measuring points	11 half meter interval points along centre line of room	
Sky model	Perez anisotropic sky	

Radiance material properties in parentheses.

Table 2
Input parameters to Radiance simulation

Ambient bounces	Ambient division	Ambient sampling	Ambient accuracy	Ambient resolution	Direct threshold	Direct sampling
7	4096	2048	0.1	256	0.03	0.02
Mkillum options		-ab 4	-s 64	-d 96		

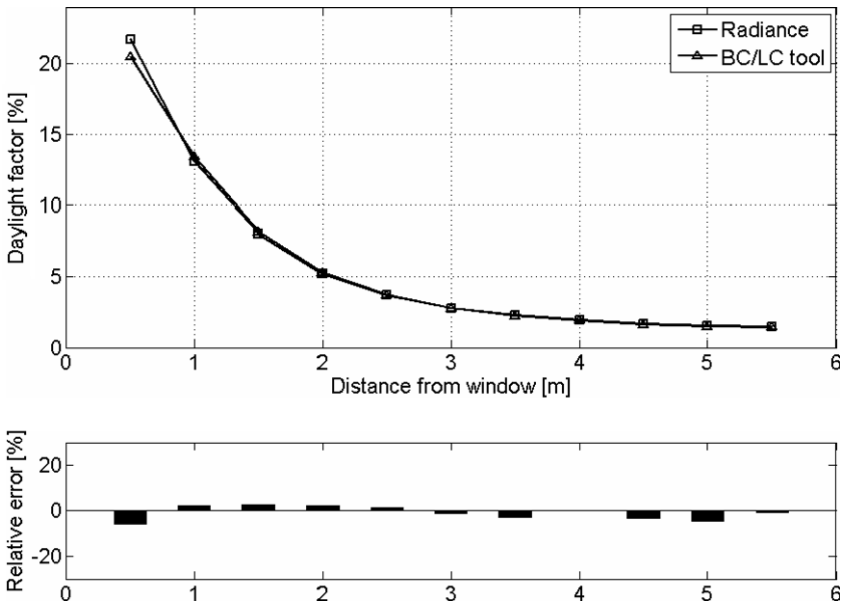

Fig. 9. Comparison of case with daylight factors from CIE standard overcast sky model and a clear double glazing with low-*E* coating.

5. Validation

Of the numerous lighting simulation programs available, Radiance has been extensively validated and repeatedly surpassed competing programs in terms of both functionality and accuracy. For these reasons, we chose Radiance as our reference model. It is a back-ward ray-tracer and was developed by Greg Ward at Lawrence Berkeley National Laboratories. It yields physically based simulations of indoor illuminance and luminance distributions for diffuse, specular and partly specular materials. We use the Radiance version 3.9 from the Learnix bootCD version 5.0.1 which is available from <http://luminance.londonmet.ac.uk/learnix/>. The validation was carried out with four setups: clear glazing, blinds, screen and opposite building façade. All four setups are validated with the anisotropic Perez sky model because it is used for the coupled simulations, but we also test the CIE standard overcast sky on a clear glazing because it is often used to quantify daylight design. The Perez sky is generated with the gendaylit package for Radiance developed by Delaunay (1994).

The test room has a south facing window and dimensions as specified on Fig. 8. The selected date for the anisotropic Perez sky is September the 21st at 3 p.m. because it

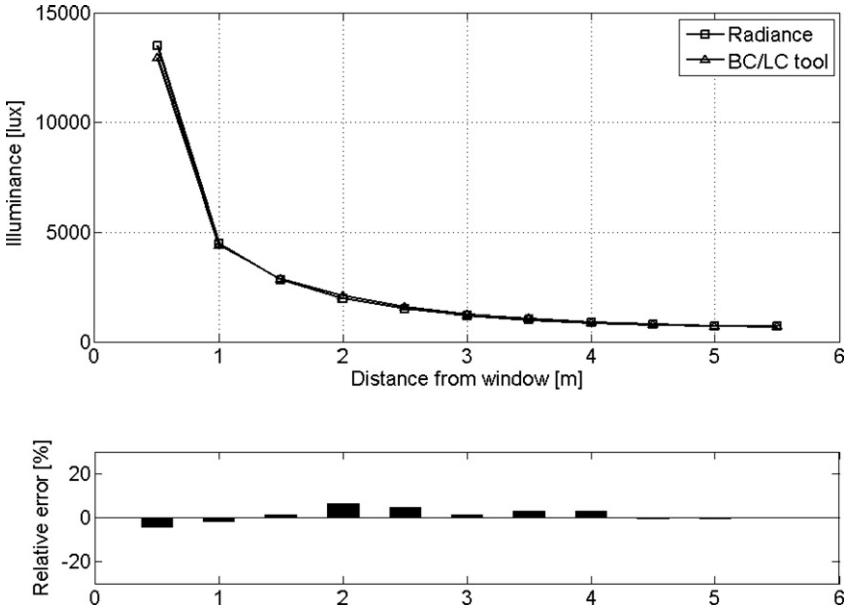

Fig. 10. Comparison of case with clear double glazing and the Perez sky model.

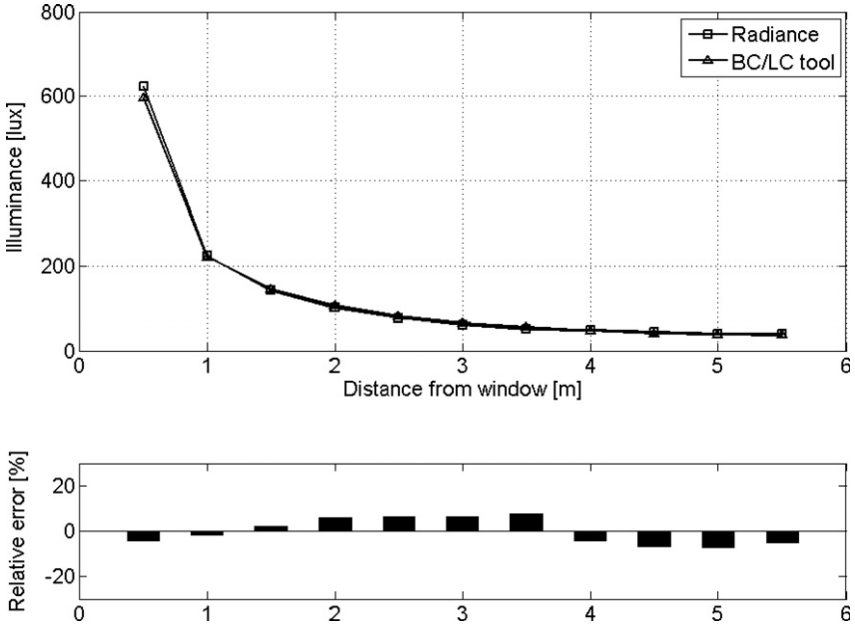

Fig. 11. Comparison of case with screen lowered.

involves complex calculation of solar position, incidence angles and cut-off slat angles. The external irradiances are obtained from the Danish Design Reference Year (see Table 1).

Generally, we use the default stochastic ray-sampling in Radiance, but the blinds were modelled with the *mkillum* program which is generally the recommended approach for treating blinds (Ward and Shakespeare, 1998). Table 2 contains input parameters to Radiance and Mkillum which are diverging from the default values.

Fig. 9 depicts the daylight factor and relative error computed with Radiance and the BC/LC tool using the CIE standard overcast sky. All the measuring points are in good agreement and the relative error is below 6%. The illuminance levels with the Perez sky and a clear glazing on Fig. 10 also show good agreement with relative errors below 6%. The same good agreement is found with the lowered screen on Fig. 11 where the largest relative error is 8%. For more complex shading devices like the lowered and cut-off adjusted external dark Venetian blinds on Fig. 12 the largest relative error is 35%. The error is due to the uni-directional light transmittances from WIS. This influences the direct light penetrating the blinds and the diffuse light distribution on the inside of the blinds. This calls for

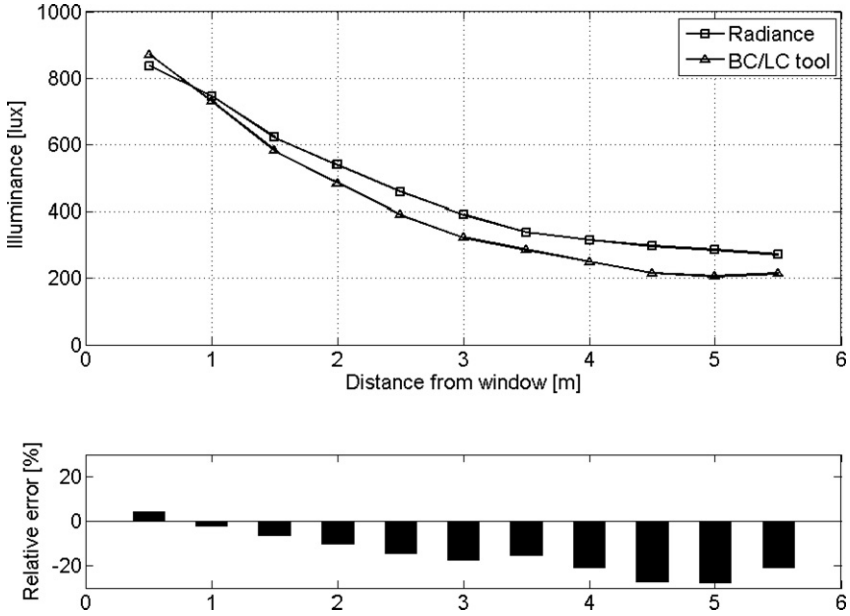

Fig. 12. Comparison of case with blinds lowered and adjusted to cut-off angle.

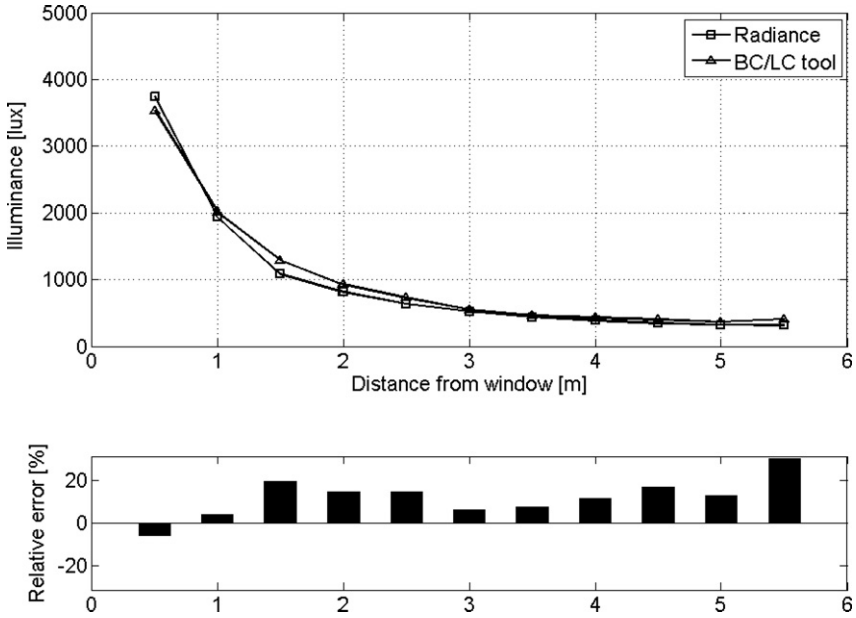

Fig. 13. Comparison of case where opposing building obscures part of the sun and sky. Clear double low-*E* glazing.

more accurate characterization of the properties of complex shading devices.

Fig. 13 depicts the influence of an opposing building façade obscuring part of the western sky vault and the solar disc. The obscured part is marked by azimuth interval [0; 60] and elevation interval [0; 45] (°). The diffuse reflectance is set to 0.3. The figure shows a maximum relative error of 30% in the back of the room and 10–20% in the rest of the room, but since the reflection algorithm is strongly simplified a certain discrepancy is expected. Buildings are almost always placed in a built environment, so further work is required to obtain satisfactory results for multiple reflections between building facades and the ground.

6. Conclusion

The tool described here is developed to evaluate the impact of incoming daylight on the energy consumption for lighting. The tool calculates the daylight distribution on the basis of a ray-tracing approach and the radiosity method to enhance accuracy while maintaining calculation speed.

The daylight distribution is calculated every hour, thus providing the information necessary for the thermal program to control the photoresponsive lighting and to calculate the heat load of the electrical lighting system. The daylight and thermal simulations are integrated meaning that the indoor temperature is recalculated if overheating or glare have caused the shading to be activated.

The daylight algorithms are validated by comparison with Radiance and they show good agreement for isotropic optical materials, and reasonable agreement for complex shading devices like blinds. The discrepancies are mainly due the fact that we use profile angle dependent light transmittances for blinds because WIS data for the time being is uni-directional. However relative errors of 20% are considered satisfactory in the early stages of daylighting design where simulation speed and ease of use is of importance. Consequently the simplified tool is adequate for predicting the electrical energy consumption of photoresponsive lighting systems, including the impact of complex shading systems such as external Venetian blinds.

References

Andersen, M., de Boer, J., 2006. Goniophotometry and assessment of bidirectional photometric properties of complex fenestration systems. Energy and Buildings 38 (7), 836–848.

Athienitis, A.K., Tzempelikos, A., 2002. A methodology for simulation of daylight room illuminance distribution and light dimming for a room with a controlled shading device. Solar Energy 72 (4), 271–281.

Clarke, J., Janak, M., 1998. Simulating the thermal effects of daylight-controlled lighting. Building Performance (BEPAC UK), Issue 1.

Crawley, D.B., Lawrie, L.K., Pedersen, C.O., Strand, R.K., Liesen, R.J., Winkelmann, F.C., Buhl, W.F., Huang, Y.J., Witte, M.J., Henninger, R.J., Glazer, J., Fisher, D.E., Shirey, D., 2002. Energyplus: new, capable and linked. In: Proceedings of Esim, Montréal, Canada, pp. 244–251.

Delaunay, Jean-Jacques, 1994. Gendaylit, manual pages, Frauenhofer Institute for Solar Energi Systems, Freiburg, Germany. <http://radsite.lbl.gov/radiance/pub/generators/index.html>.

van Dijk, D., Oversloot, H., 2003. WIS, the European tool to calculate thermal and solar properties of windows and window components. In: Proceedings of IBPSA, Building Simulation, Eindhoven, Netherlands, pp. 259–266.

Franzetti, C., Fraisse, G., Achard, G., 2004. Influence of the coupling between daylight and artificial lighting on thermal loads in office buildings. Energy and Buildings 36 (2), 117–126.

ISO, 2003. ISO 15099:2003 Thermal Performance Of Windows, Doors And Shading Devices – Detailed Calculations, International Organization for Standardization, Geneva, Switzerland.

Jenkins, D., Newborough, M., 2007. An approach for estimating the carbon emissions associated with office lighting with a daylight contribution. Applied Energy 84 (6), 608–622.

Lee, E.S., DiBartolomeo, D.L., Selkowitz, S.E., 1998. Thermal and daylighting performance of an automated venetian blind and lighting system in a full-scale private office. Energy and Buildings 29 (1), 47–63.

Lehar, M.A., Glicksman, L.R., 2007. Rapid algorithm for modeling daylight distributions in office buildings. Building and Environment 42 (8), 2908–2919.

The MathWorks, 2008. Matlab and Simulink, Version R2007a. <http://www.mathworks.com>.

Muneer, T., Gul, M., Kambezedis, H., 1998. Evaluation of an all-sky meteorological radiation model against long-term measured hourly data. Energy Conversion and Management 39 (3), 303–317.

Nielsen, T., Nielsen, T.R., Svendsen, S., 2005. Calculation of daylight distribution and utilization in rooms with solar shadings and light redirecting devices. In: Proceedings of the Seventh Symposium on Building Physics in the Nordic Countries, Reykjavik, Iceland, pp. 1011–1018.

Nielsen, T.R., 2005. Simple tool to evaluate energy demand and indoor environment in the early stages of building design. Solar Energy 78 (1), 73–83.

Park, K.-W., Athienitis, A.K., 2003. Workplane illuminance prediction method for daylighting control systems. Solar Energy 75 (4), 277–284.

Perez, R., Ineichen, P., Seals, R., Michalsky, J., Stewart, R., 1990. Modeling daylight availability and irradiance components from direct and global irradiance. Solar Energy 44 (5), 271–289.

Perez, R., Seals, R., Michalsky, J., 1993. All-weather model for sky luminance distribution – preliminary configuration and validation. Solar Energy 50 (3), 235–245.

Petersen, S., Svendsen, S., submitted for publication. Method for integrated design of low energy buildings with high quality indoor environment. In: Nordic Symposium on Building Physics 2008, Copenhagen, Denmark.

Robinson, D., Stone, A., 2006. Internal illumination prediction based on a simplified radiosity algorithm. Solar Energy 80 (3), 260–267.

Scharmer, K., Greif, J., 2000. The European Solar Radiation Atlas, École des Mines de Paris, France.

Tregenza, P.R., 1987. Subdivision of the sky hemisphere for luminance measurements. Lighting Research and Technology 19 (1), 13–14.

Tzempelikos, A., Athienitis, A.K., 2007. The impact of shading design and control on building cooling and lighting demand. Solar Energy 81 (3), 369–382.

University of Strathclyde, 2008. ESP-r Version 11, Energy Systems Research Unit, Glasgow, Scotland. <http://www.esru.strath.ac.uk/Programs/ESP-r.htm>.

US Department of Energy, 2008. EnergyPlus, Energy Efficiency and Renewable Energy, Washington DC, USA. <http://www.eere.energy.gov/buildings/energyplus>.

Walkenhorst, O., Luther, J., Reinhart, C., Timmer, J., 2002. Dynamic annual daylight simulations based on one-hour and one-minute means of irradiance data. Solar Energy 72 (5), 385–395.

Ward, G.L., Shakespeare, R.A., 1998. Rendering With Radiance – The Art and Science of Lighting Visualization, second ed. Morgan Kaufmann, San Francisco.

Wienold, J., Christoffersen, J., 2006. Evaluation methods and development of a new glare prediction model for daylight environments with the use of CCD cameras. Energy and Buildings 38 (7), 743–757.

WinDat, 2006. Window Information System software (WIS), WinDat Thematic Network, TNO Bouw, Netherlands. <http://www.windat.ucd.ie>.

Window 6.1 Research Version, 2007. Huizenga, C., Arasteh, D., Curcija, D., Klems, J., Kohler, C., Mitchell, R., Yu, T. Ver. 6.1.06. Windows and Daylighting Group, LBNL, Berkeley, California, USA.

Paper II

Submitted to Energy and Buildings, 2010

Analytical and experimental analysis of a low-pressure heat exchanger suitable for passive ventilation

Christian Anker Hviid[*,a,b], Svend Svendsen[b]

[a]*ALECTIA, Teknikerbyen 34, DK-2830 Virum, Denmark*
[b]*Department of Civil Engineering, Technical University of Denmark, Brovej, Building 118, DK-2800 Kgs. Lyngby, Denmark*

Abstract

A core element in sustainable ventilation systems is the heat recovery system. Conventional heat recovery systems have a high pressure drop that acts as blockage to naturally driven airflow. The heat recovery system we propose here consists of two separated air-to-liquid heat exchangers interconnected by a liquid loop powered by a pump ideal as a component in a heat recovery system for passive ventilation systems. This paper describes the analytical framework and the experimental development of one exchanger in the liquid-loop. The exchanger was constructed from the 8 mm plastic tubing that is commonly used in water-based floor-heating systems. The pressure loss and temperature exchange efficiency was measured. For a design airflow rate of 560 L/s, the pressure loss was 0.37 Pa and the efficiency was 75.6%. The experimental results agree well with the literature or numerical fluid calculations. Within the analytical framework, the total heat recovery of two liquid-coupled exchangers was calculated to be in the range 64.4–74.9%, depending on the parasitic heat loss in the experimental setup. The total pressure drop of the heat recovery system is 0.74 Pa. Moreover, preliminary improvement calculations promise a future total efficiency of 80% with a pressure drop of 1.2 Pa.

Key words: heat transfer, heat exchanger, hybrid ventilation, natural ventilation, heat recovery

1. Introduction

Energy performance and indoor environment have become increasingly important in building design. Building developers and designers are straining to produce end-user buildings with low energy consumption and high indoor environmental performance. This has led to an increased focus on solutions to reduce the building energy consumption. One such solution is to ventilate the building by passive means, such as stack effect and wind pressure. The term passive in this context indicates the opposite of active ventilation where fresh air is provided by fans. Passive ventilation also differs from natural ventilation because air is supplied via ducts and shafts to the building's rooms.

However, the energy reduction from the absence of fans in passive systems can be eliminated by the lack of heat recovery. An early attempt in the field of heat recovery for passive or natural ventilation solutions was based on a vertical counter-flow air-to-air heat exchanger and achieved a heat recovery efficiency of 40% [1]. Another concept used a system of stack chimneys. Passive heat pipes were interjected into the chimneys and experiments showed a heat recovery efficiency close to 43% with a total pressure loss of 1 Pa [2]. However, both attempts suffered from the inherited flow obstruction that arises when the induced flow direction is counteracted by the local buoyancy forces in the heat exchanger or heat pipes. They also lacked control of the airflow and had little flexibility in the building design.

A different concept with two air-to-liquid heat exchangers in the supply air and in the exhaust air, and connected with a pump-powered liquid loop was found to have an efficiency of 43% at a total pressure loss of 1 Pa [3]. This approach had many advantages in that the building integration was more flexible, the supply and exhaust airflows did not have to meet, and the buoyancy forces in the exchangers were fully exploited. But the total heat recovery efficiency of the system was somewhat less than the Danish Building Code requirement of 65% heat recovery for mechanical ventilation.

[*]Corresponding author. Tel.: +45 88 191 365
Email address: crh@alectia.com (Christian Anker Hviid)

Nomenclature

A	face area [m^2]
c_p	specific thermal capacity of fluid [J/kg K]
C_1	geometry parameter [-]
D	tube diameter [m]
f	friction factor [-]
F_a	geometry parameter [-]
g	gravitational acceleration [m^2/s]
h	heat transfer coefficient [W/m^2 K]
H	total heat transfer coefficient [W/K]
K_1	correction factor [-]
n	total tube length [m]
N	number of tube layers [-]
Nu	Nusselt number
P	pressure [Pa]
Pr	Prandtl number [-]
Q	supplied or transferred power [W]
Re	Reynolds number [-]
T	temperature [°C or Kelvin]
U	velocity [m/s]
$\dot{V}$	volumetric flow rate [m^3/s]
z	height [m]

Greek symbols

Φ	heat transfer, 1 unit of tube length [W/m]
λ	thermal conductivity [W/m K]
μ	dynamic viscosity [m^2/s]
ρ	density [kg/m^3]

Subscripts

a	air
app	approaching
D	diagonal
exh	exhaust
i	internal
in	indoor or inlet
out	outdoor
L	longitudinal
max	maximum
o	outer
supp	supply
T	transversal
w	water

This paper presents a heat recovery concept that has been developed specifically for innovative passive ventilation systems with heat recovery and night cooling suitable for temperate climates. The concept that we present is a newly developed heat exchanger with properties designed for passive ventilation. These include very low pressure loss (< 1 Pa) and high efficiency (≈ 70%). If the concept is integrated as a core element at the earliest stages of building design, it takes no more office space than conventional mechanical ventilation systems.

2. General considerations for developing a liquid-coupled heat exchanger

The heat recovery system is based on a well-known principle of two inter-connected air-to-liquid heat exchangers: one exchanger is placed in the inlet air and one in the outlet air, and they are inter-linked with a liquid loop powered by a pump. A schematic of the principle is depicted in Figure 1. Cold fresh air enters the heat exchanger in the inlet, heat is transferred from the hot liquid to the colder air resulting in a temperature rise in the supply air. The now cooled liquid is pumped to the heat exchanger in the outlet where it is heated by the hot exhaust air leaving the building. The warm liquid returns to the inlet heat exchanger and the cycle is repeated continuously.

The main advantage of the liquid-coupled heat exchanger principle is the flexible placing of inlet and outlet in the ventilation system because the airstreams are not required to meet. This flexibility is particularly advantageous for ventilation systems partly or purely driven by stack effect and wind pressures instead of mechanical means such as fans. The approach allows for optimum placement of the heat exchangers in the building to exploit the natural driving pressure differences fully.

A number of optimum performance objectives govern the design. Three primary objectives are listed below with two secondary objectives.

- Low frictional loss on the air side
- Low frictional loss on the water side
- Effective heat transfer between the fluids
- Low production costs
- High lifetime expectancy

Low frictional loss on the air side is critical for the heat recovery concept to be applicable in naturally driven ventilation systems. For typical operating conditions, such as an indoor temperature of 20 °C, an outdoor temperature of 5 °C, a height difference z between inlet and outlet of 12 m, and no wind, the maximum natural driving pressure is:

$$\begin{aligned} \Delta P &= (\rho_{5°C} - \rho_{20°C}) \cdot g \cdot z \qquad (1) \\ &= (1.269 - 1.204)\,\mathrm{kg/m^3} \cdot 9.81\,\mathrm{m/s^2} \cdot 12\,\mathrm{m} \\ &\approx 7.7\,\mathrm{Pa} \end{aligned}$$

Because other components also induce pressure losses in the system, we set a desired design criterion for the total pressure loss due to heat recovery of approx. 1 Pa.

The frictional loss on the water side is also important because it determines the size and energy consumption of the pump. To avoid excessive energy consumption by a secondary component in the ventilation system, we set the design criterion that a domestic circulation pump must be sufficient.

The heat transfer is governed by various factors, e.g. the velocity of the passing air, the resistance between the passing airstream and the tube fluid and the total heat transfer surface. We set an overall design criterion for the total heat recovery efficiency of 70%. This value was selected as a compromise between the heat recovery requirement in low-energy office buildings and the size of the exchanger.

The secondary objectives should also be reflected upon by the designer. For the sake of robustness and penetration in a competitive global market, production costs and lifetime expectancy are of importance. Production costs are typically proportional to material costs, and the number of fittings tends to be decisive for lifetime expectancy. The secondary objectives are essential for the exchanger to be competitive with existing heat recovery concepts and consequently cannot be disregarded for any practical implementation.

3. Theoretical design of the exchanger

Heat exchangers of the counter-flow type have the highest efficiency potential. The counter-flow type is based on a heat exchange process where a hot and a cold fluid enter the heat exchanger from opposite ends; the cold fluid is warmed and the hot fluid is cooled. Because the hot input is at its maximum temperature, it can warm the exiting hot fluid to near its own temperature. In parallel the cold input can cool the exiting cold fluid to near its own (low) temperature; in other words, the fluids 'swap' temperatures. To maintain an effective heat transfer the wall material between the fluids must have negligible heat transfer resistance compared to the surface resistances and the capacity flow of the fluids must be equal. To keep the exchanger simple and with low material costs, we used round PE plastic tubing that is commonly used for water-based floor-heating systems. Oval or even wing shaped tubes have better heat transfer and lower drag coefficient [4], but round tubes require less meticulous production procedures. The tubing used here is mass-produced, cheap, flexible and requires no fittings as it is produced in a continuous cycle and shipped on large cable drums. Equation (18) shows that the material resistance of the PE tubing accounts for 7% of the total resistance.

Equation (18) also shows that the greatest resistance to heat transfer is on the air side. This means that the heat transfer between tube surface and air is of critical importance. Many factors play a role in the overall effective heat transfer, but the air side heat transfer is typically a function of the mean Nusselt number of the tube bank. The Nusselt number is dimensionless and denotes the ratio of convective to conductive heat transfer normal to the boundary. For cylinders in cross-flow, it is defined by (13).

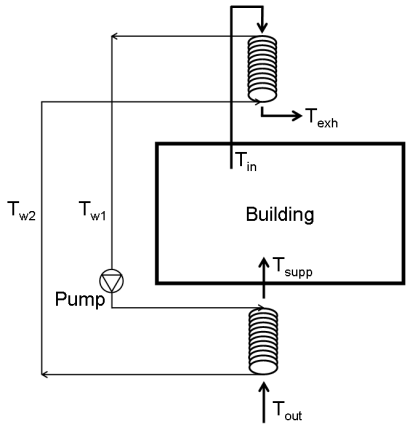

Figure 1: Schematic of the heat recovery concept.

Heat transfer is favoured by the more tortuous flow of a staggered tube arrangement particularly for small Reynolds numbers ($Re < 100$) because a greater portion of the surface area of downstream tubes remains in the path of the main flow [5]. Even so, Mandhani et.al. [6] (referring to Chen & Wung, 1989) argue that gross parameters like the mean Nusselt number are little influenced by the tube bank geometry. However, with the Chen & Wung formula, the relative difference between aligned and staggered grid is 9% for $Re = 10$ and increases to 36% for $Re = 800$. The staggered grid is chosen because, in the laminar flow range, the heat transfer will remain more robust to higher airflow rates than initially designed for. The staggered grid is depicted in Figure 3. The outer diameter D_o of the tubing is 8 mm and the internal diameter D_i is 5.8 mm. The longitudinal (streamwise) S_L pitch between the tube centroids is 11 mm, the transverse (spanwise) S_T pitch is 24 mm and the diagonal pitch S_D is 16.3 mm. This yields dimensionless longitudinal and transverse pitches of $\mathcal{S}_L = S_L/D_o = 1.375$ and $\mathcal{S}_T = S_T/D_o = 3$, respectively. The dimensionless diagonal pitch is: $\mathcal{S}_D = S_D/D_o = 2.03$.

The pitch ratios were a consequence of the brackets and tube spacers available to secure the tubing under the load of the tube fluid. The brackets fix the tubing into vertical tube columns (here: radiators) as depicted in Figure 4. In the figure two parallel tubes criss-cross the airflow. The choice of two parallel tubes was governed by the possible bend radius of a single tube, where two neighbouring single bends would overlap at both ends. With two parallel tubes there is space for both tube bends at both ends, see Figure 2. This is a compromise between the concept of counterflow and practical implementation. When the tubes are locked into the brackets forming a radiator, multiple radiators can be combined with an inter-longitudinal offset between adjacent radiators of $\mathcal{S}_L$. The resulting staggered grid with spacing is depicted in Figure 3. Thus putting multiple radiators together makes the exchanger fully scalable.

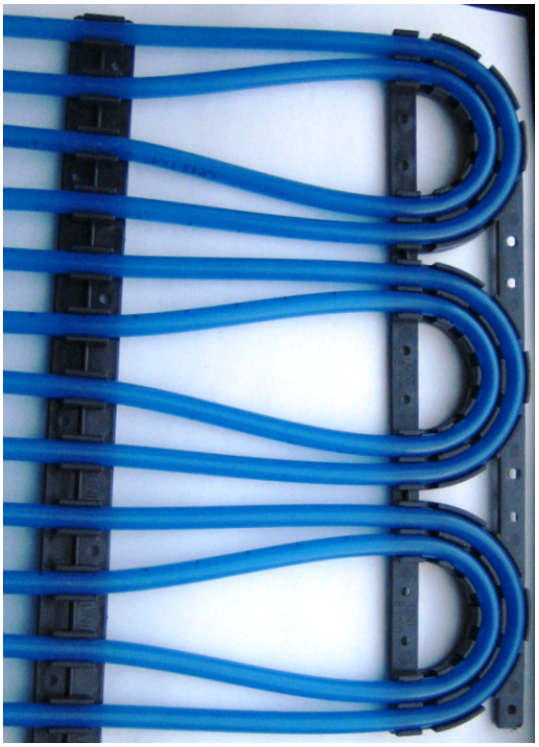

Figure 2: Photo of parallel tube bends in bracket.

The tube fluid is water, but to avoid problems with freezing and subsequent clogging and destruction of the heat exchanger, some measure of antifreeze should be considered. The efficiency drop of an aqueous solution of 30 vol-pct. propylene glycol is quantified in section 5. The mixture protects the tube fluid from freezing at temperatures below −12 °C, but propylene glycol is not harmless and requires extra safety measures and

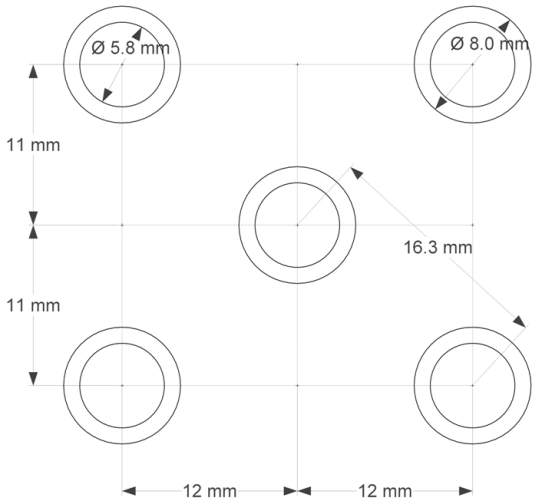

Figure 3: Tube bank spacing. Airflow from below. The pitch ratios are $\mathcal{S}_T = 24\,\text{mm}$, $\mathcal{S}_L = 11\,\text{mm}$ and $\mathcal{S}_D = 16.3\,\text{mm}$

pressure tests of the plastic tubes and manifolds.

The design of the heat exchanger was based on a desired total heat recovery efficiency η of 70%. This is defined as the temperature change of one fluid (here inlet air) divided by the temperature difference between the two inbound fluids. Using a temperature set of outdoor and indoor temperatures [$T_{\text{out}} = 5\,°\text{C}, T_{\text{in}} = 20\,°\text{C}$] which are close to realistic operation conditions, the supply temperature T_{supp} was calculated:

$$\eta = \frac{T_{\text{supp}} - T_{\text{out}}}{T_{\text{in}} - T_{\text{out}}} \Leftrightarrow T_{\text{supp}} = \eta \cdot (T_{\text{in}} - T_{\text{out}}) + T_{\text{out}} \quad (2)$$

This yields a supply temperature of 15.5 °C. If we assume that the mean temperature difference $\overline{\Delta T_{\text{a-w}}}$ between water and air is the same in both exchangers and that the temperature change in the liquid loop is zero, the temperature difference can be calculated from the temperatures T_{in} and T_{supp} from the following equations, see Figure 1:

$$\left.\begin{aligned} T_{\text{w1}} &= T_{\text{in}} - \overline{\Delta T_{\text{a-w}}} \\ T_{\text{supp}} &= T_{\text{w1}} - \overline{\Delta T_{\text{a-w}}} \end{aligned}\right\} \Leftrightarrow \overline{\Delta T_{\text{a-w}}} = \frac{T_{\text{in}} - T_{\text{supp}}}{2} \quad (3)$$

$$\overline{\Delta T_{\text{a-w}}} = \frac{20\,°\text{C} - 15.5\,°\text{C}}{2} = 2.25\,°\text{C}$$

The heat exchanger was designed for a volumetric flow rate $\dot{V}_{\text{a}}$ of $0.56\,\text{m}^3/\text{s}$ which is the ventilation requirement for 40 people in an office building according to EN15251 Indoor Climate Class II. The building is considered low polluting [7]. Given the fluid density ρ_{a},

and the thermal capacity $c_{p,a}$ of air from Table 1, the necessary supplied power Q for a temperature rise ΔT_a of the inbound fresh air in the heat exchanger is:

$$\begin{aligned} Q &= \dot{V}_a \rho_a c_{p,a} \Delta T_a \\ &= 0.56\,\mathrm{m^3/s} \cdot 1.249\,\mathrm{kg/m^3} \\ &\quad \cdot 1007\,\mathrm{J/kg\,K} \cdot 10.5\,\mathrm{K} \\ &= 7396\,\mathrm{W} \end{aligned} \tag{4}$$

when $\Delta T_a = T_{supp} - T_{out} = 15.5\,^\circ\mathrm{C} - 5\,^\circ\mathrm{C} = 10.5\,^\circ\mathrm{C}$.

In the following sections we assume the initial dimensions (length × width × height) of the exchanger to be $3.00\,\mathrm{m} \times 1.92\,\mathrm{m} \times 0.31\,\mathrm{m}$. Thus the face area A 'seen' by the approaching air is $5.76\,\mathrm{m^2}$ and with the given pitch ratio there is room for 160 tube radiators.

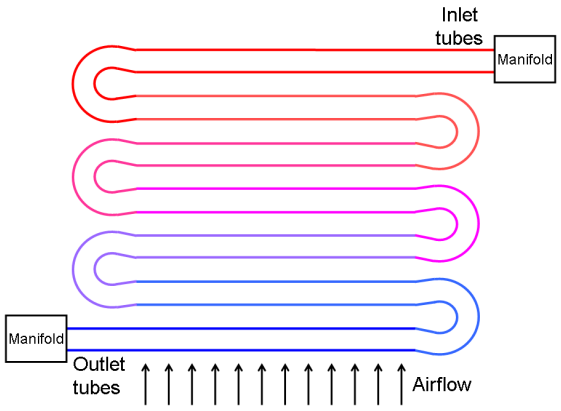

Figure 4: Layout of two parallel tubes in a radiator in crossflow.

3.1. Heat transfer coefficients

The transferred power depends on the heat transfer coefficient on both fluid sides of the heat exchanger. In the following, the heat transfer on each side is treated independently before the total heat transfer coefficient is calculated.

3.1.1. Air side

For the air side, the heat transfer depends on the local flow velocities around the tubing. The approaching air velocity U_{app} is:

$$U_{app} = \frac{\dot{V}_a}{A} = \frac{0.56\,\mathrm{m^3/s}}{5.76\,\mathrm{m^2}} = 0.10\,\mathrm{m/s} \tag{5}$$

The maximum air velocity in the tube bank is calculated from the arrangement of the tubes [8]:

$$U_{max} = max \left\{ \begin{matrix} \frac{S_T}{S_T - 1} U_{app} \\ \frac{S_T}{S_D - 1} U_{app} \end{matrix} \right\} \Leftrightarrow \tag{6}$$

$$U_{max} = \left\{ \begin{matrix} \frac{3}{3 - 1} 0.10\,\mathrm{m/s} \\ \frac{3}{2.03 - 1} 0.10\,\mathrm{m/s} \end{matrix} \right\} = 0.29\,\mathrm{m/s}$$

and the Reynolds number for the air flow is:

$$\begin{aligned} Re_{D_o} &= \frac{\rho_a U_{max} D_o}{\mu_a} \\ &= \frac{1.249\,\mathrm{kg/m^3} \cdot 0.29\,\mathrm{m/s} \cdot 0.008\,\mathrm{m}}{1.77 \cdot 10^{-5}\,\mathrm{Pa\,s}} \\ &\approx 164 \end{aligned} \tag{7}$$

The Reynolds number is much lower than the turbulent or transitional flow regime ($\ll 10^5$), so the airflow is laminar. The mean heat transfer coefficient on the air side of the tubing $\overline{h}_a$ was calculated from the Nusselt number Nu, the thermal conductivity of air λ_a and the outer tube diameter D_o, see (13). The Nusselt number is critical for the heat transfer and the literature gives several formulae for the calculation of this number. To avoid too overoptimistic predictions, we calculated the Nusselt number with three different formulae and chose the smallest number for further analysis. The formulae given for laminar flow are from Khan et.al. [8], from Beale [9], and from Hausen [10]. They all take the form $Nu = \alpha Re^{\beta} Pr^{\gamma}$ where α is a coefficient related to the geometry of the tube bank. The formula from Khan et.al. is derived analytically, Hausen's stems from experimental data, and Beale's work is based on numerical studies. Despite their initial similarities the formulas yield different results.

$$\begin{aligned} Nu_{Khan} &= C_1 Re_{D_o}^{1/2} Pr_a^{1/3} \\ &= 1.24 \cdot 164^{1/2} \cdot 0.71^{1/3} \\ &\approx 14.2 \end{aligned} \tag{8}$$

$$\begin{aligned} Nu_{Beale} &= 1.309 Re_{D_o}^{0.36} Pr_a^{0.34} \\ &= 1.309 \cdot 164^{0.36} \cdot 0.71^{0.34} \\ &\approx 7.3 \end{aligned} \tag{9}$$

Table 1: Property values of air and water.

Properties at 10 °C		Air	Water	30 vol-pct. propylene glycol
Density	ρ	1.249 kg/m^3	999.7 kg/m^3	1033 kg/m^3
Thermal capacity	c_p	1007 J/kg K	4192 J/kg K	3820 J/kg K
Thermal conductivity	λ	0.025 W/m K	0.587 W/m K	0.434 W/m K
Dynamic viscosity	μ	$1.77 \cdot 10^{-5}$ Pa s	$1.30 \cdot 10^{-3}$ Pa s	$4.52 \cdot 10^{-3}$ Pa s
Prandtl number	Pr	0.71	9.28	39.78

$$\begin{aligned} Nu_\mathrm{Hausen} &= 0.35 F_\mathrm{a} Re_{\mathrm{D_o}}^{0.57} Pr_\mathrm{a}^{0.31} \\ &= 0.35 \cdot 1.25 \cdot 164^{0.57} 0.71^{0.31} \\ &\approx 7.2 \end{aligned} \tag{10}$$

where C_1 and F_a for staggered arrangements are calculated from (11) and (12):

$$\begin{aligned} C_1 &= \frac{0.61 {\mathcal{S}_\mathrm{T}}^{0.091} {\mathcal{S}_\mathrm{L}}^{0.053}}{1 - 2\exp(-1.09\mathcal{S}_\mathrm{L})} \\ &= \frac{0.61 \cdot 3^{0.091} 1.375^{0.053}}{1 - 2\exp(-1.09 \cdot 1.375)} \\ &\approx 1.24 \end{aligned} \tag{11}$$

$$\begin{aligned} F_a &= 1 + 0.1\mathcal{S}_\mathrm{L} + \frac{0.34}{\mathcal{S}_\mathrm{T}} \\ &= 1 + 0.1 \cdot 1.375 + \frac{0.34}{3} \\ &\approx 1.25 \end{aligned} \tag{12}$$

The smallest Nusselt number was 7.2 and this was used for the heat transfer coefficient on the air side:

$$\begin{aligned} \overline{h}_\mathrm{a} &= \frac{Nu \cdot \lambda_\mathrm{a}}{D_\mathrm{o}} \\ &= \frac{7.2 \cdot 0.025\,\mathrm{W/m\,K}}{0.008\,\mathrm{m}} \\ &\approx 22.5\,\mathrm{W/m^2\,K} \end{aligned} \tag{13}$$

3.1.2. Water side

On the water side, the heat transfer coefficient depends on the water flow velocity in the tubing. The equal capacity of the fluid flows causes the temperature change and the transferred power to be the same for the two fluid sides. Thus the volumetric water flow can be calculated from (4) with the properties of water from Table 1:

$$\begin{aligned} \dot{V}_\mathrm{w} &= \frac{Q}{\rho_\mathrm{a} c_\mathrm{p,w} \Delta T_\mathrm{w}} \\ &= \frac{7396\,\mathrm{W}}{999.7\,\mathrm{kg/m^3} \cdot 4192\,\mathrm{J/kg\,K} \cdot 10.5\,\mathrm{K}} \\ &\approx 1.68 \cdot 10^{-4}\,\mathrm{m^3/s} \end{aligned} \tag{14}$$

From the schematic layout of the heat exchanger shown in Figure 4 with two parallel inlet tubes in each radiator, and with an assumed number of 160 radiators, the water flow velocity U_w is calculated:

$$\begin{aligned} U_\mathrm{w} &= \frac{\dot{V}_\mathrm{w}}{2 \cdot 160 \cdot \frac{\pi}{4} D_\mathrm{i}^2} \\ &= \frac{1.68 \cdot 10^{-4}\,\mathrm{m^3/s}}{320 \cdot \frac{\pi}{4} 0.0058^2} \\ &\approx 0.020\,\mathrm{m/s} \end{aligned} \tag{15}$$

and the Reynolds number for the water flow:

$$\begin{aligned} Re_{\mathrm{D_i}} &= \frac{\rho_\mathrm{w} U_\mathrm{w} D_\mathrm{i}}{\mu_\mathrm{w}} \\ &= \frac{999.7\,\mathrm{kg/m^3} \cdot 0.020\,\mathrm{m/s} \cdot 0.0058\,\mathrm{m}}{1.30 \cdot 10^{-3}\,\mathrm{Pa\,s}} \\ &\approx 89 \end{aligned} \tag{16}$$

The flow is laminar ($\ll 2300$) and the Nusselt number is then 4.36 [5]. With these properties the mean heat transfer coefficient for the water side of the tubing is:

$$\begin{aligned} \overline{h}_\mathrm{w} &= \frac{Nu \cdot \lambda_\mathrm{w}}{D_\mathrm{i}} \\ &= \frac{4.36 \cdot 0.587\,\mathrm{W/m\,K}}{0.0058\,\mathrm{m}} \\ &\approx 441\,\mathrm{W/m^2\,K} \end{aligned} \tag{17}$$

3.1.3. Total heat transfer

With the heat transfer coefficients established on both sides of the tubes, the total heat transfer for one meter of tube length in cross-flow Φ can be established. Given that the thermal conductivity of the plastic tubing λ_tube is 0.35 W/m K and L a unit length of tube, Φ is calculated

from [5]:

$$\begin{aligned}\Phi &= \frac{\overline{\Delta T_{\mathrm{w-a}}}}{R_a + R_{tube} + R_w} \cdot L \\ &= \frac{\overline{\Delta T_{\mathrm{w-a}}}}{\frac{1}{\pi D_{\mathrm{o}} \bar{h}_{\mathrm{a}}} + \frac{\ln(D_{\mathrm{o}}/D_{\mathrm{i}})}{2\pi\lambda_{\mathrm{tube}}} + \frac{1}{\pi D_{\mathrm{i}} \bar{h}_{\mathrm{w}}}} \cdot L \\ &= \frac{2.25\,\mathrm{K}}{(1.768 + 0.146 + 0.124)\mathrm{m^2\,K/W}} \cdot 1\,\mathrm{m} \\ &\approx 1.1\,\mathrm{W/m}\end{aligned} \tag{18}$$

This yields $\Phi \approx 1.1\,\mathrm{W/m}$ and the total tube length n is calculated from:

$$\begin{aligned}n &= \frac{Q}{\Phi} \\ &= \frac{7396\,\mathrm{W}}{1.1\,\mathrm{W/m}} \\ &\approx 6724\,\mathrm{m}\end{aligned} \tag{19}$$

The length of each tube layer is 3 m and with 14 tube layers in each radiator as depicted in Figure 4, a total of 160 radiators are necessary. The radiators were placed in a staggered grid so the number of tube layers in the streamwise direction is $N_L = 28$. With the chosen input and the pitch ratios depicted in Figure 3, the dimensions of the exchanger (length × width × height) is $3.00\,\mathrm{m} \times 1.92\,\mathrm{m} \times 0.31\,\mathrm{m}$ with a face area of $5.76\,\mathrm{m}^2$ which is the same as the initial design assumption.

3.2. Heat recovery efficiency

The total heat transfer coefficient H of one exchanger was calculated by the heat transferred from water to air Q at a given mean temperature difference $\overline{\Delta T_{\mathrm{a-w}}}$. In the experimental setup we measured the temperature differences marked in Figure 7. Knowing the differences, we could calculate the temperature difference between water and air at the air inlet ($\Delta T_{\mathrm{a,in-w,out}}$) and at the air outlet ($\Delta T_{\mathrm{a,out-w,in}}$). The mean temperature difference $\overline{\Delta T_{\mathrm{a-w}}}$ between the fluids is then $\frac{1}{2}(\Delta T_{\mathrm{a,in-w,out}} + \Delta T_{\mathrm{a,out-w,in}})$:

$$H = \frac{Q}{\overline{\Delta T_{\mathrm{a-w}}}} = \frac{Q}{1/2 \cdot (\Delta T_{\mathrm{a,in-w,out}} + \Delta T_{\mathrm{a,out-w,in}})} \tag{20}$$

We used the normal mean temperature difference and not the logarithmic mean temperature difference because we wanted to keep the temperature differences equal immediately before and after the exchanger so the normal and logarithmic temperature difference would be the same. Assuming zero temperature change in the liquid loop between the exchangers the total efficiency can be determined from the following considerations on energy conservation. From (4) and (20) we have for the inlet exchanger:

$$H \cdot \overline{\Delta T_{\mathrm{a-w}}} = \dot{V}_a \rho_a c_{p,a} (T_{\mathrm{supp}} - T_{\mathrm{out}}) \tag{21}$$

replacing ΔT_{supp} with (3) and some rearranging we have

$$\overline{\Delta T_{\mathrm{a-w}}} = \frac{\dot{V}_{\mathrm{a}} \rho_{\mathrm{a}} c_{\mathrm{p,a}} (T_{\mathrm{in}} - T_{\mathrm{out}})}{H + 2\dot{V}_{\mathrm{a}} \rho_{\mathrm{a}} c_{\mathrm{p,a}}} \tag{22}$$

From (2), (3) and (22), we are then able to calculate the total heat recovery efficiency of the system:

$$\eta = \frac{(T_{\mathrm{in}} - 2\overline{\Delta T_{\mathrm{a-w}}}) - T_{\mathrm{out}}}{T_{\mathrm{in}} - T_{\mathrm{out}}} \tag{23}$$

3.3. Pressure loss on the water side

The pressure loss in the tubing has an impact on the energy consumption of the pump. We quantified this to ensure that the heat recovered would not be eliminated by the extra electric energy consumed by the liquid loop pump. From (16) we knew that the flow was laminar which simplified the calculation of the friction factor f to:

$$f = \frac{64}{Re_{D_i}} = \frac{64}{89} \approx 0.72 \tag{24}$$

Given the friction factor f, the density ρ_{w} from Table 1, the water flow velocity U_{w}, the internal diameter D_{i}, the length of one plastic tube from manifold to manifold L ($= 3.00\,\mathrm{m} \cdot N_L/4$), and ignoring the pressure losses in the tube bends at each end of the exchanger (bending radius ≫ internal tube radius), the pressure loss in the tubes could be calculated from [11]:

$$\begin{aligned}\Delta P_{\mathrm{w}} &= f \frac{\rho_{\mathrm{w}} U_{\mathrm{w}}^2}{2D_{\mathrm{i}}} L \\ &= 0.72 \cdot \frac{999.7\,\mathrm{kg/m^3} \cdot (0.020\,\mathrm{m/s})^2}{2 \cdot 0.0058\,\mathrm{m}} \cdot 21\,\mathrm{m} \\ &\approx 521\,\mathrm{Pa}\end{aligned} \tag{25}$$

With two exchangers in the recovery system, the pump pressure loss due to the exchangers is 1042 Pa. The magnitude of this value is a fraction of the pressure loss that small energy efficient domestic circulation pumps are capable of overcoming. This means that the operating costs of the pump would largely depend on the pressure loss in the pipe loop linking the exchangers. For a well-designed pipe loop, the magnitude of the head loss would be well within the normal operation range of commercial domestic circulation pumps and would not require any special attention.

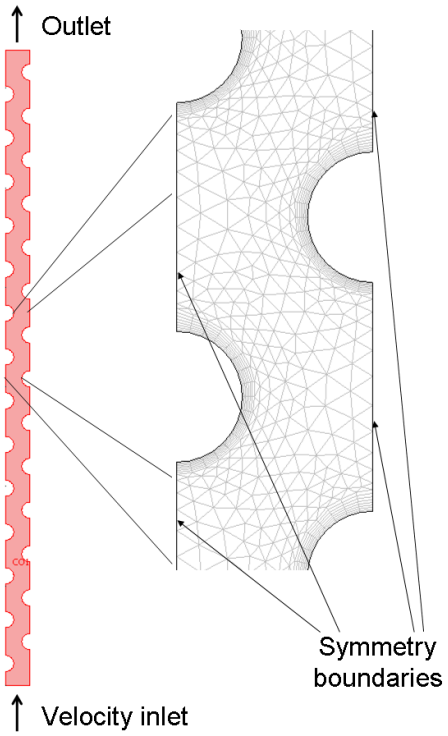

Figure 5: Comsol mesh.

3.4. Pressure loss on the air side

With the exchanger dimensions and number of tube layers established, we could calculate the pressure loss on the air side. We calculated the correction factor K_1 from the arrangement of the tubes and the Reynolds number [12]:

$$\begin{aligned} K_1 &= 1.775 \frac{\mathcal{S}_\mathrm{L}}{\mathcal{S}_\mathrm{T} Re_{\mathrm{D_o}}^{0.3124}} + \frac{Re_{\mathrm{D_o}}^{0.0807}}{2} \qquad (26) \\ &= 1.775 \cdot \frac{1.375}{3 \cdot 164^{0.3124}} + \frac{164^{0.0807}}{2} \\ &\approx 0.92 \end{aligned}$$

From K_1 and the dimensionless transverse pitch $\mathcal{S}_\mathrm{T}$ the friction factor f was calculated:

$$\begin{aligned} f &= K_1 \frac{\left[378.6/\mathcal{S}_\mathrm{T}^{13.1/S_\mathrm{T}}\right]}{Re_{\mathrm{D_o}}^{0.68/S_\mathrm{T}^{1.29}}} \qquad (27) \\ &= 0.92 \frac{\left[378.6/3^{13.1/3}\right]}{164^{0.68/3^{1.29}}} \\ &\approx 1.24 \end{aligned}$$

If N_L denotes the number of tube layers in streamwise direction, ρ_a the density of air and U_max the maximum air velocity in the tube bank, the pressure difference ΔP_a across the heat exchanger on the air side can be calculated:

$$\Delta P_\mathrm{a} = N_\mathrm{L} \cdot f \left(\frac{1}{2} \rho_\mathrm{a} U_\mathrm{max}^2 \right) \Leftrightarrow \qquad (28)$$

$$\begin{aligned} \Delta P_\mathrm{a} &= 28 \cdot 1.24 \cdot \left(\frac{1}{2} \cdot 1.249\,\mathrm{kg/m^3} \cdot (0.29\,\mathrm{m/s})^2 \right) \\ &\approx 1.82\,\mathrm{Pa} \end{aligned}$$

The total pressure drop is then 3.6 Pa, which is higher than the initial design criteria of 1 Pa. Therefore, supplemental numerical analysis of the pressure loss was carried out.

3.4.1. Numerical analysis

For supplemental pressure analysis, we used the tool *Comsol* [13]. Like CFD-codes, Comsol meshes the domain, discretises the Navier-Stokes equations, and extrapolates the boundary conditions into the domain through a series of iterations. A comparison of Comsol with validated simulation results has been performed in [14]. The simulation was performed on a 2D domain because we considered 3D effects to be negligible for most of the exchanger. Figure 5 illustrates a zoomed-in view of the calculated 2D domain with the mesh. The boundary conditions are no-slip for the tube surfaces, symmetry between tubes, pressure outlet and velocity inlet. No turbulence model was applied, i.e. we assumed laminar fluid flow. To check the quality of the mesh, it was refined once from 9074 to 22065 elements which resulted in a solution change of 0.5%.

4. Experimental setup

The dimensions of the exchanger made it unwieldy for experimental measurements at this stage of preliminary design. Consequently only a section of the total exchanger was used for measurements. This section is depicted in Figure 6 and contains 8 radiators each with 14 tube layers which results in the following effective dimensions when the spacers are subtracted (length × width × height) = 2.925 m × 0.108 m × 0.31 m. Thus the face area for the approaching air was approx. 1/18 of the design area.

The tube inlets and outlets were connected to manifolds at each end of the exchanger, making each tube layer 2.925 m in length. The manifold connection required more space than the transverse tube spacing allows for. Consequently the radiators were connected

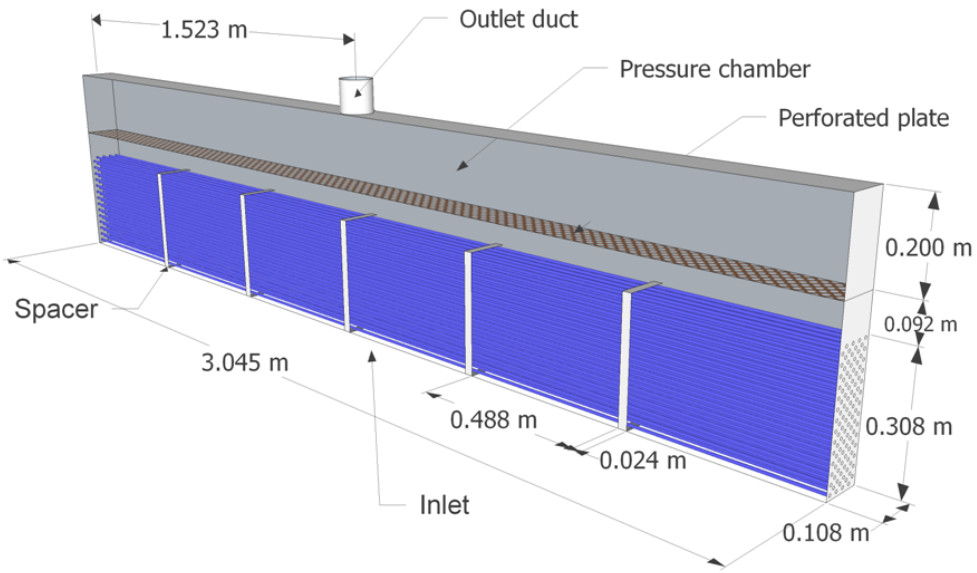

Figure 6: Cut open test exchanger box with dimensions.

to the manifolds from alternating ends. Thus the inlet water flowed in opposite directions in two adjacent radiators. To some extent, this coupling scheme cancelled out the effect of the long tube layers on the temperature distribution throughout the exchanger. Because of the long tube layers, the temperature change of the tube fluid from the start to the end of a layer is quite large. This changed the mean temperature difference and the local heat transfer between air and tube fluid locally. Moreover, where the tubing turns around and enters a new tube layer, a jump in the local temperature gradient is introduced. This was even more pronounced for the tube layout employed here, where the tube skips two layers in every second turn. As depicted in Figure 4, the tube in some turns enters the subsequent tube layer and in some turns skips to the fourth subsequent layer. The result is a quite complex varying local heat transfer between air and tube fluid, but by introducing water flow from opposite directions in adjacent radiators, the local temperature gradient shifts are smaller.

The tubes were placed in a wooded box, as depicted in Figure 6, by using the product-specific tube spacers and brackets. The box was open at the bottom and the other surfaces were insulated with 10 cm of polystyrene. The rounded tube ends were also placed inside the wooded box. The spacers were placed approx. every 0.5 m to prevent deflection due to the load of the tube fluid. Spacers and tube bend ends are not included in the effective heat transfer area. To ensure uniform distribution of inlet and outlet air in the box a chamber was placed above the tubes with an interjected perforated plate so it acted as a pressure equalization chamber. From the chamber a controllable fan drew air via an outlet duct. The setup was placed indoors and the ambient temperature was approx. 20 °C. Instead of the design temperature set of 20/5 °C, we avoided cooling of the inbound air by choosing a different operation temperature set of 40/20 °C. This is also reflected in the results section. Because the testing facility is very large, the temperature rise of the exiting air during the experiments did not affect the temperature of the inbound air significantly.

The properties measured were pressure and temperature differences at discrete points as marked in Figure 7. However, the pressure difference could vary along the length of the box because of inadequate pressure equalization. Therefore, for each measurement a uniformity check was performed by measuring the pressure differences in three positions evenly distributed along the box. The maximum difference was ±0.02 Pa and was

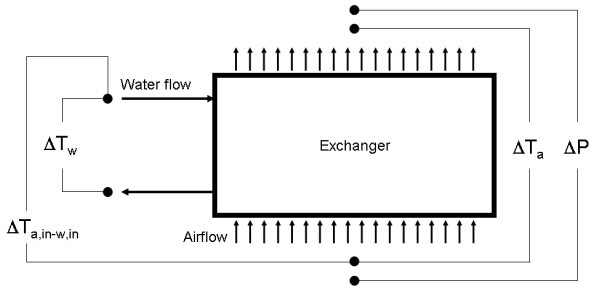

Figure 7: Measuring points of water and air temperature differences and pressure differences across the tubes.

therefore deemed negligible. The measuring device was a micromanometer FCO510 from Furness Controls with an accuracy of 0.25%. The micromanometer was also used to measure the airflow via a built-in pitot tube in a 100 mm airflow measuring duct from Veab. The micromanometer was only capable of measuring one pressure difference at a time. Consequently measurements at start and stop were averaged to the reported value.

The temperature was measured by copper/constantan thermocouples, type TT. The thermocouples producd an electric current that was converted in the datalogger to an absolute temperature with a precision of ±1 K using an internal reference loop. The precision was unsatisfactory in the present case, but for measuring temperature differences the thermocouples were coupled in series into a thermopile. This eliminates the poor accuracy of the internal reference point and augments the accuracy to ±(0.0050 + 0.0040)%. For a temperature difference of 20 K, this corresponds to ±0.0018 K. The datalogger we used is an Agilent 34970A Data Acquisition Unit.

The manifolds were connected to a cooling/heating rack with two equal lengths of connecting tube to ensure equal flow in all tubes. The cooling/heating rack provides circulation and heating of water for the test setup depicted in Figure 8. The rack automatically adjusts the necessary power to maintain a given setpoint. Furthermore, it contains a flow meter of the type Danfoss MassFlo 2100, which is used to measure the mass flow rate of water. The flow meter converts the signal to a current in the range 0–20 mA where 20 mA is the maximum mass flow rate. Because of the parasitic heat loss, manual fine-tuning was performed until conditions were steady and the temperature changes for both fluids were approximately equal and the maximum temperature efficiency was achieved.

5. Results and discussion

This section presents the measured and simulated data and compares it with various literature sources.

5.1. Pressure drop

Figure 9 shows the measured pressure drop characteristic on the air side of the exchanger. In spite of the fact that the airflow was considered to be fully laminar in the depicted range ($81 < Re < 454$), the figure exhibits some turbulent behaviour with increasing deviation from the initial linearity. This suggests that the staggered grid does introduce some turbulent wakes into the airstream especially for airflows above 150 $\mathrm{Ls^{-1}m^{-2}}$.

Figure 10 compares the measured pressure drop with two literature sources and the numerical fluid calculation performed in Comsol. It is clear that both literature sources overestimate the pressure drop across the tube banks when compared to the measured data. Particularly the model by Khan et al. [12] which was used in the design phase of the exchanger overestimates the pressure drop by more than a factor of 4. The model is based on experimental data fitting and is claimed to be valid in the laminar flow range and for the pitch ratios employed, but does not quantify the fitting error. The model by Zhukauskas [15] is valid for $Re > 10$ and shows marginally better agreement but it also overestimates the pressure drop. The numerical fluid calculation predicts the pressure drop well in most of the calculation range. The bar plot illustrates the relative error which is in the range of 3–30% with the larger error in the smaller pressure drops. It is also interesting to note the tendency for an increasing discrepancy with higher airflow rates. This suggests that the fully laminar assumption of the numerical calculation is no longer valid.

5.2. Heat transfer

Figure 13 illustrates an example of the data that was measured during the heat transfer experiments. The figure shows the heating of air when it passed the tubes, the cooling of water and the resulting temperature efficiency of the test setup. Furthermore, the fluid capacity flows were plotted because apart from being crucial for the total heat recovery of two liquid-coupled heat exchangers, they also illustrate the parasitic heat loss. Ideally, when the fluid capacity flows are equal, the fluids ‘swap’ temperatures. While the test setup was tuned to do this, the air temperature was 98.4% of the water temperature, the capacity flows remained slightly unequal with the air flow being only 91.6% of the water flow. This inequality is evidence of larger parasitic heat loss

(a) Cooling/heating rack (b) Exchanger test box

Figure 8: Photos of test setup.

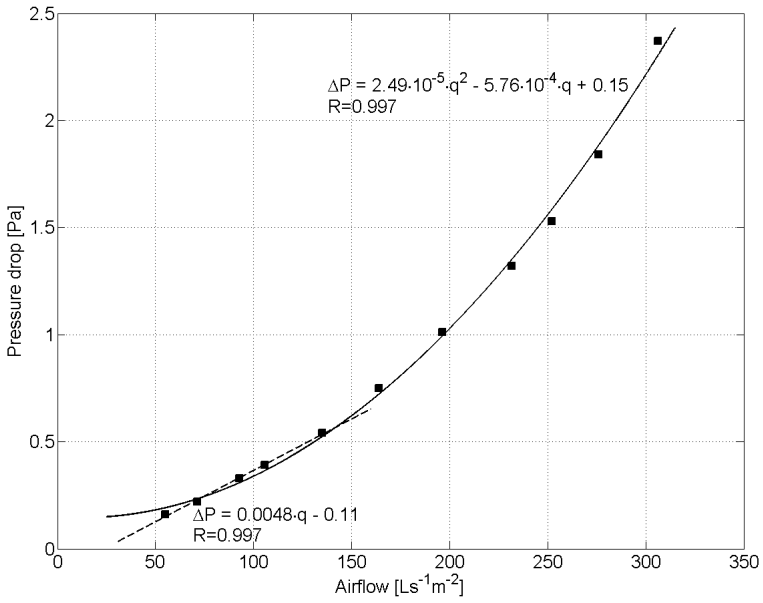

Figure 9: Pressure drop characteristic of tube bank. Below an airflow rate of $150\,\mathrm{Ls^{-1}m^{-2}}$ the characteristic corresponds closely to a linear relationship.

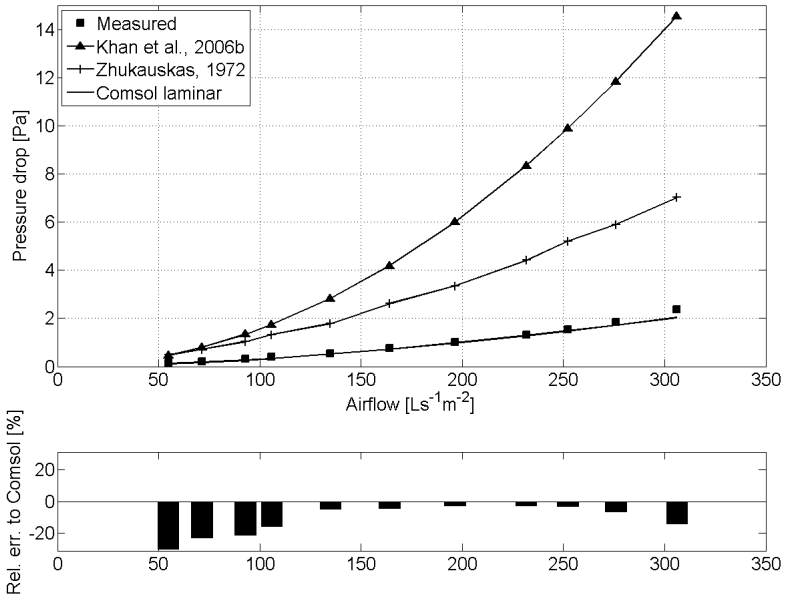

Figure 10: Comparison of measured pressure drop with the literature and Comsol. The bar plot denotes the relative error between measurements and the Comsol-derived pressure drops.

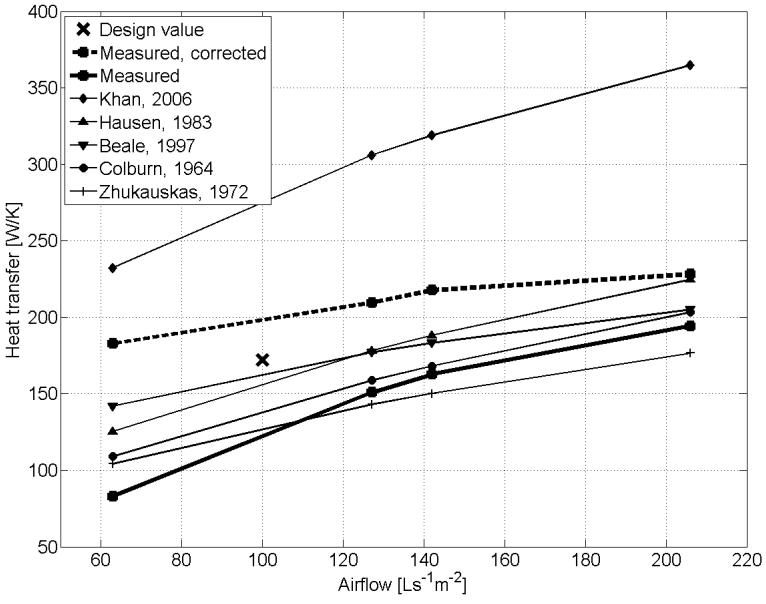

Figure 11: Comparison of measured heat transfer with the literature.

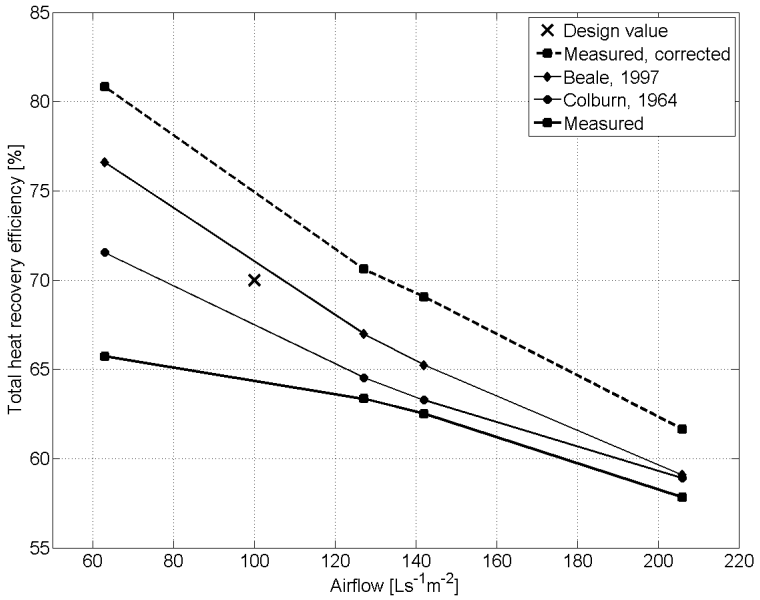

Figure 12: Total heat recovery efficiency. Comparison of measured and corrected values with the literature.

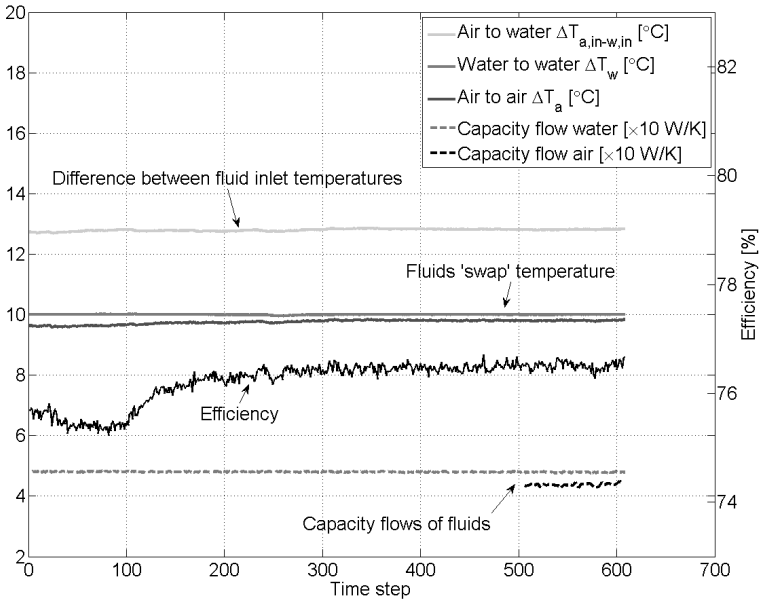

Figure 13: Example of measured data. The legend is described in detail in section 4

.

from the water tubes due to higher temperatures than from the air.

Figure 11 illustrates measured and corrected heat transfer together with a number of literature sources. The corrected values are a result of an estimate of the parasitic heat loss from the wooden test box. In order to quantify the loss a test was performed that measured the cooling of water at zero airflow. The cooling totals 1.07 K, which corresponds to 9.9 W/K. The parasitic heat loss was artificially concentrated in the water inlet, although in reality it is spread out over the entire exchanger. Thus the resulting heat transfer lies somewhere between the measured values and the corrected values. In Figure 11, it is clear that Khan et al. [8] overpredict the heat transfer while other sources, Beale, [9], Hausen [10] and Colburn [16] agree well. Comsol [13] was not used for supplemental analysis of the heat transfer because the complex temperature pattern in an operating exchanger would require a costly, full 3D model of airflow, water flow and solids.

From (2) we calculated the efficiency of the exchanger. The nominator and denominator were replaced with the measured temperature differences from Figure 7 ΔT_{a} and $\Delta T_{\mathrm{a,in-w,in}}$ resulting in an efficiency for the design flow rate $100\,\mathrm{Ls^{-1}m^{-2}}$ of 75.6%. The total system temperature exchange efficiency when two exchangers are employed was calculated from (23). This is illustrated in Figure 12, where the design airflow yields an efficiency between 64.4–74.9% depending on the source. However, if we use the Nusselt numbers from Beale [9] and Colburn [16] the interval is 67.5–71.0%, also well within the measured and the corrected values and very close to the initial design value of 70%.

We can also use Figure 12 to gain an idea of the efficiency change when the airflow differs from the design flow rate, e.g. when the exchanger is part of an operating heat recovery system in a naturally ventilated building subjected to fluctuating pressure conditions. The Colburn curve in the figure is approx. linear in a range $\pm 40\,\mathrm{Ls^{-1}m^{-2}}$ from the design value of $100\,\mathrm{Ls^{-1}m^{-2}}$. The slope is approx. -0.11 resulting in an efficiency change of ±4.4 percentage-point for airflow fluctuations of ±40% from a mean airflow value. However, this effect should be further investigated and quantified in a full-scale test setup.

Equally important for a full-scale test setup is the effect of antifreeze fluid in the liquid loop. Due to the changed properties of an aqueous solution of 30 vol-pct. propylene glycol, an efficiency drop is expected. Using the property values from Table 1, the temperature efficiency drop can be calculated to be 0.3 percentage points, which we consider negligible. However, the effect on the pump pressure loss is more significant (from 521 to 1773 Pa) due to the increased viscosity of the fluid. This is, however, still within the operating range of a small domestic circulation pump.

5.3. *Preliminary improvements*

A very direct consequence of the discrepancy between the pressure drop design value and the measured value is that this can be exploited by increasing the number of tube layers, and so increasing the heat transfer efficiency, without compromising the initial design criterion of 1 Pa. To quantify the effect, we followed the analytical framework and calculated the performance of an exchanger with twice as many tube layers. The result is shown in Table 2. The total tube length increases by 57% but the face area can be reduced by 21%. The pressure drop, based on a calculation in Comsol, increases by 62%, but the total system efficiency increases to 80% at a design flow rate of $100\,\mathrm{Ls^{-1}m^{-2}}$. Other improvement issues left for future investigations could include tube diameter, tube material thickness, pitch ratios and tube shapes.

Table 2 also includes for comparison the size and performance of a conventional commercial rotational heat exchanger from the company Hoval AG. We used the company software *CARS 2009* [17] to select a wheel with equal efficiency. This is achievable with quite small dimensions, but at the expense of the pressure drop. It is clear that the dimensions of the passive exchanger require the overall ventilation concept to be integrated as a core element at the very earliest building design phase to be economically competitive with conventional heat recovery.

6. Conclusion

The dual-sided issue of indoor environment and energy consumption have become increasingly important in building design. One possible solution is to ventilate by passive means, such as stack effect and wind pressure, but this requires the development of new concepts and components. Here we have presented the outline of a heat recovery concept suitable for passive ventilation systems where the available driving pressure is well below 10 Pa. The heat recovery concept is based on two air-to-liquid exchangers interconnected by a liquid loop powered by a pump. The core element of the concept, a prototype of a heat exchanger was developed based on initial design criteria about pressure drop, efficiency and production concerns. The performance was confirmed by comparing the pressure drop and heat transfer measured on a section with numerical fluid calculations and

Table 2: Effect of doubling the number of tube layers.

Tube layers		28	56	Commercial rotary exchanger
Dimensions	m	$3.00 \times 1.92 \times 0.31$	$3.00 \times 1.51 \times 0.62$	$1.08 \times 1.08 \times 0.32$
Face area	m^2	5.76	4.54	1.0
Total tube length	m	6724	10565	-
Total pressure drop	Pa	0.74	1.2	49
Heat transfer	W/K	172	262	-
Total efficiency	%	70	80	80

various literature sources. The measurements and calculations agree reasonably well, but also show room for improvement in the analytical pressure drop calculation technique. The properties measured were pressure drop (0.37 Pa) and heat transfer efficiency (75.6 %). Based on energy conservation, the total heat recovery efficiency for a system with two liquid-coupled heat exchangers was calculated to be between 64.4–74.9 % depending on the parasitic heat loss from the test setup. To compare with the efficiency of conventional heat recovery, the Danish Building Code requires a temperature efficiency of 65%, a value which is expected to increase in the future. However, since the pressure drop is a factor of 4 lower than initially believed in the design phase, this can be exploited by increasing the number of tube layers, and so increasing the heat transfer efficiency without compromising the initial design criterion of a pressure drop of 1 Pa. We calculated the efficiency to go from 70 to 80% by increasing the total tube length by 57% and allowing the pressure drop to rise to 1.2 Pa. An alternative benefit from more tube layers is that the size of the face area can be reduced while maintaining the efficiency.

The heat exchanger has been subjected to indoor experiments under controlled ambient conditions and not yet subjected to realistic operation conditions in a building where fluctuating ventilation flow and unexpected parasitic heat losses may exist. This should be the main research objective of a full-scale test setup.

References

[1] J.M. Schultz, B. Saxhof, Natural ventilation with heat recovery, Air Infiltration Rev. 15 (1994) 9-12.

[2] L. Shao, S.B. Riffat, G. Gan, Heat recovery with low pressure loss for natural ventilation, Energy and Buildings 28 (2) (1998) 179-184.

[3] L.L. Overgaard, E. Nørgaard, S.Ø. Jensen, and K.B. Madsen, Komponenter til naturlig ventilation - Del 2 - Luft-til-væske varmeveksler, Teknologisk Institut Energidivisionen, 2002.

[4] A. Horvat, M. Leskovar, B. Mavko, Comparison of heat transfer conditions in tube bundle cross-flow for different tube shapes, International Journal of Heat and Mass Transfer 49 (5-6) (2006) 1027-1038.

[5] F.P. Incropera, D.P. DeWitt, Introduction to Heat Transfer, John Wiley & Sons, Inc., New York, 2002

[6] V.K. Mandhani, R.P. Chhabra, V. Eswaran, Forced convection heat transfer in tube banks in cross flow, Chemical Engineering Science 57 (3) (2002) 379-391.

[7] EN 15251, Indoor environmental input parameters for design and assessment of energy performance of buildings addressing indoor air quality, thermal environment, lighting and acoustics, European Standard, European Committee for Standardization, Brussels, 2007

[8] W.A. Khan, J.R. Culham, M.M. Yovanovich, Convection heat transfer from tube banks in cross-flow: Analytical approach, Int. Jour. Heat and Mass Transfer 49 (2006), 4831-4838

[9] S.B. Beale, Tube banks, Single-phase heat transfer, in: International Encyclopedia of Heat and Mass Transfer, CRC Press, Inc., edited by G.F. Hewitt, G.L. Shires, Y.V. Polyshaev, 1997, 1181-1188

[10] H. Hausen, Heat Transfer in Counterflow Parallel Flow and Cross Flow, McGraw-Hill, Inc., New York, 1983.

[11] R.W. Fox, A.T. McDonald, P.J. Prichard, Introduction to Fluid Mechanics, 6th edition, John Wiley & Sons, New Jersey, USA, 2006

[12] W.A. Khan, J.R. Culham, M.M. Yovanovich, Optimal design of tube banks in crossflow using entropy generation minimization method, in: Proceedings of 44th AIAA Aerospace Sciences Meeting and Exhibit, Reno, Nevada, 2006.

[13] Comsol, Comsol Multiphysics version 3.5a, 2009, Available from: http://www.comsol.com

[14] A.W.M. van Schijndel, Integrated Heat Air and Moisture Modeling and Simulation, Ph.D. thesis, Technische Universiteit Eindhoven, Netherlands, 2007.

[15] A.P. Zhukauskas, Heat Transfer from Tube in Cross Flow, in: J.P. Hartnett and T.F. Irvine, Jr. (Eds.), Advances in Heat Transfer, Vol. 8, Academic Press, New York, 1972

[16] A.P. Colburn, A method of correlating forced convection heat transfer data and a comparison with fluid friction, International Journal of Heat and Mass Transfer, 7 (12) (1964), 1359-1384.

[17] CARS 2009, Hoval AG, 2009, Available from: http://www.hoval.com

Paper III

Submitted to Energy and Buildings, 2010

Experimental and numerical analysis of perforated suspended ceilings as diffuse ventilation air inlets

Christian Anker Hviid[*,a,b], Svend Svendsen[b]

[a]*ALECTIA A/S, Teknikerbyen 34, DK-2830 Virum, Denmark*
[b]*Department of Civil Engineering, Technical University of Denmark, Brovej, Building 118, DK-2800 Kgs. Lyngby, Denmark*

Abstract

Experimental and simulation analyses are reported in this paper for a diffuse ceiling ventilation concept. The analyses were carried out with two different porous surfaces mounted in a suspended ceiling: perforated tiles of aluminium and of gypsum. The experiments were carried out in a climate chamber, and the simulations were performed with CFD. The experiments documented an air change efficiency equal to fully mixed conditions with a pressure drop of 0.5 Pa and with no evidence of thermal discomfort. Furthermore, the measurements documented that the ceiling acts as a radiant cooling surface which increases the potential and applicability of the concept. The numerical analyses used an approximate method to model the pre-heating in the porous ceiling and generally supported the experimental conclusion, but it also showed risks of downdrafts especially in areas where thermal plumes do not counteract the cool supply air.

Key words: comfort ventilation, diffuse ventilation, ventilation efficiency, thermal comfort, CFD, tracer-gas

1. Introduction

The main purpose of the ventilation system in a building is to supply fresh air to the occupants and to remove heat, gases and particulate matter emitted from the building and its use. The ventilation system should do so energy-efficiently and with minimal risk of draught in the occupied comfort zone. Two major ventilation principles are commonly employed in non-industrial spaces: mixing and displacement ventilation. The mixing principle dilutes the contaminant concentration, while the displacement principle follows a stratification strategy separating stale air from fresh air.

An alternative ventilation concept of supplying fresh air is through perforations in the ceiling. The concept is known as diffuse ceiling ventilation or vertical ventilation and is characterized by air being supplied over a very large surface area occupying a substantial part of the ceiling. The inlet velocity is very small and with no fixed jet direction, hence the term diffuse. The concept is particularly known in special applications like the clean room industry where the airflow resembles piston flow [1]. Air is supplied in the laminar range, encompasses the area of interest and abolishes all convection currents due to heat or movement. Uniform air distribution is achieved by various filters in the diffuser inducing a certain pressure drop.

Another, and quite common, application is in livestock buildings where diffuse ceiling ventilation is a cheap method of providing fresh air to the animals [2, 3]. Because of the non-impulse supply from the ceiling area the mixing is dependent on the buoyant forces present from the thermal loads. The advantage is that the system does not produce draught by itself, however, insufficient mixing and high vertical temperature gradients at high heat loads are unavoidable [4].

Application of the diffuse ceiling concept to indoor spaces occupied by humans is known in practise, but the research is limited and early results are very few [5]. A recent work included laboratory experiments and numerical analysis [6] of a two-persons office. The experiments included measurements of local air velocities and temperatures for draught ratings and investigated the ventilation effectiveness with tracer-gas. The diffuse ceiling was made from 30 mm acoustic mineral fibre with a painted surface and the suspension system was similar to the one in Figure 3(b). The painted low-permeable surface caused most of the inlet air to

[*]Corresponding author. Tel.: +45 88 191 365; fax: +45 88 191 001

Email address: crh@alectia.com (Christian Anker Hviid)

penetrate through cracks between tiles and suspension. The overall conclusion was very beneficial for the diffuse ceiling. Compared to other means of air supply the diffuse inlet exhibited superior performance in terms of possible concurrent flow rate and low inlet temperature without causing draught in the comfort zone [7]. Similar findings was reported by Jacobs et.al. [8] in a study of a classroom with two different types of perforations. While Nielsen et.al. [7] did not reflect on the limited pressure drop of the diffuse ceiling, and its positive impact on the energy consumption, Jacobs et.al. commented on the simultaneous low fan energy consumption, modest investment costs, and low noise levels that the diffuse ceiling has to offer.

The objective of the research reported in this paper is to assess the applicability of porous ceiling tiles for diffuse ceiling ventilation in premises for humans with high thermal load. Subsequently it is to investigate the sensitivity of the thermal comfort in the occupied zone from inlet temperature and flow rate and to disclose performance deficiencies. The deficiencies for low-pressure drop ceilings are possibly inadequate air change efficiency caused by poor air distribution above and below the ceiling. Poor air change is characterized by stagnant zones and short circuiting of the ventilation air. Alternatively poor air distribution may produce downdraughts from the cool inlet air resulting in local discomfort. Also measurements of the pressure drop and pre-heating in the porous ceiling is reported, and we discuss the radiant cooling potential and the energy transfer between inlet air and ceiling material. We also reflect on the constructive and economic advantages that are the consequences of reduced ductwork, no diffusers and reduced fan power due to the low pressure drop in the ceiling.

2. Diffuse ceiling ventilation

The conventional mixing principle supplies air from one or multiple diffusers. The diffusers are placed outside the occupant zone, and mixing is induced by a high impulse air stream that acts through entrainment of the room air. Numerous mixing diffusers has been tested and reported in the literature [9]. The displacement principle exploits the thermal load in the room and the associated buoyancy effects to create stratification that replaces the contaminated air with fresh air. Mixing ventilation is generally often the better choice in single offices where the heat load is limited, while displacement has proven superior in rooms with high occupant density and high thermal load, e.g. conference rooms and classrooms [10]. To avoid draught both principles require optimization and accurate operating control of two basic design parameters: inlet temperature and supply air velocity.

The risk of draught effectively limits the cooling capacity particularly in premises with high occupant density and thermal load. Fitzner, referred in [11], constructed a rough guide to what system is most likely not to cause draught. Similarly, a design chart based on the Archimedes number was constructed [12].

However, in premises with high occupant density and thermal load, increased ventilation flow rate and lower supply temperature augments the risk of draught. Considering a classroom with an occupant density of $2\,\mathrm{m}^2$/person the comfort ventilation rate that complies with indoor class I (low-polluting building) is $5.1\,\mathrm{Ls}^{-1}\mathrm{m}^{-2}$ [13]. With this flow rate the thermal load requires cooling of the inlet air by 9.7 °C and half of that if the flow rate is doubled. Both operation modes are close to the upper limit of mixing flow [11], and applying displacement flow requires an adjacent zone ($l_{0.2}$) that is too large in a confined space with high occupant density [10]. According to Nielsen et.al. [7] displacement is not an option at all. A possible solution includes the combination of air ventilation with hydronic radiant cooled ceilings [14, 15, 16, 17], but to achieve comfort the simultaneous control of radiant cooling and air flow is challenging.

Diffuse ceiling ventilation does not mix or displace the room air by itself. Rather it depends on the buoyant forces in the room to mix the air. Jacobsen et.al. [18] showed how the location of the heat sources governs the prevailing air flow pattern in livestock buildings with diffuse ceiling ventilation. The thermal plume is the strongest current in the enclosure, and it acts by deflecting the downward cool air current from the ceiling. Thus the ventilation pattern takes the form of room size vortices that act through a mixture of displacement and mixing.

In livestock buildings the ceiling material is mineral fibres, glass fibres, or wood concrete plates with a thickness of 25–200 mm and with high permeability. Typical pressure drops are 20–40 Pa [19] in effect making the plenum a pressure chamber where the supply air penetrates the ceiling material equally and unidirectionally over the entire surface. The porous material pre-conditions the fresh air by a combination of radiative and convective energy transfer. The solid material absorbs radiative energy from the enclosure, and convection in the pores of the material pre-heats the inlet air to a temperature where the radiative and convective energy transfer balances. At low temperature

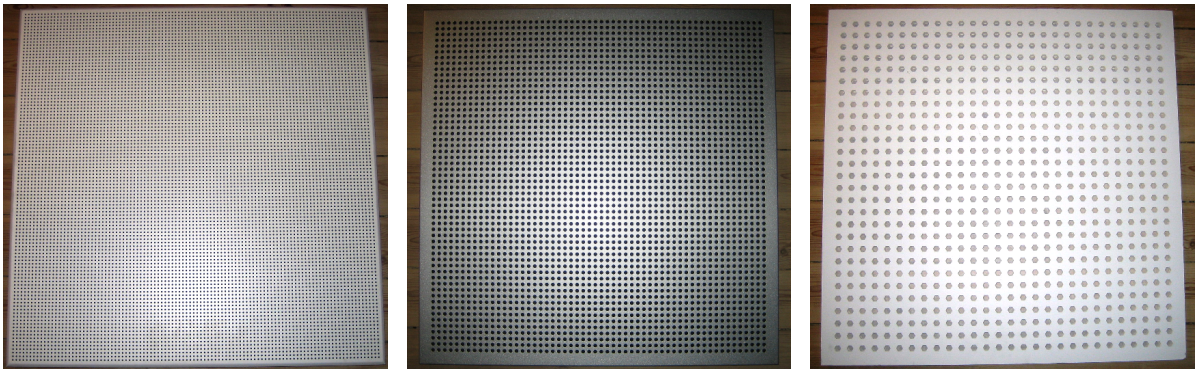

(a) Alu-16 (b) Alu-28 (c) Gyp-17

Figure 1: Photos of experimental ceiling tiles.

differences, the relative energy transfer due to radiative exchange becomes the governing heat transport process [3]. This expands the applicability of the diffuse ceiling to be a combination of ventilation supply and radiant cooling ceiling.

The heat exchanger effect that occurs when air penetrates counterflow insulation has been extensively investigated in housing by Elmroth et.al. [20]. He pointed out that the small pressure drop across the insulation made it difficult to achieve uni-directional airflow and uniform heat transfer over the entire surface area. In his study the heated room air rose above the insulation, displaced the colder fresh air, and deteriorated the heat transfer. Jacobsen [3] found that the room air penetrated the ceiling material to some degree, but reverse flow was not observed. Neither was it observed at pressure differences of approx. 1.5–4.5 Pa [6].

2.1. Porous acoustic ventilation ceilings

In this study we exploit the properties of the suspended acoustic ceiling. The assessed suspended ceilings comprise two types of tiles. One tile is a perforated aluminium sheet, and another is a perforated gypsum board. Furthermore, a second aluminium tile with higher permeability is assessed in terms of pressure drop. Figure 1 shows photos of the three tiles, Table 1 lists the experimental tile types and Figure 2 illustrates the perforation characteristics. All tiles are commercial products and are sold as acoustic ceiling tiles with specific suspension systems. The acoustic performance stems largely from the textile that is glued to the backside. The textile on the aluminium tiles is 0.22 mm thick [21] while the textile on the gypsum tile is of a denser undocumented type. We expect that the textile accounts for a large part of the pressure drop.

Table 1: Ceiling tiles.

Name	Material	Thickness mm	Open area %
Alu-16	Aluminium	0.6	16.2%
Alu-28	Aluminium	0.6	28.3%
Gyp-17	Gypsum	12.5	17.0%

The suspension systems are custom made to the tile type. The aluminium tiles are fixed by pushing the taps into the squeezer of the suspension profile. Only two opposite tabs are used to fixate the tile. The gypsum tiles simply rests on a reverse T-profile. The systems are illustrated in Figure 3.

3. Experimental analysis

The experiments were carried out in a test facility located at the Technical University of Denmark. The experiments included measurements of pressure drop across two types of porous tiles mounted in the suspension system in the room and for comparison across unmounted single tiles. Tracer-gas was used to measure air change efficiency and identify stagnant zones. Local discomfort was estimated in multiple locations by measuring air velocity and temperature. Also room air temperature gradient and ceiling temperature was measured and reported.

3.1. Test chamber

The test facility consists of a climate chamber with walls of gypsum and upper and lower deck of concrete. The inner dimensions of the test chamber are

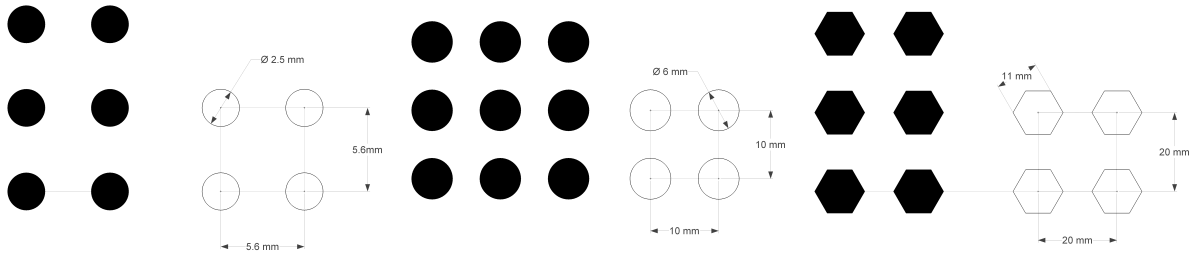

(a) Alu-16 (b) Alu-28 (c) Gyp-17

Figure 2: Schematic of ceiling tile perforations.

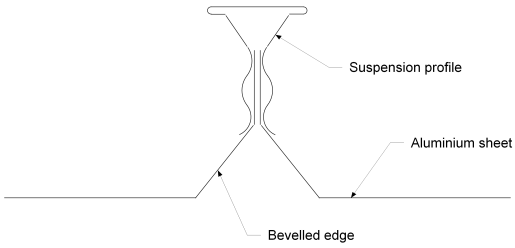

(a) Aluminium tile

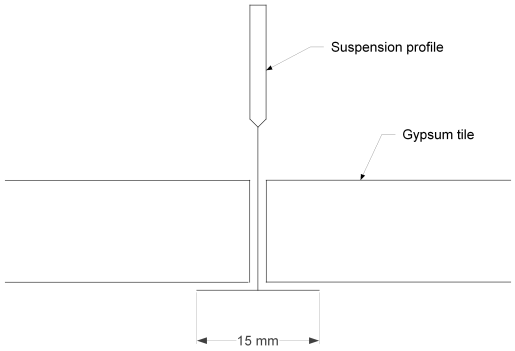

(b) Gypsum tile

Figure 3: Schematic of ceiling suspension systems.

$3.6 \times 6.0 \times 3.5$ m as depicted in Figure 4. The porous ceiling was suspended approx. 0.6 m from the upper concrete deck which makes the volume of the ventilated room 62.6 m^3. The suspension length was longer than required due to constructional obstructions in the test chamber. The inlet was located above the suspended ceiling slightly off-center, and the outlet was located below the ceiling, also off-center. Both ducts are marked in the Figure 4. The inlet and outlet of the test chamber was connected to a neighbouring cooling chamber by two 200 mm ducts. Air was drawn from the test facility space into the cooling chamber by means of a fan, cooled when it passes through the chamber, and supplied to the test chamber. The extract air was drawn directly from the test chamber and exhausted to the test facility space. The ventilation system was not balanced so the amount of extracted air through the outlet duct was a function of the exfiltration of the test chamber. The airflow rate was measured in the inlet duct by the relation of flow rate and static pressure change across an orifice from Fläkt model EHBA-012-1. The pressure drop was measured by a micromanometer from Furness Controls model FCO510 with an accuracy of 0.25%. The accuracy of the orifice is ±5%.

Nine black-painted metal barrels each equipped with two 60 W light bulbs imitated 9 persons with a latent heat release of 120 W which corresponds to 1 Met for adults or a heat gain of 50 W/m^2 floor. The diameter and height of the barrels are 28 cm and 46 cm, respectively. The barrels are arranged with three at each table generating a concentrated yet diffuse heat source in the room, see Figure 4.

3.2. Measurements

The conducted investigations included tracer-gas experiments, comfort measurements in critical points and pressure drop measurements. The pre-heating potential

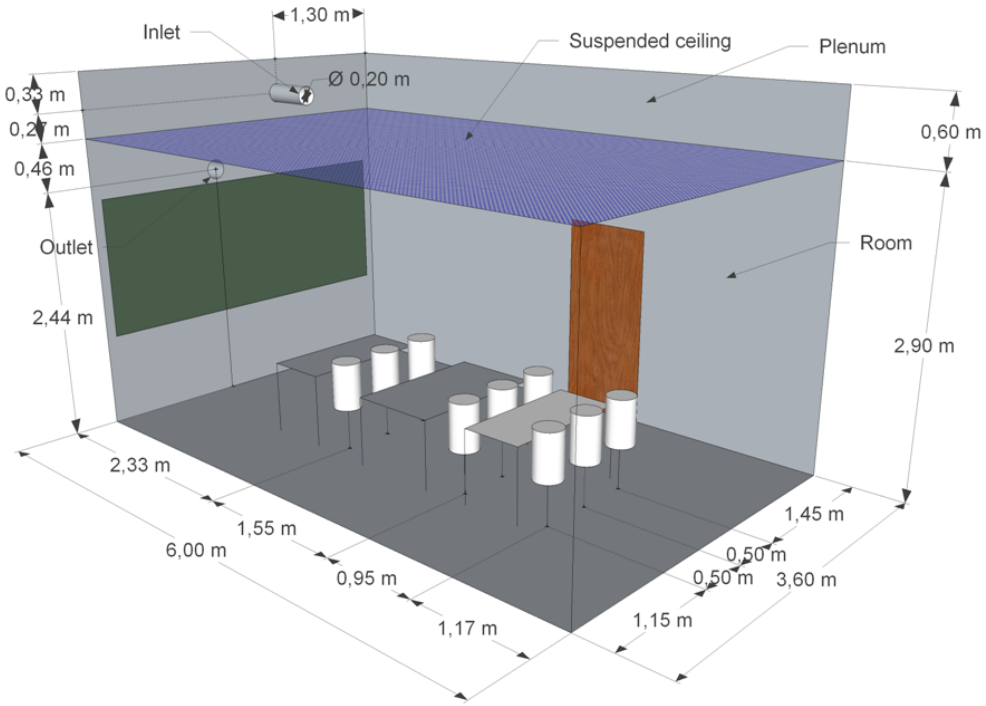

Figure 4: Dimensions of test chamber and experimental setup.

Figure 5: Photo of the arrangement of the test chamber.

Table 2: Test cases.

Case	Air change h^{-1}	Flow rate m^3/s	Internal load W	Inlet temp. $°C$
1	2.3	0.040	1080	-3.2
2	3.0	0.053	1080	3.2
3	6.0	0.105	1080	11.2

of the suspended ceiling was also investigated. The investigations were all carried out for three cases in terms of flow rate and inlet temperature. The cases are described in detail in Table 2 and cover a wide range of ventilation flow rates from approx. indoor climate category 1 to 3 by the European Standard [13]. The inlet temperatures were determined so that an approximate steady state condition of 20 °C applied to the test setup during measurements. The ambient temperature was approx. 20 °C, hence steady state implied that the walls surfaces of the test chamber were approx. 20 °C.

Two indices can be derived from the tracer-gas experiments that characterizes the performance of the perforated ceiling: the air change efficiency of the room and the local mean age of air in discrete points. The air change efficiency index characterizes the room averaged mixing capability of the diffuse ceiling ventilation

and the local mean age of air index discloses zones of short-circuiting or stagnant ventilation air.

Local air velocities and air temperatures together with the temperature gradient of the room were measured to disclose local discomfort in the occupied zone due to unpremeditated downdrafts by the cooled inlet air. Radiant asymmetry was also quantified by logging the ceiling surface temperature. From the temperature difference across the ceiling and the surface temperature of the concrete deck in plenum, the pre-heating potential was quantified.

3.3. Tracer-gas

The tracer-gas experiments followed the concentration-decay method where tracer-gas is injected into the chamber until constant concentration is achieved. During the injection the chamber was fully mixed by means of domestic swivel fans. When the gas build-up was finished with a constant concentration in all sampling points the dosing was stopped and the domestic fans switched off. The following concentration decay was logged in each individual sampling point, and from this the local mean age of air in each point was derived. By comparing inter-point values problematic zones can be revealed. The decay was started from a constant concentration of approx. 5 or 10 ppm depending on air change and initial background concentration. The gas concentration was sampled from a total of 12 points: eight points within the room, two points in plenum, one point in the exhaust duct, and one point sampled the background concentration in the inlet. Figure 6 marks the positions of the sampling points. The eight points in the room were placed at the height of 1.1 m with six points along the perimeter and two points placed among the heat sources. The locations in the room were selected to uncover inadequate mixing in the occupied zone while the plenum locations were selected to investigate the possibility of reverse flow. The background concentration was monitored because extract air was exhausted to the test facility space where also the intake air was drawn from. Consequently the background concentration increased with time depending on the test facility air volume and the ventilation rates. The background concentration was subtracted from all other concentrations, and if it was allowed to rise to too high levels, e.g. by inadequate air change in the test facility, the resulting noise at the end of the decay, where concentrations within the test chamber decrease to the same level of the background, would render the measured values unusable. We used freon R-134a as tracer-gas ($C_2H_2F_4$) which has a density of 4.25 kg/m^3, about 3.5 times heavier than air. To avoid spillage the gas was mixed with chamber air by a domestic fan. The dosing location is marked on Figure 6. Four other domestic swivel fans located in the corners ensured that fully mixed conditions applied to the entire chamber. Gas dosing and sampling equipment comprised a photo-acoustic multi-gas monitor from Innova model 1312 and two multipoint sampler and doser from Innova/Brüel & Kjær model 1303.

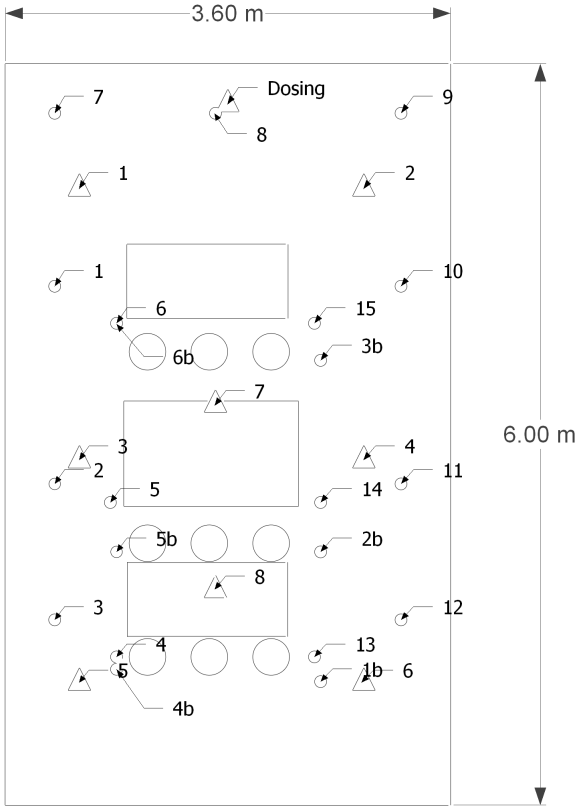

Figure 6: Measurement locations of local velocity and air temperatures (small circles) and tracer-gas (triangles.)

3.3.1. Age of air

The age of the air characterizes the 'freshness' and diluting capabilities of the air, and it can be calculated by continuously monitoring the concentration at the point in question. If stagnant zones exist or short circuiting occurs the local age will be higher or lower, respectively, than the room mean age. The concept was introduced by Sandberg [22] and has proven to be a useful tool in evaluating ventilation effectiveness [10]. For a comprehensive description of the concept, refer to [23]. In short the concept pictures the air particles coming from the ventilation system and arriving at a given location p after a time τ. Because there is a large number

Table 3: Air change efficiencies for some flow patterns.

Flow pattern	Air change efficiency, ϵ^a
Ideal piston	100%
Displacement	50-100%
Fully mixed	50%
Short-circuited flow	<50%

of particles the time will vary from one particle to the other and the statistical age distribution of all particles that arrive at the point p over time is the local mean age of air $\overline{\tau}_p$. Using the notation in [10]:

$$\overline{\tau}_p = \int_0^\infty \frac{c_p(t)}{c_e(0)}\, dt \tag{1}$$

where $c_p(t)$ is the tracer-gas concentration at point p as a function of time t. The room mean age of air is then the spatial average of all local mean ages in the room and is found by logging the decay in the exhaust:

$$\langle\overline{\tau}\rangle = \frac{1}{\tau_n}\int_0^\infty t\,\frac{c_e(t)}{c_e(0)}\, dt \tag{2}$$

where τ_n is the nominal time constant being the inverse of the air exchange. In the exhaust τ_n is equal to the local mean age of air.

3.3.2. Air change efficiency

The air change efficiency ϵ^a is a measure of the average time it takes to replace the air in the room $\overline{\tau}_r$ compared to the shortest possible air change time. It is the ratio of the shortest possible air change time in the room, i.e. the nominal time constant τ_n, and the actual air change time $\overline{\tau}_r$ [10].

$$\epsilon^a = \frac{\tau_n}{\overline{\tau}_r}\cdot 100\% \tag{3}$$

The actual air change time $\overline{\tau}_r$ can be derived from the room mean age of air by:

$$\overline{\tau}_r = 2\langle\overline{\tau}\rangle \tag{4}$$

If the room is fully mixed the actual air change time $\overline{\tau_r}$ is twice the shortest possible time τ_n. Thus fully mixing gives a maximum result of 50% air change efficiency. Table 3 compares the expected air change efficiencies for different ventilation principles

3.4. Temperature measurements

Temperatures were measured with copper-constantan thermocouples, type TT. The thermocouples produced an electric current that was converted in a datalogger to an absolute temperature with a precision of ±1 K using an internal reference circuit. The datalogger sampled every ten seconds, and the precision of the thermocouples was improved by always averaging over 10 samples. In the reported results the standard deviation is always listed if it has an impact on the last digit. The datalogger was an Agilent 3497A Data Acquisition Unit. The sampled temperatures were the ventilation inlet and outlet, the upper concrete deck surface temperature, the ceiling lower surface temperature denoted ceiling temperature, the temperature difference between the lower and upper ceiling side and the difference between lower ceiling side and plenum temperature. The two latter temperatures were derived from two thermopiles. Nine thermocouples were also used to measure the vertical temperature gradient. Each thermocouple was placed in a small open aluminium cylinder that acted as a radiative shield and subsequently positioned on a pole at different heights from 0.14 to 2.9 m. The heights are marked in Figure 16.

3.5. Thermal comfort

Mixing is governed by buoyant forces in diffuse ceiling ventilation. Consequently good mixing may be an indicator of strong convective flows with augmented risk of draught. To assess discomfort local air velocity and air temperature measurements were performed with an Indoor Climate Analyzer from Brüel & Kjær model 1213. Figure 6 marks the positions of measurements which were selected to cover the occupied zone, i.e. to disclose cold downdrafts from the ceiling. This means that the points were located close to the ankles and neck of the occupants and additional points were placed along the perimeter of the room. The positions numbered 1–15 were performed at 1.1 m and numbers 1b–6b at 0.1 m. Each measurement was averaged over 3 minutes.

From the measurements we derive the local draught rating, i.e. the percentage of dissatisfied people due to draught from ISO7730 [24]:

$$DR = (34 - T_{a,l})(\overline{v}_{a,l} - 0.05)^{0.62}(0.37\overline{v}_{a,l}Tu + 3.14) \tag{5}$$

where index a, l denotes the local air in question, T is the temperature, $\overline{v}$ is the mean air velocity and Tu is the turbulence intensity. The definition of Tu is the fraction of the standard deviation σ to the mean air velocity $\overline{v}$ over the specified time period of 3 minutes:

$$Tu = \frac{\sigma}{\overline{v}} \tag{6}$$

According to ISO7730 the indoor climate categories A, B and C, allow a draught rating up to 10, 20 and 30%,

respectively. Requirements in ISO7730 for vertical temperature difference between head and feet and radiant asymmetry are commented upon.

4. Numerical analysis

Numerical simulation of a total of six cases is presented in this section. The numerical cases comprise simulations of the three experimental cases in the test chamber and three simulations of a classroom with high thermal load. The numerical analyses were conducted to further investigate the performance of porous suspended ceilings as diffuse ventilation inlets and widen the applicability of the concept. We used the commercial computational fluid dynamics software Fluent [25] with the standard k-ϵ-turbulence model. Heat transfer was modelled with standard wall functions and adapted grid so the dimensionless wall grid distance y^+ complied with the requirements in the Fluent manual for heat transfer at walls. First-order discretization was used for all variables to make the simulation robust against the convergence challenges that a porous zone pose. The suspended ceiling was modelled as a narrow 2 cm thick porous zone with imposed properties corresponding to the measured pressure drop of the gyp-17 ceiling. The gyp-17 ceiling was chosen for numerical simulation because it had the lowest pressure drop and thus was the most critical in terms of reverse flow and air distribution in plenum.

4.1. Representation of porous ceiling

The suspended ceiling acts as a resistance to the fluid flow and must be correctly modelled in the numerical analysis. Fluent [25] incorporates a porous medium model that is capable of modelling the pressure jump by adding a momentum source term in the governing momentum equations. The source term S contributes to the pressure gradient Δp in the porous medium with thickness Δn by a quadratic relationship between flow rate and pressure difference where μ/α is the laminar term and $C_2 \frac{1}{2}\rho$) is the turbulent term:

$$\Delta p_i = -\left(\frac{\mu}{\alpha} v_i + C_2 \frac{1}{2} \rho v_i^2\right) \Delta n \tag{7}$$

From Figure 12 we derived velocity and pressure drop for the gyp-17 ceiling, while we remembered that the porous ceiling thickness in the Fluent model was 2 cm due to grid size issues. This yielded the following input to the porous model perpendicular to the ceiling: a viscous resistance factor $1/\alpha$ of $1.109 \cdot 10^9$ and an inertial resistance factor C_2 of $5.212 \cdot 10^6$. The Fluent manual [26] recommends that the laminar and turbulent term of the secondary directions, even though the resistance is infinite, are multiplied with a factor 100. However due to unachievable convergence a factor 10 was used instead. Furthermore, we suppressed the calculation of turbulence transport in the porous medium because the linear relationship that we observe in Figure 12 indicated laminar flow through the ceiling fabric.

4.1.1. Radiation model

Accurate modelling of heat transfer in the porous medium is a complex issue. The porous zone model in Fluent does not participate in inter-surface radiative exchange, and indeed no CFD tool incorporates such a model that we know of. However, modelling the heat transfer due to radiation is important for correct comfort estimation. The measurements documented the pre-heating in the ceiling to be in the range 3.2–5.8 °C (Table 6). Furthermore, the ceiling temperature was lower than the room temperature (Figure 16). This means that the radiative exchange from the room surfaces to the ceiling surface plays a role for pre-heating the inlet air when it passes through the holes in the porous ceiling. In the three test cases the pre-heating power was put in manually as an artificial heat source in the porous zone. The magnitude of the source was based on the ceiling temperature difference and mass flow rate. It is an approximate approach that requires laminar flow to prevail. Reynolds number for the three test cases immediately after the inlet was 1700, 2200, and 4100 based on a characteristic length twice the suspended distance. Only the latter case is in the turbulent/transitional range ($Re > 2300$), dropping to 2050 halfway through the plenum, and therefore we believe the approach to be adequate.

A more general approach for cases where no measured data is available is described here. First, we set up a radiative heat balance for room zone and plenum. Figure 8 illustrates two adjacent zones with air nodes, surface nodes and convective resistances. The balance assumes the following:

- the convective resistance between inlet air and upper deck ($R_{c,1}$) is infinite. This is intuitively correct for a laminar inlet flow that is colder than the upper deck surface temperature. Assuming infinite convective resistance is a worst-case scenario because any pre-heating by the concrete deck is neglected

- the vertical flow rate through the porous ceiling is distributed equally

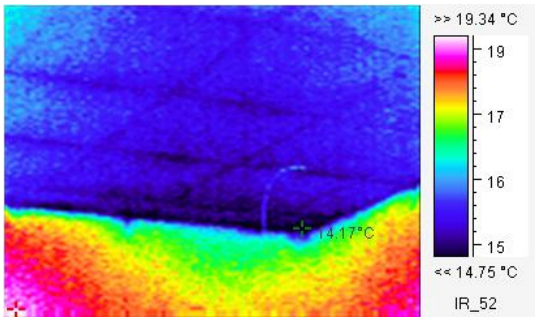

(a) Alu-16 ceiling

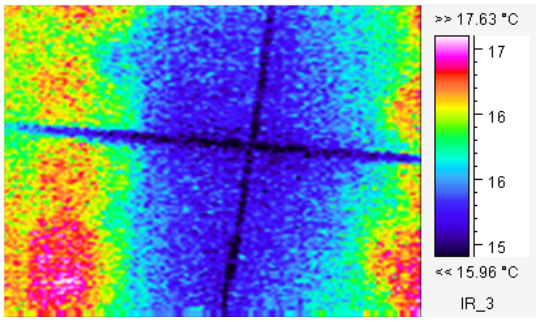

(b) Alu-16 close up

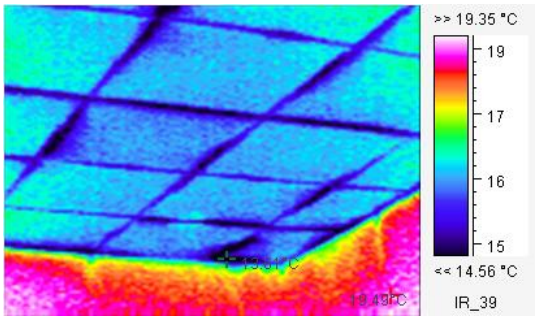

(c) Gyp-17 ceiling

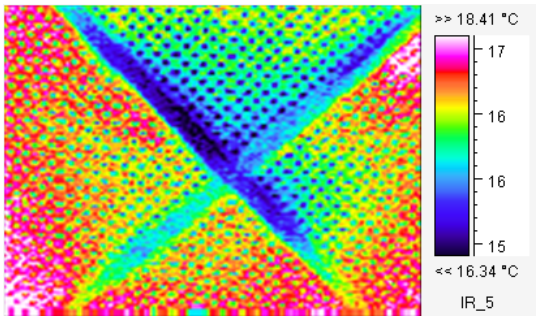

(d) Gyp-17 close-up

Figure 7: Thermovision of alu-16 and gyp-17 ceilings.

- because the flow penetrates the ceiling unidirectionally, the convective resistance between the ceiling surface and the plenum air node ($R_{c,2}$) is zero. Consequently the convective resistance between the ceiling surface and the occupied zone node ($R_{c,3}$) is infinite. This is a also a worst-case scenario because pre-heating due to convection is neglected
- when the inlet air penetrates the ceiling, both ceiling and air acquire the same temperature
- each surface of the enclosure is isothermal and is characterized by uniform radiosity and irradiation
- the enclosure air is taken to be non-participating in the radiation exchange

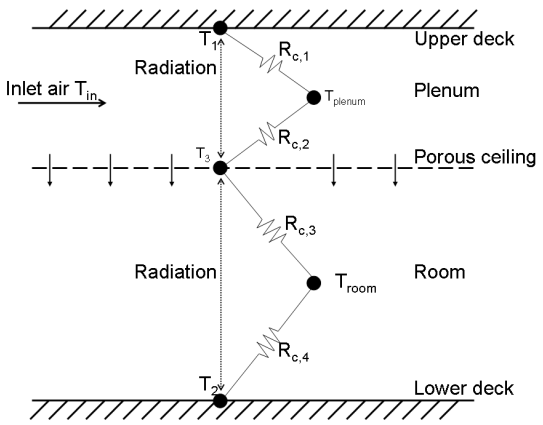

Figure 8: Radiative exchange balance model for two adjacent zones with one common surface.

Assuming that the convective resistance in plenum is infinite for the upper deck and zero for the ceiling, the following applies $T_{plenum} = T_{in}$. Likewise, because $R_{c,3}$ is infinite, $T_{room} = T_2$ applies. For the three simulated class room cases in Table 4 this means that the inlet air is purely heated by the radiative net gain that the suspended ceiling receives from the upper and lower decks and occupants. We solve the net radiative gain by a simple radiation exchange method, see Appendix A and applied it as an artificial heat source in the porous zone.

4.2. Test chamber

The calculation domain of the test chamber was subdivided into plenum and room by the porous media, and the 9 heat sources were distributed in accordance with Figure 6. We simulated the three test cases from Table 2 with the surface boundary conditions described in Table 4.

Table 4: Boundary conditions for numerical analysis.

Case	Boundary	Condition
Test chamber	Convective heat load	120 W/occupant
	Radiative heat load	10/12/32 W/m^2 ceiling
	Floor	20.0 °C
	Room surfaces	20.0 °C
	Plenum surfaces	13.5/14.4/15.3 °C
	Velocity-inlet	1.27/1.65/3.31 m/s
	Inlet temp.	−3.2/3.2/11.2 °C
Class room	Occupant heat load	105 W/occupant
	Radiative heat load	33 W/m^{2}ceiling
	Floor	20.0 °C
	Room surfaces	20.0 °C
	Plenum surfaces	18.0 °C
	Velocity-inlet	0.235 m/s
	Inlet temp.	8 °C

4.3. Class room with high thermal load

Figure 9 illustrates the numerical model of a real size class room. The model is intended to mimick a situation with high air change, high thermal load and low inlet temperature in a confined space. In this case the application of conventional mixing carries an elevated risk of draught, and diffuse ceiling ventilation reportedly reduces that risk [12]. The dimensions of the calculation domain is 12 × 6.3 × 3.5 m, and the ceiling is suspended 0.5 m. The 30 heat sources are formed as real-size manikins with a prescribed sum of convective and radiative heat gain of 120 W/manikin. However, the radiative contribution from each occupant to the ceiling is ≈15 W/manikin, see Appendix A. Consequently we reduced the heat gain per occupant to 105 W/manikin and applied the summed radiative ceiling gain as an artificial heat source in the porous ceiling. Solar gain was not considered because effective solar shading is a requirement in future low-energy buildings. Other boundary conditions are described in Table 4.

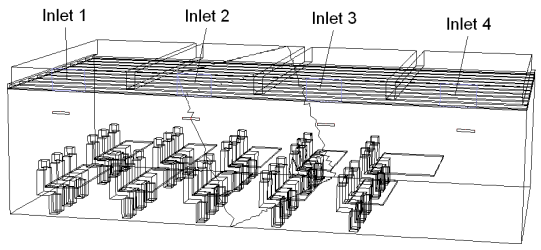

Figure 9: Modelled class room.

Three class room cases were simulated with different subdivision of the ceiling in high and low permeability zones, see Figure 19. The cases were selected to

investigate possible qualitative mixing differences between them. The first case supplies air over the entire ceiling surface, also in areas without counteracting thermal plumes. The second case supplies air through 75% of the ceiling surface corresponding to the area above the manikins, and the third case employs a chess pattern with alternating high and low permeability. Ideally the latter case should increase the mixing interface between supply air and room air. Plenum was served by four velocity inlets each with an area of 0.4 m^2 as depicted in Figure 9. The 75% pattern was only served by inlet 1–3.

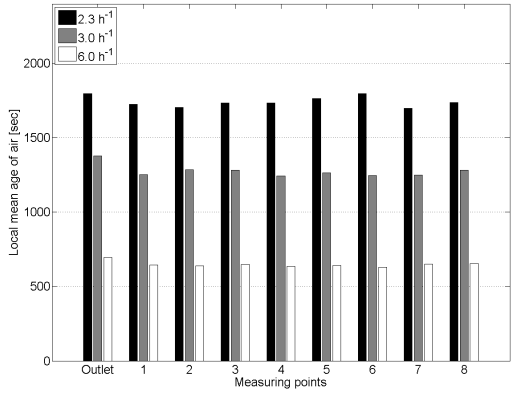

(a) Alu-16

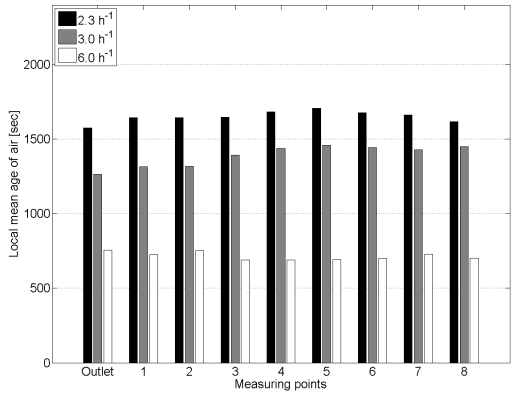

(b) Gyp-17

Figure 10: Mean local age of air. Outlets, i.e. mean room age of air, are included for comparison.

5. Results and discussion

5.1. Pressure drop

The pressure drop of three types of single acoustic tiles is reported together with the pressure drop of two of the tiles mounted in the ceiling suspension system. Figure 11 illustrates the pressure drop of single tiles for different flow rates, and Figure 12 illustrates the same relation for mounted tiles. From the linearity of the curves we conclude that the flow trough the perforations was indeed laminar as expected. The aluminium tiles in Figure 11 exhibit expected behaviour in terms of lower pressure drop with larger open area ratio. The drop is approx. 30% when the open area ratio shifts from 16 to 28%. The gyp-17 tile has approx. 75% higher pressure drop than the alu-16 tile yet the open area ratio is almost the same. This is caused by the acoustic textile on the backside of the tiles which is of a different brand and also of a denser type on the gypsum tile. This suggests that the fabric of the acoustic textile is of greater importance to the pressure drop than the open area ratio of the ceiling. However, the picture is reversed when the tiles are mounted in a ceiling. Figure 12 illustrates this showing that the gypsum ceiling has the lowest pressure drop. This suggests that the suspension system is of greatest importance to the operating pressure drop. The importance of the suspension system is also illustrated in the thermovision pictures in Figure 7, where cracks between tiles and the suspension light up as less air tight.

However, the measured data does not allow for a conclusive statement because while the mounted gypsum tile has a lower pressure drop the mounted aluminium tile has a higher pressure drop. It is clear that the pressure drop is influenced by the open area ratio because alu 28% has lower pressure drop than alu 16%, yet the figures also indicate that the acoustic textile on the backside is the main contributor to the pressure drop since the curve for gypsum 17% lies significantly higher than alu 28%. Comparing with previous work [6] which had a single-mounted pressure drop ratio of 14–39, the ratio here is only 1.2–3 which means that the inlet air is more likely to be distributed over the entire ceiling surface.

5.2. Air change efficiency and age of air

The air change efficiencies are illustrated in Figure 13. It shows almost perfect mixing for all test cases and ceiling types with a slight transition into displacement ventilation for high air change rates, something that could indicate increased risk of downdrafts.

Figure 14 elaborates the room mean air change efficiency by showing the local mean age of air in multiple

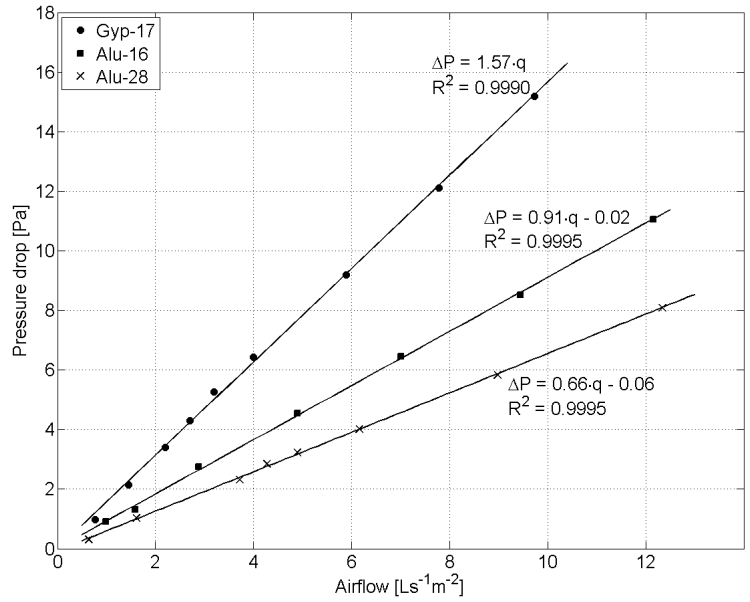

Figure 11: Correlation between pressure drop and airflow for three suspended single tiles.

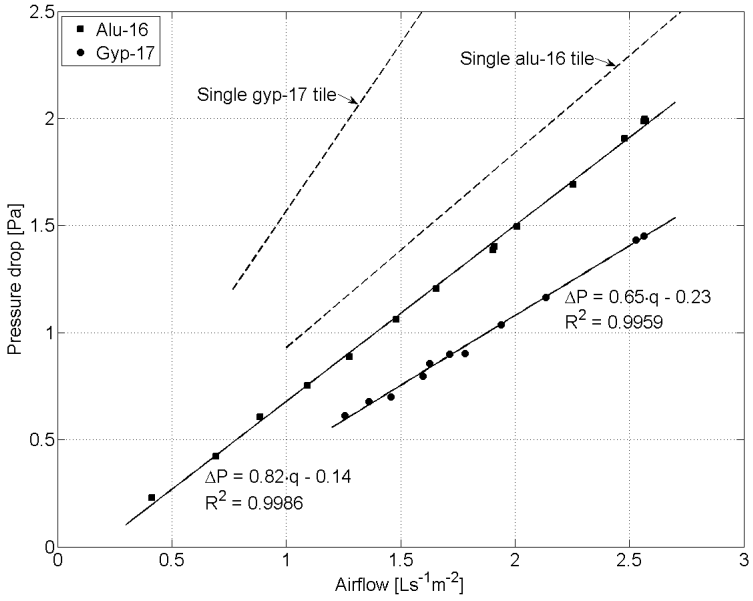

Figure 12: Correlation between pressure drop and airflow for two mounted suspended ceilings. Comparison with single tiles from Figure 11.

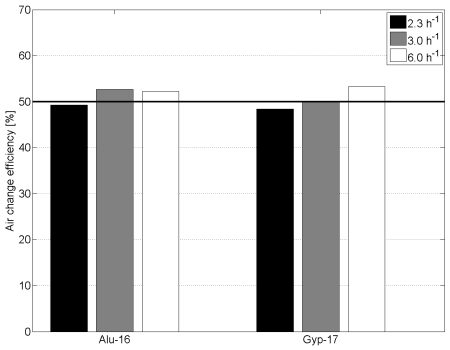

Figure 13: Air change efficiency.

Table 5: Comparison of air changes derived from inlet and tracer-gas measurements and relative differences.

Case	Inlet h^{-1}	Alu-16 Tracer h^{-1}	Rel. diff. %	Gyp-17 Tracer h^{-1}	Rel. diff. %
1	2.3	2.0	-10	2.2	-4
2	3.0	2.8	-7	2.9	-3
3	6.0	5.4	-10	5.1	-15

sampling points. The local age of air is used as an indicator for stagnant zones or short-circuiting ventilation air. If the room is fully mixed the renewal of air locally denoted the local age of air equals the room mean age of air. It is evident that the relative difference in age from the outlet value was small for both ceiling types and all air changes. For alu-16 the maximum relative difference from the outlet value is 10% for all air changes and for the gyp-17 the maximum difference is 16%.

A comparison of the room average age of air in the outlet with the expected nominal time constant shows some discrepancy caused by exfiltration. Exfiltration occurred because of overpressure in the test chamber due to the use of an unbalanced ventilation system in the test setup. Table 5 lists the relative error between the air changes derived from inlet measurements and tracer-gas measurements. In this respect it is worth noting that the inlet flow rate was measured with an orifice with an accuracy of ±5%. The impact on the tracer-gas results are deemed negligible because exfiltration does not influences the air flow in the room.

5.3. Thermal comfort

Evidence of cold downdrafts are further investigated in Figure 15 which shows local discomfort due to draught in the occupied zone. The figure does not allow for a conclusive statement on draught risk in terms of

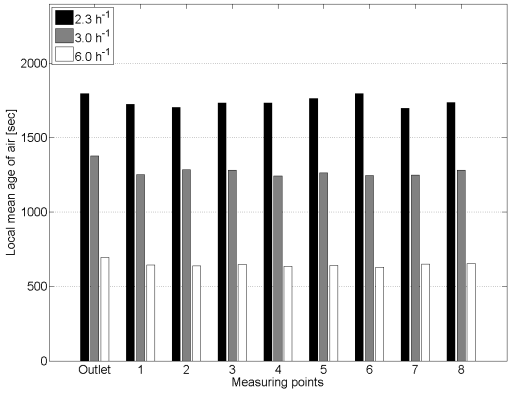

(a) Alu-16

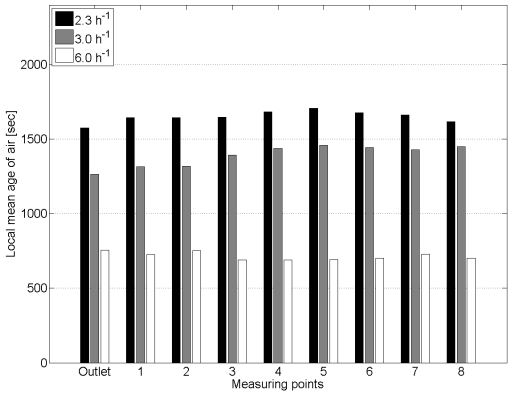

(b) Gyp-17

Figure 14: Mean local age of air. Outlets, i.e. mean room age of air, are included for comparison.

overall air change or ceiling type, but a slight tendency towards higher ratings at ankle height may be observed. Furthermore, the two corner points 7 and 9 shows elevated readings. This could indicate downdrafts that, when they hit the floor, spilled out and caused elevated readings at ankle height of the closest occupants in points 3b and 6b. It is worth noting, however, that within the occupied zone, the velocities dropped to values that places the diffuse ventilation into category B of ISO7730 [24].

The temperature gradients in Figure 16 do not support evidence of downdrafts even though they show a vertical temperature gradient between head and ankle height of approx. 0.5 °C. Nor do the gradients confirm the statement put forward by [4] that high vertical gradients are unavoidable. On the contrary the temperature difference from the floor to below the ceiling was close to zero which suggests that with the employed room size and heat source density temperature gradients can be eliminated by self-sustained mixing.

In terms of dissatisfied occupants the gradient between head and feet and the radiant asymmetry caused by the cold ceiling do not generate a notable amount of percentage dissatisfied. In fact according to ISO7730 [24] the ceiling may be cooled to 6 °C, if condensation is handled in some way, before surpassing the category A radiant asymmetry limit of 5% dissatisfied.

5.4. Reverse flow

The pressure drop in the ceiling made the plenum act as a pressure chamber causing flow to be unidirectional. However, with a pressure drop below 1 Pa and strong convective currents two-directional flow may occur and cause a warm air buffer to form in plenum [20]. Jakubowska [6] performed tracer-gas experiments, but did not observe reverse flows. She performed her experiments at pressure differences of approx. 1.5–4.5 Pa. In general no serious reverse flow was observed in the tracer-gas experiments yet Figure 17 shows reverse flow for case 1 (low air change rate) for the alu-16 ceiling. Reverse flow was observed because the concentration level in plenum was higher than in the background. The concentration divergence can only stem from the higher concentration of 10 ppm in the room below plenum. However, the largest divergence in the figure is 5.1% and in the other test cases divergence ranges from 1.3% to 2.6%.

5.5. Numerical results

5.5.1. Test chamber

In Figure 18 the temperature distribution of the numerical test cases are illustrated. In the figures the horizontal planes are placed at the height of 0.1 m and 1.1 m, and the vertical plane is placed one third from the back wall. In addition, streamlines that emanate from the lower surface of the porous ceiling is plotted to illustrate the downdrafts that occur in all cases. The streamlines are also coloured by temperature. The numerical figures illustrates well the phenomena that the thermal plumes above the heat sources counteracts the colder supply air and pushes it to the nearest corner where it drops down and flows unto the floor. This downdraft is also observable, however weak, in Figure 15(b) where draught ratings in the two corners of the inlet wall (point 7 and 9) are slightly elevated. The effect is repeated in the readings at ankle height which are also elevated. In general the plenum air was heated up to 19 °C due to the deck surface temperature and the radiation source in the ceiling. We have not measured the temperature in multiple locations in plenum and therefore cannot verify this result.

It should be noted that no flows from room to plenum is observed despite the low pressure drop of the ceiling. This is in agreement with the experimental evidence where only very small counterflow was observed, see Figure 17.

In general the experiments do not support the downdrafts found via CFD simulation. This could be due to the properties of the suspension system where leakage through the ceiling creates microjets that mixes the air more efficiently. This effect has been observed by [31] and indeed the temperature gradients in Figure 16 could indicate that the supply air is mixed thoroughly with room air above the occupied zone.

5.5.2. Class room

Three cases of ceiling permeability patterns in a full size class room were also simulated numerically. The three patterns are illustrated in Figure 19, and similar to the numerical simulation of the test chamber, the results are reported at ankle height and at neck height in Figure 20 and Figure 21. Of the three cases, the 75%-pattern with only three inlets exhibits the worst performance in terms of cold downdrafts. The 100%-pattern is slightly better but shows evidence of a downdraft in the corner closest to the viewer as does the chess pattern, however, on a smaller scale. The downdrafts are reflected in airspeeds up to 0.25 m/s where the air is accelerated between the occupants legs, but in general airspeeds are below 0.15 m/s in all cases. The chess pattern has the best overall performance which emphasizes the importance of the buoyant convection on the thermal comfort in diffuse ceiling ventilation.

Table 6: Measured temperatures during the experiments. The temperature of the suspended ceiling is measured on the lower side.

		Gyp-17					Alu-16				
Case	Air change h^{-1}	Inlet $°C$	Susp. ceil. $°C$	Deck $°C$	$\Delta T_{in \to ceil}$ $°C$	ΔT_{ceil} $°C$	Inlet $°C$	Susp. ceil. $°C$	Deck $°C$	$\Delta T_{in \to ceil}$ $°C$	ΔT_{ceil} $°C$
1	2.3	-3.2	15.0	13.5	18.2	4.4	-2.2	14.3	14.7	16.4	5.7
2	3.0	3.2	17.7	14.4	14.5	3.7	3.2	16.0	14.9	12.7	4.7
3	6.0	11.2	17.6	15.3	6.4	5.2	11.6	16.9	15.6	5.3	4.7

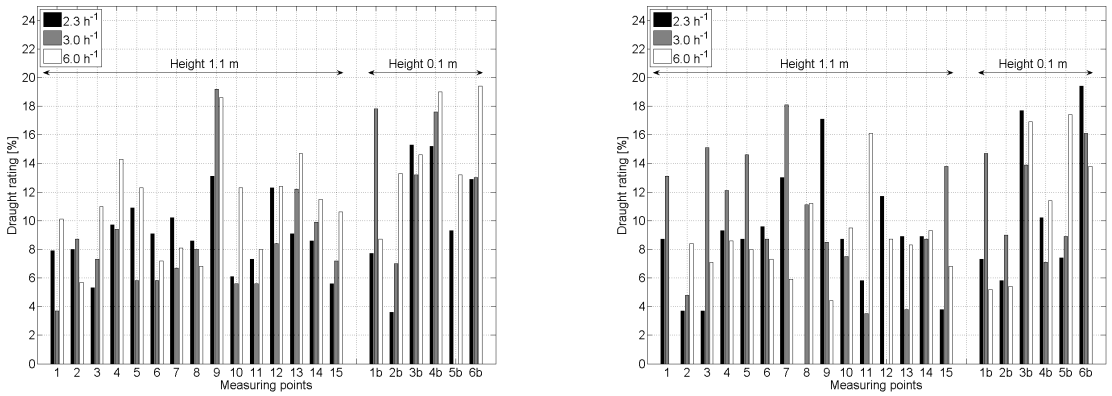

(a) Alu-16 (b) Gyp-17

Figure 15: Draught ratings at the height of 1.1 m and 0.1 m.

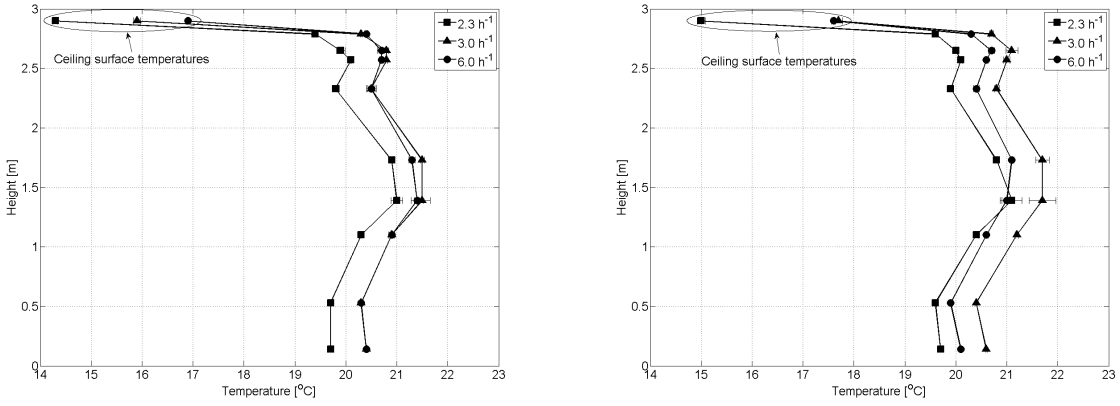

(a) Alu-16 (b) Gyp-17

Figure 16: Temperature gradients. Standard deviations are shown.

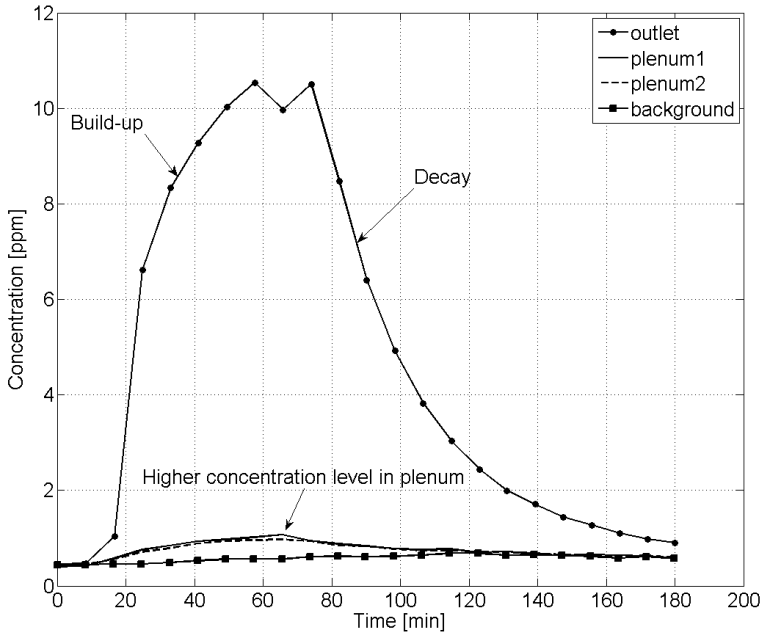

Figure 17: Higher concentration levels in plenum compared to background indicates counterflow.

The Reynolds number in plenum immediately after the inlets is 4400, which renders the assumption of the radiation model invalid for half of the plenum, see Section 4.1.1. This is reflected by the heating of plenum air from 8 to 20 °C partly by the ceiling, partly by the deck. However, it does not differ from the expected heating of plenum air when it passes from inlet to the furthest end. At the end we would expect the temperature to lie somewhere in between the room air (21 °C) and the plenum deck (18 °C), and therefore we deem the approach valid. It highlights, however, the need for a more direct modelling procedure for CFD that includes the interaction of radiative, convective and conductive heat transfer in the ceiling as well as microjets from the suspension system.

6. Conclusion

The objective of the present work was to investigate the performance of a porous suspended ceiling as diffuse ventilation inlet. Two types of porous ceiling material was investigated both experimentally as well as computationally. The experiments included measured pressure-drop, air change efficiency, mean age of air and local discomfort. The experiments were conducted in a test chamber and compared with computational fluid dynamics simulations of the same test chamber. In the literature diffuse ceiling ventilation have proven superior in terms of comfort for a wide range of flow rates and cooling. The experimental results are generally in good agreement with the literature sources in terms of comfort and air change efficiency. No local discomfort in the vicinity of the imitated occupants is found and no stagnant zones is identified anywhere. The CFD simulations showed some problems with cold downdrafts especially below the inlets and in areas without counteracting plumes. The discrepancy could be caused by microjets from the suspension system which were absent in the CFD simulation. Both experiments and numerical analysis showed significant pre-heating in plenum as well as in the ceiling, but further work is needed to understand the physics of the pre-heating. Also the effect of the plenum height and pressure drop should be investigated. However, the radiant cooling potential of the ceiling is evident as well as the low pressure drop and air change efficiency. This reduces the ductwork and necessary fan power when comparing with conventional mixing ventilation which makes the concept ideal for low-energy ventilation.

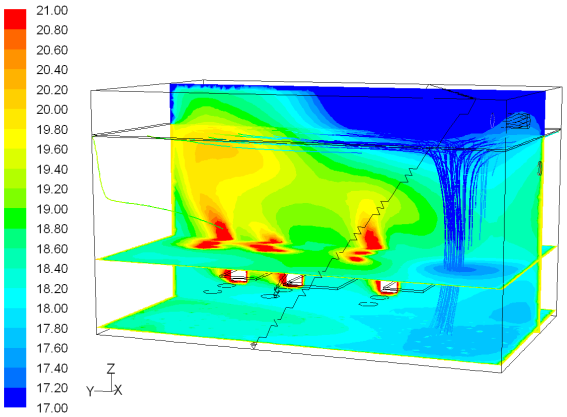

(a) Case 1

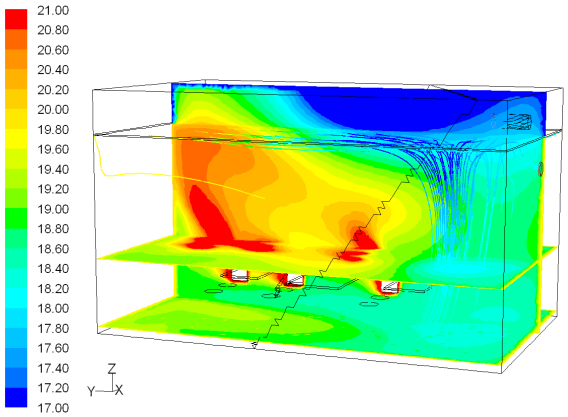

(b) Case 2

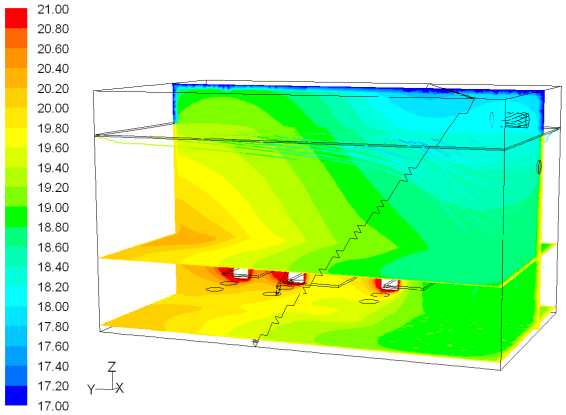

(c) Case 3

Figure 18: Temperature distribution for the three test cases described in Table 2.

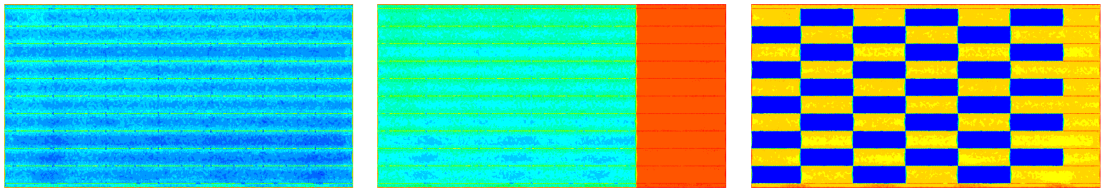

(a) 100% pattern (b) 75% pattern (c) Chess pattern

Figure 19: Three ceiling patterns showing high and low permeability. Z-velocity in m/s in the range -0.03–0.0

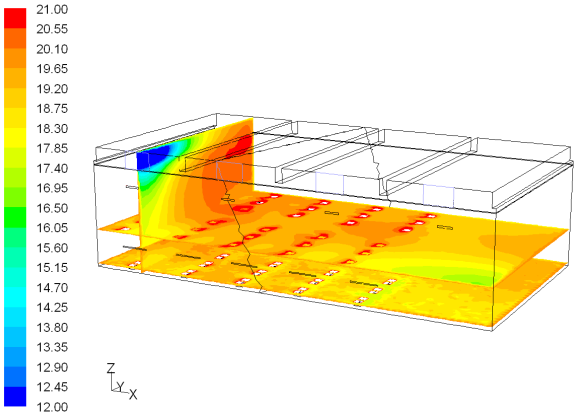

(a) 100% pattern

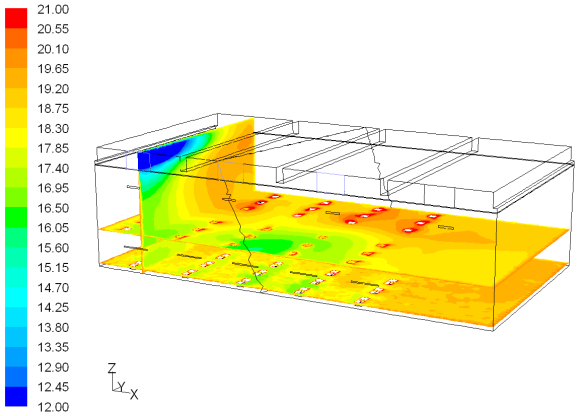

(b) 75% pattern

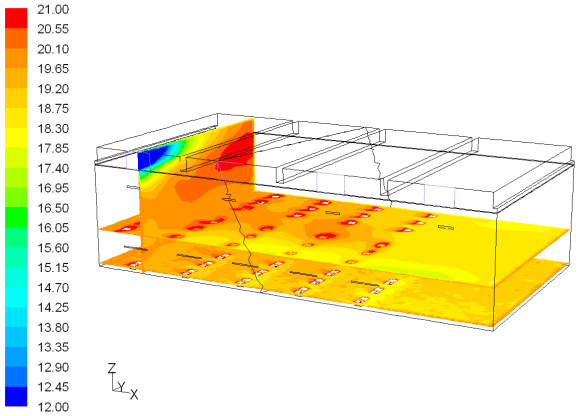

(c) Chess pattern

Figure 20: Temperature distribution in $^{\circ}C$ for three ceiling patterns in class room.

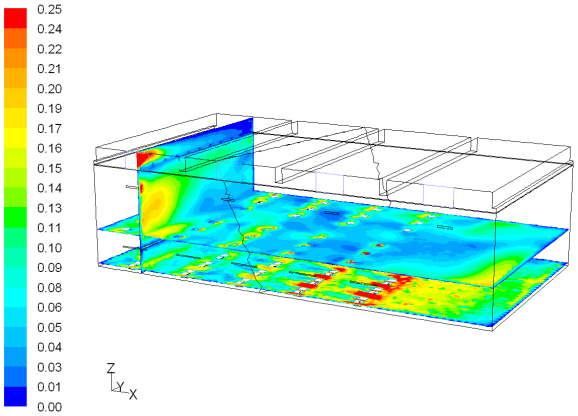

(a) 100% pattern

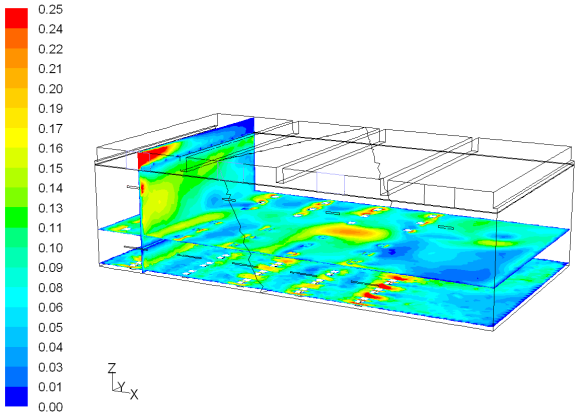

(b) 75% pattern

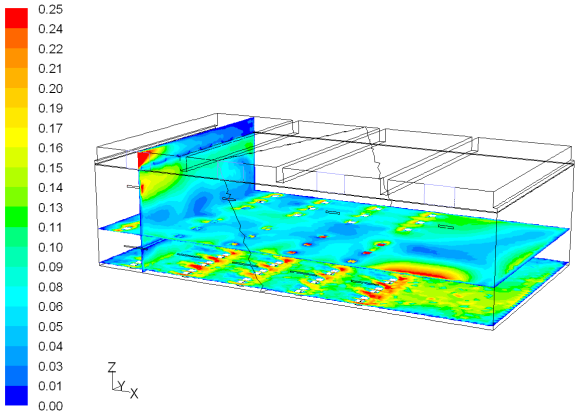

(c) Chess pattern

Figure 21: Velocity magnitude in m/s for three ceiling patterns in class room.

7. Acknowledgements

The work was gratefully funded in collaboration with ALECTIA A/S and the Danish Ministry of Science, Technology and Innovation.

A. Radiative exchange

The porous ceiling acts as a pre-heater of the supply air trough the radiative exchange between the surfaces in the room, see Figure 8. Assuming that convective heat transfer in the ceiling zone is zero for upper deck and the suspended ceiling ($h_{c,1} = h_{c,2} = 0$), the following applies: $T_{plenum} = T_{in}$. Likewise, because $h_{c,3} = 0$, $T_{room} = T_2$ applies. This means that the inlet air is purely heated by the radiative net gain that the suspended ceiling receives from the upper and lower decks. The following three equations can be set up for the radiative heat balance between the suspended ceiling, plenum and room:

$$\phi_{13} = F_{13} \cdot \epsilon_1 \cdot \epsilon_3 \cdot \sigma \cdot A_1 \cdot (T_1^4 - T_3^4) \quad (8)$$

$$\phi_{23} = F_{23} \cdot \epsilon_2 \cdot \epsilon_3 \cdot \sigma \cdot A_2 \cdot (T_2^4 - T_3^4) \quad (9)$$

$$\phi_{13} + \phi_{23} = \dot{V} \cdot \rho \cdot c_p \cdot (T_3 - T_{\text{in}}) \quad (10)$$

where the radiative exchange ϕ_{ij} is calculated with the viewfactor F between surface i and j, the emissivity ϵ, Stefan-Boltzmann's constant $5.6697 \cdot 10^{-8}\,\mathrm{W/m^2\,K^4}$, and the absolute surface temperature T.

Additionally the radiosity of the occupants contribute to the net gain. The contribution is calculated as the radiant heat loss from a person and weighted with viewfactors between each individual and the ceiling [27]. From ASHRAE [28] we have that the convective and radiative heat losses $C + R$ from each individual equals the heat loss by conduction

$$C = f_{\text{cl}} h_{\text{c}} (T_{\text{cl}} - T_{\text{a}}) \quad (11)$$

$$R = f_{\text{cl}} h_{\text{r}} (T_{\text{cl}} - \overline{T}_{\text{r}}) \quad (12)$$

$$C + R = \frac{T_{\text{sk}} - T_{\text{cl}}}{0.155 I_{\text{cl}}} \quad (13)$$

For the convective and radiative heat transfer coefficients h_{c} and h_{r} ASHRAE states the values for sedentary persons $3.1\,\mathrm{W/m^2\,K}$ and $4.7\,\mathrm{W/m^2\,K}$, respectively. The clothing area factor $f_{\text{cl}} = 1.0 + 0.3 I_{\text{cl}}$ where $I_{\text{cl}} = 1\,\text{clo}$ and $\overline{T}_{\text{r}}$ is the viewfactor-weighted mean radiant temperature. The skin temperature is found by $T_{\text{sk}} = 35.7 - 0.0275(M - W)$ where $M = 70\,\mathrm{W/m^2}$ and $W = 0$. From Equation 13 the clothing surface temperature is found iteratively, and, knowing that the body surface area is approx. $1.8\,\mathrm{m^2}$, and the emissivity of skin and clothes is approx. 0.97, we use Equation 8 to calculate the net radiative energy transfer from each individual to the porous ceiling.

References

[1] T.T. Chow, X.Y. Yang, Ventilation performance in operating theatres against airborne infection: Review of research activities and practical guidance, J. of Hospital Infection 56 (2) (2004) 85-92

[2] A. Wagenberg, M.A.H.H. Smolders, Contaminant and heat removal effectiveness of three ventilation systems in nursery rooms for pigs, Transactions of the American Society of Agricultural Engineers 45 (6) (2002) 1985-1992

[3] L. Jacobsen, Air motion and thermal environment in pig housing facilities with diffuse inlet, Ph.D. thesis, Department of Civil Engineering, Aalborg University, Denmark, 2008

[4] H. Awbi (Ed.), Ventilation systems - Design and performance, Taylor and Francis, 2008

[5] Handbuch der Klimatechnik band 2: Berechnung und Regelung, Arbeitskreis Dozenten für Klimatechnik, 2nd ed., C.F. Müller, Karlsruhe, 1986

[6] E. Jakubowska, Air distribution in rooms with diffuse ceiling inlet, M.Sc. thesis, Department of Civil Engineering, Aalborg University, Denmark, 2007

[7] P.V. Nielsen, E. Jakubowska, The performance of diffuse ceiling inlet and other room air distribution systems, in: Proceedings of Cold Climate HVAC, Sisimiut, 2009

[8] P. Jacobs, E.C. van Oeffelen, B. Knoll, Diffuse ceiling ventilation, a new concept for healthy and productive classrooms, in: Proceedings of Indoor Air, paperID #3, Copenhagen, Denmark, 2008

[9] E. Lee, J.A. Khan, C.E. Feigley, M.R. Ahmed, J.R. Hussey, An investigation of air inlet types in mixing ventilation, Building and Environment 42 (3) (2007) 1089-98

[10] H. Skistad (Ed.), E. Mundt, P.V. Nielsen, K. Hagström, J. Railio, Displacement ventilation in non-industrial premises, Rehva Guidebook No.1, Federation of European Heating and Air-conditioning Associations, 2002

[11] P.E. Nilsson (Ed.), Achieving the desired indoor climate - energy efficiency aspects of system design, Commtech Group, Studentlitteratur, 2003

[12] P.V. Nielsen, Analysis and design of room air distribution systems, HVAC & R Research 13 (6) (2007) 987-997

[13] EN 15251, Indoor environmental input parameters for design and assessment of energy performance of buildings addressing indoor air quality, thermal environment, lighting and acoustics, European Standard, European Committee for Standardization, Brussels, 2007

[14] H.E. Feustel, C. Stetiu, Hydronic radiant cooling - preliminary assessment, Energy and Buildings 22 (3) (1995) 193-205.

[15] M. Behne, Indoor air quality in room with cooled ceilings. Mixing ventilation or rather displacement ventilation?, Energy and Buildings 30 (1999) 155-166

[16] A. Novoselac, J. Srebric, A critical review on the performance and design of combined cooled ceiling and displacement ventilation systems, Energy and Buildings 34 (5) (2002) 497-509

[17] S.P. Corgnati, M. Perino, G.V. Fracastoro, P.V. Nielsen, Experimental and numerical analysis of air and radiant cooling systems in offices, Building and Environment 44 (3) (2009) 801-806

[18] L. Jacobsen, P.V. Nielsen, S. Morsing, Prediction of indoor airflow patterns in livestock buildings ventilated through a diffuse

Paper IV

Submitted to Energy and Buildings, 2010

Detailed whole-year simulation of a building integrated ventilation concept with heat recovery and night cooling for low-energy offices

Christian Anker Hviid[*,a,b], Svend Svendsen[b]

[a]*ALECTIA A/S, Teknikerbyen 34, DK-2830 Virum, Denmark*
[b]*Department of Civil Engineering, Technical University of Denmark, Brovej, Building 118, DK-2800 Kgs. Lyngby, Denmark*

Abstract

Hybrid ventilation systems seek to exploit the advantages of both natural ventilation and mechanical ventilation. Hybrid systems are typically two-mode with two fully autonomous systems or mixed-mode systems where a fan helps the natural ventilation system. Here we present a one-mode system of balanced mechanical ventilation with substantial assistance from stack and wind. The state-of-the-art building simulation program ESP-r is used to model heat and air flows in a fictive building and indoor climate and energy consumption is quantified. The system employs heat recovery with a newly developed heat exchanger, filtration with an electrostatic precipitator and distributes air using diffuse ceiling ventilation. Conventional blade dampers control the airflow and free cooling is provided as night ventilation through the existing supply ducts. The pressure loss is 5 Pa, and the specific fan power (SFP), which is commonly used to compare the energy performance of different ventilation systems, is calculated to 155 J/m^3 including the power consumption of the electrostatic precipitator. The SFP value is approx. 6% of the currently upper limit for VAV systems in the Danish Building Code. The total primary energy consumption of the building is 16.3 kWh/m^2 which makes the ventilation concept suitable for near-zero emission buildings.

Key words: hybrid ventilation, building simulation, heat recovery, low energy buildings, night ventilation

1. Introduction

While ventilation technologies are constantly improving energy-wise and efficiency-wise, it is not possible to meet tomorrow's demand of better indoor climate while cutting energy consumption as demanded by the risk of global warming. This leads to a widening gap between the required fossil fuel reductions and the demand for improved indoor climate. One solution is to shift the ventilation use from active (mechanical) to passive ventilation systems. Passive in this context means ventilation solutions that exploit natural driving forces and the building envelope physics to establish and maintain a satisfying indoor climate without the consumption of electrical energy. The concept has particular potential in temperate climates where high wind speeds and large daily temperature differences prevail. In order for a passive ventilation system to be competitive, efficient heat recovery and filtration are essentials. This paper proposes a one-mode hybrid ventilation system with very small pressure loss yet with superior or equal performance in indoor climate compared to conventional mechanical ventilation systems. The objective of the proposal is to achieve whole-year comfort ventilation at extremely low fan power consumption, low primary energy consumption and to provide sufficient free cooling by night ventilation using the existing supply ducts. A parallel objective is to use components with measured performances whether they are commercially available or developed prototypes. The system proposed here employs a newly developed heat recovery concept [1], filtration by electrostatic precipitators and diffuse ceiling ventilation for air distribution [2, 3]. The proposal is backed by detailed simulation of the heat and mass transfer in a test case building. Furthermore, it discusses air flow control, thermal comfort, filtration, operation/maintenance, and cost as a whole.

2. Hybrid ventilation systems

The term 'hybrid' covers a multitude of different ventilation concepts. Hybrid is generally used in the sense

[*]Corresponding author. Tel.: +45 88191365; fax: +45 88191001
Email address: crh@alectia.com (Christian Anker Hviid)

that the ventilation system employs some sort of mixture between mechanically driven air change and naturally driven air change. The definition of a hybrid ventilation system given by the IEA Annex 35 [4] is a two-mode ventilation system where the two modes refer to natural and mechanical driving forces. Heiselberg [5] expands the definition to a two-mode system of natural and mechanical ventilation that takes advantage of the different features of both systems at any given time. Furthermore, Heiselberg states, the main difference from a conventional mechanical ventilation system is the intelligent control that the hybrid system is equipped with. The control provides the hybrid system with the ability to switch diurnally or seasonally between natural and mechanical air supply to take maximum advantage of the given ambient conditions. The criteria for mode-switching is minimization of energy consumption and to keep the level of CO_2 below a certain limit.

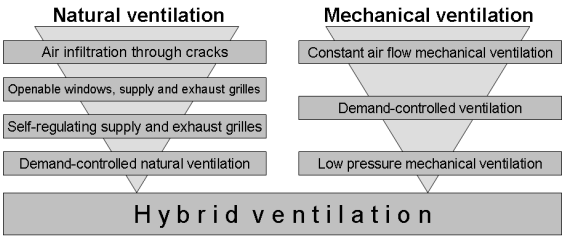

Figure 1: Development of hybrid ventilation from natural and mechanical systems [5, 6]

The development of hybrid ventilation from natural and mechanical ventilation is illustrated in Figure 1. The figure illustrates the development towards minimal energy use and comfortable indoor environment. The process has been separate yet approaching through time driven by the recognition of experts that the ventilation must provide indoor air quality *and* passive cooling, and that this dual task reaches beyond the limits of fully natural or fully mechanical systems [5, 7, 8]. Thus the motivation for hybrid ventilation is access to both ventilation modes and to combine the advantages of each mode to achieve mechanical control, thermal comfort and heat recovery with low power consumption while eliminating some disadvantages of each mode. The most important limiting factor for natural and hybrid ventilation is air humidity because in humid regions removal of water vapour from the supply air requires active air-conditioning [9].

Basically three categories covers the hybrid approach [5]:

- Two-mode system of natural and mechanical ventilation
- Mixed mode system of fan-assisted natural ventilation
- One mode system of stack- and wind-assisted mechanical ventilation

The first category provides fresh air by two fully autonomous ventilation systems where the active system typically is mechanical when heat recovery is needed and natural when night cooling is used. Apart from that, any of the two systems may be active depending on time, building and season. The second category is a mixed mode system where the ventilation primarily is driven by natural ventilation but in periods of insufficient natural driving pressure an assisting fan is switched on. The third category does not fully comply with the hybrid definition of a two-mode system and is in reality a low-pressure balanced mechanical ventilation system. Due to the low pressure drop, pressure rise from stack and wind aids in driving the air flow. This difference from conventional ventilation that fully relies on mechanical pressurization to work, however, justifies the hybrid label. The distinction between the second and third category is vague and indeed we have observed different sources enlist the same project in both categories [5, 6, 10].

While the IEA Annex 35 [4] was committed to develop and explore various hybrid approaches only a few detailed simulations on energy performance were reported [11, 12, 13]. By detailed we mean simulations on a macroscopic level with a combined thermal and airflow model that includes heating and electricity consumption, indoor air quality and thermal comfort. Indeed combined thermal and airflow simulation is a powerful tool for whole-year analysis of hybrid ventilation buildings [5] and is also reported to show good accuracy with measurements [14, 15]. In one Finnish energy performance study simulated in IDA ICE [16] a fan-assisted natural ventilation system of a five-storey building was found to consume 15% less energy compared to a mechanical VAV system and 73% less fan energy [12]. The annual primary energy consumption was 92 $\mathrm{kWh/m^2}$ when electricity was multiplied with 2.5. The system was characterized by central intake at ground level and exhaust at roof level. During heating and cooling seasons the supply air was conditioned in the air handling unit and distributed with supply ducts to the rooms. Extraction happened centrally through an atrium and heat recovery was achieved with liquid-coupled heat exchangers. The air-conditioning com-

ponents were bypassed during mild periods to lower the pressure drop. Apart from fan energy savings, the results showed significant divergences between the intended air change rate on the different floor levels and the actual value due to stack differences. No attempt was made to correct the problem, e.g. through dampers on each floor.

While the estimated pressure drop in the Finnish study was reported to be < 100 Pa in bypassed mode and < 500 Pa otherwise, a Norwegian state-of-the-art implementation reached a measured total of approx. 100 Pa [10]. The Mediå School in Grong, Norway is considered a successful practical implementation of a balanced mechanical ventilation system with substantial assistance from stack and wind [17]. The ventilation system has central intake through an underground culvert that dampens the seasonal fluctuations of the outdoor temperature and central exhaust through a stack-enhancing wind tower. Heat is recovered by liquid-coupled heat exchangers and filtration is partly achieved through settlement of particles in the culvert, partly in a EU7 filter. The primary energy consumption is measured to 107 kWh/m^2. A combined thermal and airflow simulation of the school was performed using ESP-r [13, 18], but the model was cursory and the simulation period limited.

3. Building integrated ventilation concept proposal

The hybrid ventilation system that we present here is a one-mode system of balanced mechanical system with extremely low pressure losses. Despite their advantages over two-mode or mixed-modes systems, one-mode hybrid systems have not had much published attention. We believe that the hybrid approach where only one mode exists has several advantages in temperate climatic conditions:

- One-mode systems do not require the implementation and inordinate investment of two separate ventilation systems in the same building
- One-mode systems require only one control system which makes it simpler to control
- Ducted systems distribute fresh supply air as intended because conventional dampening systems may be applied
- Ducted systems may easily employ heat recovery and filtration
- Ducted systems with heat recovery do not suffer from draught risks in the occupied zone
- Frequency-controlled fans ensures steady and continuous performance by levelling out natural fluctuations while allowing stack and wind to assist
- One-mode systems do not suffer from shifts in the neutral plane due to thermal stratification [19]
- One-mode systems may exploit the stack from temperature drop in summer nights to provide night ventilation
- Conventional low-pressure mechanical systems suffer from uncontrollable stack. In the approach here the system is designed to actively exploit the stack effect

The strategy to design hybrid ventilation systems in low-energy offices is to aim for low air speeds. It is achieved by letting the building rooms be part of the flow path or by sizing ducts and components to lower pressure drop. However, large dimensions on ducts and components consumes useful space. This can be minimized by designing the building with fewer stories, place intake and extract ducts below and above useful levels, i.e. in the basement and on the roof, and to use building rooms, hallways, staircases and atria as exhaust paths wherever it is within fire regulations [7].

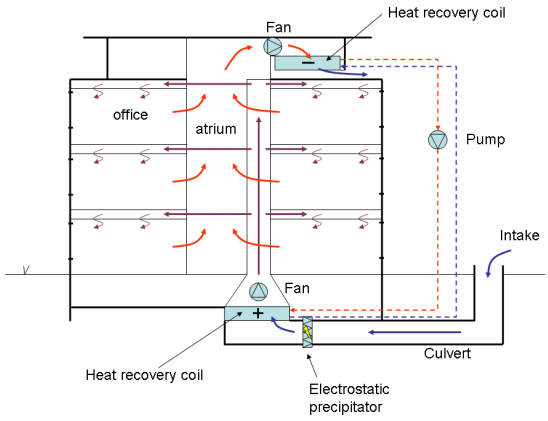

Figure 2: Building integrated ventilation concept.

Figure 2 illustrates the building integrated ventilation concept following these guidelines. The concept is designed for maximum stack effect and for maximum responsive building integration. A 30 m long embedded concrete duct leads the fresh air through an electrostatic precipitator, through the heat recovery inlet coil and distributes it to the floors via the main shaft placed in the atrium. On each floor supply ducts feeds the diffuse ceiling ventilation. The extract air flows from all floors

via the atrium to the heat recovery outlet coil above the roof. Heat is recovered by linking the recovery coils with a pump-powered liquid loop. No office space is used for ventilation because the installations are placed in the basement and above the roof or they exploit the space of the atrium for supply and exhaust. In the following sections we go into detail on the used components and concepts.

3.1. Test case building

The principles mentioned in the above sections are used in a fictive test case office building with three stories, see Figure 3. The design of the building is intended to match many newly erected office buildings while showing the applicability and energy savings potential of building integrated ventilation. It comprises three blocks forming a U-shape around an atrium with the open face of the atrium pointing westward. This means that a substantial part of the offices are facing either North of South which is a worst-case scenario. The footprint of the building is 38×24 m with a total floor area of 2256 m^2. The office floor area is 2016 m^2 and the floor height is 3.4 m. The height of the atrium roof is 12.2 m.

3.2. Duct sizing

Usually the pressure loss in natural ventilation is less than 10 Pa, whereas the pressure loss in hybrid systems is 30–100 Pa [7]. Here we wish the system to be operable only on stack and to quantify the design criterium of allowable pressure loss we perform a preliminary calculation of the stack effect. With three storeys and indoor temperature of 20 °C and outdoor temperature of 5 °C, a height difference z between inlet and outlet of 12.2 m and no wind, the maximum thermal driving pressure is:

$$\begin{aligned} \Delta p &= (\rho_{5^\circ\mathrm{C}} - \rho_{20^\circ\mathrm{C}}) \cdot g \cdot z \qquad (1) \\ &\approx 6.5\,\mathrm{Pa} \end{aligned}$$

Duct sizing is performed with the computer program PFS which is developed at Lund University [20]. The program is very versatile and may be used for any kind of flow system. It accepts a mixture of visual and textual input, transforms the input into a number of loop equations and solves the equations using an iterative Newton-Raphson technique. We use it to resolve the sizing of ducts from the criterium maximum pressure drop per meter: 0.01 Pa/m. The program selects the closest fitting size from a number of user entered sizes. An illustration of the supply ductwork is depicted in Figure 4 and a comprehensive description is placed in Appendix A.

3.3. Diffuse ceiling ventilation

In a conventional mechanical ventilation system fresh air is supplied to the room through mixing or displacement diffusers. The diffusers act through a pressure drop that is too large for non-conventional systems. In recent years a new concept where fresh air is supplied through perforations in the acoustic suspended ceiling has been investigated [2, 3, 21, 22, 23]. The plenum space above the acoustic ceiling is used as a pressure chamber reducing ductwork and diffusers and fresh air is supplied through almost the entire suspended ceiling surface. The air velocity through the ceiling is very low and consequently has very low pressure drop. The concept has several advantages in low-pressure ventilation systems:

- the pressure drop is below 1–4 Pa
- the air distribution is reported to equal conventional mixing ventilation
- the concept requires less ductwork and no diffusers
- with no ductwork the space above the ceiling can be reduced and the room height increased at no extra cost
- commercial acoustic ceiling tiles are available

Another advantage is the extra thermal mass that may be activated during night cooling because the upper concrete deck is not shielded from the room by the suspended ceiling [24]. The level of activation is dependent on convective and radiative heat transfer in plenum and investigations made by the authors [2] showed significant pre-conditioning of the supply air partly due to heat transfer in plenum and partly due to the radiative net gain received by the suspended ceiling from the other room surfaces. An in-depth investigation of the effects and possibly optimization, however, is beyond the scope of this paper. Thus we only make use of the ceiling properties regarding air distribution at low pressure drop in the reported simulations, and we disregard the effect of extra thermal mass and pre-conditioning.

3.4. Embedded culvert and main shaft

In building integrated ventilation the exposure of the ventilation air to thermal mass is exploited as a heating/cooling buffer that evens out thermal fluctuations. Exposure in an embedded culvert will pre-heat the ventilation air in winter and cool it in summer [10]. In winter, defrosting of the heat recovery unit may be avoided [9]. Embedded ducts also provide some filtration effect

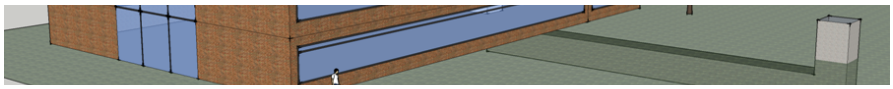

Figure 3: 3D schematic of the test case building.

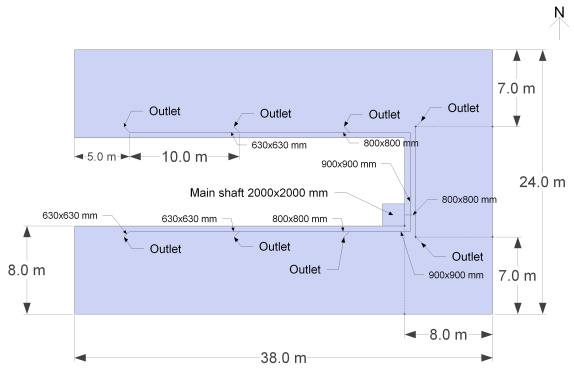

Figure 4: Schematic of north, south and east ducts, distribution ducts and supply on one floor.

because of settling of large particles. In one study of a 15 m long culvert the decrease of $>0.3\,\mu$m particles was 85% and 95% for larger particles [17]. This emphasizes the need for the duct to be passable for manual cleaning.

Horizontal embedded ducts experiences significant stratification. Cold intake air will flow as a gravity current in the bottom of the duct while warmer air flows backwards in the top and opposite in summer [15]. Consequently we performed a numerical investigation in the commercial computational fluid dynamics software *Fluent* with the standard k-ϵ-turbulence model [25]. Heat transfer was modelled with standard wall functions and to ensure proper heat transfer between the duct surfaces and the bulk flow, the grid was automatically adapted so the dimensionless grid characteristic y^+ complied with the wall function validity interval of 30–300 [25]. The roughness of the surfaces were set to 3 mm due to the raw concrete walls. The length was 30 m and the cross-sectional dimensions were 2×2 m. The inlet flow rate was $3\,\mathrm{m}^3/\mathrm{s}$, slightly higher than the comfort ventilation rate (see Section 4.2), with a turbulence intensity of 10%. The inlet temperature was 0 °C and the walls were fixed at 10 °C. The mean outlet temperature was then 2.2 °C and the mean heat transfer coefficient was calculated to be $3.5\,\mathrm{W/m^2\,K}$. The value was applied to the inner culvert surfaces in the ESP-r model and the thermal inertia of the ground was modelled by 1 m of earth and the monthly mean ground temperatures in Table 4. Condensation will certainly occur in summer when humid air outdoor air is cooled in the culvert, but the raw concrete walls act as a hygroscopic buffer that absorbs moisture in the day and desorbs during night ventilation. This effect seems to work as intended [9, 10]. The CFD-result is shown in Figure 5(a).

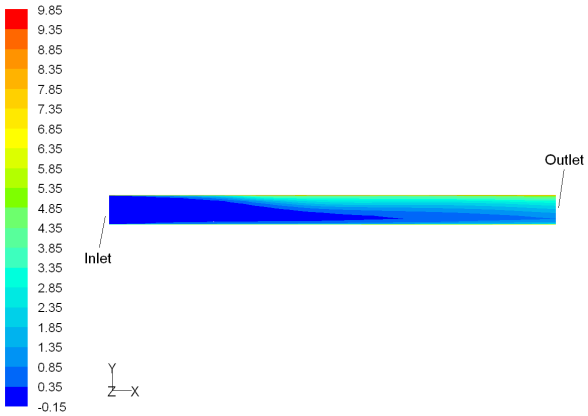

(a) Culvert

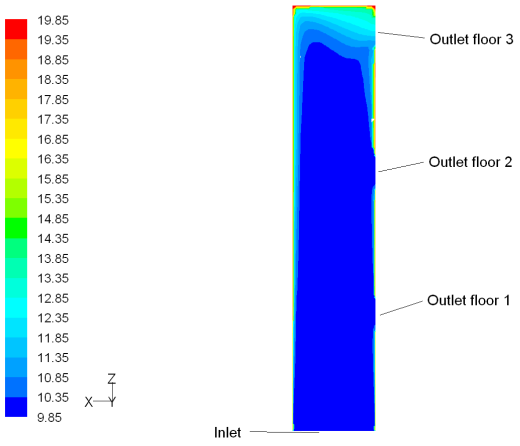

(b) Main shaft

Figure 5: Temperature development in underground culvert and main shaft.

We also performed a numerical investigation of the heat transfer of the concrete main shaft because it may also exhibit considerable pre-conditioning of the intake

Table 1: Main shaft heat transfer coefficients.

Zone	Surf. area m^2	Mass flow kg/s	Inlet temp. °C	Outlet temp. °C	Power W	Heat trans. coef. $W/m^2\,K$
1	27.2	1.17	10.0	10.7	824	3.0
2	27.2	1.17	10.3	10.8	589	2.2
3	31.2	1.17	10.9	12.3	1648	6.9

air. The shaft has a height of 10.2 m with a cross-section equal to the culvert. The temperature of the duct surfaces was set to 20 °C which is representative for the yearly indoor temperature and the inlet temperature was set to 10 °C. The result is shown in Figure 5(b) where some vertical stratification is observed. For this reason the main shaft is divided in three sections and the mean heat transfer coefficient is calculated for each section, see Table 1. The values are applied to the inner surfaces of the main shaft.

3.5. Heat recovery

Heat is recovered with two prototype heat recovery coils which are linked by a liquid loop powered by a domestic pump [1]. Figure 2 shows how cold fresh air enters the heat recovery coil in the inlet, heat is transferred from the hot liquid to the colder air resulting in a temperature rise of the supply air. The now cooled liquid is pumped to the heat exchanger in the outlet where it is heated by the hot exhaust air leaving the building. The warm liquid returns to the inlet heat exchanger and the cycle is repeated continuously. The total pressure drop of the coils is 0.74 Pa with a system efficiency of 70% and an active area of each coil of 25 m^2. A smaller prototype with a face area of 6 m^2 is depicted in Figure 6.

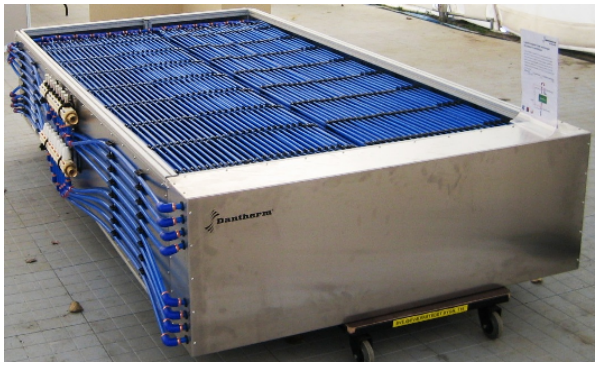

Figure 6: Photo of used heat exchanger.

Figure 7 illustrates the heat recovery plant model that we modelled in ESP-r. The illustration includes only

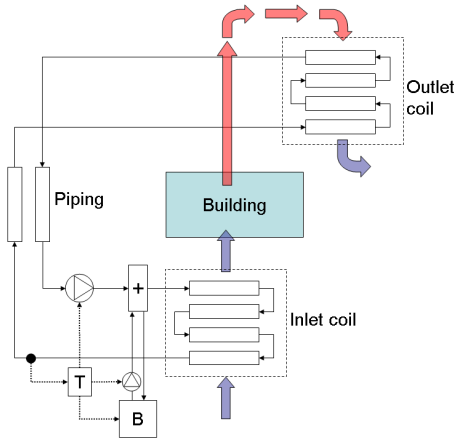

Figure 7: The heat recovery plant modelled in ESP-r.

4 tube layers in the inlet and outlet coil. In the simulation each coil consisted of 10 tube layers. We used the special feature of ESP-r where we may overlay the plant network used to model heat fluxes with a mass flow network. This means that mass flows in the plant network are determined by the mass flow network and the thereon imposed control strategies. We used the air-to-water heat transfer tubes that exists in ESP-r for the coils and linked them in counterflow. The linking loop comprises two 24 m pipes, a frequency controlled pump and a calorifier fed by a pump and a boiler. The latter is added for multiple reasons. In real-life operation the transporting media most likely would be an aqueous solution of glycol. This would allow the outlet temperature of the inlet coil to achieve subzero temperatures in cold weather. Subsequently the outlet coil would cool the exhaust air to subzero temperatures which would cause freezing of excess water, clogging and after some time, destruction of the outlet coil. To avoid subzero pipe temperatures we increase the pump flow speed which causes the temperature efficiency to drop. However, rarely and for short periods, even with embedded intake culvert and increased loop flow, the inlet air temperature drops to subzero temperatures. This would in real life not lead to problems with the outlet coil but because ESP-r is incapable of simulating sub-zero fluid temperature we add the calorifier in the liquid loop and use it to inject heat if necessary during the whole-year simulation. The overall reported heat consumption includes the boiler contribution and the extra pump is included in the power consumption.

Increasing the flow rate in the liquid-loop during cold weather causes the capacity flows of the exchanger fluids to be unequal. In the counterflow coil arrangement

the exit liquid temperature of the inlet coil is shifted in upward direction because the liquid is not cooled as well as in normal operation. Neither is it heated as well in the outlet coil. The result of less cooling and less heating is a smaller temperature difference in the liquid loop and thus reduced efficiency.

The length of the liquid loop is important because the time constant of the system is higher than the rapid changes of the natural pressure. High efficiency is based on equal capacity flow and steady temperature differences in both coils. Changes in the air flow rate or changes in inlet temperature that are faster than the time constant will have a negative impact on the efficiency. The time constant was modelled by the transport delay mechanism that the air-to-water heat transfer tubes employ. Furthermore the loop pipes were insulated so the temperature change between coils are below 0.1 °C. The properties of the tubes were adjusted so the yearly mean efficiency of the system approximated 70%. The length of the layers were also adjusted so the time of one coil pass for the water flow equals that for a 4×6.3 m (25 m^2) prototype coil [1].

3.5.1. Filtration

Filtration has two objectives: to filter outdoor pollutants, primarily pollen and traffic soot, and to protect the inlet heat exchanger and the duct system from soiling. Filtration is conventionally done in mechanical ventilation systems by bag filters which are soiled during ventilation operation with subsequent negative impact on the indoor air quality [26, 27]. In this concept we employ two types of filtration, passive settlement of particulate matter in the culvert and active filtration by an electrostatic precipitator. The former technique is described in more detail in Section 3.4. The latter is an active efficient filtration device that minimally impede the airflow and easily removes fine particulate matter such as dust and smoke from the airstream. An electrostatic precipitator charges passing particles and aerosols and removes them with an electrical field and like bag filters they must be cleaned regularly to avoid depletion of the efficiency. The pressure drop of an electrostatic precipitator is a fraction of a conventional bag filter and therefore is used in some hybrid ventilation projects [17]. The filter employed here induces 2 Pa pressure drop at the design flow speed [28]. On the down-side electrostatic precipitators are costly to buy and run because they are power consuming. The amount depends on the amount of ionized particles and the ionization level of each particle. Therefore, it is difficult to accurately quantify the power consumption, especially in a relatively particle free environment like the present. An in-depth investigation of the aspects of filtration efficiency, pressure drop, fan power and filter power is beyond the scope of this paper. We added the power consumption to the total energy consumption as well as to the reported specific fan power of the ventilation system.

4. Simulation setup

The ventilation system was simulated using the state-of-the-art building simulation program ESP-r from University of Strathclyde, Glasgow, Scotland [18]. ESP-r is capable of combined thermal and airflow modelling and has been used to model natural ventilation with good accuracy [15, 24]. Also it has several build-in plant components that we used for the dynamic heat recovery loop. On the down-side ESP-r is, although improving, less than user-friendly, and requires a strong opinion on the physics of buildings and environmental systems. Other tools that has been used for similar purposes is IDA ICE [16], used by [12], and TRNSYS [29], used by [11]. Other simpler tools include HYBCELL1.0 and a SPARK tool by [30]. We chose ESP-r because it is continuously developing and has a comprehensive validation history [31]. The program stems from a unix-based environment but it was run on a Microsoft Windows machine using the Linux-emulator Cygwin. The used version was 11.6.

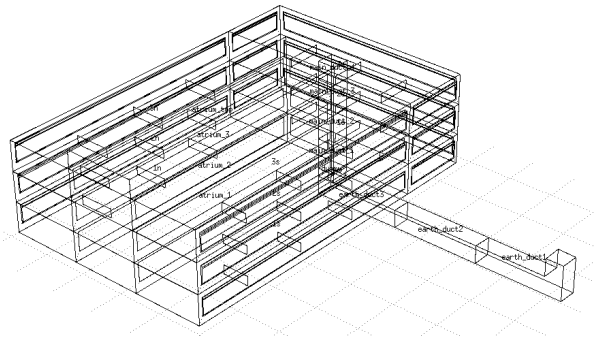

Figure 8: Model in ESP-r.

Weather data from the Danish Design Reference year was used in the simulations. The Danish climate is within the temperate zone and to give a general idea of the weather conditions the annual mean outdoor temperature is 7.8 °C and the mean wind velocity is 4.4 m/s with prevailing direction southwest and east. The design temperature for heating is −12 °C.

4.1. Simulations

The system and it's components were designed to provide sufficient ventilation during winter and most of

the transitional periods without fans. However, during the day time in the summer season, the stack effect is eliminated and a helping fan is required to create driving pressure. Therefore, the reported results include yearly simulations of the test case building without and with fans. At night, when the outdoor temperature drops, the stack was exploited to create night ventilation without the help of fans. The exchangers and fans were bypassed but to avoid soiling of the inlet ducts, the electrostatic filter was kept active. The consumed energy for this purpose was included in the reported total energy consumption.

4.2. Indoor climate criteria

The European standard for indoor environment [32] states the required fresh air supply and temperature comfort ranges for four different categories 1–4 where 4 is out of category. We chose category 2 as design criterium which states ventilation of $7\,\mathrm{Ls}^{-1}$ per person and building ventilation of $0.7\,\mathrm{Ls}^{-1}\mathrm{m}^{-2}$ for the low-polluting category. Assuming daily average occupancy of $15\,\mathrm{m}^2$/person, the total comfort ventilation rate is $2.5\,\mathrm{m}^3/\mathrm{s}$. However, it was difficult to accurately control the flow rate to all localities and for this reason we increased the ventilation rate to $3.0\,\mathrm{m}^3/\mathrm{s}$.

The temperature comfort range for category 2 is 20–24 °C in winter and 23–26 °C in summer. The subdivision into seasonal ranges is due to the expected clothing level of the occupants. In winter a clo-value of 1 is expected while it drops to 0.5 in summer. However, in a temperate climate where the transitional periods are long and the distinction between cooling and heating periods is vague, we assume that the occupants are able to change their clo-value over the course of a working day. Thus the resulting yearly comfort range 20–26 °C was our design criterium.

4.3. Constructions

Table 2 contains descriptions of the constructions with heat transfer properties. The test case building has open plan offices and to compensate for lightweight partitions, furniture, binders and paper stacks, $18\,\mathrm{m}^2$ of bookshelf is put into each open plan office.

4.4. Internal loads

Table 3 specifies the internal loads during working hours and outside working hours. The periods were constant throughout the year and weekends were considered outside working hours. The lighting load was also applied in the atrium.

Table 2: Constructional details from outside to inside with heat transfer coefficients.

	Materials	U-value $\mathrm{W/m^2\,K}$
Facade	Brick 100 mm Mineral fibre 250 mm Breeze block 100 mm	0.18
Roof	Roofing felt 12 mm Mineral fibre 400 mm Concrete 200 mm Air 200 mm Gypboard 13 mm	0.12
Decks	Flooring 13 mm Cement screed 10 mm Concrete 200 mm Air 200 mm Gypboard 13 mm	–
Ground	Flooring 12 mm Air 50 mm Cement screed 10 mm Concrete 200 200 mm EPS 300 mm Gravel 150 mm	0.09
Culvert	Concrete 100 mm Gravel 100 mm Earth 1000 mm	0.84
Internal partitions	Concrete 200 mm	–
Window	Low-e Glaz.: 4SN-12Ar-4-12Ar-SN4 Frame part: 15% Transp. façade area 51%	0.8 g-value: 0.49

Table 3: Office hours and internal heat gain in office zones. Lighting is the only heat gain in the atrium.

	Hours		Load $[\mathrm{W/m^2}]$	
	Work hours	Outside work h.	Work hours	Outside work h.
People	8–17	17–8	4	0
Lighting	8–17	17–8	6	0.6 (10%)
Equipment	8–17	17–8	6	0.6 (10%)

4.5. Solar shading

The predefined transparent constructions in ESP-r are not suitable for high-performance offices in temperate climates. For this reason we used WIS [33] to construct a triple glazing with retractable external blinds. The thermal and angular optical properties were added and the resistance-value of the air-gaps were adjusted, so the overall thermal heat loss coefficient was in accordance with the value calculated by WIS. Due to the limited capabilities of automatic shading devices in ESP-r, the yearly shading of the window was modelled as a glazing with external venetian blinds with incremental tilt angle of 30 ° for the internal temperature interval 23–25 °C. Thus shading was activated and adjusted to a tilt angle of 0 ° at the indoor air temperature of 23 °C, 30° tilt at 24 °C and 60° tilt at 25 °C. The risk of glare was handled by including a setpoint of incident radiation of 170 W/m^2 which, if exceeded, caused the shading to be activated and adjusted to a tilt angle of 60° between 8 and 17. This control also allowed passive solar gain to heat up the room air when night ventilation had cooled the constructions. The only exception was the east-facing third floor that did not need such a high morning solar gain. Here glare control was activated from 6 to 17. The effect of shading on daylight levels and subsequently the effect on artificial lighting and thermal load is beyond the scope of this article.

4.6. Ground temperature

The temperature variation at different depths in the ground around the culvert and below the building was modelled on monthly basis as ESP-r accepts mean monthly soil temperature input. The following equation referred by [34] predicts the ground temperature for any depth x_s and any Julian day t:

$$\begin{aligned} T(x_s,t) \;=\; & T_\mathrm{m} \\ & -A_\mathrm{s}\exp\left\{-x_s\left(\frac{\pi}{365\alpha}\right)^{1/2}\right\} \\ & \cos\left\{\frac{2\pi}{365}\left[t-t_0-\frac{x_s}{2}\left(\frac{365}{\pi\alpha}\right)^{1/2}\right]\right\} \end{aligned} \quad (2)$$

T_m is the yearly mean soil temperature, A_s is the annual surface temperature amplitude (=(maximum temperature–minimum temperature)/2), t_0 is the day of minimal soil surface temperature and α the thermal diffusivity of the soil in m^2/day. The sinusoidal annual outdoor temperature was estimated from Equation 3 where M is the number of the month [35]. The resulting mean monthly soil temperatures at the depth of 2 and 4 m are listed in Table 4.

$$\theta_e = 8.0 - 8.5\cos\left(2\,\pi\,\frac{M-1}{12}\right) \quad (3)$$

4.7. Mass flow network

The ventilation system with heat recovery was modelled using the coupled plant and mass flow network option in ESP-r. The mass network was established by specifying internal nodes representing the pressure and temperature in each zone and linking them with components. The external nodes represents the outdoor pressure and temperature conditions. The components consisted of ducts, dampers, openings, grilles and other pressure drop inducing elements in the mass flow network.

A schematic of the principal mass flow network is depicted in Figure 9. To ease the understanding, fictitious mass nodes are not depicted and some parts are simplified. Neither the modelling of infiltration by building fabric cracks is depicted, nor the division of each floor into North-facing, South-facing and East-facing open plan offices each equipped with separate supply ducts. In order to inject recovered heat from the plant network back into the mass flow network a dummy zone was created. The plant network is depicted in greater detail in Figure 7. The flow path through the building responsive elements, culvert and main shaft were modelled as thermal zones with CFD-derived heat transfer coefficients, see Section 3.4. Appendix A describes in detail the duct sizes and local losses due to bends and components that was put into the mass flow network.

The pressure conditions at the boundary nodes were determined from the default ESP-r pressure coefficients for a building with length/width ratio of 2:1. The pressure coefficients are associated with great uncertainty and to avoid unrealistically high wind pressure and to make the results more robust, the boundary nodes were set to either sheltered or semi-exposed. The wind profile was based on the power law model with urban environment parameter values.

The fan performance characteristic were derived from [36]. The absorbed energy of pumps and fans is in ESP-r based on the linear relationship of rated power at the rated flow rate. The absorbed power is passed on to the fluid. The absorbed fan power was 50 W at 12 Pa and 3 m^3/s. The liquid-loop heat recovery pump was a circulation pump with the absorbed power 41.6 W at the design flow rate 3.6 m^3/h and 2 meters of head loss. The pump performance characteristic was derived from [37]. The flow in normal operation mode was only 39%

Table 4: Monthly ground temperatures.

Depth m	Jan	Feb	Mar	Apr	May	Jun	Jul	Aug	Sep	Oct	Nov	Dec
							°C					
2	5.5	4.2	3.9	4.7	6.5	8.7	10.9	12.3	12.6	11.8	10.0	7.7
4	8.2	7.1	6.3	5.9	6.2	7.1	8.2	9.4	10.3	10.6	10.2	9.4

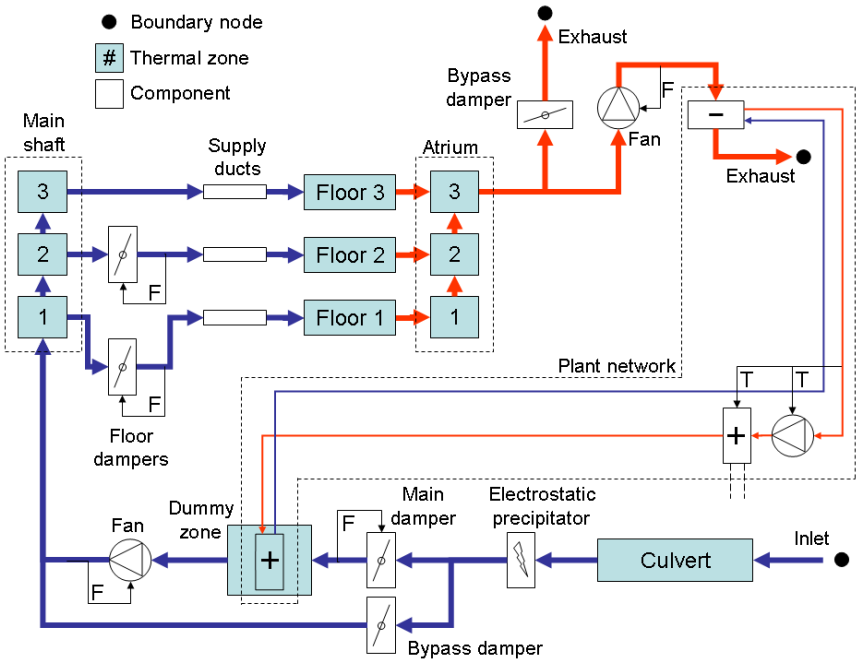

Figure 9: Schematic of mass flows and controls.

of the design flow rate because there had to be some excess power for situations where sub-zero temperatures threatened to freeze the outlet heat exchanger. Thus the absorbed power was 25.6 W. The dampers were rectangular with opposing blades. Their characteristics were derived from [38] and include leakage.

4.8. Control strategies

Table 5 summarizes the control strategies and setpoints. The heating control was ideal while the damper, fan and pump were controlled by proportional ramps, i.e. they varied from closed to fully open within a specified sensor range. The sensed properties were mass flow rates or temperatures. In order to achieve stable results, the building timestep was set to 4 steps per hour with 5 plant time steps for each building time step. This meant that the flow controls, dampers, fans, and pumps, were updated every 15 minutes which also reflects a practical update rate.

The sensed property for the actuation of freeze protection was the exiting water temperature of the inlet exchanger, see Figure 7. The control was a proportional ramp that kept the flow rate at 39% for exiting temperatures above 4 °C and increased it to 100% when the temperature dropped to 2 °C. This was on the safe side in practise, but it was required in order to avoid simulation crashes due to sub-zero temperatures. For the same reason the pump was also started 1 time step earlier (15 minutes) than the ventilation. During the transitional seasons high exchange efficiency can cause too high supply temperatures. The ramp control was then changed so it started decreasing the mass flow when the exiting temperatures exceeded 8 °C and reduced it down to 10% at 12 °C. During summer there was no heat recovery but the exchanger's were not bypassed except in night ventilation mode.

In ESP-r version 11.6 the same control law cannot perform differently from one season to the next season. Consequently the yearly simulation was split in four season and the results put together afterwards. Each season was started with 12 days of pre-conditioning simulation.

5. Results

The ventilation rate and thermal performance results for the yearly simulation are reported as footprints for the occupied time in all offices (Figure 10 and Figure 11). Duration curves elaborate the results for selected offices (Figure 12 and Figure 13).

Figure 14 illustrates in detail the operation of the heat recovery system over the span of five winter days. The

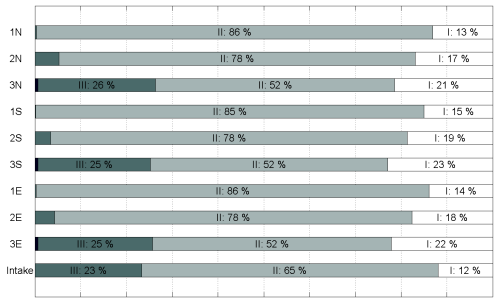

(a) Without fans

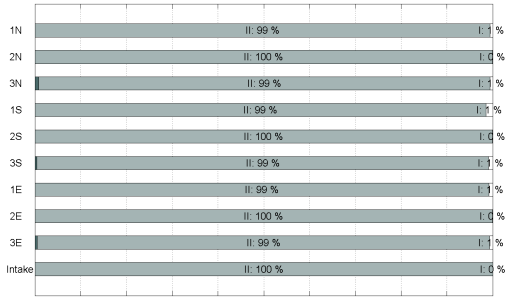

(b) With fans

Figure 10: Ventilation rate according to [32] in the different offices of the atrium building.

Table 5: Control strategies.

	Winter		Spring/autumn		Sum	
	8-17	17-8	8-17	19-7	8-17	17-7
Heating[a]	On	On	On	On	Off	Off
Heat rec. pump	On	Off	On	Off	Off	Off
Main damper[b]	On	Off	On	Off	On	Off
Bypass damper	Off	Off	Off	On[c]	Off	On[d]
Fans (if applicable)[b]	On	Off	On	Off	On	Off

[a] Heating setpoint 20.05 °C air temperature.

[b] Fans and main damper are shut down in weekends.

[c] Cooling setpoint 21 °C operative temperature measured in 1N.

[d] Cooling setpoint 20 °C operative temperature measured in 1N.

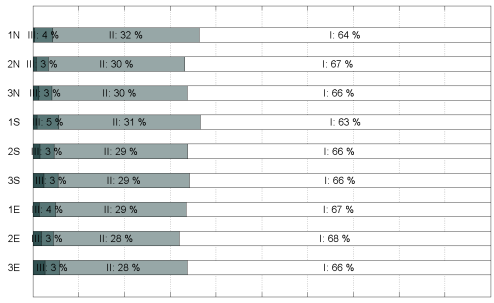

(a) Without fans

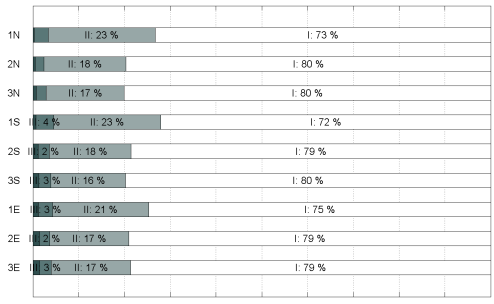

(b) With fans

Figure 11: Indoor thermal climate according to [32] in the different office floors of the atrium building.

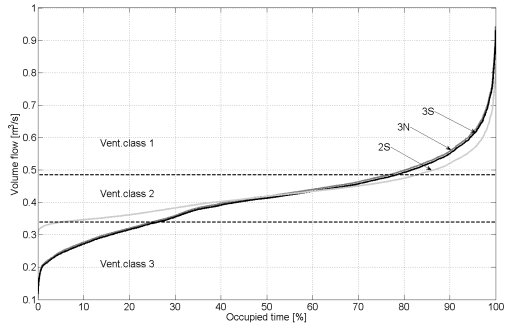

(a) Without fans

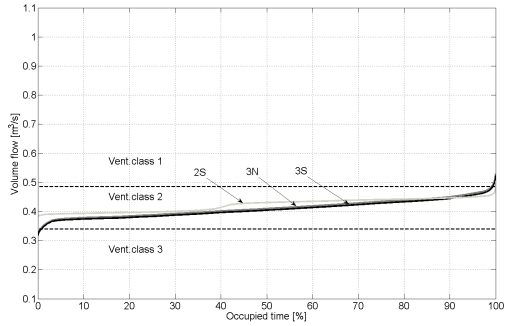

(b) With fans

Figure 12: Selected ventilation duration curves of ventilation supply.

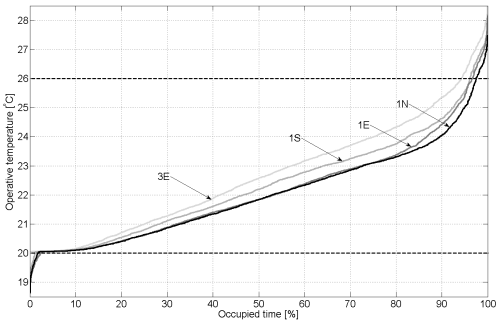

(a) Without fans

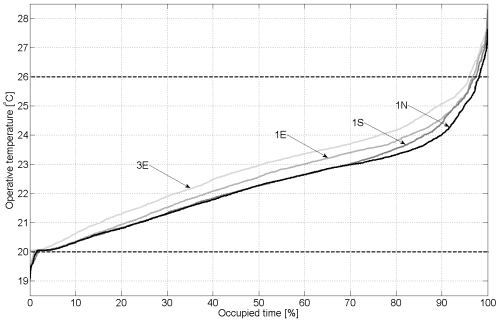

(b) With fans

Figure 13: Selected duration curves of operative temperature.

number of time steps was increased to 12 steps per hour, i.e. every 5 minutes. The outdoor temperature is heated slightly in the culvert before it is heated by the inlet coil to supply temperature. The indoor temperature is plotted for reference. The freeze protection control is illustrated towards the end of the period where the exiting temperature of the inlet coil drops below 4 °C which activates the pump to increase the water flow. The heat exchange efficiency during operation is approx. 66% but drops when the airflow rate is unstable due to inadequate damper control.

Figure 15 illustrates the necessary fan pressure rise over a year. In the summer, the fan pressure rise is approx. 4 Pa. In the winter, the fan pressure rise is negative because the natural driving pressure is so large that to achieve the desired flow rate, the fans have to act as dampers. This can be achieved in practise by either stopping them or letting them rotate slower than the flow. The latter option is advantageous in terms of ensuring constant air supply because it evens out natural fluctuations. Figure 15 also illustrates that fans are needed for the warm part of the year. The outdoor temperature is included for reference.

Figure 16 shows the results of exploiting building integration in conditioning of the supply air. The figure shows results for peak summer and winter values with fan driven flow. The outdoor air is pre-conditioned by the culvert and further pre-conditioned in the main concrete shaft for the three floors F1–F3. The airflow is shown for reference. In Figure 16(b) the night ventilation is visible.

The primary energy consumption is reported in Table 6. Yearly lighting and hot water was separately calculated with an external program [39] which is normally used to document the primary energy consumption in Denmark. The boiler in the heat recovery loop is included in the heating consumption. The mean specific fan power (SFP) is calculated and to compare it with the SFP of conventional mechanical ventilation, the value includes the power consumption of the electrostatic precipitator and the extra pumps that are required for the passive building integrated ventilation system to run. In Table 7 the contributors to the mean SFP is listed. The SFP values were calculated by the mean value of the sum of all power consumption divided with the total amount of comfort ventilation.

6. Discussion

The building was simulated as a fully naturally ventilated building and as a balanced mechanical system with extremely low pressure loss. The ventilation footprint in

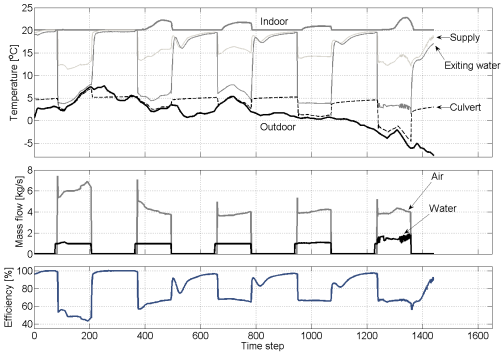

(a) Without fans

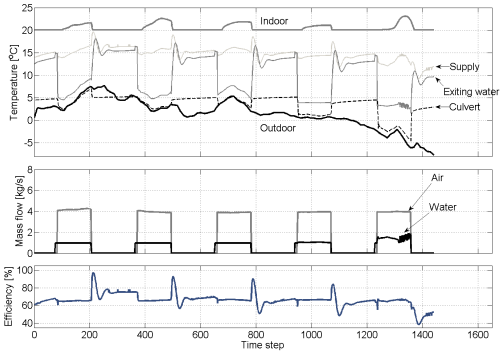

(b) With fans

Figure 14: Detailed illustrations of operation results.

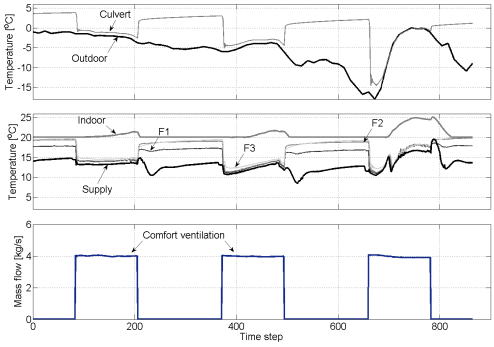

(a) Winter

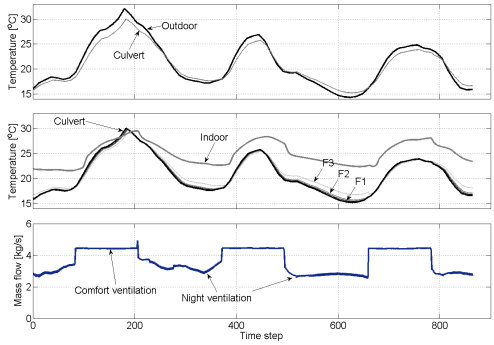

(b) Summer

Figure 16: The temperature effect of building integration with fans.

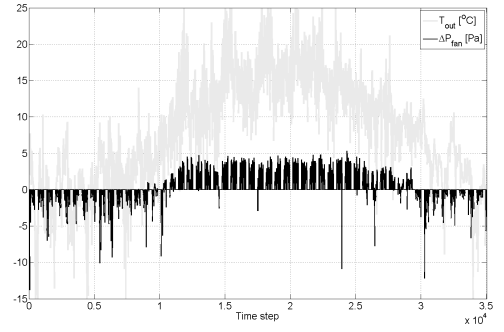

Figure 15: Fan pressure rise.

Table 6: Comparison of yearly primary energy consumption. Conversion factor to primary energy: 2.5.

Primary energy kWh/m^2	w/o fans	w/ fans
Heating	4.93	3.63
Cooling	0.00	0.00
Fans	0.00	0.03
Filter	2.20	2.20
Pumps	0.03	0.03
Hot water	6.05	6.05
Lighting	6.95	6.95
Total	20.16	18.90
Mean SFP [J/m^3]	155.6	155.0

Table 7: Breakdown of mean SFP.

Specific fan power J/m^3	w/o fans	w/ fans
Fans	0	1.1
Pumps	19.7	16.4
Filter	135.9	137.5
Sum	155.6	155.0

Figure 10 documents that the system is dependent on the fans to comply with the minimum required ventilation rate in indoor class II [32]. However, the natural driving pressure was sufficient for 75% of the operation time for class II and 100% of the time for class III. In practise, performance drops below the minimum ventilation rate is seldom allowed but Figure 10(a) also shows that compensation is often achieved in terms of ventilation class I. It is important to note that the compensation allows for better productivity in the indoor environment [40] without increasing the fan energy consumption. The extra ventilation heat loss is minimal, see Table 6. The performance deficiency is further illustrated in Figure 12 where the fan-controlled flow was kept within the limits of ventilation class II, whereas without fans, the flow fluctuated much more. The lower ventilation rate values stem from insufficient natural driving pressure in the summer. Too high values stem from the limitations of the dampers. The logarithmic properties of blade dampers means that is has a clear angle-flow response only for a small range of blade angles. This limits the lower open area of the main damper which sometimes results in too high flow rates. Whether this limitation is specific to the ESP-r simulation environment or a general limitation for blade dampers is unknown, however poor angle-flow response causes control difficulties also in practise. Because floor 1 and 2 have damper controlled flow, floor 3 suffers the most in both cases. The airflow fluctuations are illustrated in detail in Figure 14.

Figure 14 also shows results from the heat recovery system in detail. The time constant of the the liquid-loop is visible by observing the supply temperature and exiting temperature every time the airflow is shut down. The ESP-r simulation does not allow the circulation flow to be completely stopped and therefore the temperatures 'balance' to find a new steady state. In Figure 14(a) (without fans) there is no exhaust damper. Hence infiltration and slowly circulating water flow cause the steady state temperature to lie closer to the indoor temperature.

Figure 11 shows the operative temperature in all offices during occupied time. It documents that the thermal comfort is slightly better with fans. The excessive thermal load is removed by: (1) the normal comfort ventilation, and (2) free cooling by night ventilation. The night ventilation is provided purely by stack and wind through the culvert and existing ventilation ducts and is sufficient to maintain a maximum of 5% deviation in all offices. Only the fans and exchanger coils were bypassed. Figure 13 depicts the duration curves of selected offices which show that some of the deviation in the first floor offices is due to operative temperatures below 20 °C. This is due to the control of the night ventilation where the sensed property is the operative temperature of the North-facing floor 1 office. When the night ventilation is activated, the floor dampers direct the air first to floor 1 and 2, and then to floor 3. This means that floor 1 is cooled down effectively to 20 °C but because it has higher transmission loss than floor 2, the temperature subsequently drops below 20 °C overnight. Thus sensing the North-facing floor 1 office is a lesser-of-evil in terms of minimizing too low temperatures.

The thermal comfort was achieved by night ventilation, effective solar shading, effective lighting and the embedded culvert. In Figure 16 the peak temperatures are shifted 2 °C in summer and 3 °C up in winter. This corresponds to a heat transfer of 33–50 W/m^2 culvert surface, equivalent to the cooling/heating power of 3.6/5.6 W/m^2 floor area. In comparison the Mediå School in Grong, Norway [17] experienced a cooling power maximum of 80 W/m^2 culvert surface at slightly higher air speed. The cooling power in Grong was much higher than the models predicted [15]. Consequently, higher impact of the culvert in practise may be experienced. The effect of the main shaft on the supply temperatures in Figure 16 is low due to the small temperature gradients. The primary advantage of using embedded culverts and other building integration is not the cooling and heating potential but the peak temperatures and consequently on the installation of heating and cooling coils. In this building (with fans) neither heating nor cooling coils were necessary because the supply temperature never reaches more than 8 °C below indoor temperature (Figure 16(a)), and the temperature deviation is below 5% (Figure 11(b)). The building integration effect due to the diffuse ceiling ventilation remains to be quantified.

The total energy consumption of the building is summed up in Table 6. The power consumption is converted to primary energy with a conversion factor of 2.5. The only major difference between the two cases is the heating consumption which is due to differences in ventilation heat loss. The power required for fans is extremely small. This is supported by Figure 15 which

illustrates that the required fan pressure rise is very low (< 5 Pa) and only necessary during the warm season. This is comparable to the design criterium of 6.5 Pa and the pressure loss in natural ventilation which is typically less than 10 Pa [7]. Some of the low fan power is replaced by the power consumption in the electrostatic precipitator. This results in a mean specific fan power of 155 J/m^3 including fans, pumps and filter. For comparison the maximum SFP value in the Danish Building Code is 2500 J/m^3. The total energy consumption is 18.9 kWh/m^2 with a heat recovery efficiency of approx. 66% and a pressure drop of approx. 5 Pa. This is significantly lower than those obtained by [10], and by [12].

The major cost difference to a conventional mechanical system is due to the culvert, the main concrete shaft, and the heat exchanger coils. On the up-side no air-conditioning coils are necessary, no office space is consumed for ventilation purposes, and increased ventilation rates, e.g. due to higher future indoor climate demands, are 'free'. In total, a near-zero emission building is obtained without employing costly renewables.

7. Conclusion

With the results in this paper we have made probable that a realistic building can be ventilated by a one-mode hybrid ventilation system. The building is almost naturally ventilated, employs heat recovery, filtration, diffuse ceiling ventilation and flow control and uses a fraction of the energy for air transport required in a new building by the Danish Building Code. The indoor air quality is improved because filtration is performed with an electrostatic precipitator where the fresh air is not polluted by dirty bag filters, and the thermal comfort is maintained through an embedded culvert and free cooling by night ventilation without fans using the existing supply ducts. Heating coils and cooling coils are not necessary. The proposed ventilation concept is not optimized with regard to investment and running costs but we have made probable that buildings with near-zero emissions are within reach.

8. Acknowledgements

The work was gratefully funded in collaboration with ALECTIA A/S and the Danish Ministry of Science, Technology and Innovation.

A. Air flow network input

The appendix documents the ductwork and the local loss coefficients employed (Table 8). Table 9 documents the various components.

References

[1] C.A. Hviid, S. Svendsen, Analytical and experimental analysis of a low-pressure heat exchanger suitable for passive ventilation, Submitted to Energy and Buildings, 2010

[2] C.A. Hviid, S. Svendsen, Experimental and numerical analysis of perforated suspended ceilings as diffuse ventilation air inlets, Submitted to Energy and Buildings, 2010

[3] P.V. Nielsen, R.L. Jensen, L. Rong, Diffuse ceiling inlet systems and the room air distribution, submitted to Clima 2010, 10th REHVA World Congress, Antalya, 2010

[4] A. Delsante, T. Arvik (Eds.), Hybrid ventilation, State-of-the-art review, IEA Annex 35 Hybrid ventilation in new and retrofitted office buildings, Hybrid Ventilation Centre, Aalborg University, Denmark, 2002

[5] P. Heiselberg (Ed.), Principles of hybrid ventilation, IEA Annex 35 Hybrid ventilation in new and retrofitted office buildings, Hybrid Ventilation Centre, Aalborg University, Denmark, 2002

[6] P. Wouters, N. Heijmans, C. Delmotte, L. Vandaele, Classification of hybrid ventilation, Technical paper, in: Proceedings of Hybvent Forum 99, IEA Annex 35, Sydney, Australia

[7] S. Aggerholm, P. Heiselberg, N.C. Bergsøe, Hybrid ventilation i kontorer og institutioner, Danish Building Research Institute, Hørsholm, Denmark, 2008

[8] W. de Gids, Hybrid ventilation concepts, classification and challenges, Technical paper, in: Proceedings of HybVent Forum 01, IEA Annex 35, Delft, Netherlands, 2001

[9] H. Awbi (Ed.), Ventilation systems - Design and performance, Taylor and Francis, 2008

[10] P.O. Tjelflaat, Pilot study report: Mediå school, Grong, Norway, Case study, IEA Annex 35, 2000

[11] J. Seifert, A. Perschk, M. Rösler, W. Richter, Coupled air flow and building simulation for a hybrid ventilated educational building, Technical report, IEA Annex 35, Dresden, Germany, 2001

[12] J. Heikkinen, J.S. Heinonen, T. Laine, K. Liljeström, M. Vuolle, Performance simulation of hybrid ventilation concepts, Technical report, IEA Annex 35, Espoo, Finland, 2002

[13] Y. Jeong, F. Haghighat, Modeling of a hybrid-ventilated building, Journal of Ventilation 1 (2) (2002) 127-139

[14] U. Meinhold, M. Rösler, Hybrid ventilation in the Bertolt-Brecht Gymnasium - Results of the monitoring phase, Technical paper, in: Proceedings of HybVent Forum 02, IEA Annex 35, Montreal, Canada, 2002

[15] B.J. Wachenfeldt, Natural ventilation in buildings - detailed prediction of energy performance, PhD Thesis, Department of Energy and Process Engineering, Norwegian University of Science and Technology, NTNU, Trondheim, 2003, ISBN 82-471-5624-5

[16] IDA Indoor Climate and Energy, version 4.0, Available from: http://www.equa.se

[17] P.G. Schild, An overview of Norwegian buildings with hybrid ventilation, Technical paper, in: Proceedings of HybVent Forum 01, IEA Annex 35, Delft, The Netherlands, 2001

[18] Energy Systems Research Unit, ESP-r, version 11.8, 2010. Available from: http://www.esru.strath.ac.uk/Programs/ESP-r.htm

Table 8: Airflow network input for passive system.

Component	Characteristics	Face area m^2	Velocity m/s	Local loss coefficient C[a]
Culvert	2000 × 2000 mm	4.000	0.75	-
Main shaft	2000 × 2000 mm	4.000	0.25–0.75	-
North supply duct	900 × 900 mm	0.810	0.42	-
South supply duct	900 × 900 mm	0.810	0.42	-
East supply duct	800 × 800 mm	0.640	0.42	-
Distribution ducts	Not applicable	-	-	-
Floor dampers	1800 × 830 mm	1.494	10.5 m^3/s[b]	-
Main/bypass damper	2000 × 2000 mm	4.000	105 m^3/s[b]	-
1 elbow bend 90°	900 × 900 mm	0.063	-	0.15[c]
2 wye fittings 45°	900 × 900 mm	-	-	0.17[c]
1 elbow bend 45°	900 × 900 mm	-	-	0.09[c]
Room supply	Porous suspended ceiling[d]	2016	0.0015	-
	Pressure drop 0.5 Pa	-	-	6.97[e]
Room exhaust	Through atrium	-	-	-

[a] Local loss coefficient denoted by C is used in ESP-r simulation.

[b] Rectangular opposed blade damper, flow at a pressure difference of 100 Pa and fully open blade angle [38]

[c] [41]

[d] [2]

[e] Calculated from and applied to the supply ducts.

Table 9: Component data.

Component	Characteristics
Fans[a]	Ø 1600 mm Rated volume flow 3 m^3/s Rated pressure rise 12 Pa Rated power 50 W Efficiency 78%
Liquid-coupled heat exchangers[b]	Pressure drop 0.74 Pa Efficiency 70%
Loop pipe size Loop pump	0.05 m Grundfos Magna 25-60[c] Rated volume flow 3.6 m^3/h Rated power 41.6 W Efficiency 46%
Electrostatic precipitator[d]	Pressure drop 2 Pa Power consumption 476 W Local loss coefficient 5.05

[a] [36]

[b] [1]

[c] [37]

[d] [28]

[19] Y. Li, A. Delsante, L. Chen, Integrating thermal stratification in natural and hybrid ventilation analysis, Technical paper, in: Proceedings of HybVent Forum 99, IEA Annex 35, Sydney, Australia, 1999
[20] L. Jensen, PFS, version 1.0, 2000. Available from: http://www.hvac.lth.se/PFS/PFS.HTML
[21] E. Jakubowska, Air distribution in rooms with diffuse ceiling inlet, M.Sc. Thesis, Department of Civil Engineering, Aalborg University, Denmark, 2007
[22] P. Jacobs, E.C. van Oeffelen, B. Knoll, Diffuse ceiling ventilation, a new concept for healthy and productive classrooms, in: Proceedings of Indoor Air 2008, paperID #3, Copenhagen, Denmark
[23] P.V. Nielsen, E. Jakubowska, The performance of diffuse ceiling inlet and other room air distribution systems, in: Proceedings of Cold Climate HVAC, Sisimiut, Greenland, 2009
[24] R. Høseggen, H.M. Mathisen, S.O. Hanssen, The effect of suspended ceilings on energy performance and thermal comfort, Energy and Buildings 41 (2) (2009) 234-245
[25] Fluent manual, version 6.2.16, Fluent Inc., 2005
[26] G. Bekö, G. Clausen, C.J. Weschler, Is the use of particle air filtration justified? Costs and benefits of filtration with regard to health effects, building cleaning and occupant productivity, Building and Environment 43 (10) (2008) 1647-1657
[27] G. Bekö, M.O. Fadeyi, G. Clausen, C.J. Weschler, Sensory pollution from bag-type fiberglass ventilation filters: Conventional filter compared with filters containing various amounts of activated carbon, Building and Environment 44 (10) (2009) 2114-2120
[28] S. Terkildsen, Udvikling af ventilationsanlg med lavt elforbrug, M.Sc. thesis, Department of Civil Engineering, Technical University of Denmark, 2009
[29] TRNSYS. Available from: http://sel.me.wisc.edu/trnsys/
[30] M. El Mankibi, F. Cron, P. Michel, C. Inard, Predicition of hybrid ventilation performance using two simulation tools, Solar Energy 80 (8) (2006) 908-926.
[31] P.A. Strachan, G. Kokogiannakis, I.A. Macdonald, History and development of validation with the ESP-r simulation program, Building and Environment 43 (4) (2008) 601-609
[32] EN 15251, Indoor environmental input parameters for design and assessment of energy performance of buildings addressing indoor air quality, thermal environment, lighting and acoustics, European Standard, European Committee for Standardization, Brussels, 2007
[33] D. van Dijk, H. Oversloot, WIS the European tool to calculate thermal and solar properties of windows and window components, in: Proceedings of IBPSA, Building Simulation, Eindhoven, Netherlands, 2003, 259-266
[34] D.P. Jenkins, R. Tucker, R. Rawlings, Modelling the carbon-saving performance of domestic ground-source heat pumps, Energy and Buildings 41 (6) (2009) 587-595.
[35] DS418, Calculation of heat loss from buildings, Danish Standards, 2002
[36] Airbox, version 2.0.0.2, Novenco, 2009. Available from: http://www.novencogroup.com/Downloads/Software.aspx
[37] Product catalog, WebCAPS, Grundfos, 2010. Available from: http://www.grundfos.com
[38] Catalogue, Lindab, 2009. Available from: http://www.lindab.com
[39] Be06, version 4,8,11,14. Danish Building Research Institute, Hørsholm, 2010. Available from: http://www.sbi.dk/miljo-og-energi/energiberegning/anvisning-213-bygningers-energibehov/
[40] O. Seppänen, W. Fisk, Q. Lei, Ventilation and performance in office work, Indoor Air 16 (1) (2006) 28-36.
[41] ASHRAE, Handbook — Fundamentals SI-edition, American Society of Heating, Refrigerating and Air-Conditioning Engineers, Atlanta, GA, USA, 2005

Paper V

Submitted to Buildings and Environment, 2010

A morphological method for investigation of the problem complex of choosing the ventilation system for a new building

Christian Anker Hviid[*,1], Svend Svendsen[b]

[a]*ALECTIA A/S, Teknikerbyen 34, DK-2830 Virum, Denmark*
[b]*Department of Civil Engineering, Technical University of Denmark, Brovej, Building 118, DK-2800 Kgs. Lyngby, Denmark*

Abstract

The application of a ventilation system in a new building is a multidimensional complex problem that involves both quantifiable and non-quantifiable data e.g. energy consumption, indoor environment, building integration and architectural expression. This paper presents a structured method for evaluating the performance of a ventilation system in the design process by treating quantifiable and non-quantifiable datasets together. The method is based on general morphological analysis and applies cross-consistency assessment to reduce the problem complex, thus treating the multi-dimensionality, the uncertainty and the subjectivity that arise in the design process on a sound methodological and scientific basis. Using a distance analysis of the shared values, the solution scenarios may be plotted relative to each other, which provides the designer with an illustrated 'space of solutions'. Herein the designer may view multiple ventilation solutions and navigate between them, evaluate the differences and choose the best ventilation system scenario in terms of energy consumption, indoor environment and architectural quality.

Key words: Product development, Morphological analysis, Ventilation, Multidimensional scaling

1. Introduction

The design of ventilation systems for low-energy offices requires insight of the engineer/architect into multiple fields of building design and ventilation. Integrated design process is a holistic method that facilitates the design of buildings in the initial design phase. The process is to combine architectural and functional quality of a building. Part of the process is the selection of the ventilation scheme.

Analysing problem complexes like choosing the ventilation system for a new building presents us with a number of methodological difficulties. The issue involves both quantifiable and non-quantifiable variables that are inter-correlated to some extent and perhaps incomplete, with missing or undetermined information due to the early stage in the design phase or simply the subjective nature of judgements.

In this contribution, we use morphological analysis to decompose and structure the problem complex into both objective (technical) and subjective (psychological) variables while treating incomplete information in a structured manner. One of the advantages of morphological analysis is that such combinations are valid. General morphological analysis was developed by Fritz Zwicky [1] and has been used for many purposes in relation with buildings e.g. for integral design methods or to improve the comfort of various ventilation concepts [2, 3]. Here we propose a coupling of morphological analysis with cross-consistency assessment (CCA) [4] and multidimensional scaling (MDS) [5] to establish the feasible 'space of solutions' for various ventilation schemes within various building envelopes. This process is time-consuming, but it can be automated if it is implemented in a dynamic building simulation program. For this purpose a transparent building simulation application developed at the Technical University of Denmark is useful [6, 7, 8]. The application works on room level to facilitate the design of the building to maximize the indoor climate and minimize the energy consumption at the pre-design stage where changes are cost-free. In the following we explain how the software application was expanded in terms of it's ventilation design capabilities and how the method with relative little effort can be implemented generally in the program.

[*]Corresponding author. Tel.: +45 88 191 365; fax: +45 88 191 565 001

Email address: crh@alectia.com (Christian Anker Hviid)

Nomenclature

A	face area [m^2]
a	constant [-]
B	width [m]
b	constant [-]
C	wind pressure coefficient [-]
c	constant [-]
D	diameter [m]
d	constant [-]
E	power, [W], empirical [-]
e	constant [-]
f	friction factor [-]
H	height [m]
k	price [€/m^2]
K_{Dr}	diffuser constant [m^{-1}]
L	length [m], logical
l	adjacent zone [m]
M	momentum [N]
Q	heat load [W]
q	flow [m^3/s, L/s]
r	constant [-]
SFP	specific fan power [J/m^3]
T	temperature [°C]
U	air velocity [m/s]
v	air velocity [m/s]
x	distance [m]

Greek symbols

α	constant [-]
β	constant [-]
ϵ	ventilation effectiveness [-]
η	heat recovery efficiency [-]
κ	constant [-]
ρ	density [kg/m^2]
τ	running time [h], $\sqrt{A_{\mathrm{o}}}T_{\mathrm{o}}$ [m K]

Subscripts

a	ambient, outdoor
b	building
bend	bend
conn	connection
demp	damper
duct	duct
e	energy
f	floor, friction
fan	fan
h	hydraulic
hx1	inlet heat exchanger
hx2	outlet heat exchanger
i	indoor, index
m	mean, material
main	main
met	meteorological
min	minimum
o	outlet
opt	optimal
oz	occupied zone
p	pressure
red	reduction
s	supply
sil	silencer
stack	stack
T	T-junction
v	volumetric flow

Other pre-design tools have been developed by Massachusetts Institute of Technology [9] and by Lawrence Berkeley National Lab [10], but both tools are based on scenario generation and neglects the procedure to produce energy-efficient scenarios. In the IEA-ECBCS Annex 35 a simple method was developed that enables the building designer to determine the feasibility of natural or hybrid ventilation systems in a given building based on the site and permeability of the building envelope [11] but this approach is too specific to include all types of ventilation systems. An even simpler design guide chart meant to quantify the probability of success for natural, hybrid and mechanical systems is also available [12].

The method that we propose is based on an existing simulation tool that already employs the approach of low/medium/high values for an integrated design concept. The tool and method are described in [8] and uses a parametric study approach where all medium values constitute the reference, and for all the variables that the user selects, a parametric study with high and low values is performed. This method is quick and advantageous in a practical working situation between architect and ventilation engineer, yet it depends on the ventilation engineer to be able to find a suitable reference. For the design of low-energy buildings finding a suitable reference is tiresome and challenging. It requires multiple iterations and for each variable iteration, alternative options are excluded. The method that we propose uses the same low/med/high approach but to generate a morphological chart, i.e. combinations of all variable values. While this method is less practical in a working situation due to the calculation time, it generates low-energy designs automatically and does not exclude any alternative options. With the statistical method of multi-dimensional scaling, the reference (all medium values) can be visualized in relation to a number of alternatives

which enables the design team to find the low-energy solution that suits them best.

2. Methods

The methodology that we propose comprises three main elements or three steps: generation of input to the morphological chart, cross-consistency assessment and use of multidimensional scaling to visualize the *n*-dimensional result in two-dimensions. The overall objective is not to provide the building designer with the final answer but to visualize the feasibility of different building ventilation concept and to place them in relation to each other. The following sections discusses the methodological elements separately.

2.1. Morphological analysis

The first step is to generate the input that forms the problem complex and for this purpose we employ the morphological box. General morphological analysis identifies and investigates the total set of scenarios or relationships contained in a problem complex from the input parameters. Problem complexes are also denoted 'messes', which are complex issues without well-defined form and where the elements have a high degree of interaction. The purpose of the morphological approach is to structure the mess into problems of unambiguous form and dimension [4]. In this contribution, morphological analysis is used to generate a problem laboratory that enables us to decompose the problem complex into sets of functional subsystems. The decomposition is carried out hierarchically and continues until we arrive at simple building functional components each of which can be described with a single variable. Typically the variable could be of technical nature and denote some technical aspect, but there are no formal requirements that the variables are of the same unit. Technical, physical or psychological elements, known or hypothesized, can be treated together to create a space of solutions for the designer. Thus the method is flexible and fully scalable. To start the morphological analysis we need to:

1. Identify the aspects of the problem complex. Aspects are also referred to as dimensions because they represent the sides in the *n*-dimensional morphological box. In Table 1, comfort, cost, building characteristics, and phycological aspects are chosen as the dimensions.
2. Each dimension is governed by a set of variables. Comfort is e.g. achieved through fresh air supply and the air speed in the occupied zone (Table 1).
3. Each variable may attain a well-defined range of values or conditions. In practice, the ranges are discretised on the basis of a user perception of low, medium and high values. Thus uncertain or hypothesized values are represented on a backward-traceable methodological basis.

The decomposed problem is put into a 'box', which is depicted as a chart in Table 1. The dimensions and variables are listed in the left-hand columns and the values are listed in rows. The imaginative values (high, medium, low) are exchanged with real numbers that the user regards as representing high, medium and low values whenever possible. The values may be arbitrarily selected or based on e.g. three classes from a standard. The depicted chart does not encompass all the possible ventilation variables and indeed has been reduced for the purpose of illustration. The number of non-quantifiable variables is unlimited and the number of quantifiable parameters is only limited by the software tool.

2.2. Cross consistency assessment

After the initial setup and definition of the dimensions of the problem, the user can apply cross-consistency assessment (CCA). This is to accomplish two things: eliminate the illogical or empirically unwanted scenarios and to detect input garbage. Input garbage consists of vaguely defined problems, terms or variables with no clear meaning or with more than one meaning, etc. If anything is insufficiently defined the user must go back to the morphological box and either refine or redefine the input. All values are pairwise compared by the user for logical (denoted by L) or empirical (denoted by E) incompatibility. In the assessment, it is important to focus on each value pair to avoid biased judgments that unintentionally exclude value combinations that may be perfectly compatible but are normatively incompatible. In the assessment there is no reference to causality, but only to consistency and in general only strictly illogical combinations should be excluded. If the intersection between two values is marked, all the scenarios containing the value pair are excluded from the simulation. Blank intersections are included.

Examples of questions for assessing the CCA matrix are:

- Is it possible to have a building scenario where a cooling coil in the second cooling system coexists with a night cooling system in the first cooling system? Clearly this is possible, so no marking is used.

Table 1: Morphological box for the ventilation system in a building. Input is example values.

		Values		
	Dimensions and variables	Low $i = 1$	Medium $i = 2$	High $i = 3$
$k = 1$	Comfort-dimension			
$j = 1$	Ventilation rate[a]	Class III	Class II	Class I
$j = 2$	Ventilation effectiveness[b]	0.7	1.0	1.3
$j = 3$	Thermal comfort[a]	Class III	Class II	Class I
$j = \ldots$	Supply method[c]	Wall jet	Circular diffuser	Displacement
	Draught rating[d]	Class C	Class B	Class A
$k = 2$	Building-dimension			
	Site	City	Urban	Open field
	Inlet exch. coil height, m	2.7	3.2	3.4
	Outlet exch. coil height, m	10.0	12.0	15.0
	Room floor height, m	2.7	3.2	3.4
	Room height, m	2.7	3.2	3.4
	Internal gain, W/m^2	5	10	20
	Thermal capacity[e]	Light	Middle light	Middle heavy
	Window size, % of facade	20	40	60
	Solar shading	None	Blinds	Screen
$k = \ldots$	Cost-dimension			
	Material costs, €/m^2	50	100	300
	Energy price, €/kWh	0.15	0.25	2.0
	Fan efficiency, -	0.4	0.6	0.8
	Running time, hours	2000	2500	4000
	Air handling unit[f], Pa	50	100	200
	Length[g], m	20	30	50
	Heat recovery, -	0.65	0.75	0.9
	Night ventilation, -	None	Venting	Mech. vent.
	Heating system efficiency, -	0.6	0.8	1.0
	Cooling system efficiency, COP[h]	2.0	3.0	5.0
$k = n$	Psychological-dimension			
	Aesthetics (integration)	Visible	Invisible	Somewhat visible
$j = m$	Occupant satisfaction	No control	Low control	Individual control

[a] [13]

[b] Example values for natural ventilation, mechanical mixing and mechanical displacement.

[c] A fourth option, linear slot diffuser, is also available.

[d] [14]

[e] Influences the thermal load that has to be removed by ventilation/cooling system.

[f] Additional losses due to air handling unit.

[g] Local losses in the ductwork should be included as equivalent lengths.

[h] Coefficient of performance.

- Is it possible to have an efficient heat recovery of 85% and a specific fan power of zero? This is illogical, so the pair is marked with an L.

- Is it possible to have a room height of 2.5 m together with a natural ventilation system? This is a possibility, but the literature states that natural ventilation is unsuitable for room heights below 2.7 m [10]. So an E is used because the user assesses that on an empirical basis this particular combination is undesirable.

In a computer simulation it is possible to implement a general algorithm that asks for each value pair: "Is dimension$_k$: variable$_j$: value$_i$ compatible with dimension$_k$: variable$_j$: value$_i$?" where $i = 1, 2, 3$, $j = 1, 2, \ldots n$ and $k = 1, 2, \ldots m$. It is then possible to assign for each pair an L or and E for logical or empirical incompatibility, respectively.

2.3. Distance analysis

One of the most important goals in visualizing data is to provide the viewer with a sense of the distance between the plotted points. While it is straightforward to plot scenarios based on two criteria, e.g. energy consumption and draught rating, the designer is not provided with the overall picture. With more dimensions than 3, it is very difficult to visualize distances, unless the number of dimensions may be reduced to two or three. So a reduction in the number of dimensions is necessary. Non-metric multidimensional scaling (MDS) is a set of statistical methods for addressing this type of problem. The methods are available in a toolbox in Matlab and we use them to plot the selected scenarios relative to each other to obtain an instant sense of the distances between them. The inter-scenario distances are not Euclidean but the configurational or technical distances, or more precisely the pairwise dissimilarities between the scenarios. So a technical distance of 1 between two scenarios indicates that they have been produced from the same set of values except for one value that has been replaced by its horizontal neighbour in the morphological box. A technical distance of 2 means that two values have been replaced by its horizontal neighbour.

It is evident that a certain amount of distortion has to be tolerated when a multidimensional dataset is reduced to two or three dimensions. In typical MDS applications, an investigation into the significance of the error can be conducted using Kruskal's normalized stress criterion (stress1) [15], in which values below 0.05 are good and values above 0.20 are poor. If the criterion is exceeded, the user must reduce the number of selected scenarios or raise the number of depicted dimensions from two to three.

3. Simulation tool

The basis of the simulation software is a simplified thermal and daylighting model [6, 7]. The tool is capable of evaluating the thermal indoor environment and heating and cooling loads in a building with very few input parameters while providing the option of sophisticated system controls. The thermal model is based on a two-nodal equation system with one node representing the air temperature and one the internal temperature of the constructions. The mean surface temperature represents the internal surfaces where heat is exchanged with the indoor air and the effective heat capacity of the constructions. The equation system has an analytical solution and by the end of each time step the temperatures are calculated based on the initial temperatures of the time step. The daylighting model is based on simple ray-tracing between the room surfaces and the sky and internal radiosity. Shading transmittances are derived from WIS [16]. The systems control strategy is ideal yet satisfactory for quick design suggestions. During each time step the shading/cooling systems are activated to control the risk of glare and the indoor air temperature which changes the analytical solution and causes the equation system to be solved several times within a time step to achieve a given setpoint.

3.1. Ventilation model

In order to properly evaluate different ventilation concepts, e.g. natural ventilation versus mechanical ventilation, the natural driving forces become important. The ventilation model described here is implemented in the software application thus expanding the ideal ventilation model by introducing stack, wind effects and pressure characteristic in the ventilation system. Figure 1 depicts a schematic of the model with two possible inlets, either central inlet or facade inlet, and one outlet. All heights relate to the ground level and can be selected arbitrarily, i.e. inlet and outlet heights can be equal, e.g. in the case of air-to-air heat recovery.

The wind speed at reference height (building height) is based on a power law wind profile model in Equation 1 where U_{met} is the meteorological wind speed, H_{b} is the building height and κ and α are terrain constants. Four terrains are available: flat country, open fields, suburban and city center.

$$U_{\text{ref}} = U_{\text{met}} \cdot \kappa \cdot H_{\text{b}}^{\alpha} \tag{1}$$

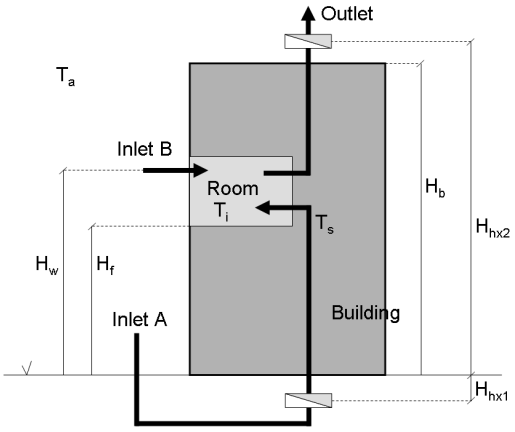

Figure 1: Stack model.

The wind pressure difference between the inlet and outlet opening is:

$$\Delta p_{\mathrm{w}} = (C_{\mathrm{p,i}} + C_{\mathrm{p,o}}) \cdot \frac{1}{2} \cdot \rho_{\mathrm{a}} \cdot U_{\mathrm{ref}}^2 \tag{2}$$

where C_{p} is the tabulated wind pressure coefficient based on wind direction and exposure. The supply temperature is derived from the heat recovery efficiency η:

$$T_{\mathrm{supp}} = \eta\, T_{\mathrm{i}} + (1 - \eta)\, T_{\mathrm{a}} \tag{3}$$

The mean temperature of the air column for the room in question is calculated as a weighted average of the vertical distance between the heat exchangers. The terms are shown in Figure 1

$$T_{\mathrm{in,mean}} = \frac{T_{\mathrm{s}}\,(H_{\mathrm{f}} - H_{\mathrm{hx1}}) + T_{\mathrm{i}}\,(H_{\mathrm{hx2}} - H_{\mathrm{f}})}{H_{\mathrm{hx2}} - H_{\mathrm{hx1}}} \tag{4}$$

The total pressure rise is the sum of wind pressure from Equation 2, stack pressure and fan pressure:

$$\begin{aligned} \Delta p_{\mathrm{tot}} &= \Delta p_{\mathrm{fan}} + \Delta p_{\mathrm{w}} + \\ &= \rho_{\mathrm{a}} g\,(H_{\mathrm{hx2}} - H_{\mathrm{hx1}}) \frac{T_{\mathrm{i,m}} - T_{\mathrm{a}}}{T_{\mathrm{i,m}} + 273.15} \end{aligned} \tag{5}$$

The implementation of the model has been validated by comparison with a commercial building simulation program [17].

The simplified pressure loss characteristic of the system follows a power law relation:

$$\Delta p = r\,(q_{\mathrm{v}})^n \tag{6}$$

where r is a system specific constant, see Equation 9, and $n = 2$ for turbulent currents. The relation is depicted in Figure 2 where only part of the desired flow rate q_{min} is achieved through stack. In order to achieve q_{min} an additional, optional fan pressure rise is needed. If the stack flow rate q_{stack} surpasses q_{min}, the ideal ventilation control adjust the flow rate down to q_{min}.

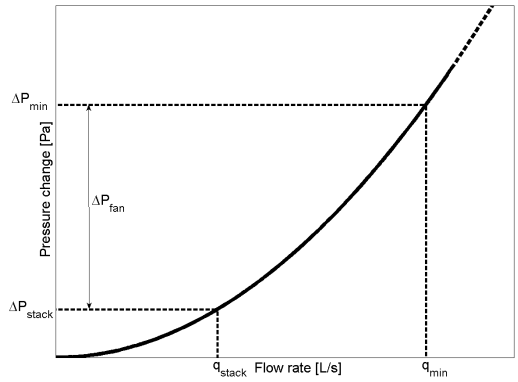

Figure 2: Relation between flow rate and pressure change.

Separating the room from the building in the ventilation model is outright possible for natural stack ventilation because the pressure loss of the airflow is the same for all rooms in the building. A mechanical ventilation system usually serves the whole building or a large part of it. The system will ideally be regulated based on the largest pressure loss in order to provide the desired flow rates to all rooms. This means that the pressure loss is the same for all rooms. The largest pressure loss is usually in the duct to the room furthest away from the fan and this must be considered when the pressure drop characteristic is entered in the tool. Similar considerations may apply to the floor location of the simulated room, because the thermal driving force is affected by the height and temperature of the air column. Without heat recovery the difference between a bottom floor and a top floor is significant, but with pre-heating of supply air in the inlet exchanger, see Figure 1, the difference is much smaller and inversely proportional to the heat recovery efficiency. A worst-case scenario where stack is reduced to a minimum will be achieved by placing the room on the top floor.

The fan pressure rise is used to calculate the specific fan power (SFP), which is the ratio of absorbed fan energy and the transported volume of air in units J/m^3. Figure 2 and Equation 7 show that SFP can be calculated from just the pressure rise attributable to the fan

and the fan efficiency.

$$\mathrm{SFP} = \frac{E}{q_\mathrm{v}} = \left[\frac{(\Delta p_\mathrm{min} - \Delta p_\mathrm{stack})\, q_\mathrm{v}}{\eta}\right] \Big/ q_\mathrm{v} = \frac{\Delta p_\mathrm{fan}}{\eta} \quad (7)$$

In the pressure loss characteristic we ignore the fact that the fan component does not exhibit a continuous pressure characteristic. When the fan is stopped the blades depending on the flow rate are either turning with the flow or standing still [18], both of which induces a variable pressure loss.

3.2. Economical optimization

Sizing of a ventilation systems depends on construction costs, running costs and desired mean ventilation rate. Therefore an optimization method is needed. The one suggested here is by [19]. The method only requires little input and can be used both as stand-alone tool or as an integrated part of a morphological analysis.

For fluid flow in a conduit, friction losses and local losses can be calculated by the Darcy equation [20]

$$\Delta p_\mathrm{f} = \left(\frac{f\,L}{D_\mathrm{h}}\right) \cdot \frac{\rho\, v^2}{2} \quad (8)$$

where f is the dimensionless friction factor, L the conduit length in m, D_h the hydraulic diameter in m, ρ the density in kg/m^3, and v the mean velocity in m/s. Rewriting Equation 8 using round ducts yields:

$$\Delta p_\mathrm{f} = \frac{a\, L\, q_v^2}{D^5} = R\, L \quad (9)$$

where $a = \rho f \pi^2/32$ ($Pa\, s^2/m^2$) is assumed to be constant and q_v is the volumetric flow rate in m^3/s. The constant a can also be described as the pressure loss (Pa/m) at the flow rate 1 m^3/s and the diameter 1 m. R is the frictional loss per meter.

The total costs are the sum of running costs and construction costs. The running cost is determined by the fan energy consumption ($= \Delta p_\mathrm{f}\, q\, \tau/\eta$ kWh) where τ is the running time in hours, η the fan efficiency and k_e the energy price in €/kWh. The construction cost (k_m in €/m^2 duct surface) is the sum of material costs and installation costs. Here we lump them together and assume that they are proportional to the duct surface area. Furthermore, if we assume that the energy price is the mean value over the lifespan discounted to present worth, the objective function for total costs C is:

$$C(D) = \frac{\Delta p\, q_v}{10^3\, \eta}\, \tau\, k_\mathrm{e} + \pi\, D\, L\, k_\mathrm{m} \quad (10)$$

Rewriting the objective function using Equation 9 yields:

$$C(D) = \frac{a\, L\, q_v^3}{10^3\, \eta\, D^5}\, \tau\, k_\mathrm{e} + \pi\, D\, L\, k_\mathrm{m} \quad (11)$$

The objective function shows that the energy cost is proportional to D^{-5} and the construction cost is proportional to D. Simplifying the objective function by replacing the constants with $\alpha = a\, L\, \tau\, k_\mathrm{e}/(10^3 \eta)$ and $\beta = \pi\, L\, k_\mathrm{m}$, and taking the derivative and set it equal to zero we can find minima:

$$5\, \alpha\, q_\mathrm{v} = \beta\, D^2 \quad (12)$$

We see that q_v is proportional to D^2 which implies that the optimal solution dictates constant velocity in all ducts. Replacing $q_\mathrm{v} = v\, \pi\, D^2/4$, the optimal velocity is:

$$v_\mathrm{opt} = \frac{40}{\pi}\left(\frac{\pi\, k_\mathrm{m}\, \eta}{5\, a\, k_\mathrm{e}\, \tau}\right)^{1/3} \quad (13)$$

Constant velocity in all ducts has the great advantage that it is easy to calculate. It yields low pressure drops in large ducts and subsequently low minor losses. The greatest disadvantage is high frictional losses and noise generation in smaller ducts. Instead of constant velocity we can also choose to optimize using constant frictional loss. If we rewrite the objective function in a more general form we get:

$$C(D) = \frac{a\, L\, q_v^{b+1}}{10^3\, \eta\, D^c}\, \tau\, k_\mathrm{e} + \pi\, D^e\, L\, k_\mathrm{m} \quad (14)$$

where b used to be 2, c was 5 and e was 1. Simplifying and setting the derivative equal to zero we get:

$$c\, \alpha\, q_v^{b+1} = e\, \beta\, D^{c+e} \quad (15)$$

From Equation 9 we see that for constant friction d^5 is proportional to q^2, which means that:

$$\frac{c+e}{b+1} = \frac{5}{2} \quad (16)$$

From earlier $b = 2$, and $c = 5$, which yields $e = 2.5$. Other reasonable exponents could be 1.8, 4.8, and 2.2. Putting the former values into Equation 17, the optimal diameter is:

$$\begin{aligned} D_\mathrm{opt} &= \left(\frac{5\, \alpha\, q_\mathrm{v}^3}{2.5\, \beta}\right)^{1/7.5} \\ \Rightarrow D_{\mathrm{opt},i} &= 0.275\left(\frac{\rho\, f\, \pi\, k_{\mathrm{e},i}\, q_{\mathrm{v},i}^3\, \tau_i}{\eta_i\, k_{\mathrm{m},i}}\right)^{1/7.5} \end{aligned} \quad (17)$$

where $i = 1, 2, 3$ corresponds to low/medium/high values in the morphological analysis.

The constant frictional loss method carries some advantages over the constant velocity method. One advantage is reasonable duct sizes in terms of frictional loss and noise in the smaller ducts. The second advantage is that the maximum pressure loss of the system is readily available through multiplication with the duct length. Economical optimization as a pre-processor to the morphological analysis reduces the number a cost-related parameters significantly. Looking at Equation 17, four variables of the cost-dimension is included: material costs k_m, energy price k_e, and fan efficiency η and running time τ. These can be reduced to one variable of optimal duct dimension D_{opt} which means that the preprocessing has reduced the number of cost-related combinations from 3^4 to 3. With the optimal diameter the pressure loss can be calculated from Equation 9 where q_v is replaced with q_{min}/ϵ where ϵ is the ventilation effectiveness. The economical optimization is made with mechanical ventilation in mind and cannot be used with natural ventilation, however, natural ventilation can be included by specifying values for diameter and length that yields the correct pressure drop in Equation 9 for a given flow rate.

The installation and material costs k_m in Equation 13 and Equation 17 are not easily quantified, however, [21] made the attempt. The following adapted Equation 18–Equation 23 quantifies the cost of different duct components on the basis of a Swedish building component database from 2004. The original equations are in Swedish currency and here we have adapted them to € and added the Swedish inflation for 2004–2009. The diameter D is in m.

$$C_{duct} = (13.9 + 144.9\, D^{1.19}) \cdot L \quad (18)$$

$$C_T = 10.1 + 121.5\, D_{main}^{1.91} + 222.3\, D_{conn}^{2.49} \quad (19)$$

$$C_{red} = 4.4 + 102.7\, D^{1.83} \quad (20)$$

$$C_{bend} = 7.3 + 298.2\, D^{2.34} \quad (21)$$

$$C_{sil} = 62.3 + 430.6\, D^{1.91} \quad (22)$$

$$C_{damp} = 11.3 + 137.2\, D^{2.12} \quad (23)$$

Equation 18–Equation 23 can be used to calculate k_m for use in Equation 17. However, it requires an initial guess of diameter and perhaps multiple iterations to find the optimal diameter.

3.3. DR-hours

In order to properly evaluate the performance of a ventilation system, the possible generation of draught must be included in the analysis. In the design phase this is often ignored due to lack of relevant information on the air movement and neither the risk of discomfort because of draught nor the limitations on air flow rate or cooling capacity is quantified [22]. For the purpose of hourly estimation of draught risk we employ a number of empirical formulae that relates the type of inlet and supply temperature with the mean room speed in the occupied zone [23, 24]. Four types of inlets are considered, three of which are mounted in the ceiling or wall and employ the mixing principle and one displacement type mounted in the wall, see Figure 3. The possible inlets are a displacement diffuser, a circular ceiling diffuser, a ceiling slot diffuser, and a wall jet. The latter can be employed for natural ventilation from bottom-hung windows. All air distribution system can be typically found in single and open plan offices. For ceiling-mounted air terminal devices, the following empirical relation for the mean room speed is [23]:

$$v_r = 0.42\, a\, Q \frac{\left[0.3 \left(\frac{H\tau^2}{Q}\right)^2\right]^{1/4}}{\tau \sqrt{0.25L^2 + H^2}} \quad (24)$$

where the empirical constant a has a value of 1.0 for linear diffusers and 1.2 for circular diffusers, $Q = \rho\, C_p\, q\, \Delta T_o\, 10^{-3}$ is the room heat load in kW, $\tau = \sqrt{A_o}\Delta T_o$, and L and H are room length and height. A_0 is the effective area of the supply terminal and T_o the difference between supply and extract temperature. Equation 24 assume a centrally mounted diffuser in a square ceiling of area L^2. If the ceiling or the considered airflow zone is not square, then for a circular diffuser $L = \sqrt{BL}$, where B is the width of the room. For a slot diffuser, the room dimension normal to the slot is L [23]. For side-wall supply the relation for mean room speed is:

$$v_r = 0.73 \sqrt{\frac{M_o}{B\, H}} \quad (25)$$

where the momentum $M_o = \rho\, (q_v^2/A_o)$.

For a wall-mounted displacement diffuser there is no relation for mean room speed. Instead the maximum air velocity in the occupied zone depends on the length of the adjacent zone l_n to the 0.2 m/s isovel. The velocity at the distance x from the diffuser is [24]:

$$v_x = 10^{-3}\, q_s\, K_{Dr}\, \frac{1}{x} \quad (26)$$

where q_s is in L/s, K_{Dr} is stated to be in the range 6–11 with newer designs in the lower end [25]. K_{Dr} is dependent on the Archimedes number and Equation 27 is

therefore adapted from a figure in [24] where θ denotes temperature.

$$K_{Dr} = 1.277 \ln\left(\frac{\theta_{oz} - \theta_s}{q_s^2} 10^3\right) + 2.963 \qquad (27)$$

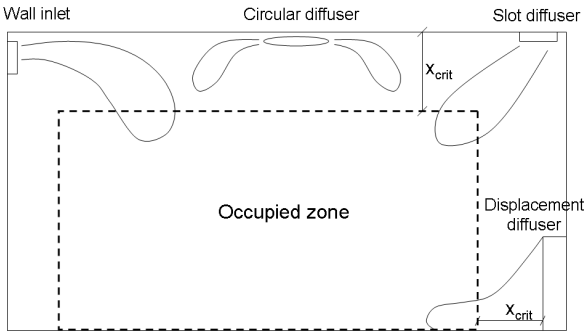

Figure 3: The critical distance between supply inlets and the occupied zone.

With the empirical formulae in Equation 25 – Equation 27 flow rate and supply temperature are related with mean room air speed, and to quantify the performance of different air distribution systems, one can e.g. use the sum of hours that surpasses a user-specified threshold of air velocity within the occupied zone. This can furthermore be coupled with the room air temperature to form draught risk assessment. Consequently the critical distance from the inlet to the occupied zone must also be specified by the user, see Figure 3, and the supply temperature must be controllable with respect to system capacity.

4. Method test case

The suggested method is tested on a simple case to illustrate the possible outcome. Figure 4 illustrates the procedure that starts with selecting the simulation variables and inputting the non-quantifiable variables as well. Four quantifiable variables and one non-quantifiable were simulated. We did not perform cross consistency assessment because we did now want to exclude any scenarios. Neither did we perform any economical optimization but simply stated the pressure loss for three different mechanical ventilation systems. The simulation input is listed in Table 2. The five variables are marked with bold font.

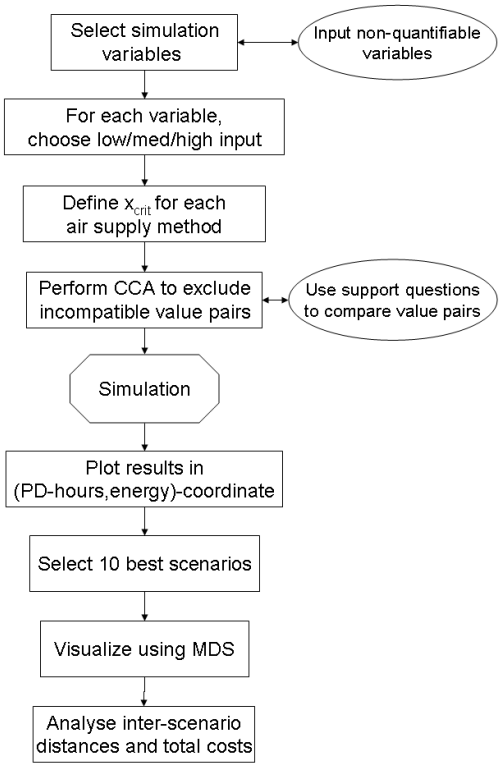

Figure 4: Method procedure.

Table 2: Input values for test run.

Dimensions and variables	Values		
	Low	Medium	High
Comfort-dimension			
1 Ventilation rate	Class III	Class II	Class I
2 Ventilation effectiveness	0.7	1.0	1.3
Thermal comfort	Class II	Class II	Class II
Supply method	Circular diffuser	Circular diffuser	Circular diffuser
Draught rating	Class B	Class B	Class B
Building-dimension			
Site	City	City	City
Orientation	South	South	South
Inlet exch. height, m	-2.0	-2.0	-2.0
Outlet exch. height, m	12.0	12.0	12.0
Room floor height, m	6.0	6.0	6.0
Room height, m	3.0	3.0	3.0
Internal gain, W/m^2	17	17	17
Thermal capacity	Middle light	Middle light	Middle light
Window size, %	50	50	50
Solar shading	Blinds	Blinds	Blinds
Cost-dimension			
3 Pressure loss, Pa	5[a]	200	800
4 Fan efficiency, -	0.4	0.6	0.8
Heat recovery, -	0.8	0.8	0.8
Night ventilation, -	Mech. vent	Mech. vent	Mech. vent.
Heating system efficiency, -	1.0	1.0	1.0
Cooling system efficiency, COP	2.5	2.5	2.5
Psychological-dimension			
5 Aesthetics (integration)	Visible	Invisible	Somewhat visible

[a] Value for mechanical-hybrid system developed by the authors in [26]

4.1. Results

The simulation generated $3^n = 3^4 = 81$ scenarios. We carry out the evaluation on the basis of total primary energy consumption and hours of draught risk above 20% (class B). For power consumption a primary energy factor of 2.5 is used. With 81 combinations, the simulation took approx. 120 minutes on a laptop with a Pentium M processor running at 1.86 GHz and with 1 GB of RAM. Yearly daylight simulation was included.

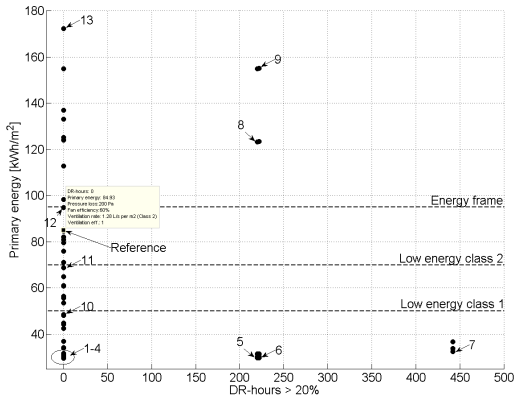

Figure 5: The simulated scenarios are depicted with respect to draught and energy.

Figure 5 depicts most of the scenarios derived from Table 2. With the software tool it should then be possible to pick the most interesting scenarios, typically with respect to low energy consumption and low DR-hours. By holding the mouse over the scenario, the properties should 'pop up'. An example of a 'pop up' box is shown for the reference.In Figure 5 we have pre-selected some interesting scenarios 1–13.

In Figure 6 we establish a linear correlation between bubble size and energy and use the MDS method to plot the selected scenarios relative to each other. The stress criterion is 0.01 which means that the scaling to two dimensions is good. The bubble size could also have been dependent on the total cost using Equation 10.

The distances between the bubble centroids are expressed in terms of 'technical distance'. Where two bubbles are closely spaced, this represents two ventilation scenarios that are very similar to one another. The MDS method visualizes the morphological chart for the engineer, and he is then able to navigate between them and explore their dissimilarities simply by clicking on the bubbles with the mouse.

Figure 7 depicts the predominant value settings of the optimal performing scenarios 1–4. The variable num-

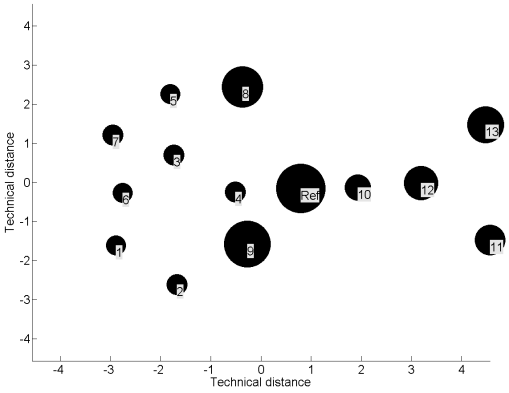

Figure 6: Distance analysis chart.

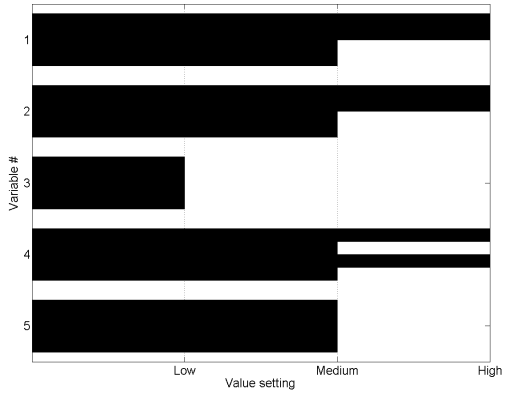

Figure 7: Predominant values.

bers refer to the five simulated variables in Table 2.

5. Discussion

The investigated scenarios are visualized in Figure 6. The low-energy scenarios 1–7 are all close together which means that the poor draught performance when going from scenario 1–4 to 5–7 is due to small solution changes. If scenario 1 is not entirely acceptable to the engineer or the architect, they can go to scenario 2, 3, and 4 which are close by. Scenario 10–12 which are selected for their compliance with the different energy requirements are also closely spaces in terms of solution. The reference is made of medium values for all variables and thus is close to the middle. Quite interestingly it is close to both scenario 4, which is very good, and scenario 9 which is very poor. This emphasizes the importance of making the correct design decisions on the final performance of the building. So Figure 6 illustrates the space of solutions, where it is clear that when standing in the reference, moving to scenario 4 is better than moving to 10 even though the change in solution is nearly the same. In fact moving to 4 means the pressure loss has to be changed from 200 to 5 Pa and moving to 10 means shifting of the ventilation rate from class II to class III. This difference in cost for the two scenarios is significant and therefore it is important in a future version to let the bubble size reflect the total costs instead of energy, i.e. by using the cost objective function in Equation 10.

If we compare the values to the morphological chart we see that the best performance is with a combination of high ventilation rates and high ventilation effectiveness. This is due to the fact that high effectiveness reduces the necessary ventilation rate. Also low-pressure systems with moderate or high fan efficiency shows up. Furthermore, all of the selected scenarios have the aesthetics label: invisible. If none of the scenarios fulfilled the required energy consumption or draught rating, the predominant values could be used as refined starting points in a reformulation of the morphological box and the simulation repeated.

The MDS method has several limitations. The distortion of the solution increases with more scenarios and the information contained in the distance plot depends on the variable resolution; too few attainable values for each variable increases the risk of large unanticipated ‘jumps’ between the scenarios. But the MDS method provides an excellent visualization and overview of feasible scenarios for engineers and architects to discuss in the design phase and the overall methodological approach has the great advantage that a natural pressure is exerted on engineers and architects to produce buildings that perform better because un-conventional scenarios are considered.

6. Conclusion

This paper has sketched the idea for an optimization tool capable of illustrating the ventilation solutions in a given situation. The method offers the possibility of deep insight into the problem complex involved in choosing a ventilation system for a new building. The morphological approach exempts the engineer from generating biased scenarios, and by coupling the morphological analysis with cross-consistency assessment we ensure that the subsystems are unambiguously defined. The approach does require a certain amount of skill and practice to be able to setup the morphological box, cross-assess and iterate, but the procedure in itself helps keep out garbage input and decompose the problem complex correctly.

The different solutions are related to on another by multidimensional scaling which shows the ‘closeness’ or distance of all the alternatives. One great advantage of the method is that it does not exclude non-quantifiable variables but visualizes them with the quantifiable variables side-by-side. With this methodology the architect and the ventilation engineer together have a tool that enables them to find a common optimal solution. The distance analysis gives them a roadmap to a system with a good performance which most closely resembles each person’s idea. The evaluation criteria are here chosen to be energy and draught risk as we believe they address a broad range of interests from the building owner, the engineer and the architect. However, total costs should also be included to give the method credibility.

7. Acknowledgements

The work was gratefully funded in collaboration with ALECTIA A/S and the Danish Ministry of Science, Technology and Innovation.

References

[1] Zwicky F. Discovery, invention, research - through the morphological approach. Toronto: The Macmillan Company; 1969.

[2] Quanjel E, Zeiler W, Borsboom W, Spoorenberg, H. Integral design methodology for collaborative design of sustainable roofs. In: Proceedings of Passive and Low Energy Architecture: Geneva; 2006. p. 195-200.

Paper VI

Published in Proceedings of CLIMA, Helsinki, 2007

A method for evaluating the problem complex of choosing the ventilation system for a new building

Christian Anker Hviid[1] and Svend Svendsen[2]

[1]Birch & Krogboe A/S, Consulting Engineers, Denmark
[2]Dept. of Civil Engineering, Technical University of Denmark, Denmark

Corresponding email: crh@birch-krogboe.dk

SUMMARY

The application of a ventilation system in a new building is a multidimensional complex problem that involves both quantifiable and non-quantifiable data e.g. energy consumption, indoor environment, building integration and architectural expression. This paper presents a structured method for evaluating the performance of a ventilation system in the design process by treating quantifiable and non-quantifiable datasets together. The method is based on general morphological analysis and applies cross-consistency assessment to reduce the problem complex, thus treating the multi-dimensionality, the uncertainty and the subjectivity that arise in the design process on a sound methodological and scientific basis. Using a distance analysis of the shared values, the solution scenarios may be plotted relative to each other, which provides the designer with an illustrated 'space of solutions'. Herein the designer may view multiple ventilation solutions and navigate between them, evaluate the differences and choose the best ventilation system scenario in terms of energy consumption, indoor environment and architectural quality.

INTRODUCTION

Analysing problem complexes like choosing the ventilation system for a new building presents us with a number of methodological difficulties. The issue involves both quantifiable and non-quantifiable variables that are intercorrelated to some extent and perhaps incomplete, with missing or undetermined information due to the early stage in the design phase or simply the subjective nature of the judgements.
In this contribution, we use morphological analysis to decompose and structure the problem complex into both objective (technical) and subjective (architectural) variables while treating incomplete information in a structured manner. One of the advantages of morphological analysis is that such combinations are valid.
General morphological analysis was developed by Fritz Zwicky [1] and has been used for many purposes in relation with buildings e.g. for integral design methods [2] or to improve the comfort of various ventilation concepts [3]. Here we couple morphological analysis with cross-consistency assessment (CCA) [4] and multidimensional scaling (MDS) [5] to establish the feasible 'space of solutions' for various ventilation schemes within various building envelopes. This process is time-consuming, but we have automated it by implementing it in a simplified yet fully dynamic building simulation program: BuildingCalc [6] programmed in Matlab [7].
In the methods section we describe the requirements and general theory behind this approach and illustrate it with a limited example. Then we give the results obtained using this

methodology, and finally we discuss the design-stage significance of the method and results for both architects and engineers.

METHODS

The section contains a chronological description of the methodological approach beginning with the building requirements, the morphological analysis, the cross-consistency analysis, and the evaluation criteria and tools.

Requirements

The requirements for ventilation systems are specified in prEN15251 [8] and we use these to establish the initial design criteria for the ventilation system. In prEN15251 the ventilation and thermal comfort criteria are specified for different building types. The criteria are given as intervals in three categories I, II, and III for different building types. So the first thing we need is for the building owner to specify the use of the building, the desired category of indoor climate, the type of materials to establish the building pollution, and the overall placement of the building on the premises to establish external shadows and prevailing wind conditions. The example values are listed in Table 1.

Table 1. The overall requirements specified by the building owner. Data is obtained from prEN15251 [8] and Danish Building Regulations [9].

Building type	Indoor climate category	Building pollution (no smoking)	Total vent. rate [l/s/m^2]	Temp. range [°C]	Energy frame [kWh/m^2]	External shadows	Wind conditions
Single office 18m^2	I	very low (0.5 l/s/m^2)	1.5	21.0-25.5	95.5[1]	None	Good enough for nat. vent.

Morphological analysis

The background for general morphological analysis is to identify and investigate the total set of relationships or scenarios contained in a problem complex. The purpose is to structure *messes*, which are complex issues without well-defined form, into *problems* of unambiguous form and dimensions.
In this contribution, morphological analysis is used to generate a problem laboratory that enables us to decompose the problem complex into sets of functional subsystems. The decomposition is carried out hierarchically and continues until we arrive at simple building functional components each of which can be described with a single variable. There are no formal requirements that the variables are in the same unit; technical, aesthetical and architectural elements, known or hypothesised, can be treated together to create a space of solutions for the designers. Thus the method is flexible and fully scaleable.
The decomposed problem is put into a ‘box’, which is depicted as a chart in Table 3. The dimensions and variables are listed in the left-hand columns and the values are listed in rows. The combination of variables with arrays of values makes up the morphological box.

[1] With a heated floor area of 3000 m^2.

To start the morphological analysis we need to:

1. Identify the *aspects* of the problem complex. Aspects are also referred to as *dimensions* because they represent the sides in the n-dimensional morphological box. In Figure 1, comfort, energy and building characteristics, and aesthetics are chosen as the dimensions.
2. Each dimension is governed by a set of variables. E.g. comfort is achieved through fresh air supply and the ability to cool or heat when necessary (Figure 1).
3. Each variable may attain a well-defined range of values or conditions. In practice, the ranges are discretised on the basis of a user perception of low, medium and high values.[2] Thus uncertain or hypothesised values are represented on a backward-traceable methodological basis.

Table 3 illustrates the morphological chart. The imaginative values (high, medium, low) are exchanged with real numbers that the *user* regards as representing high, medium and low values. The chart does not encompass all the possible ventilation variables or dimensions and indeed has been reduced for the purpose of illustration and to reduce computation time. For example, the variables in Table 2 are fixed. The comfort systems each consist of two systems as is often the reality in real buildings. In the simulations the second system acts as backup if the first system is unable to meet the specified requirements.

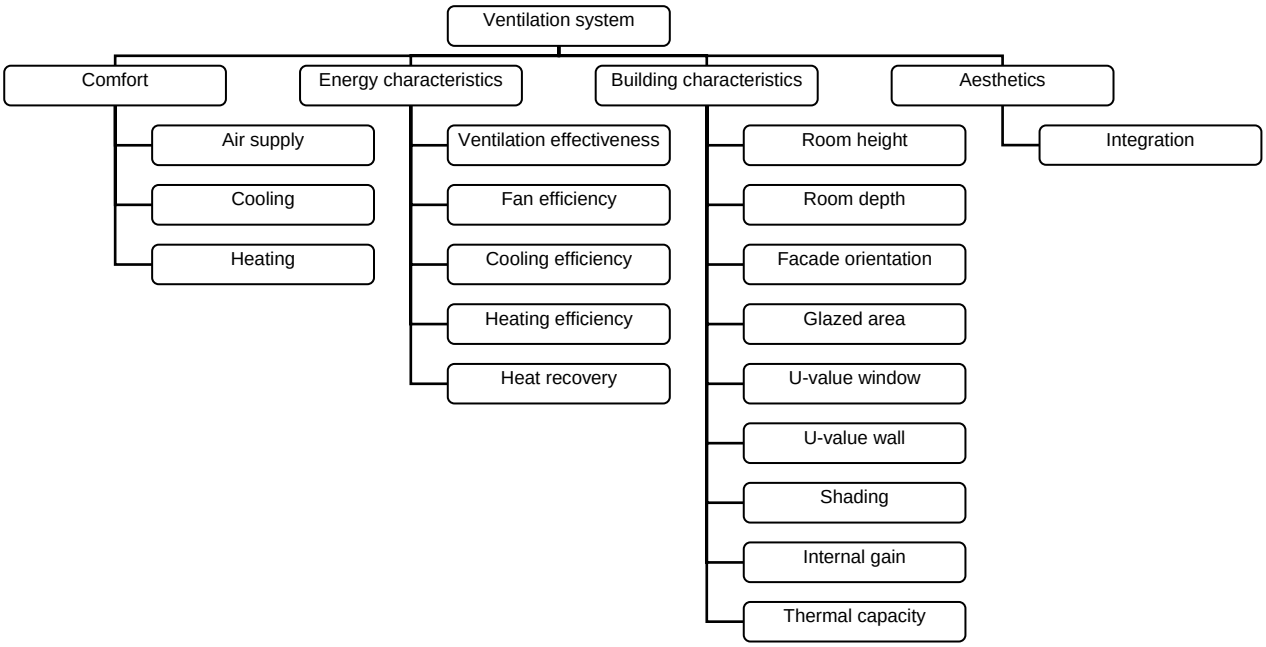

Figure 1. The problem complex decomposed into dimensions and variables.

Table 2. Fixed and excluded values from the morphological chart in Table 3.

Depth of room	Average U-value of window	Average U-value of wall	Façade length	Façade orientation	Min. shading factor
6 m	1.4 W/(m^{2}K)	0.15 W/(m^{2}K)	4 m	South	0.2

Four system/user profiles were specified: working hours, outside working hours, heating season and outside heating season.

[2] The exact number of discrete values is user-defined.

Table 3. Example of a morphological box for a ventilation system in a new building. The greyed-out areas represent the reduced problem which is used in CCA in Table 4.

Dimensions	**Variables**	**Values**			
Comfort systems	Ventilation 1 Supplied air* [l/s/m^2]	Natural **calculated**	Fan-assisted **1.5-3.0**	CAV **3.0**	VAV **1.5-7.5**
	Ventilation 2 Supplied air* [l/s/m^2]	Natural **calculated**	Fan-assisted **1.5-3.0**	CAV **3.0**	VAV **1.5-7.5**
	Cooling 1 Max cool. power [W]	Mech. increa-sed vent. rate **calculated**	Night cooling **calculated**	Cooling unit **10**	Chilled beams **30**
	Cooling 2 Max cool. power [W]	Mech. increa-sed vent. rate **calculated**	Night cooling **calculated**	Cooling unit **10**	Chilled beams **30**
	Heating 1 Max heat. power [W]	Radiator ∞	Heating coil **10**	Heat pump **10**	
	Heating 2 Max heat. power [W]	Radiator ∞	Heating coil **10**	Heat pump **10**	
Energy characteristics	Ventilation effectiveness [-]	Low **0.7** (natural)	Medium **0.9** (mixing)	High **1.3** (displacement)	
	Fan efficiency SFP** [kJ/m^3]	Low **0** (no fan)	Medium **1** (extract only)	High **2**	Very high **2.5**
	Cooling efficiency COP† [-]	Low **1** (cooling w/ outdoor air)	Medium **3**	High **4**	
	Heat recovery [%]	Low **0** (no heat req.)	Medium **65**	High **85**	
	Heating efficiency [-]	Medium **1** (water-based)	High **3** (heat pump, COP)		
Building characteristics	Room height [m]	Low **2.5**	Medium **3**	High **3.5**	
	Glazed area [%]	Low **25**	Medium **40**	High **60**	Very high **80**
	Internal gain [W/m^2]	Low **10**	Medium **25**	High **40**	
	Thermal capacity [kJ/(m^{2}K)]	Light **144**	Medium **288**	Heavy **432**	Very heavy **576**
Aesthetics	Integration of vent. system	Visible	Somewhat visible	Invisible	

* 'Supplied air' is the required minimum in accordance with prEN15251 during occupancy. Some of the systems (CAV, VAV) may be able to supply additional air (for cooling purposes). The user defines the desired ventilation ranges of the systems.

** SFP: annual average specific fan power – a measure of the efficiency of the ventilation fans and the pressure loss in the system.

† COP: annual average coefficient of performance – a measure of the efficiency of the cooling system.

Cross-consistency assessment

After the initial setup and definition of the dimensions of the problem, the user must apply cross-consistency assessment (CCA). This is to accomplish two things: eliminate the illogical or empirically unwanted scenarios and to detect *input garbage*. Input garbage consists of vaguely defined problems, terms or variables with no clear meaning or with more than one meaning, etc. If anything is insufficiently defined the user must go back to the morphological box and either refine or redefine the input.
Table 4 demonstrates the cross-consistency assessment derived from the morphological box in Table 3. All values are pairwise compared by the user for logical (denoted by L) or empirical (denoted by E) incompatibility. In the assessment, it is important to focus on each value pair to avoid biased judgments that unintentionally exclude value combinations that may be perfectly compatible but are incompatible normatively. In the assessment there is no reference to causality, but only to consistency and in general only strictly illogical combinations should be excluded.
If the intersection between two values is marked, all the scenarios containing the value couple are excluded from the simulation. Blank intersections are included.

Table 4. The CCA matrix from the morphological chart in Table 3. 'L' denotes logically incompatible value pairs, 'E' empirically unwanted value pairs.

		Vent1		Vent2		Cool1		Cool2		Heat1	Heat2	Effectiveness			SFP				COP			Heat rec.		Hieght		Glazed area			Internal gain			Capacity		
		Nat.	VAV	Nat	VAV	Increase	Night	CoolCoil	Beams	Raidtator	Raidtator	0.7 (nat.)	0.9 (mech. mix)	1.3 (displcment)	0 (÷fan)	1	2	2.5	1 (nat)	3	4	0 (none)	0.85	2.5	3	25	40	60	10	25	40	144	288	432
Vent2	Nat.																																
	VAV	E																															
Cool1	Increase	L		L																													
	Night																																
Cool2	CoolCoil	L		L																													
	Beams	L																															
Heat1	Radiat.																																
Heat2	Radiat.																																
Effectiv.	0.7		E		E	L		L																									
	0.9	L		L																													
	1.3	L		L																													
SFP	0 (÷fan)		L		L	L		L					L	L																			
	1	L		L								L																					
	2	L		L								L																					
	2.5	L		L								L																					
COP	1 (out.air)							L	L					E																			
	3					L	L																										
	4					L	L																										
Rec.	0 (none)		E		E								E	E																			
	85	L		L								L			L																		
Height	2.5	E		E								E																					
	3																																
Glaz.	25								E																								
	40																																
	60																																
Gain	10								E																								
	25																																
	40																																
Capac.	144	E		E			E					E							E														
	288																																
	432																																
Integrt	Visible		E		E								E	E																			
	Somewht																																
	Invisible	L	L	L	L				L			L	L	L																			

Examples of questions for assessing the CCA matrix:

- Is it possible to have a building scenario where a cooling coil in the second cooling system coexists with a night cooling system in the first cooling system? Clearly this is possible, so no marking is used.

- Is it possible to have an efficient heat recovery of 85% and a specific fan power of zero? This is illogical, so the pair is marked with an L.
- Is it possible to have a room height of 2.5 m together with a natural ventilation system? This is a possibility, but the literature states that natural ventilation is unsuitable for room heights below 2.7 m [10]. So an E is used because the user assesses that on an empirical basis this particular combination is undesirable.

Evaluation criteria

The morphological approach generates a large number of scenarios as depicted on Figure 2. We carry out the evaluation on the basis of total energy consumption, indoor climate (PPD-hours), and annual total cost. For electrical appliances a primary energy factor of 2.5 is used [9].
PPD-hours are calculated from the annual sum of hourly values of predicted percentage dissatisfied [11]. Local discomfort is not considered and relative humidity and air velocity is fixed at 50% and 0.15 m/s respectively. Nor do we consider the ventilation rate because we assume that the minimum ventilation requirements are always met.
Total cost is based on the sum of the annualised construction and annual running costs of the ventilation system.

Distance analysis

One of the most important goals in visualising data is to provide the viewer with a sense of the distance between the plotted points. While it is straightforward to plot scenarios based on two criteria, e.g. energy consumption and PPD-hours, the designer is not provided with the overall picture.
With more dimensions than 3, it is very difficult to visualise distances, unless the number of dimensions may be reduced to two or three. So a reduction in the number of dimensions is necessary. Non-metric multidimensional scaling (MDS) is a set of statistical methods for addressing this type of problem. The methods are available in a toolbox in Matlab and we use them to plot the selected scenarios relative to each other to obtain an instant sense of the distances between them. The inter-scenario distances are not Euclidean but the *configurational* or technical distances, or more precisely the pairwise dissimilarities between the scenarios. So a technical distance of 1 between two scenarios indicates that they have been produced from the same set of values except for one value that has been replaced by its horizontal neighbour in the morphological box.
It is evident that a certain amount of distortion has to be tolerated when a multidimensional dataset is reduced to two or three dimensions. In typical MDS applications, an investigation into the significance of the error can be conducted using Kruskal's normalized stress criterion (stress1) [12], in which values below 0.05 are good and values above 0.20 are poor. If the criterion is exceeded, the user must reduce the number of selected scenarios or raise the number of depicted dimensions from two to three.

RESULTS

In this section we show the results of the method. The initial requirements established by the fictive building owner are shown in Table 1 and the simulation took approximately 80

minutes on a laptop with a Pentium M processor running at 1.86 GHz and with 1 GB of RAM.[3]

In Figure 2, all the scenarios derived from Table 3 and Table 4 have been simulated and depicted with respect to energy consumption and PPD-hours. With the BuildingCalc tool it is possible to pick the most interesting scenarios, typically with respect to low energy consumption and low PPD-hours. Figure 3 depicts the predominant value settings of 30 selected scenarios. With the predominant values as starting points, it is possible to reformulate the morphological box and repeat the simulation with refined values.

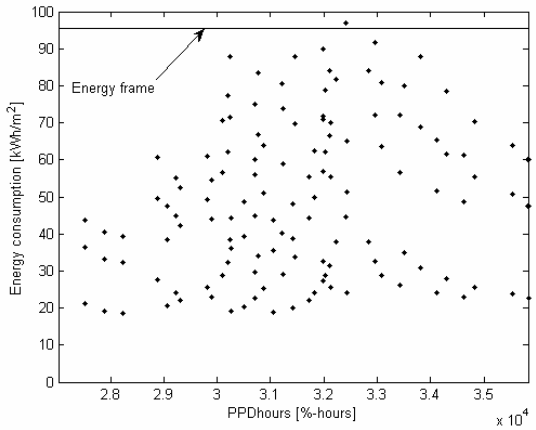

Figure 2. The distribution of ventilation scenarios produced via the morphological box.

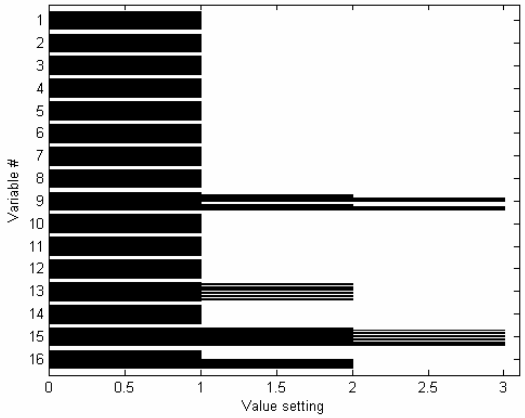

Figure 3. Predominant values for the 30 selected scenarios. The variables are numbered consecutively as in Table 3.

In Figure 4 we establish a linear correlation between bubble size and total costs, and use the MDS method to plot the selected scenarios relative to each other. We can navigate between them and explore their dissimilarities simply by clicking on the bubbles with the mouse.

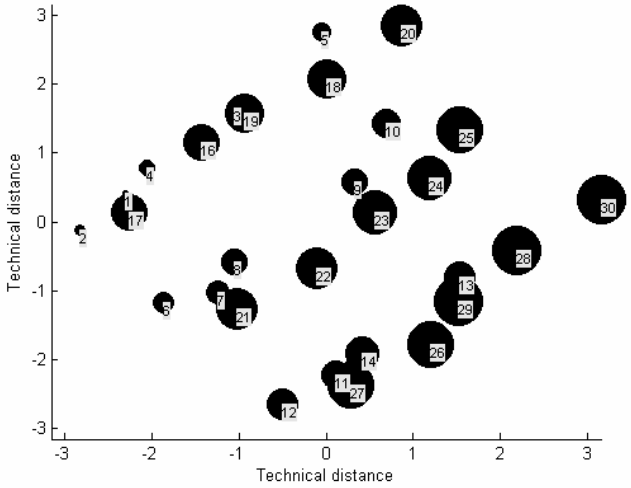

Figure 4. The relative technical distance between the 30 selected scenarios. Large bubbles have lower total costs than small ones. The stress1-value is 0.12.

The distances between the bubble centroids are expressed in terms of 'technical distance'. Where two bubbles are closely spaced, this represents two ventilation scenarios that are very similar to one another. The MDS method visualises the morphological chart for the engineer

[3] Only a portion of the total number of scenarios required lengthy thermal simulation time.

and he is able to distinguish between multiple scenarios because their visual distance is a measure of their dissimilarity. So Figure 4 illustrates a space of solutions, where it is clear that scenario 22 is better than 7, if 21 is not entirely acceptable to the engineer or the architect.

DISCUSSION

The method described in this paper offers the possibility of deep insight into the problem complex involved in choosing a ventilation system for a new building. The morphological approach exempts the engineer from generating biased scenarios, and by coupling the morphological analysis with cross-consistency assessment we ensure that the subsystems are unambiguously defined. The approach does require a certain amount of skill and practice to be able to setup the morphological box, cross-assess and iterate, but the procedure in itself helps keep out garbage input and decompose the problem complex correctly.
The evaluation criteria are here chosen to be total cost, energy and thermal comfort in terms of PPD as we believe they address a broad range of interests from the building owner, the engineer and the architect. However the indoor air quality, apart from what is initially speficied by the building owner, is not considered.
The MDS method has several limitations e.g. the distortion of the solution increases with more scenarios and the information contained in the distance plot depends on the variable resolution; too few attainable values for each variable increases the risk of large unanticipated 'jumps' between the scenarios. But the MDS method provides an excellent visualisation and overview of feasible scenarios for engineers and architects to discuss in the design phase and the overall methodological approach has the great advantage that a natural pressure is exerted on engineers and architects to produce buildings that perform better because 'unusual' scenarios are considered.

REFERENCES

1. Zwicky, F., 1969. Discovery, invention, research - through the morphological approach, The Macmillan Company, Toronto, Canada.
2. Quanjel, E., Zeiler, W., Borsboom, W., Spoorenberg, H. 2006. Integral design methodology for collaborative design of sustainable roofs. Proceedings of Passive and Low Energy Architecture, PLEA2006, pp 195-200.
3. Zeiler, W., Savanovic, P., Borsboom, W. 2006. Integral design workshop for sustainable comfort systems to improve ventilation concepts. Proceedings of Healthy Buildings, pp 131-136.
4. Ritchey, T. 2006. Problem structuring using computer-aided morphological analysis. Journal of the Operational Research Society. Vol. 57 (7), pp 792-801.
5. Cox, T., Cox, M., 1994. Multidimensional scaling, Chapman & Hall, London.
6. Nielsen, T.R. 2005. Simple tool to evaluate energy demand and indoor environment in the early stages of building design. Solar Energy. Vol. 78 (1), pp 73-83.
7. The Mathworks Inc., Natick, USA.
8. prEN 15251 DRAFT. 2005. Criteria for the Indoor Environment including thermal, indoor air quality, light and noise. European Standard, European Committee for Standardization, Brussels.
9. Danish Building Regulations 2007, National Standard, National Agency for Enterprise and Construction, Denmark
10. Andersen, K.T., Heiselberg, P., Aggerholm, S., 2002. Naturlig ventilation i erhvervsbygninger - Beregning og dimensionering, By og Byg anvisning 202, Hørsholm, Denmark.
11. Fanger, P.O. 1970. Thermal comfort. Danish Technical Press, Copenhagen, Denmark.
12. Kruskal, J. 1964. Multidimensional scaling by optimizing goodness of fit to a nonmetric hypothesis. Psychometrika. Vol. 29, pp 1-27.

Paper VII

Published in Proceedings of Nordic Symposium on Building Physics, Copenhagen, 2008

Simple tool to evaluate the impact of daylight on building energy consumption

Christian Anker Hviid, Indutrial Ph.D. student,
Alectia A/S;
crh@alectia.com

Toke Rammer Nielsen, Assoc. prof.,
Depatment of Civil Engineering, Technical University of Denmark;
trn@byg.dtu.dk

Svend Svendsen, Professor,
Department of Civil Engineering, Technical University of Denmark;
ss@byg.dtu.dk

KEYWORDS: Simulation, daylight, validation, radiosity, integration, building design

SUMMARY:
This paper presents a simple building simulation tool for integrated daylight and thermal analysis. The tool is capable of importing the thermal and visual properties for different glazings and shading positions from the Window Information System (WIS) program. Radiosity methodology is used to derive the daylight levels for different sky conditions on an hourly basis. The daylight levels are fed into an existing simple thermal simulation program capable of calculating energy demand and the indoor environment. Straightforward control systems for general and task lighting systems have been implemented together with a shading control strategy that adjusts the shading according to the indoor operative temperature and the profile angle of the sun. The implemented daylight calculation method allows for shades from the window recess and overhang. Comparisons with the ray-tracing program Radiance show that the accuracy of this approach is adequate for predicting the energy implications of photoresponsive lighting control.

1. Introduction

For integrated daylight and thermal simulations several approaches and programs have been developed. One approach which is implemented in the program Adeline (Fraunhofer-Institut für Bauphysik 2006) generates an annual output file for lighting which may be used as an internal load file in a thermal simulation program. However, this method lacks interactivity between daylight, lighting, solar shading and the thermal performance of the building. Another approach is to use Radiance (Ward, G.L. and Shakespeare, R.A. 1998) in combination with a thermal simulation program. This approach has been implemented in ESP-r (Clarke, J. and Janak, M. 1998). Generally lighting simulation packages involve a lengthy learning effort, which restricts their use to expert designers, and they are computationally costly for general architectural and engineering purposes, especially during the initial design stage. In order to reduce the computational burden the daylight coefficient method has been suggested as a third approach (Tregenza,P.R. and Waters, I.M. 1983; Reinhart, C.F. and Herkel, S. 2000).

The tool described in this article encompasses an integrated thermal and lighting simulation approach for evaluating the impact of daylight and dynamic shading device design on energy demand. The amount of input is small yet it provides detailed hourly output of the daylight level, the electrical energy consumption for lighting, heating load, cooling load and indoor operative temperature. An existing simplified thermal simulation tool BuildingCalc (Nielsen, T.R. 2005) and a daylight simulation tool LightCalc (Nielsen, T. 2005) formed the starting point for the work.

2. Calculation procedures

There are several different methods and tools for determining daylight distribution in rooms. Methods vary from simple factor calculations through radiosity methods to complex computer algorithms, such as ray-tracing. In this tool, the radiosity method is employed for internal daylight reflections, while the incident initial light is calculated using a ray-tracing approach. This gives a reasonable balance between accuracy and calculation time.

2.1 External light distribution

External daylight may be divided into direct light from the solar disc, diffuse light due to the scattering properties of the atmosphere, and diffuse light reflected from the ground and surroundings. The diffuse light is modelled using the approach in Robinson and Stone (2006) and summarized here. An upper sky dome for atmospheric light and a lower (inverted) sky dome for ground reflections (one above and one below the horizontal plane) are used to model diffuse light. Each sky vault is divided into 145 patches using a discretization scheme proposed by Tregenza (1987). Each patch subtends a similar solid angle Φ (Sr), which enables every patch to be treated as a point source with insignificant error. The sky vault is divided into seven azimuthal bands of equal angular height ($\sin \gamma_{i,max}$ -$\sin \gamma_{i,min}$), in which the azimuthal range $\Delta\alpha$ increases towards zenith (12°, 12°, 15°, 15°, 20°, 30°, 60°).

$$\Phi_i = \Delta\alpha_i \left(\sin \gamma_{i,\max} - \sin \gamma_{i,\min}\right) \tag{1}$$

Let L denote the luminance (Lm m^{-2} Sr^{-1}) of the i'th patch, ξ the mean angle of incidence (rad), and σ ($0 \le \sigma \le 1$) the visible proportion of the patch, then the illuminance E_{sky} on an external plane due to diffuse light from the sky vault is expressed as:

$$E_{sky} = \sum_{i=1}^{145} \left(L \Phi \sigma \cos \xi\right)_i \tag{2}$$

Let E_n denote the direct normal illuminance and ξ the incidence angle (solar zenith angle), then the illuminance on an external inclined plane due to direct light E_{sun} is expressed (Scharmer, K. and Greif, J. (2000):

$$E_{sun} = E_n \cos \xi \tag{3}$$

Having determined the light sources, the reflecting ground can be represented as a luminous up-side down sky with constant brightness. Given the ground patch luminance L^*, the illuminance due to reflected light E_{ground} is written as:

$$E_{ground} = \sum_{j=i}^{145} \left(L^* \Phi \sigma \cos \xi\right)_j \tag{4}$$

where L^* is expressed as a function of the total horizontal diffuse illuminance E_{sky}, the direct illuminance E_{sun} on a horizontal plane and the mean ground reflectance ρ (albedo):

$$L^* = \frac{\rho}{\pi}\left(E_{sun} + E_{sky}\right) \tag{5}$$

The Perez anisotropic sky model (Perez et al. 1993) is amenable to implementation in a computer program while maintaining good overall performance. The luminance of a sky point L_i is given here:

$$L_i = \frac{lv_i dh}{\sum_{j=1}^{145} \left(lv \Phi \cos \xi\right)_j} \tag{6}$$

where the relative luminance lv is normalized to diffuse horizontal illuminance dh as recommended by Perez et al. (1993). Diffuse horizontal and direct normal illuminances are obtained from measured horizontal and direct normal irradiances respectively by a luminous efficacy η given in Perez et al. (1990).

The visible proportion σ is calculated by establishing a 10x10 grid of each patch and evaluating the visibility of each grid point for all internal surfaces. Thus σ is a function of both distant objects (other buildings, the landscape) and near shades like the window recess and overhang. Reflected light from opposing building façades is not yet treated.

2.2 Internal daylight distribution

The calculation of the internal distribution of light is based on the luminous exitance method. This method is analogous to the radiosity method, in that all the restrictions and assumptions are the same. Internal subsurfaces hit by transmitted direct and diffuse light act as light sources, with the initial exitance *Mo,* if we assume these

surfaces have Lambertian optical characteristics and reflect incident light perfectly diffusively and ignore any specular properties. The methodology and implementation of the daylight distribution algorithms are described in detail by Park (2003).

2.3 Coupling of external and internal light distribution

To establish the initial light exitance *Mo* of a subsurface the amount and the direction of the light and the reflectance of the surface has to be known. Therefore the external and internal light distributions is coupled in a simple ray-tracing approach that assumes the luminance of the sky hemisphere and ground hemisphere patches can be considered as point sources.

2.3.1 Diffuse light

For diffuse sky and ground light penetrating into the room, the exitance for each internal subsurface is calculated using eq. (2) and eq. (4) multiplied by the profile-angle dependent light transmittance τ_θ and the surface reflectance ρ:

$$Mo_i = \rho\left(\sum_{i=1}^{145}\left(L\Phi\sigma\cos\xi\tau_\theta\right)_i + \sum_{j=1}^{145}\left(L^*\Phi\sigma\cos\xi\tau_\theta\right)_j\right) \tag{7}$$

The profile angle θ is defined as the line of elevation projected unto the vertical normal plane of a surface. We may also name it the perpendicular incidence angle on a vertical surface. The profile-angle dependent light transmittance is used because it is calculated directly by the WIS program (van Dijk, D. and Oversloot, H. 2003), see section 2.4. However for clear glazings with isotropic optical properties we use the profile-angle dependent data directly as dependent on incidence angle.

2.3.2 Direct light

For direct light a different approach is applied. It is evident that all direct light transmitted through the glazing hits a subsurface. Subdividing the internal surfaces, however, may result in false prediction of the amount of incoming direct light. Let E_{dir} denote the incident sun light on the window plane obtained by eq. (3), A_g the glazing area, A_j the area of the *j*'th internal subsurface and *m* the total number of internal subsurfaces. If we define a normalization factor $\chi = E_{dir}A_g\tau_\theta \Big/ \sum_{j=1}^{m} E_n A_j \tau_\theta \cos\xi_j$ then the initial exitance *Mo* of the *i*'th subsurface is written:

$$Mo_i = E_n\rho_i\tau_\theta\cos\xi_i\,\chi = E_{dir}A_g\rho_i\tau_\theta\frac{\cos\xi_i}{\sum_{j=i}^{m}A_j\cos\xi_j} \tag{8}$$

When the direct light is transmitted through the glazing, some of the direct light may be transformed into diffuse light in a diffusing device, e.g. blinds placed in conjunction with the glazing. This effect is taken into consideration by calculating the light contribution from sun, sky, and ground on the window plane by using eq. (2), (3), and (4). The exitance of the inner glazing surface Mo_g is determined by multiplying the total light contribution with the light transmittance for direct light that is diffused when it passes the glazing/shading system: $\tau_{dir\rightarrow dif}$. This light transmittance is calculated by WIS, see section 2.4.

$$Mo_g = \left(E_{sun} + E_{sky} + E_{ground}\right)\tau_{dir->dif} \tag{9}$$

Devices that redirect the incoming light, e.g. a specular light shelve are modelled using a simple implementation. It is achieved by setting a special redirecting light transmittance τ_{redir} to a value between 0 and 1 where 0 means that no light is redirected and 1 that all incoming light is redirected. This means that for an incoming ray of light with a given profile angle θ the following applies: $\tau_\theta + \tau_{dir\rightarrow dif,\theta} + \tau_{redir,\theta} = 1$ (FIG. 1). The inclination angle β of the slat or light shelve determines the reflection angle. Only fully specular devices are considered and any specular interreflections between slats and between slats and glazing are ignored.

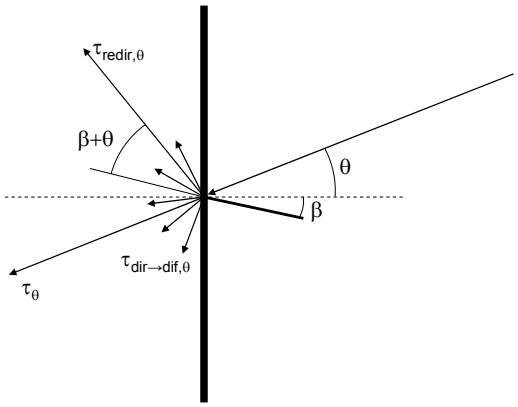

FIG. 1. Illustration of how an incoming ray of light from the sky, sun or ground is transmitted directly, diffused in the combined glazing and shading, or redirected specularly with equal inbound and outbound angle.

2.4 Light transmittances

A critical element in the daylight calculation routine is the light transmittance of the combined glazing/shading system. For this purpose the European software tool called WIS (van Dijk, D. and Oversloot, H. 2003) is used. This tool implements algorithms from the ISO standard 15099 (ISO 15099 2003) capable of calculating the light transmittance of a transparent system for both direct and diffuse light.

WIS calculates the thermal and solar performance of multilayered window systems, allowing the user unlimited combinations of glazing and solar shading devices. This makes WIS a very powerful tool for evaluating various integrated daylight designs. Currently the improvement and verification of WIS, and its database format and database population are the responsibility of the EU Thematic Network WinDat, which consists of major European research institutions and manufacturers of window components.

The output from a WIS calculation may be in the format of a text file. The file includes the light transmittances and solar energy transmittances for different solar profile angles (-90° to 90° at 10° increments), and may be loaded seamlessly into the tool described in this article. If the shading device has multiple shading positions, e.g. Venetian blinds, the user may generate and load files for every position required. The tool will linearly interpolate between the transmittance data loaded, thus making the number of loaded positions a question of desired accuracy.

Because the employed method of calculating incident light on internal subsurfaces is equivalent to a ray-tracing technique, the WIS transmittance for direct light is employed for both diffuse and direct light. WIS cannot yet handle specular shading devices, e.g. light shelves or light redirecting devices.

3. CONTROL STRATEGIES

3.1 Thermal simulation

The simplified thermal model is described in detail in Nielsen (2005). It is capable of evaluating the thermal indoor environment and heating and cooling loads in a building with very few input parameters while providing the option of sophisticated controls.

3.2 Electrical lighting

The electrical lighting system can be divided into general and task lighting. Both systems are defined by the power consumption of the lighting fixtures in W/m^2 when providing an illuminance of 100 lux, and the minimum (standby) power consumption. The linear relationship is shown on FIG. 2. The values for power density and corresponding illuminance are often supplied by the producers of lighting fixtures, and the maximum illuminance is calculated using the maximum power density.

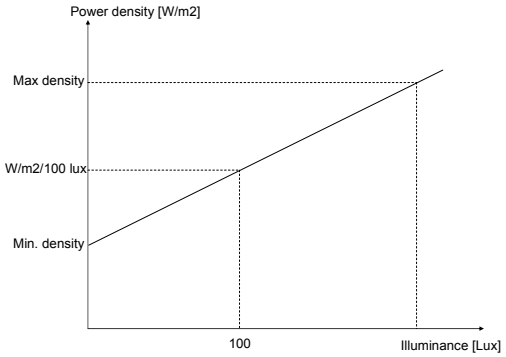

FIG. 2. Definition of illuminance and power density relationship for lighting systems in the tool.

Both systems can be defined and controlled separately with respect to daylight in two arbitrary points within the simulated enclosure. The possible control strategies are 'always max', 'always min', 'on-off', and 'continuous'. The hourly incoming daylight in the point is evaluated and the electrical lighting is switched on/off or dimmed according to the chosen control strategy. The 'on-off' control switches between the maximum and minimum power consumption when the daylight level is below or above the illuminance setpoint. The 'continuous' control interpolates linearly between the maximum and minimum power consumption in order to meet the specified setpoint. Electrical losses in the ballasts must be included in the power density.

3.3 Shading

The indoor air temperature controls the systems including the shading. This means that shading is activated only when excess heat gains occur, thus ignoring the risk of glare for the time being. In the case of screens or similar, the controls are limited to screen up or screen down.

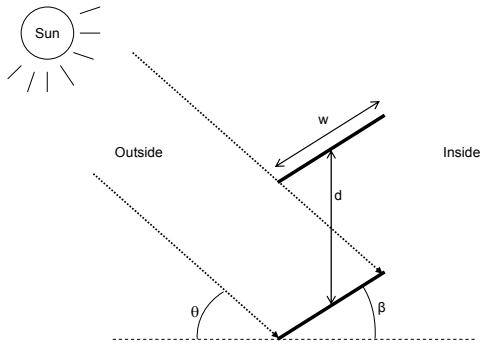

FIG. 3. Illustration of the cut-off shading control strategy for adjustable slats.

In the case of adjustable slats or similar the shading is lowered and adjusted to 'cut-off' angle when the indoor air temperature exceeds the specified cooling setpoint. Let d denote the distance between two slats (m), θ the profile angle of the sun (degrees), and w the width of the slats (m), then the cut-off angle is calculated:

$$\beta_{cut\,off} = \arcsin\left(\frac{d\cos\theta}{w}\right) - \theta \tag{10}$$

3.4 Thermal simulation coupling

It requires a sophisticated coupling to calculate the incoming daylight, the effect of shading on daylight levels, and thus electrical lighting consumption and indoor air temperature. This is achieved by pre-calculating the hourly daylight levels in the room *without* shading, initiate the thermal simulation, evaluate the hourly indoor operative temperature with respect to the cooling setpoint, possibly lower the shading and adjust the slat angle (for blinds) to cut off direct sunlight, and calculate the daylight levels again. If the operative temperature still exceeds the cooling setpoint, venting, increased ventilation, and mechanical cooling are employed in that order. The daylight levels are evaluated at two arbitrary points specified by the user.

4. Validation

Of the numerous lighting simulation programs available, Radiance has been extensively validated and repeatedly surpassed competing programs in terms of both functionality and accuracy. For these reasons, we chose Radiance as our reference model. The validation of the daylight calculation algorithm is carried out for a single office room as depicted on FIG. 4. Three different setups are carried out for a clear glazing, external blinds adjusted to cut-off angle and an external screen. The property data is listed in TABLE. 1

TABLE. 1: Input data for validation.

Properties	WIS Code	Property	Value [-]	Remarks
Glazing	4-15Ar-SN4	Light transmittance	0.782	Double glazing w/ lowE coating
Blinds	Windat #01	Diffuse reflectance	0.096	Slat width: 0.08m, slat distance: 0.072m
Screen	Verosol Silverscreen	Light transmittance	0.035	Total transmittance for screen+glazing

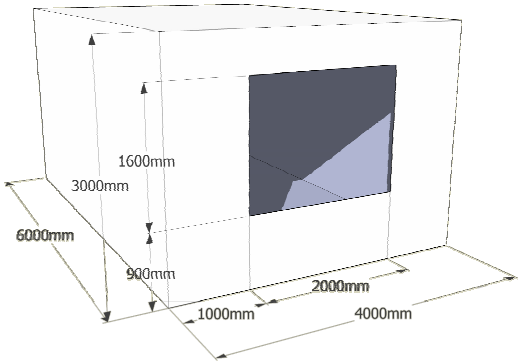

FIG. 4. Room dimensions for validation.

The chosen validation date is the 21st of September at 3 p.m. because it involves complex calculation of solar position, incidence angles and cut-off angle. The radiation data is from the Danish Design Reference Year and the measurements are performed at desktop height 0.85m in interval points along the centre line of room.

FIG. 5 to FIG. 7 compares the illuminance levels computed by Radiance and by the simple tool. The relative error is within ±20% for the clear glazing and for the blinds which is considered satisfactory in daylight research. However the largest discrepancy is for the screen, but this is due to two facts: the light transmittances from WIS are unidirectional but screens have bidirectional properties and the screen is defined in Radiance as a glazing with reduced transmittance ignoring the diffusing properties of the real screen.

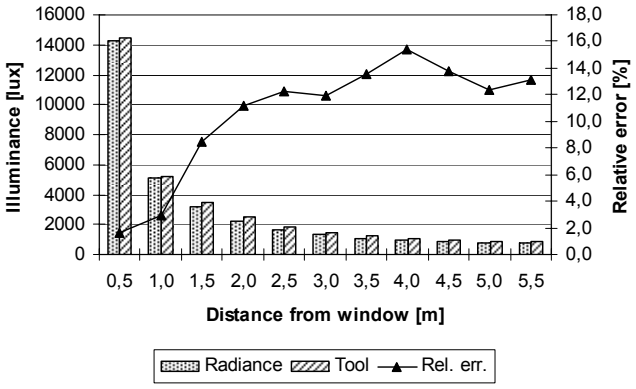

FIG. 5. Clear glazing. Absolute illuminance levels and relative error.

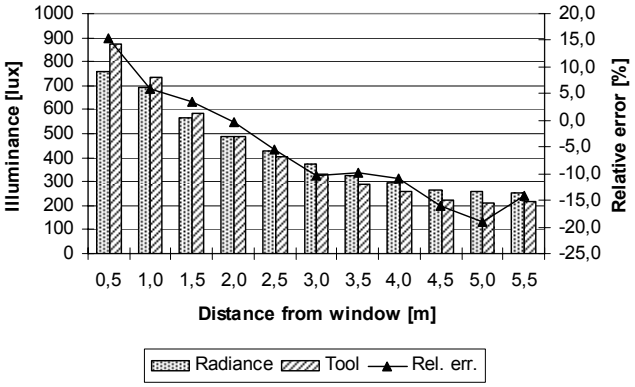

FIG. 6. External blinds at cut-off angle. Absolute illuminance levels and relative error.

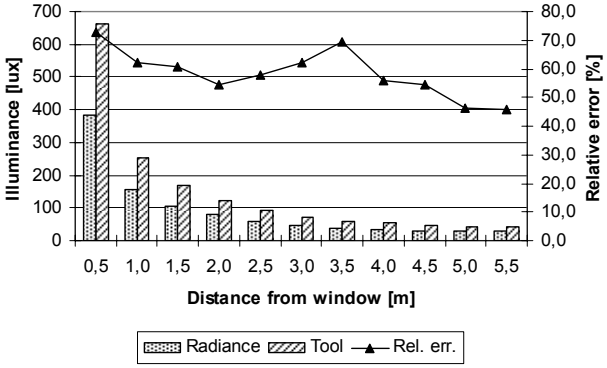

FIG. 7. External screen. Absolute illuminance levels and relative error.

5. Combined simulation

FIG. 8 depicts the implications of daylight responsive lighting systems. The artificial lighting system adjusts continuously with respect to the incoming daylight complementing the illuminance deficit. If overheating occurs the shading device is activated and the effect on daylight, casual gain and the thermal balance is quantified. Consequently the tool aids in producing daylight friendly design and quantifies the effect of 'smart' solar shadings that allows the maximum amount of direct sunlight to be tranferred diffusively in order to save electrical energy.

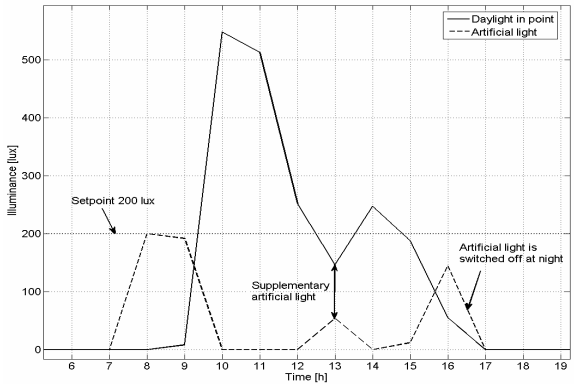

FIG. 8. Daylight and artificial light in a point. Continuous dimming control of the lighting system.

6. Conclusion

The tool described here is developed to evaluate the impact of incoming daylight on the energy consumption for lighting. The tool calculates the daylight distribution on the basis of a ray-tracing approach and the radiosity

method to enhance accuracy while maintaining calculation speed. The sky is divided into patches with individual luminances in order to imitate the energy distribution of the real sky. Rays are traced from each individual sky patch to the surfaces of the room through glazing and shading giving the initial input to the radiosity algorithm which is employed for internal light distribution. Window overhang and recess as well as distant objects like other buildings reduce the visible proportion of the sky.

The daylight distribution is calculated every hour, thus providing the information necessary for the thermal program to control the photoresponsive lighting and to calculate the heat load of the electrical lighting system. The daylight and thermal simulations are integrated meaning that the indoor temperature is recalculated if overheating has caused the shading to be activated.

The daylight algorithms were validated by comparison with the state-of-the-art ray-tracing program, Radiance, using the Perez anisotropic sky. The results show agreement within 20 % relative error, thus the simplified tool is adequate for predicting the electrical energy consumption of photoresponsive lighting systems, including the impact of complex shading systems such as external Venetian blinds.

7. References

Clarke, J. and Janak, M. (1998). Simulating the thermal effects of daylight-controlled lighting. *Proceedings of Building Performance (BEPAC UK)*, Issue 1.

Fraunhofer-Institut für Bauphysik, 2006. ADELINE 3.0, Abteilung Wärmetechnik, Stuttgart, Germany. Available from: http://www.ibp.fhg.de/wt/adeline/

ISO 15099 (2003). ISO 15099:2003 Thermal performance of windows, doors and shading devices – Detailed calculations, International Organization for Standardization, Geneva, Switzerland.

Nielsen T.R. (2005a). Simple tool to evaluate energy demand and indoor environment in the early stages of building design, *Solar Energy*, Vol. 78, No. 1, 73-83.

Nielsen, T., Nielsen, T. R. and Svendsen, S. (2005b). Calculation of daylight distribution and utilization in rooms with solar shadings and light redirecting devices. *Proceedings of 7th Symposium on Building Physics in the Nordic Countries*, 1011-1018.

Park K.-W. and Athienitis A.K. (2003). Workplane illuminance prediction method for daylighting control systems, *Solar Energy*, Vol. 75, No. 4, 277-284.

Perez R., Ineichen P., Seals R., Michalsky J. and Stewart R. (1990). Modeling daylight availability and irradiance components from direct and global irradiance, *Solar Energy*, Vol. 44, No. 5, 271-289.

Perez R., Seals R. and Michalsky J. (1993). All-weather model for sky luminance distribution - preliminary configuration and validation, *Solar Energy*, Vol. 50, No. 3, 235-245.

Reinhart C.F. and Herkel S. (2000). The simulation of annual daylight illuminance distributions - a state-of-the-art comparison of six RADIANCE-based methods, *Energy and Buildings*, Vol. 32, No. 2, 167-187.

Robinson D. and Stone A. (2006). Internal illumination prediction based on a simplified radiosity algorithm, *Solar Energy*, Vol. 80, No. 3, 260-267.

Scharmer, K. and Greif, J. (2000). The European Solar Radiation Atlas. École des Mines de Paris, France.

Tregenza P.R. (1987). Subdivision of the sky hemisphere for luminance measurements, *Lighting Research & Technology*, Vol. 19, No. 1, 13-14.

Tregenza P.R. and Waters I.M. (1983). Daylight coefficients, *Lighting Research & Technology*, Vol. 15, No. 2, 65-71.

van Dijk, D. and Oversloot, H. (2003). WIS, the European tool to calculate thermal and solar properties of windows and window components. *Proceedings of IBPSA, Building Simulation*, Vol. 1, 259-266.

Ward, G. L. and Shakespeare, R. A. (1998). Rendering with Radiance - The art and science of lighting visualization. Morgan Kaufmann, San Francisco.

Paper VIII

Published in Proceedings of International Conference on Air Infiltration and Ventilation (AIVC), Kyoto, 2008

Passive ventilation systems with heat recovery and night cooling

C.A. Hviid
Alectia A/S, Teknikerbyen 34, DK-2830 Virum, Denmark
S. Svendsen
Technical University of Denmark
Department of Civil Engineering, Brovej bygn. 118, DK-2800 Lyngby

ABSTRACT

In building design the requirements for energy consumption for ventilation, heating and cooling and the requirements for increasingly better indoor climate are two opposing factors. This paper presents the schematic layout and simulation results of an innovative multifunctional ventilation concept with little energy consumption and with satisfying indoor climate. The concept is based on using passive measures like stack and wind driven ventilation, effective night cooling and low pressure loss heat recovery using two fluid coupled water-to-air heat exchangers developed at the Technical University of Denmark. Through building integration in high performance offices the system is optimized to incorporate multiple functions like heating, cooling and ventilation, thus saving the expenses of separate cooling and heating systems. The simulation results are derived using the state-of-the-art building simulation program ESP-r to model the heat and air flows and the results show the feasibility of the proposed ventilation concept in terms of low energy consumption and good indoor climate.

1. INTRODUCTION

Several investigations document the effect of indoor climate on the performance of office workers (Seppänen et al., 2006). Other investigations show that the productivity increase of an improved ventilation system with higher air change and better temperature control is significantly larger than the total costs of the ventilation system (Wargocki and Djukanovic, 2005)

While the ventilation technologies are always improved energy-wise and efficiency-wise it is not possible to meet tomorrows demand of better indoor climate while cutting energy consumption as demanded by the Kyoto-protocol. This leads to a widening gap between the required reduction in the use of fossil fuels and the demand for improved indoor climate. One solution is to shift the ventilation use from active (mechanical) to passive ventilation systems. Passive in this context means ventilation solutions that exploit natural driving forces and the building envelope physics to establish and maintain a satisfying indoor climate without the consumption of electrical energy. The concept has particular potential in temperate climates with moderate wind velocities and large daily temperature differences (Kolokotroni and Aronis, 1999; Olsen and Chen, 2003). In order for a passive ventilation system to be competitive efficient heat recovery is essential. A master thesis by Anderson and Vendelboe (2007) performed at the Technical University of Denmark tests a prototype of a heat exchanger suitable for passive systems.

This paper describes and simulates a proposed passive ventilation system with equal performance – in terms of indoor climate – to conventional mechanical ventilation and cooling system while saving significant amounts of energy.

2. PASSIVE VENTILATION DESIGN

The proposed passive ventilation systems have been developed with several performance parameters in mind:

- Low energy consumption
- Equal indoor climate quality compared to mechanical ventilation
- Low total costs
- Flexible solution
- Does not occupy more space than a conventional mechanical ventilation system

In order to meet these demands we propose a ventilation system with intake at ground level and exhaust above the roof. The duct system consists of large main ducts for intake and exhaust. Via a diverging duct smaller supply ducts feed fresh air to the work-spaces that are situated vertically above each intake. Exhaust ducts from each work-space extracts the stale air and via a converging duct and a large main duct is exhausted to the outside. Figure 1 shows the schematic layout of the proposed system.

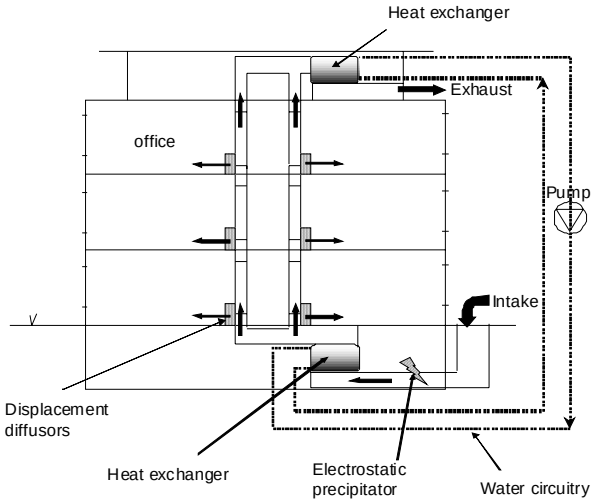

Figure 1: Cross-section of a building with a passive ventilation system.

There are several advantages to this duct layout:

- Vertical supply and exhaust ducts enhances the stack effect
- Intake and exhaust are placed where the prevailing wind pressures are – respectively – positive and negative. This enhances the effect of wind
- Central intake and exhaust is required for heat recovery and filtering capabilities. Filtering is done by an electrostatic precipitator in the supply air with very low pressure loss, high efficiency and low energy consumption
- Duct sizing and not presssure-loss inducing dampers ensures equal ventilation rates to all rooms
- Evenly distributed intakes and exhausts along the building maintains the flexibility of the building
- Duct layout is simple, requiring more floor area but saving space above acoustic ceilings

3. SIMULATION SETUP

The passive ventilation system is simulated using the state-of-the-art building simulation program ESP-r from University of Strathclyde, Glasgow, Scotland, (ESP-r, 2008). ESP-r is a unix-based program and as such we have been running ESP-r under the Linux emulator Cygwin. Cygwin enables the user to run unix-based software in a Linux environment on a Microsoft Windows computer. ESP-r is chosen because it is continuously developing and has a comprehensive validation history. The employed version of ESP-r is 11.5.

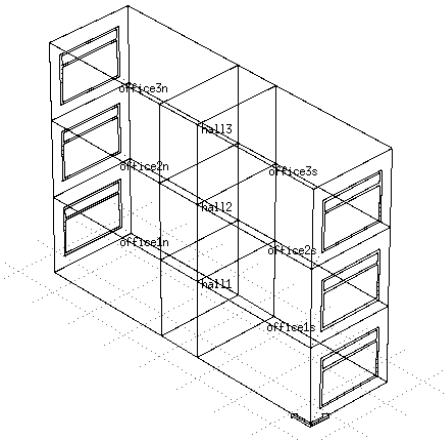

Figure 2: Cross-section of simulated building.

3.1 Dimensions, layout

The simulated part is a cross section of a long flat-roofed building with rectangular 2:1 footprint.
In order to evaluate the proposed system we establish a reference based on a cross section of a three-storey office building as shown on Figure 1. The cross section comprises six single offices with connecting hallways. The basement which contains the ventilation system intake is not shown.
The façades are oriented towards North and South because these orientations represent worst-case with regard to ventilation and night cooling efficiency.

3.2 Constructions

Table 1 contains descriptions of the constructions with the calculated heat transfer coefficients.

Table 1: Constructional details from outside to inside with heat transfer coefficients.

	Materials	U-value W/m²K
Façade	Brick 100 mm Mineral fibre 200 mm Breeze block 100 mm	0.18
Roof	Roofing felt 12 mm Mineral fibre 300 mm Concrete 200 mm Air 100 mm Gypboard 13 mm	0.12
Decks	Flooring 13 mm Cement screed 10 mm Concrete 150 mm Air 100 mm Gypboard 13 mm	-
Ground	Gravel 150 mm EPS 300 mm Concrete 150 mm Cement screed 10 mm Air 50 mm Flooring 12 mm	0.09
Internal partitions	Gypsum 13 mm Mineral fibre 100 mm Gypsum 13 mm	-
Window	Wooden frame 4-15Ar-SN4 Frame part: 19%	1.2 g-value: 0.51

Transparent area of the façade: 40%.

3.3 Internal load

Table 2 specifies the internal loads during working hours and outside working hours. The periods are constant through the year and weekends are considered outside working hours. The lighting load is also applied in the hallways.

Table 2: Internal loads in offices.

	Hours		W/m²	
	Work hours	Outside work h.	Work hours	Outside work h.
People	8-17	17-8	5	0
Lighting	8-17	17-8	7	0.7
Equipm.	8-17	17-8	4	0.4

3.4 Solar shading

The predefined constructions in ESP-r are not suitable for high-performance offices in temperate climates. For this reason we use WIS (van Dijk and Oversloot, 2003) to construct a new double glazing with retractable blinds. The thermal and angular optical properties are added and the resistance-value *R* of the air-gap is adjusted, so the overall thermal heat loss coefficient *U* was in accordance with the *U*-value calculated by WIS. Due to the limited capabilities of automatic shading devices in ESP-r, the yearly shading of the window was modelled as a glazing with external venetian blinds with incremental tilt angle of 30° in the interval 23-26 °C. Thus shading is activated and adjusted to a tilt angle of 0° at the indoor air setpoint of 23°, 30° at 24.5°C and 60° at 26°C. The risk of glare is handled by including a setpoint of incident radiation of 270 W/m² causing the shading to activate and adjust to a tilt angle of 60°.

3.5 Air flow network

The passive ventilation system is modelled using the coupled plant and air flow network option in ESP-r. The network is established by specifying internal nodes representing the pressure and temperature in each room and the temperature in the ducts and linking them with external nodes representing the outdoor weather conditions. The links consists of ducts, grilles and other pressure loss inducing elements in the air network. Typically the rela-

tion between mass flow and pressure difference is expressed with power formulas.

3.6 Heat exchangers

The heat exchangers are represented with the following expression:

$$\dot{m} = a \times \Delta P^{b} \quad (1)$$

where:
a: dimensionless coefficient set to 0.19
b: dimensionless coefficient set to 0.43
m: mass flow rate in kg/s
ΔP: pressure drop in Pa

A heat exchanger comprises several hundred meters of plastic tubes arranged in a staggered grid. Air flows across the tubes at velocities ~0.25 m/s and the heat capacity flows of the tube fluid and the air are kept equal. Thus energy is transferred in a counter-flow manner. Heat recovery is achieved by coupling two heat exchangers using a water circuitry with a domestic pump. The details of the heat exchangers and heat recovery system are described in Anderson and Vendelboe (2007).
The heat exchangers are bypassed outside the heating season to reduce the pressure loss.

3.7 Duct system

The intake is placed near the ground on the north façade and the outlet is placed on the roof. The ducts listed in Table 3 are all of standard sizes.
Dynamic pressure losses from bends are specified with a loss factor for the average air velocity.
The wind pressures on the building are calculated from pressure coefficients for a 2:1 building.

Table 3: Duct sizes.

	mm
Main intake duct at ground level	1000-630
Supply & exhaust 1st floor rooms	250
Supply & exhaust 2nd floor rooms	250
Supply & exhaust 3rd floor rooms	315
Main exhaust duct on roof	630

From coefficient tables we know that negative pressure prevailes on a flat roof and on the façade positive pressure in the wind direction and negative pressures on the opposite side.
Open grilles are placed at the intake and exhaust and between ducts and rooms.

3.8 Controls

The desired ventilation rate is specified by CEN 15251 indoor climate class II. This gives a required minimum airflow in the main intake duct of 0.160 m³/s. The ventilation system is controlled by a damper in the main intake duct. The control is proportional meaning that the damper is 100 % open for zero airflow and 10 % open for airflow 4 times the desired airflow. A number of 10 % is due to simulation aspects in ESP-r. Outside heating season in the working hours ventilation is achieved with openings in the façade and single-side and/or cross ventilation. The passive system – however – continues to contribute to the night cooling. Table 4 lists the activation of the different systems.
In order to achieve stable results, the building timestep is set to 6 steps/hour with a plant timestep of 20 steps/building timestep.

Table 4: The activation of passive system and windows

	Heating season		Summer	
	Work hours	Outside work h.	Work hours	Outside work h.
Passive system	On	Off	Off	On
Openings in façade	Off	Off	On	Off

4. RESULTS

The results shown are chosen to represent critical performance parameters: indoor air temperature and ventilation rate in critical rooms.
Air temperature is shown for South-facing rooms and ventilation rate for North-facing rooms. The latter is due to the fact that colder rooms contribute less to the stack effect.
Figure 3 depicts the whole-year ventilation rate through the main supply duct.
Figure 4 depicts duration curves of ventilation rate for critical rooms during the heating season filtered by occupancy. Figure 5 depicts whole-year duration curves of indoor air tem-

perature in critical rooms filtered by occupancy.

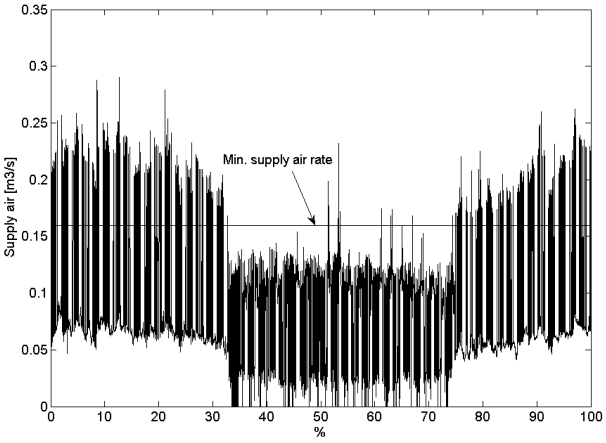

Figure 3: Yearly airflow in main intake duct.

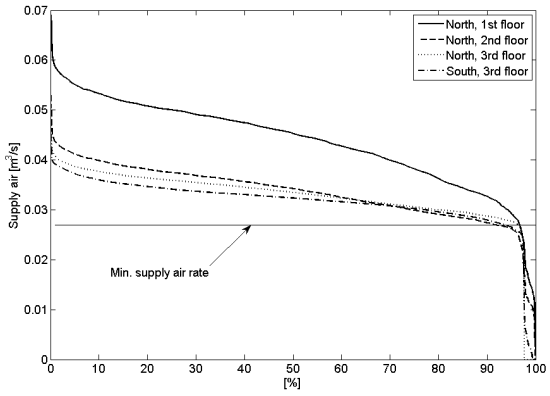

Figure 4: Duration curves of ventilation rates of hand-picked rooms during heating season.

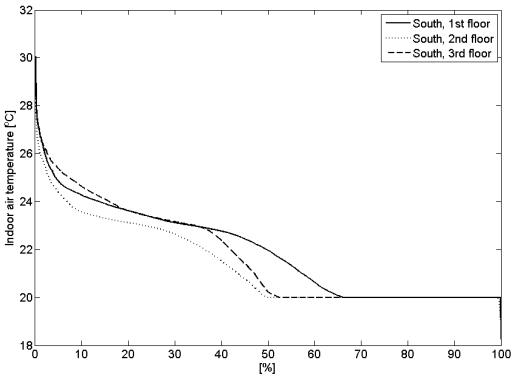

Figure 5: Yearly duration curves of indoor air temperatures.

4.1 Energy consumption

The amount of energy consumed by the building is listed in Table 5 together with the 2008 energy frame for new buildings in Denmark. The energy demand is calculated by the Danish energy frame documentation tool Be06 (2008), because several of the elements of the energy frame require special and time-consuming setup and simulation in ESP-r.
We use ESP-r to show the feasibility of the passive system in terms of ventilaton rate and indoor climate and Be06 in terms of energy. Thus the ventilation rate keyed into Be06 is the required minimum supply air rate from Figure 3, because in practise the intake damper would be controlled to obtain this air rate.
With regard to the cooling effect of the night ventilation during summertime, the keyed-in ventilation rate value in Be06 is set to 0.11 m³/s as an average value obtained from Figure 3.

Table 5: Relative energy consumption

Primary energy kWh/m²	Mech. vent. and cool.	Passive vent., night cool., mech cool.
Heating	100 %	103 %
Cooling	100 %	55 %
Fans	100 %	0 %
Lighting	100 %	100 %
Hot water	100 %	100 %
Total	100 %	60 %
Danish	2006	2010
Building Code	100%	53%

The energy delivered is in primary energy (electric energy consumption is multiplied by 2.5) and includes energy for heating, cooling, fans, lighting and domestic hot water. The reduction in the Danish energy frames from 2006 to 2010 is included to demonstrate how a passive ventilation system with night cooling reduces the mechanical cooling load and thus is an efficient energy measure on the road to the future frame of 2010.

5. DISCUSSION

It is clear from Figure 3, Figure 4 and Figure 5 that the passive system is able to provide suf-

ficient ventilation during the heating season. The distribution of air between offices may be further optimized by choosing duct sizes that correspond to equal pressure losses. This however requires non-standard duct sizes. Introducing dampers is not desirable as the air velocities in the ducts are outside the working interval of dampers and that dampers introduce unnecessary pressure losses.

From Figure 3 it is clear that the ventilation rate provided by the passive system becomes unstable during the summer due to small stack effect and less wind. Hence comfort ventilation during the summer must be provided by other means, e.g. through openings in the façade. Despite the inadequacy of the passiv system to provide ventilation in a summer day situation, the system does provide a significant amount of free cooling on a whole-year basis even with no more thermal mass than that of the decks and the façade.

The proportional damper control in ESP-r is not adequate for controlling the ventilation system in terms of energy consumption. This is illustrated on Figure 3 where the minimum setting of the damper (10 % open) lets 40 % of the minimum supply airflow through. However this also illustrates the driving potential of stack and wind in ventilation.

Thus the energy consumption in the building is compared to the current and future energy frame of the Danish Building Code showing a significant decrease in energy consumption. This said, the energy required for the electrostatic precipitator and the circuitry pump is not quantified but rather assumed to be negligible.

6. CONCLUSION

The simulations performed in this paper indicate that passive ventilation has potential over conventional mechanical ventilation. In conjunction with adequate night cooling both ventilation and cooling tasks are performed satisfactorily. Consequently energy consumption for fans and mechanical cooling can be saved in a passive ventilation system. If the system is equipped with low pressure loss heat recovery and electrostatic filtering it may perform the task of ventilation, cooling and heating in high performance offices with comparable flexibility and total costs to that of conventional mechanical systems.

REFERENCES

Anderson, M., and Vendelboe, M., 2007. Passiv ventilation med varmegenvinding. Master thesis, Department of Civil Engineering, Technical University of Denmark, Copenhagen. In Danish.

Be06, 2008. SBi. Ver. 2.7.3.30. Danish Building Research Institute, Hørsholm, Denmark. Available from http://www.sbi.dk

ESP-r, 2008. Version 11.5. Energy Systems Research Unit, University of Strathclyde, Glasgow, UK. Available from http://www.esru.strath.ac.uk

Kolokotroni, M., Aronis, A., 1999. Cooling-energy reduction in air-conditioned offices by using night ventilation. Applied Energy 63, 241-253.

Olsen, E.L., Chen, Q., 2003. Energy consumption and comfort analysis for different low-energy cooling systems in a mild climate. Energy and Buildings 35 (6), 560-571.

Seppänen, O., Fisk, W., Lei, Q., 2006. Ventilation and performance in office work. Indoor Air 16 (1), 28-36.

van Dijk, D., Oversloot, H., 2003. WIS, the European tool to calculate thermal and solar properties of windows and window components. Proceedings of IBPSA, Building Simulation, Eindhoven, Netherlands, pp. 259-266.

Wargocki, P., Djukanovic, R., 2005. Simulations of the potential revenue from investment in improved indoor air quality in an office building. ASHRAE Transactions 111 PART 2, 699-711.

List of Figures

List of Tables